The Dynamic Neuron: Cellular Mechanisms Maintaining Neural Activity and the Consequences of Phosphatidylinositol 3,5-bisphosphate Biosynthesis on Synapse Function

by

Amber Joyce McCartney

A dissertation submitted in partial fulfillment
of the requirements for the degree of
Doctor of Philosophy
(Neuroscience)
in the University of Michigan
2014

Doctoral Committee:

Associate Professor Michael A. Sutton, Chair
Professor Miriam H. Meisler
Associate Professor Geoffrey G. Murphy
Professor Michael D. Uhler
Professor Lois S. Weisman
Associate Professor Haoxing Xu

ACKNOWLEDGEMENTS

This dissertation is the result of a tight collaboration between the laboratories of Dr. Michael Sutton and Dr. Lois Weisman. I greatly appreciate the support and enthusiasm for taking on strongly collaborative projects. And, I am deeply grateful for the contributions of members of both groups. Multiple people contributed directly to experimental design, data collection and analysis – these specific contributions are indicated throughout this dissertation. Collectively, through their contributions, support and willingness to collaborate, my scientific peers inspire me to continue to tackle challenging scientific questions.

I would like to acknowledge the following people for their encouragement, support and helpful discussions early in my scientific career: Dr. Lu Chen, Dr. Herman Dierick, Dr. Bruno van Swinderen, Dr. Weimin Zhang and Dr. Robert Zucker.

I am grateful for the training that I have received throughout graduate school from friends, dissertation committee and colleagues that aided my investigations. I would like to thank Christian Althaus, Dr. Rafiqa Ameziane, Cindy Carruthers, Nick Carducci, Dr. Jonathan Demb, Dr. Adam Iliff, Emily Kauffman, Dr. Jeremy Kennard, Dr. Rich Hume, Dr. Michael Manookin, Dr. Miriam Meisler, Dr. Geoffrey Murphy, Dr. Michael Uhler, Dr. Hishashi Umemori, Dr. Bethany Strunk, Dr. Michael Sutton, Dr, Akiko

Terauchi, Dr. Lois Weisman, Dr. Haoxing Xu, Dr. Masa Yasuda, Dr. Yanling Zhang and Dr. Sergey Zolov.

My training has been supported in part by the following sources: training grants T32EY017878 and T32MH014279-33, National Research Service Award (F31-07474001) from the National Institute of Neurological Disorders and Stroke, and the Rackham Predoctoral Fellowship. Additionally, I am grateful for the support that I have received to attend scientific meetings from the Neuroscience Graduate Program, the Society for Neuroscience graduate student travel award, the Rackham Graduate School Travel Award (multiple years) and the Keystone Graduate Student Travel Award.

I would like to thank the Neuroscience Graduate Program for providing an enriching environment for graduate education and always striving to improve the experience of every student. The current and past directors of the program during my tenure (Dr. Peter Hitchcock, Dr. Stephen Maren and Dr. Edward Stuenkel) deserve special recognition for their dedication to the students and the University of Michigan. I am deeply grateful for Rachel Flaten and Valerie Smith, both of whom provide outstanding support of all aspects of the program.

Finally, I thank my parents, siblings and husband for enduring support, encouragement and inspiration: Douglas, Virginia D., Willie, Janelle, Derek, Alex, Jeff, Annie, Emily, Joshua, Johnny, Jeremy, Tim, Lois, Virginia K., and Julia.

Table of Contents

LIST OF FIGURES

LIST OF TABLES

LIST OF APPENDICES

LIST OF ABBREVIATIONS

ALS	amyotrophic lateral sclerosis
AMPA	α-Amino-3-hydroxy-5-methyl-4-isoxazolepropionic acid
APV	(2R)-amino-5-phosphonovaleric acid
BDNF	brain-derived neurotrphic factor
Bic	bicuculline
Ca	calcium
CDK	cyclin-dependent kinase
CFD	Francois-Mouchetee Fleck Corneal Dystrophy
Clavesin	clathrin vesicle associated Sec14 protein
cLTD	chemical long-term depression
CMT	Charcot Marie Tooth
CNQX	6-cyano-7-nitroquinoxaline-2,3-dione
DIV	days in vitro
DNA	deoxyribonucleic acid
EEA1	early endosome antigen 1
EGF	epidermal growth factor
EGFR	epidermal growth factor receptor
ER	endoplasmic reticulum
FBS	fetal bovine serum
Fwd	forward
g	gram
GFP	green fluorescent protein
GluA1	glutamate receptor 1
GluA2	glutamate receptor 2
Glut4	glucose transporter 4
h	hour
HBS	HEPES buffered saline
HEAT	Huntingtin, elongation factor 3, protein phosphatase 2A, and the yeast kinase TOR1
IgG	immunoglobulin G
ILV	intraluminal vesicle
Lamp1	lysosomal-associated membrane protein 1
Lamp2	lysosomal-associated membrane protein 2
LBPA	lysobisphosphatidic acid

LTD	long-term depression
LTP	long-term potentiation
M	molar
MAP2	microtubule associated protein 2
MEF	mouse embryonic fibroblast
mEPSC	miniature excitatory postsynaptic current
Mg	magnesium
min	minute
MTMR	myotubularin-related
mTOR	mammalian target of rapamycin
MVB	multivesicular body
N	number
Na_V	voltage-gated sodium channel
NIH	National Institute of Health
NMDA	N-methyl-D-aspartate
nNOS	neuronal nitric oxide synthase
pAb	polyclonal antibody
PCR	polymerase chain reaction
PDZ	postsynaptic density protein (PSD95), Drosophila disc large tumor suppressor (Dlg1), zonula occludens-1 protein (zo-1)
pHluorin	pH sensitive green fluorescent protein
PI	phosphatidylinositol
PI(3,4)P2	phosphatidylinositol 3,4-bisphosphate
PI(3,4,5)P3	phosphatidylinositol 3,4,5-trisphosphate
PI(3,5)P2	phosphatidylinositol 3,5-bisphosphate
PI(4,5)P2	phosphatidylinositol 4,5-bisphosphate
PI3P	phosphatidylinositol 3-phosphate
PI4P	phosphatidylinositol 4-phosphate
PI5P	phosphatidylinositol 5-phosphate
Plk2	polo-like kinase 2
PLS	primary lateral sclerosis
PSD95	postsynaptic density protein 95
PTEN	phosphatase and tensin homolog
Rev	reverse
RNA	ribonucleic acid
RNAi	RNA interference
RyR	ryanodine receptor
sec	second
sEPSC	spontaneous excitatory postsynaptic currents
sGluA2	surface GluA2
shRNA	small/short hairpin RNA

TNF	tumor necrosis factor
TPC	two-pore channel
TRPML	transient receptor potential cation channel, mucolipin subfamily
TTX	tetrodotoxin
vGlut	vesicular glutamate transporter
vol	volume
VPS	vacuolar protein sorting

ABSTRACT

Proper trafficking of neurotransmitter receptors through endosomal compartments is important for the development, maintenance and plasticity of neural circuits in the brain. However, little is known about the signaling cues orchestrating these intracellular events. Phosphoinositide lipids are excellent candidates for these roles because they regulate multiple types of membrane trafficking, but their specific functions are poorly understood. There are seven unique phosphoinositide lipids that are synthesized from the structural lipid, phosphatidylinositol, by lipid kinases and phosphatases. They function in part through the recruitment of complex protein machines to specific membrane subdomains. That multiple neurological disorders are linked to mutations in phosphoinositide lipid-related genes suggests that they may be particularly important in neurons. A major goal of this dissertation was to identify novel roles for phosphoinositide lipids, as well as identify cellular mechanisms involved in maintaining normal neural function. The specific hypothesis tested was that the low abundant phosphoinositide lipid, phosphatidylinositol 3,5-bisphosphate, is important for synapse function. Notably, Vac14, a regulator of phosphatidylinositol 3,5-bisphosphate biosynthesis is enriched at synapses, which raised the possibility that this lipid impacts synaptic function and plasticity. Additionally, this dissertation examined the roles of phosphatidylinositol 3,5-bisphosphate in determining the fate of internalized AMPA-

type glutamate receptors following stimulus-induced internalization. Evidence presented shows that phosphatidylinositol 3,5-bisphosphate acts as a negative regulator of synapse strength. These data reveal that phosphatidylinositol 3,5-bisphosphate synthesis is required for maintenance of homeostatic synaptic weakening and suggest that phosphatidylinositol 3,5-bisphosphate impacts synapse function by altering AMPA-type glutamate receptor trafficking. These data identify the activity-dependent synthesis of phosphatidylinositol 3,5-bisphosphate as a novel mechanism for regulating synapse strength and suggest that synaptic dysfunction may contribute to the pathogenesis of neurological diseases arising from loss of dynamic phosphatidylinositol 3,5-bisphosphate regulation. In addition, this dissertation examined the role of intrinsic neuronal excitability in the homeostatic response to AMPA-receptor blockade. The ability to adapt to changes in levels of activity is critical for stability of neural networks. These studies identify that relatively brief blockade of AMPA-type glutamate receptor activity triggers at least three forms of homeostatic compensation: postsynaptic strengthening, increased presynaptic probability of release and increased intrinsic excitability.

CHAPTER 1

PHOSPHATIDYLINOSITOL 3,5-BISPHOSPHATE: LOW ABUNDANCE, HIGH SIGNIFICANCE

1.1 SUMMARY

[1]Recent studies of the low abundant signaling lipid, phosphatidylinositol 3,5-bisphosphate ($PI(3,5)P_2$), reveal an intriguingly diverse list of downstream pathways, the intertwined relationship between $PI(3,5)P_2$ and PI5P, as well as links to neurodegenerative diseases. Derived from the structural lipid phosphatidylinositol, $PI(3,5)P_2$ is dynamically generated on multiple cellular compartments where interactions with an increasing list effectors regulate many cellular pathways. A complex of proteins that includes Fab1/PIKfyve, Vac14 and Fig4/Sac3 mediates the biosynthesis of $PI(3,5)P_2$, and mutations that disrupt complex function and/or formation cause profound consequences in cells. Surprisingly, mutations in this pathway are linked with neurological diseases, including Charcot-Marie-Tooth Syndrome and Amyotrophic Lateral Sclerosis. Future studies of $PI(3,5)P_2$ and PI5P are likely to expand the roles of these lipids in regulation of cellular functions, as well as provide new approaches for treatment of some neurological diseases.

[1] This chapter was published as a literature review: McCartney AJ*, Zhang Y* and Weisman LS. 2014. Phosphatidylinositol 3,5-bisphosphate: Low abundance. High significance. *Bioessays,* 36**,** 52-64. DOI 10.1002/bies.201300012

1.1 INTRODUCTION

Phosphorylated phosphatidylinositol (PIP) signaling lipids play regulatory roles. These low-abundance lipids are produced from phosphatidylinositol (PI), an abundant structural component of membranes, which can be phosphorylated in any combination on positions three, four or five. Highly regulated PIP kinases and phosphatases generate and turn over the resultant seven PIP lipids (Figure 1-1).

PIP lipids provide spatial and temporal regulation of complex protein machines. The interconvertibility of PIPs enables rapid changes in the identity of the signaling lipid to dynamically recruit effector proteins to specific membranes at the right time. For example, synthesis of phosphatidylinositol 3-phosphate (PI3P) (Gary et al., 1998) at a confined region is predicted to assemble a large complex of multiple PI3P binding proteins and their associated binding partners. Notably, the lipid kinase, Fab1, binds PI3P (Burd and Emr, 1998) (Figure 1-2) and catalyzes the conversion of PI3P to PI(3,5)P_2 (Gary et al., 1998). Recruitment of Fab1 causes local depletion of PI3P and an increase in the levels of PI(3,5)P_2, which releases PI3P binding proteins and recruits a distinct set of PI(3,5)P_2 binding proteins.

Since the discovery of PI(3,5)P_2 in 1997 (Dove et al., 1997, Whiteford et al., 1997), the number of known PI(3,5)P_2 regulated pathways has expanded greatly. Identification of a comprehensive list of these pathways and downstream effector proteins will be required to fully understand PI(3,5)P_2 signaling. Similarly, stimuli that regulate PI(3,5)P_2 levels remain to be identified. Here we assess current knowledge and suggest future directions for the study of this very low abundance lipid.

$PI(3,5)P_2$ is much less abundant than most PIPs, including PI4P and $PI(4,5)P_2$. $PI(3,5)P_2$ is present at about 0.1% and 0.04% of total phosphatidylinositol in yeast and mammalian fibroblasts, respectively. The amount of $PI(3,5)P_2$ is 17-fold and 125-fold less abundant than $PI(4,5)P_2$ in yeast (Bonangelino et al., 2002) and mammalian fibroblasts (Zolov et al., 2012), respectively. The scarcity of $PI(3,5)P_2$ likely contributed to the twenty-five year delay in its discovery (Dove et al., 1997, Whiteford et al., 1997) relative to PI4P and $PI(4,5)P_2$ (Brockerhoff and Ballou, 1962). Utilizing dilute perchloric acid to precipitate cells followed by deacylation of lipids significantly improved the yield of glycerol-inositol head-groups and the identification of $PI(3,5)P_2$ over the traditional Folch extraction (Whiteford et al., 1997, Bonangelino et al., 2002).

1.1 SYNTHESIS AND TURNOVER OF $PI(3,5)P_2$ IS TIGHTLY CONTROLLED BY A LARGE PROTEIN COMPLEX

In yeast, Fab1 (Yamamoto et al., 1995) is the sole PI3P 5-kinase (Gary et al., 1998, Cooke et al., 1998) and Vps34 is the sole PI 3-kinase (Schu et al., 1993). Both $PI(3,5)P_2$ and PI3P levels dynamically and transiently change in response to specific stimuli. Prolonged introduction of yeast into hyperosmotic media causes a 20-fold transient elevation of $PI(3,5)P_2$ (Dove et al., 1997) that lasts for about ten minutes before a precipitous drop to basal levels (Duex et al., 2006a). Concomitant with the rise in $PI(3,5)P_2$, synthesis of PI3P increases. These data suggest that $PI(3,5)P_2$ and PI3P play early roles in adaptation of yeast to hyperosmotic stress. Similarly, these lipids may regulate adaptation in plants and animals, such as transient responses to hormonal or sensory stimuli.

Fab1, commonly called PIKfyve in mammals, is present in most eukaryotes (McEwen et al., 1999). In this review, "Fab1" refers to Fab1 in all non-mammalian species and "PIKfyve" to mammals. "Fab1/PIKfyve" refers to the mammalian and non-mammalian enzyme. In yeast and mouse embryonic fibroblasts (MEF), Fab1/PIKfyve provides all of the PI(3,5)P_2 (Cooke et al., 1998, Gary et al., 1998, Morishita et al., 2002, Jeffries et al., 2004, de Lartigue et al., 2009, Ikonomov et al., 2011, Zolov et al., 2012, Sbrissa et al., 2012, Takasuga et al., 2013). Across species, the domain structure is similar (Figure 1- 2).

1.1.1 The PI(3,5)P_2 synthesis complex

The dynamic and rapid changes in PI(3,5)P_2 observed in yeast suggest that Fab1 is tightly regulated. Moreover, overexpression of Fab1 does not increase PI(3,5)P_2 levels (Gary et al., 1998). Indeed, Fab1 activity requires formation of a complex of regulatory proteins, including Fig4, Vac14, Vac7 and Atg18.

Fig4, a PI(3,5)P_2 5-phosphatase, catalyzes the turnover of PI(3,5)P_2 in yeast (Gary et al., 2002, Rudge et al., 2004, Duex et al., 2006a, Duex et al., 2006b). Unexpectedly, Fig4 is also required for the activation of Fab1/PIKfyve (Duex et al., 2006a, Duex et al., 2006b, Chow et al., 2007, Zolov et al., 2012). Mutations in the catalytic site of Fig4 negatively affect both the turnover of PI(3,5)P_2 and the elevation in PI(3,5)P_2 in response to hyperosmotic stress (Duex et al., 2006b). In addition to Fig4 catalytic activity, other regions in Fig4 may play a role. Several disease mutations in *Fig4* reside in a non-catalytic, N-terminal domain (Manford et al., 2010). Analysis of a corresponding mutation (Fig4-I59T) in yeast revealed a defect in hyperosmotic shock induced activation

of Fab1 (Chow et al., 2007). Analysis of this N-terminal domain may provide insight into how Fig4 activates Fab1/PIKfyve.

Vac14 regulates both Fab1 and Fig4 (Bonangelino et al., 2002, Dove et al., 2002) and is required for the synthesis and turnover of $PI(3,5)P_2$ (Duex et al., 2006a). Vac14, composed of virtually all HEAT repeats (Figure 1- 2), functions as a scaffold protein that nucleates the formation of a complex including Fab1, Fig4 and other regulators (Botelho et al., 2008, Jin et al., 2008) (Figure 1- 3). Vac14 forms dimers or oligomers (Dove et al., 2002, Jin et al., 2008, Botelho et al., 2008, Alghamdi et al., 2013). In the cytoplasm, Fig4 and Vac14 interact without Fab1 (Botelho et al., 2008). There may be additional proteins required to form the complex.

Similarly, mammalian Vac14 (ArPIKfyve) forms a complex with PIKfyve, and Fig4 (Sac3) (Sbrissa et al., 2007, Jin et al., 2008, Sbrissa et al., 2008, Ikonomov et al., 2009b, Ikonomov et al., 2010). The interaction sites between the yeast and mammalian complexes are likely conserved. The binding site for Fab1 on Vac14 is conserved in the mammalian complex (Jin et al., 2008, Ikonomov et al., 2009b). Fig4 binds to Vac14 through the conserved C-terminal region (Ikonomov et al., 2009b). Additionally, the N-terminal pathogenic point mutation, Fig4-I41T, disrupts the interaction of Fig4 with Vac14 and destabilizes Fig4 (Ikonomov et al., 2010, Lenk et al., 2011). These observations raise the possibility that both the N- and C-termini of Fig4 interact with Vac14.

Yeast Vac7, a critical activator of Fab1, has no recognizable motifs; its mode of action is unknown (Bonangelino et al., 1997, Gary et al., 1998, Bonangelino et al., 2002,

Gary et al., 2002, Duex et al., 2006a, Duex et al., 2006b). Vac7 resides within the Fab1 complex, but is not required for formation or localization of the complex (Gary et al., 1998, Rudge et al., 2004, Jin et al., 2008). This is surprising because Vac7 is the only protein in the complex with a transmembrane domain (Bonangelino et al., 2002). Vac7 function is likely conserved in metazoans. However, based on sequence similarity, Vac7 is only present in some fungi. Either alternative mechanisms activate Fab1/PIKfyve in metazoans or proteins with functions analogous to Vac7 cannot be identified by BLAST search.

Yeast Atg18, a negative regulator of $PI(3,5)P_2$ levels, resides within the Fab1 complex. Through two adjacent binding sites (Baskaran et al., 2012, Watanabe et al., 2012, Krick et al., 2012), Atg18 binds to $PI(3,5)P_2$ and PI3P (Dove et al., 2004). These sites are essential for Atg18 to negatively regulate $PI(3,5)P_2$ levels and for localization of Atg18 on the vacuole (Efe et al., 2007). Relief of Fab1 inhibition in an *atg18Δ s*train requires Fab1 activators. Thus, Atg18 likely inhibits the activators rather than acting on Fab1 directly. Metazoans may have unidentified proteins that function similarly to yeast Atg18. The mammalian genes *WIPI1*, *WIPI2, WIPI3* and *WIPI4* encode proteins with greater than 20% identity to yeast Atg18 (Jeffries et al., 2004, Proikas-Cezanne et al., 2007). WIPI1 and WIPI2, like Atg18, function in autophagy. However, whether they function as negative regulators of $PI(3,5)P_2$ levels has not been tested.

1.1.1.1 Orchestrating Fab1/PIKfyve activity

At least three mechanisms within the Fab1 complex contribute to the dynamic regulation of $PI(3,5)P_2$. First, the lipid kinase and phosphatase reside within the complex.

Second, the Fab1 activator, Vac7, and inhibitor, Atg18, bind overlapping sites on Vac14 and likely compete for access to Fab1. Third, catalytic activity of Fig4 is required for the activation of Fab1. Tight coordination between synthesis and turnover of PI(3,5)P_2 likely explains how a sustained stimulus of hyperosmotic shock causes a steep transient increase in PI(3,5)P_2 levels.

Other opposing lipid kinases and phosphatases reside in the same complex or have coordinated regulation (reviewed in (Botelho, 2009)). MTM1, a lipid 3-phosphatase, resides in a complex with the PI3-kinase, Vps34. Inositol polyphosphate 4-phosphatase is in a complex with a class I PI3-kinase. The added complexity in the Fab1 complex, that the opposing lipid phosphatase has a second role as activator of the lipid kinase, underscores the importance of directly measuring phosphoinositide lipid levels to determine cellular functions of predicted lipid phosphatases.

1.1.1.1 Comparison of PI(3,5)P_2 synthesis in yeast and metazoans

In metazoans, several PI 3-kinases, in addition to Vps34, may produce the PIKfyve substrate, PI3P. Indeed, knockdown of either PIKfyve or PI3K-C2α, but not Vps34, affects TORC1 activity in adipocytes (Bridges et al., 2012). Thus, in some cases PI3K-C2α may provide the pool of PI3P utilized to generate PI(3,5)P_2.

A major difference between the yeast and mammalian Fab1/PIKfyve complex are the lipid pools that they control. Surprisingly, in MEF cells the PIKfyve complex is required for most of the PI5P and all of the PI(3,5)P_2 pool (Zhang et al., 2007, Ikonomov et al., 2011, Sbrissa et al., 2012, Zolov et al., 2012). An independent study concluded that PIKfyve does not contribute to PI5P levels (Jones et al., 2012); however, that study

assumed that PIKfyve inhibition did not impact the lipids used to standardize the samples.

The relative importance of Vac14 for Fab1/PIKfyve activity differs between the yeast and mammalian complexes. In *vac14Δ* yeast, PI(3,5)P_2 levels are reduced at least 10-fold (Duex et al., 2006a, Duex et al., 2006b), while Vac14$^{-/-}$ and Fig4$^{-/-}$ MEF cells reveal a more modest 2-fold reduction in PI(3,5)P_2 and PI5P (Zhang et al., 2007, Chow et al., 2007, Zolov et al., 2012). Since Vac14 or Fig4 are required for only half of the PI(3,5)P_2 pool and PIKfyve is required for the entire pool, PIKfyve either retains partial function in the absence of Vac14 or Fig4 and/or PIKfyve has additional regulators.

1.1.2 Localization of Vac14, Fab1/PIKfyve and Fig4

In yeast, Fab1, Vac14, Fig4 are found on the limiting membrane of vacuoles and adjacent foci, which are likely endosomes (Rudge et al., 2004, Jin et al., 2008, Botelho et al., 2008). In metazoan cells, Fab1/PIKfyve and Vac14 are found on early and late endosomes, lysosomes and in the cytosol (Shisheva et al., 2001, Sbrissa et al., 2004, Cabezas et al., 2006, Ikonomov et al., 2006, Rutherford et al., 2006, Rusten et al., 2006, Zhang et al., 2012). Questions remain about how the complex is associated with membranes. Is the FYVE domain of Fab1/PIKfyve sufficient for localization of the complex? Are there other lipid-binding or transmembrane containing subunit(s)?

1.1.3 PI(3,5)P_2 is a precursor for PI5P synthesis

PI(3,5)P_2 likely serves as a precursor for most of the cellular PI5P pool. The strongest evidence for this hypothesis comes from heterologous expression of PIKfyve in yeast, which greatly increases PI(3,5)P_2 and decreases its precursor, PI3P. Importantly,

the combined total of PI3P, PI5P and PI(3,5)P_2 remains constant in the presence or absence of heterologous PIKfyve (Zolov et al., 2012). If PI5P were generated directly by PIKfyve, then new direct conversion of PI to PI5P would raise the combined total of PI3P, PI5P and PI(3,5)P_2. Additionally, transient activation or inhibition of endogenous PIKfyve in fibroblasts causes PI(3,5)P_2 levels to reach a new steady-state faster than PI5P, an outcome consistent with a precursor-product relationship (Zolov et al., 2012).

Generation of PI5P from PI(3,5)P_2 requires proteins with 3-phosphatase activity (Zolov et al., 2012), which may be provided by myotubularins (MTMRs) (Tronchere et al., 2004). Indeed, mouse MTMR2 and *Drosophila* MTMR3 function with Fab1/PIKfyve to control PI5P and PI(3,5)P_2 (Vaccari et al., 2011, Oppelt et al., 2013). That both PI(3,5)P_2 and PI5P are embedded in membranes, and cannot freely diffuse, raises the possibility that MTMRs reside within the PIKfyve complex. This would provide rapid access of MTMRs to the newly synthesized PI(3,5)P_2.

An alternative hypothesis, that PIKfyve directly generates most of the cellular PI5P, has been recently reviewed (Shisheva, 2012). Briefly, there is controversy between independent *in vitro* studies about whether PIKfyve directly generates PI5P (McEwen et al., 1999). In some studies PIKfyve was immunoprecipitated from cells that express many lipid 3-phosphatases. Tight association of PIKfyve with 3-phosphatases during immunoprecipitation may explain some discrepancies. Strong *in vitro* evidence that PIKfyve can directly generate PI5P comes from studies of PIKfyve expressed from insect Sf9 cells (Sbrissa et al., 2000). Development of a general inhibitor of myotubularin

function may help resolve whether most of the cellular PI5P pools are generated directly or indirectly by PIKfyve.

That PIKfyve is either directly or indirectly responsible for most of the PI5P in fibroblasts raises questions about whether PI(3,5)P_2 and PI5P reside on the same membrane. Localization of Vac14, Fab1/PIKfyve, and Fig4 provide insights into the subcellular locations of PI(3,5)P_2 in yeast and metazoans. If MTMRs are associated with this complex, then MTMR localization would provide information for the subcellular distribution of PI5P as well (Figure 1- 4A). However, the presence of Vac14, Fab1/PIKfyve, and Fig4 does not *a priori* indicate enzymatic activity. Thus, development of probes will be critical to determine the spatial and temporal dynamics of PI(3,5)P_2 and PI5P.

1.2 PI(3,5)P_2 BINDING PROTEINS

Based on the pleiotropic defects observed in cells and organisms with defects in PIKfyve activity, most PI(3,5)P_2 binding proteins are likely not yet identified. To date, multiple types of motifs as well as novel sequences have been shown to interact with PI(3,5)P_2. PI(3,5)P_2 binds directly to some WD40 domain containing proteins, including Atg18, Atg21, Hsv2, Tup1 (in yeast) and Raptor (in adipocytes), and regulates their functions *in vivo* (Dove et al., 2004, Han and Emr, 2011, Bridges et al., 2012). Additionally, sorting nexin proteins SNX1 and SNX2 (PX domain) (Carlton et al., 2004, Carlton et al., 2005), Cti6 (PHD domain) (Han and Emr, 2011), clavesin (Sec14 domain) (Katoh et al., 2009) and class II formins (PTEN domain) (van Gisbergen et al., 2012) interact with PI(3,5)P_2. TRPML1 and RyR1 also bind PI(3,5)P_2 (Shen et al., 2009, Dong et

al., 2010). In these latter examples, no lipid binding motif is apparent. Thus, bioinformatic approaches are not sufficient to determine which proteins bind PI(3,5)P_2.

Atg18 binds PI(3,5)P_2 with a high affinity, in the nanomolar range (Dove et al., 2004), likely due to tandem lipid binding sites. Lower affinity interactions may be of equal biological significance but are more difficult to detect. Moreover, some effectors require simultaneous interactions with other proteins (reviewed in (Lemmon, 2008)). For example, the FYVE domain containing protein, EEA1, associates with membranes via simultaneous interaction with PI3P and Rab5 GTPase. The development of strategies to detect relatively low affinity binding will be necessary to identify the full set of PI(3,5)P_2 and PI5P effectors.

1.3 PATHWAYS REGULATED BY VAC14, FAB1/PIKFYVE AND FIG4

Mutants deficient in Fab1 or its regulators provide information on its cellular (Table 1) and physiological roles (Table 2). The PIKfyve inhibitors YM201636 and MF4 have also facilitated studies of cellular functions of PIKfyve (Jefferies et al., 2008, de Lartigue et al., 2009). However, off-target effects need to be considered (Ikonomov et al., 2009c). Recently, apilimod was also found to be a potent inhibitor of PIKfyve (Cai et al., 2013).

In mammals, loss of PIKfyve function decreases both PI(3,5)P_2 and PI5P (Zhang et al., 2007, Ikonomov et al., 2011, Zolov et al., 2012), thus phenotypes linked to mutations in this pathway may be due to loss of PI(3,5)P_2, PI5P or both lipids. In addition, disagreement among studies about whether a specific pathway requires PIKfyve may be due to differences in the extent of decrease of PIKfyve activity. In most cell-based

studies some PIKfyve function remains, including mutant cells and RNAi experiments. For example, in *PIKfyve*$^{\beta geo/\beta geo}$ MEF cells, 5% of the normal levels of PIKfyve provide half of the normal levels of PI(3,5)P_2 and PI5P (Zolov et al., 2012). Here, we present pathways that require PIKfyve. Those known to be directly regulated by PI(3,5)P_2, because PI(3,5)P_2 protein effectors have been identified, will be indicated. In other cases, the regulatory lipid may either be PI(3,5)P_2 or PI5P.

1.3.1 Formation of large vacuoles

A striking feature in PI(3,5)P_2 deficient organisms is enlarged vacuoles (Yamamoto et al., 1995, Bonangelino et al., 1997, Ikonomov et al., 2001, Rutherford et al., 2006, Zhang et al., 2007, Chow et al., 2007, Jefferies et al., 2008, Whitley et al., 2009, Hirano et al., 2011, Takasuga et al., 2013). In mutant yeast, the vacuole/lysosome is enlarged. In *Vac14*$^{-/-}$ and *Fig4*$^{-/-}$ MEF cells, the vacuoles are heterogeneous, arising from both late endosomes and lysosomes, as well as enlarged autophagosomes (Zhang et al., 2007, Chow et al., 2007, Ferguson et al., 2009, Zhang et al., 2012). Complete inhibition of PIKfyve causes vacuoles to form from early endosomes as well (Jefferies et al., 2008).

The enlarged vacuoles in PI(3,5)P_2-defective yeast mutants cannot release water even when exposed to hyperosmotic shock (Bonangelino et al., 2002), which suggests an inability to regulate the water content of the vacuole. Similarly, vacuoles in mammalian cells are likely due to defects in the regulation of osmolarity within the endomembrane system. The *Vac14*$^{Ingls/Ingls}$ and *Fig4*$^{-/-}$ mouse mutants exhibit extreme hydrocephalus (Jin et al., 2008, Lenk et al., 2011), and the vacuoles that form in *Vac14*$^{-/-}$ or *Fig4*$^{-/-}$ MEF cells are not filled with lipid (Zhang et al., 2007, Chow et al., 2007).

1.3.2 PI(3,5)P_2 regulates some ion channels

The defects in water homeostasis may be linked to defects in ion homeostasis. Indeed, overexpression of the TRPML1 calcium channel in *Vac14*$^{-/-}$ MEF cells suppresses the formation of vacuoles (Dong et al., 2010). In *S. pombe*, mutations in a calcium permease (SPAC521.04c) rescue the enlarged vacuoles in the *fab1Δ* mutant (Onishi et al., 2003). Suppression in both cases may be due to regulation of calcium flux.

A role for phosphoinositide regulation of ion channels is better understood on the plasma membrane where multiple ions channels are activated by PI(4,5)P_2. In some cases, PI(4,5)P_2 directly interacts with the channel; in other cases, PI(4,5)P_2 recruits regulators (Falkenburger et al., 2010). Similarly, PI(3,5)P_2 activates ion channels on endosomes and lysosomes, including mucolipin transient receptor potential channels (TRPML1, TRPML2, TRPML3) and yeast homolog, yeast vacuolar conductance (Yvc1), and two-pore channels (TPC1, TPC2, TPC3) (Dong et al., 2010, Wang et al., 2012). While the mechanism of PI(3,5)P_2 regulation of TPCs is not known, PI(3,5)P_2 interacts directly with the cytoplasmic N-terminus of TRPML1. PI(3,5)P_2 is also important for calcium dynamics in muscles. PI(3,5)P_2 directly activates the ryanodine receptors (RyR1, RyR2), which release calcium from the sarcoplasmic reticulum in skeletal and cardiac muscles, respectively (Shen et al., 2009, Touchberry et al., 2010).

1.3.3 PI(3,5)P_2 plays a role in the acidification of the vacuole

Vacuoles in *fab1Δ*, *vac7Δ*, and *vac14Δ* yeast are less acidified than wild-type vacuoles (Yamamoto et al., 1995, Bonangelino et al., 1997). Similar phenotypes occur in *Schizosaccharomyces pombe*, *Caenorhabditis elegans*, *Drosophila melanogaster* and

Arabidopsis thaliana (Augsten et al., 2002, Nicot et al., 2006, Rusten et al., 2006, Hirano et al., 2011, Bak et al., 2013). These acidification defects may contribute to the formation of large vacuoles; vacuolar ATPase function is required for both vacuole fission and fusion (Baars et al., 2007). However, $PI(3,5)P_2$ plays additional roles in vacuole morphology. A limited increase in $PI(3,5)P_2$ corrects acidification of the vacuole without correcting vacuole size (Gary et al., 1998, Bonangelino et al., 2002). $PI(3,5)P_2$ effectors involved in acidification have not been identified, although the vacuolar ATPase is a likely candidate. While assembly of the vacuolar ATPase does not require $PI(3,5)P_2$ (Bonangelino et al., 2002), $PI(3,5)P_2$ may regulate vacuolar ATPase activity.

1.3.4 Fab1/PIKfyve is required for multiple pathways in the endomembrane system

Membrane trafficking defects also contribute to the formation of enlarged vacuoles. In yeast, $PI(3,5)P_2$ and Atg18 are required for fission of the vacuole (Efe et al., 2007, Zieger and Mayer, 2012) and retrograde traffic from the vacuole to the Golgi (Bryant et al., 1998, Dove et al., 2004). These defects contribute to but do not fully account for the large vacuoles in the *fab1Δ* mutant. The vacuoles in *atg18Δ* are not as enlarged as observed in *fab1Δ* yeast (Efe et al., 2007). Thus, defects in water and ion homeostasis, vacuole acidification, as well as defects in membrane trafficking and vacuole fission, each contribute to the enlarged vacuoles caused by low levels of $PI(3,5)P_2$ (Figure 1- 4B).

1.3.4.1 Roles for Fab1/PIKfyve in the multivesicular body pathway

Fab1/PIKfyve function has been linked to multivesicular body (MVB) formation, a protein degradation pathway. MVB formation involves the ubiquitination and capture of cargoes on the limiting membrane of late endosomes, which are then internalized via invagination and formation of intraluminal vesicles (ILV). Degradation of protein cargoes occurs when the MVB fuses with the lysosome. In *fab1Δ* yeast, fewer ILVs are formed (Gary et al., 1998). Formation of ILVs requires several ESCRT proteins, including Vps24. While controversial (Michell et al., 2006), one study suggested that Vps24 binds $PI(3,5)P_2$ (Whitley et al., 2003). Thus, the partial defect in ILV formation may be due to a requirement for $PI(3,5)P_2$ in Vps24 function. In addition to a possible role in forming ILV vesicles, $PI(3,5)P_2$ may be required for sorting some protein cargoes (reviewed in (Ho et al., 2012)). How $PI(3,5)P_2$ regulates cargo sorting remains to be determined.

Loss of PIKfyve activity has also been linked to events that occur after cargo sorting. *Drosophila* Notch, Wingless and Dpp (a fly homologue of TGFβ) accumulate in the MVB and are not degraded in a *Drosophila fab1* mutant. Thus, Fab1 may also function downstream of cargo internalization (Rusten et al., 2006). Delayed epidermal growth factor receptor (EGFR) degradation due to inhibition of PIKfyve (Jefferies et al., 2008, Er et al., 2013) may also be due to similar defects: either trafficking problems after sorting ligands into the MVB or loss of protease activity in lysosomes that are not properly acidified.

1.3.4.2 PIKfyve is required for protein trafficking from endosomes to the TGN

Similar to yeast (Bryant et al., 1998, Dove et al., 2004), PIKfyve is required for retrograde traffic of proteins from endosomes to the trans-Golgi network (TGN). Knockdown of PIKfyve inhibits retrograde traffic of the cation-independent mannose-6-phosphate receptor (CI-MPR), sortillin (a related receptor) and furin (Rutherford et al., 2006). In *Vac14*$^{-/-}$ fibroblasts (Zhang et al., 2007), or following inhibition of PIKfyve (de Lartigue et al., 2009), CI-MPR localizes to endosomes and cathepsin D, one of its ligands, is missorted (Zhang et al., 2007). Inhibition of PIKfyve also delays trafficking of the Shiga Toxin B subunit from endosomes to the TGN (de Lartigue et al., 2009). These defects may be due in part to dysregulation of SNX1 and SNX2, retromer proteins that bind directly to $PI(3,5)P_2$. In addition, PIKfyve binds to two proteins required for retrograde trafficking: p40, a Rab9 effector, and JLP, a kinesin adaptor required for microtubule based transport from endosomes to the TGN (Ikonomov et al., 2003, Ikonomov et al., 2009a).

1.3.4.3 Regulation of PIKfyve in response to insulin

PIKfyve is required for insulin-mediated Glut4 translocation. Insulin stimulates the glucose transporter (Glut4) to transiently translocate to the plasma membrane, which facilitates glucose uptake. Regulated Glut4 trafficking occurs in both adipocytes and muscle. Suppression of PIKfyve activity reduces insulin induced Glut4 translocation in cultured adipocytes (reviewed in (Shisheva, 2012)). PIKfyve is also required for Glut4 trafficking in animals; a muscle-specific knock-out of *PIKfyve* in mice causes a defects in

Glut4 translocation and glucose uptake (Ikonomov et al., 2013). The precise role(s) of PIKfyve in Glut4 translocation are not known.

Insulin stimulation regulates PIKfyve activity (Shisheva et al., 2001, Berwick et al., 2004, Bridges et al., 2012), in part by Akt, which phosphorylates PIKfyve on serine 318 (Berwick et al., 2004). Moreover, EGF stimulation, which promotes EGFR internalization and degradation, also induces Akt phosphorylation of PIKfyve on serine 318 (Er et al., 2013). However, in cells the degree of activation of PIKfyve due to phosphorylation of serine 318 is relatively modest. Thus, there are may be additional Akt phosphorylation sites on PIKfyve, as well as additional PIKfyve activators.

One outcome of insulin activation of PIKfyve in adipocytes is an effect on mTOR, a major regulator of cell metabolism. Insulin-induced translocation of mTOR to the plasma membrane, as well as mTOR activity, requires PIKfyve (Bridges et al., 2012). The recruitment of mTOR to the plasma membrane in response to insulin may occur through direct interactions with $PI(3,5)P_2$. However, whether $PI(3,5)P_2$ is found on the plasma membrane of adipocytes is not known.

1.3.4.4 Fab1/PIKfyve is required for autophagy in metazoans

Autophagy requires Fab1/PIKfyve. Autophagy delivers cargoes to the lysosome for degradation. Suppression of Fab1/PIKfyve results in impaired clearance of autophagic organelles. In *C. elegans*, mutations in PPK-3 (Fab1) cause an increase in autophagosomes (Nicot et al., 2006). Similarly, *Drosophila fab1* mutant larvae accumulate autophagosomes and amphisomes (Rusten et al., 2007). In NIH3T3 or HEK293 cells, and in primary cultured hippocampal neurons, inhibition of PIKfyve with

YM201636 or MF4 causes an accumulation of autophagosomes and the autophagic marker, LC3-II (Jefferies et al., 2008, de Lartigue et al., 2009, Martin et al., 2013). Similarly, the brains of mice with mutations in *Fig4* have elevated levels of LC3-II and p62, another marker of autophagy (Ferguson et al., 2009, Vaccari et al., 2011, Lenk et al., 2011, Katona et al., 2011). Together, the above studies indicate that PIKfyve has multiple roles in the endomembrane system.

1.3.4.5 Roles for lysosomal PI(3,5)P_2 in the regulation of transcription

Endosomal PI(3,5)P_2 may also regulate some transcriptional pathways. Expression of pheromone responsive genes in *S. pombe* is defective in a *fab1Δ* mutant (Morishita et al., 2002). Similarly, in *S. cerevisiae* PI(3,5)P_2 modulates transcription via interaction with Tup1 and Cti6 (Han and Emr, 2011). PI(3,5)P_2 provides a site on the yeast vacuole for assembly of the Tup1/Cyc8/Cti6 transcription complex. These findings predict that PI(3,5)P_2 on lysosomes may regulate additional transcription pathways.

1.3.4.6 Fab1/PIKfyve may function at the plasma membrane

In addition to multiple functions on endosomes, a small pool of Fab1/PIKfyve may function at or near the plasma membrane. In adipocytes, PIKfyve activity may contribute to localization of mTORC1 to the plasma membrane. Furthermore, PIKfyve has been implicated in phagocytosis and pinocytosis (Kerr et al., 2010, Hazeki et al., 2012). Further evidence for a potential role for Fab1/PIKfyve at the plasma membrane comes from the *Physcomitrella patens* class II formins, which bind PI(3,5)P_2 (van Gisbergen et al., 2012) and require Fab1 activity for their localization at the cell cortex. PIKfyve has also been implicated in actin remodeling in mammalian cells (reviewed in

(Shisheva, 2012)). In addition, when expressed heterologously in *Xenopus* oocytes, several plasma membrane localized ion channels and carrier proteins require PIKfyve activity (reviewed in (Dove et al., 2009, Ho et al., 2012, Shisheva, 2012)). Thus, while most PIKfyve is associated with endosomal membranes, PIKfyve may also have roles at the plasma membrane.

1.4 FAB1/PIKFYVE, VAC14 AND FIG4 IN PLANT AND ANIMAL PHYSIOLOGY

PIKfyve plays critical roles in development. Knockout of *PIKfyve* in mice results in very early lethality: *PIKfyve*$^{-/-}$ embryos did not survive past E3.5 (Ikonomov et al., 2011) and, in an independent knock-out, embryos did not survive past E8.5 (Takasuga et al., 2013). Similarly, *Drosophila fab1* and *C. elegans* (*ppk*-3) mutants display early lethality (Rusten et al., 2006, Nicot et al., 2006). In *Arabidopsis thaliana* the two *Fab1* genes, *FAB1A* and *FAB1B*, play critical roles in development (Whitley et al., 2009, Hirano et al., 2011)}, perhaps due in part to hyposensitivity to auxin signaling (Hirano and Sato, 2011).

Analysis of a *PIKfyve*$^{\beta geo/\beta geo}$ hypomorphic mutant mouse with partial PIKfyve activity, which dies perinatally, has revealed post-development roles of PI(3,5)P_2 and PI5P in animal physiology (Zolov et al., 2012). Similarly, *Vac14*$^{-/-}$ mutant mice, which also have less Fig4 protein (Lenk et al., 2011, Zolov et al., 2012), die perinatally (Zhang et al., 2007). *Fig4*$^{-/-}$ mice can live up to 6 weeks (Chow et al., 2007). *Vac14*$^{Ingls/Ingls}$, a missense mutation that disrupts binding of Vac14 with PIKfyve, survives up to 3 weeks (Jin et al., 2008). Differences in lethality may be largely due to differences in strain background. Early lethality is rescued in *Fig4*$^{-/-}$ mice by neuronal-specific, but not astrocyte-specific, expression of *Fig4* (Ferguson et al., 2012). Thus, loss of PI(3,5)P_2 and PI5P in neurons

likely contributes to early lethality of the *Fig4*$^{-/-}$ mice and other PIKfyve-related mouse models.

1.4.1 Multiple tissues require PIKfyve

Vac14, *Fig4* and *PIKfyve* are expressed globally. Accordingly, defects in the corresponding mouse mutants occur in multiple tissues. Hearts of the *Vac14*$^{-/-}$, *Fig4*$^{-/-}$ and *PIKfyve* hypomorph mutants have vacuoles (Zolov et al., 2012) and in the two latter mutants, there is a spongiform-like phenotype in the spleen as well. Moreover, the lungs and kidneys of the *PIKfyve* hypomorph have a spongiform-like appearance. Conditional knock-out of *PIKfyve* (*PIPKIII*), in intestinal cells, causes vacuole formation and defects in membrane trafficking in the gut epithelia, which ultimately lead to early lethality (Takasuga et al., 2013).

Vac14, PIKfyve and Fig4 proteins are most abundant in the nervous system, which fits with findings that the nervous system is profoundly affected in the corresponding mutant animals (Zhang et al., 2012, Zolov et al., 2012). *Fig4*$^{-/-}$, *Vac14*$^{-/-}$ and *Vac14*$^{Ingls/Ingls}$ mice display degeneration of the brain, including enlarged ventricles, increased apoptosis and severe spongiform encephalopathy; large vacuoles in the cell bodies of neurons are also observed in the peripheral nervous system (Chow et al., 2007, Zhang et al., 2007, Jin et al., 2008). The *PIKfyve* hypomorph has similar defects (Zolov et al., 2012). Consistent with the importance of PI(3,5)P_2 and PI5P in the nervous system, a mouse with a neuron-specific knock-out of *Vps34*, displays juvenile lethality and neurodegeneration, and has reduced PI3P and PI(3,5)P_2. PI5P was not measured (Zhou et al., 2010).

Myelination is reduced in the central and peripheral nerves of *Fig4*$^{-/-}$ mice (Chow et al., 2007, Winters et al., 2011, Ferguson et al., 2012). Fig4 may be particularly abundant during development of myelinating cells and dorsal root ganglia sensory neurons (Guo et al., 2012), although *Fig4*$^{-/-}$ controls, which would indicate whether the antigen detected by the anti-Fig4 antibody was bona fide Fig4, were missing. Interestingly, hypomyelination in *Fig4*$^{-/-}$ mice is rescued by neuron-specific expression of Fig4 (Winters et al., 2011). Heterozygous *Fig4*$^{+/-}$ mice show no signs of neurodegeneration or increased susceptibility to trauma induced degeneration (Yan et al., 2012). *Mtmr2*$^{-/-}$*Fig4*$^{-/-}$ double mutant mice have more severe hypomyelination and neurodegeneration, which suggest that loss of PI5P contributes to these phenotypes (Vaccari et al., 2011).

1.4.2 PIKfyve in neurons

Vac14, PIKfyve and Fig4 have specialized roles at the synapse. AMPA-type glutamate receptors, which mediate fast neurotransmission in the brain, cycle between endosomes and the plasma membrane. Notably, trafficking of the AMPA receptor subunits, GluA1 and GluA2, are modulated by the PIKfyve complex. shRNA silencing of PIKfyve impairs trafficking of GFP-HA-GluA2 (Tsuruta et al., 2009), and addition of PI(3,5)P_2 promotes trafficking of heterologously expressed GluA1 (Seebohm et al., 2012). In *Vac14*$^{-/-}$ cultured hippocampal neurons, GluA1 and GluA2 are increased on the plasma membrane with a concomitant increase in postsynaptic strength (Zhang et al., 2012). Similarly, in cultured cortical neurons, internalization and degradation of the L-

type voltage-gated calcium channel subunit, $Ca_V1.2$, requires PIKfyve (Tsuruta et al., 2009).

In addition to postsynaptic defects, *Vac14*$^{-/-}$ neurons also displayed an increased probability of presynaptic vesicle fusion (Zhang et al., 2012). Similarly, PIKfyve is a negative regulator of calcium-dependent exocytosis in neurosecretory cells (Osborne et al., 2008). Together, PIKfyve and potentially $PI(3,5)P_2$, PI5P or both negatively regulate the excitatory response of neurons, which may explain why defects in the PIKfyve complex are linked to excitotoxic neuronal death.

Further determination of roles for $PI(3,5)P_2$ and PI5P signaling at the synapse will likely come from identification of proteins that binds these lipids and/or interact with Vac14, PIKfyve, or Fig4. Potential candidates include clavesin and nitric oxide synthase (nNOS). Clavesin (clathrin vesicle-associated Sec14 protein), is expressed solely in the brain and binds $PI(3,5)P_2$. Knockdown of clavesin causes enlarged late-endosomes/lysosomes similar to those seen with suppression of PIKfyve activity (Katoh et al., 2009). nNOS, which functions at the synapse in the regulation of neurotransmission, binds Vac14 through a PDZ domain *in vitro* (Lemaire and McPherson, 2006); a functional interaction between Vac14 and nNOS at the synapse has not been tested.

1.5 MUTATIONS IN GENES THAT ENCODE THE VAC14, PIKFYVE, AND FIG4 COMPLEX ASSOCIATED WITH HUMAN DISEASES

Mutations in *FIG4* underlie a severe form Charcot Marie-Tooth (CMT) type 4J (Chow et al., 2007). In CMT, progressive deterioration of nerves and/or demyelination

throughout the peripheral nervous system results in reduced nerve conduction velocity and sensory sensation. These defects overlap with those observed in the *Fig4*$^{-/-}$ mouse. The most common genotype in CMT4J patients is *FIG4* compound heterozygosity: one null allele and the other encoding the missense mutation, isoleucine 41 to threonine (I41T) (Chow et al., 2007). The mutation retains partial function. In *Fig4*$^{-/-}$ mice, overexpression of a *Fig4-I41T* transgene significantly suppresses the early lethality (Chow et al., 2007, Lenk et al., 2011). That *Fig4-I14T* has a modest functional defect, yet causes peripheral neuropathy, underscores the importance of precise modulation of PI(3,5)P_2 and/or PI5P levels in the nervous system.

CMT4B1 and CMT4B2 are caused by loss-of-function mutations in MTMR2 and MTMR13 respectively (reviewed in (Bolis et al., 2007)) and have clinical symptoms that overlap with those observed in CMT4J. The clinical symptoms in common between CMT4B and CMT4J may be due to either less PI5P or elevated PI3P.

A range of mutations in *FIG4* were found in 7 out of 473 patients with ALS and 2 patients with PLS (Chow et al., 2009). Mutations in *FIG4* may be causative in other neurological diseases as well. Moreover, mutations in *FIG4* can cause defects in additional tissues. Homozygous null mutations in *FIG4* cause Yunis-Varón syndrome, a severe autosomal-recessive congenital disorder, which affects multiple tissues, including the heart, skeletal muscle, skeleton and brain (Campeau et al., 2013). The diversity of affected tissues underscores the importance of the Vac14/PIKfyve/Fig4 complex in human physiology.

To date, neither *PIKfyve* nor *Vac14* have been linked to neurological disease. Heterozygous null mutations in *PIKfyve* are associated with Francois-Mouchetee Fleck Corneal Dystrophy (CFD) (Li et al., 2005), which results in white flecks throughout the corneal stroma of the eye that do not affect vision. Corneal flecks are thought to be enlarged vacuoles in swollen keratocytes (Kotoulas et al., 2011). Interestingly, Vac14 mRNA is down-regulated in a large subset of patients with chronic fatigue syndrome (Carmel et al., 2006). Based on the common molecular functions of PIKfyve, Vac14 and Fig4, it is tempting to speculate that mutations in *PIKfyve* and *Vac14* will be discovered that are linked to neurological disorders.

1.6 CONCLUSIONS

The roles and regulation of PI(3,5)P_2 parallel those of other PIP species. Notably, PI3P is a precursor for PI(3,5)P_2, which in turn is a precursor for PI5P. The interconversion between these lipids predicts that there are pathways where these lipids spatially and temporally control multi-step pathways.

Compared with PI3P, PI4P and PI(4,5)P_2, the levels of PI(3,5)P_2 are exceedingly low. The difficulty of measuring the low levels of PI(3,5)P_2 in cells, and the lack of a fluorescent probe to monitor its spatial and temporal dynamics have provided major hurdles towards elucidating the roles and regulation of PI(3,5)P_2. A more complete picture of the pathways that rely on PI(3,5)P_2 and PI5P will likely provide insights into how minor defects in the regulation of these lipids leads to profound human diseases. Recent observations that mutations in *Fig4* cause defects with striking similarities to lysosomal storage disorders may also provide insight into the links between these lipids

and disease (Martyn and Li, 2013). Moreover, as whole exome sequencing of patients continues, more diseases linked to this pathway will likely be discovered. The severity of CMT4J, ALS and Yunis-Varon syndrome underscores the importance of uncovering the molecular mechanisms that regulate the Vac14/PIKfyve/Fig4 complex, as well as the discovery of new cellular pathways that are regulated by $PI(3,5)P_2$ and PI5P.

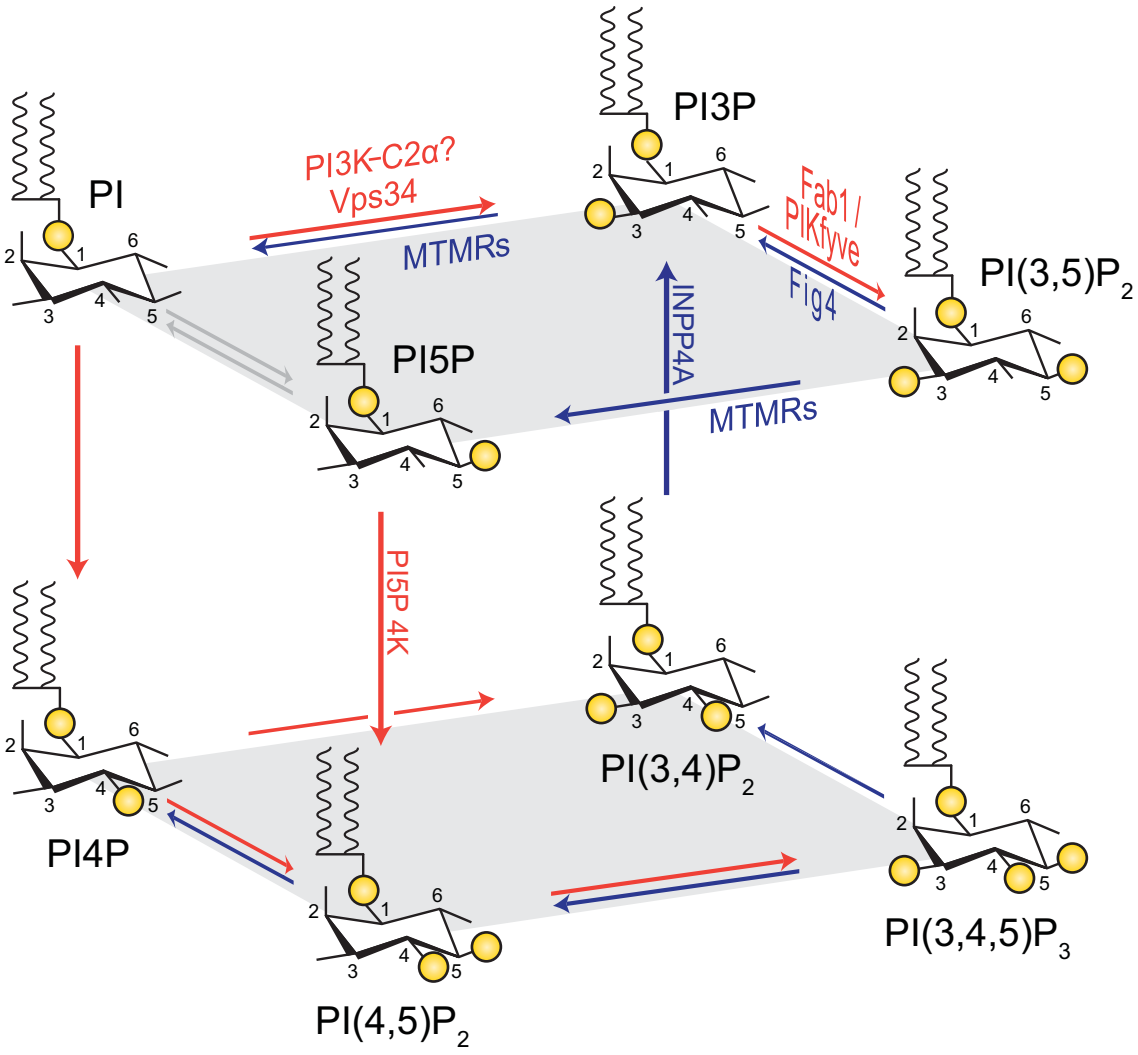

Figure 1-1. Interconversion among the seven known phosphoinositide lipids
Interconversion among the seven known phosphoinositide lipids occurs via action of specific lipid kinases (red arrows) and phosphatases (blue arrows). Selected kinases and phosphatases are shown. While controversial, direct conversion of PI to PI5P via PIKfyve activity may contribute to the PI5P pool (gray arrows). INPP4A phosphatase, which causes neurodegeneration in mice (Norris et al., 1995), and the type II PI5P 4-kinase (Carricaburu et al., 2003, Rameh et al., 1997), which has a role in the regulation of PI5P levels, were not discussed in this chapter.

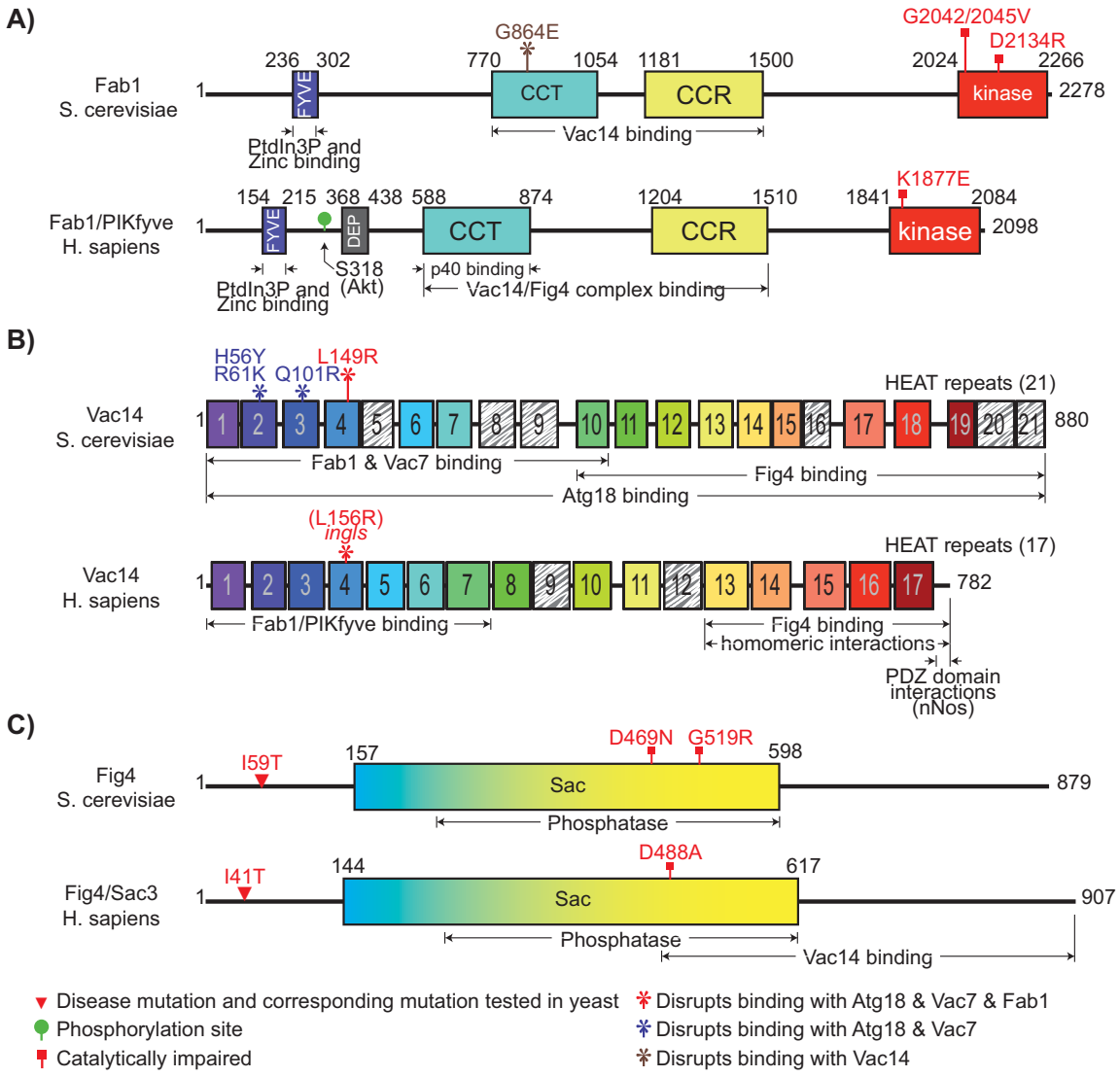

Figure 1-2. Fab1/PIKfyve, Vac14 and Fig4 are conserved in most eukaryotes
Domains of *S. cerevisiae* and human Fab1/PIKfyve, Vac14 and Fig4/Sac3 are shown. **(A)** Fab1 domains include FYVE (binds PI3P), DEP (unknown function; present in chordate and insect Fab1), CCT (homologous to the chaperone Cpn60/TCP-1 family; mediates interactions with Vac14), CCR (a conserved cysteine rich domain found only in Fab1/PIKfyve; part of the Vac14 binding region), kinase (catalytic site for conversion of PI3P to PI(3,5)P_2). **(B)** Vac14 is composed of tandem HEAT repeats, which are rod-like helical structures that mediate protein-protein interactions. **(C)** Fig4 contains a Sac domain, which is a module found in several lipid phosphatases. Note, the number of amino acids in mouse PIKfyve and human PIKfyve are not identical. The catalytically impaired mutation in mouse PIKfyve, K1831E, is indicated on the schematic of human PIKfyve, K1877E. The boundaries for FYVE, CCT, CCR, kinase, and Sac domains were identified as follows: 1) conserved in multiple sequence alignments and 2) contained unbroken secondary structure elements predicted by the program Jpred. Sequences for Fab1/PIKfyve were from the following species: *Saccharomyces cerevisiae* (budding

yeast, NP_116674), *Schizosaccharomyces pombe* (fission yeast, NP_596090), *Candida albicans* (human pathogen, CAC42810), *Ashbya gossypii* (cotton pathogen, NP_985045), *Arabidopsis thaliana* (plant, NP_001078484), *Drosophila melanogaster* (fly, NP_611269), *Apis mellifera* (honey bee, XP_393666), *Anopheles gambiae* (mosquito, XP_314118), *Caenorhabditis elegans* (worm, CAA19436), and *Homo sapiens* (human, NP_055855). The Sac domain in Fig4 was defined through alignment of the following Sac domain proteins in S. cerevisiae: Inp51, Inp52, Inp53, Sac1 and Fig4.

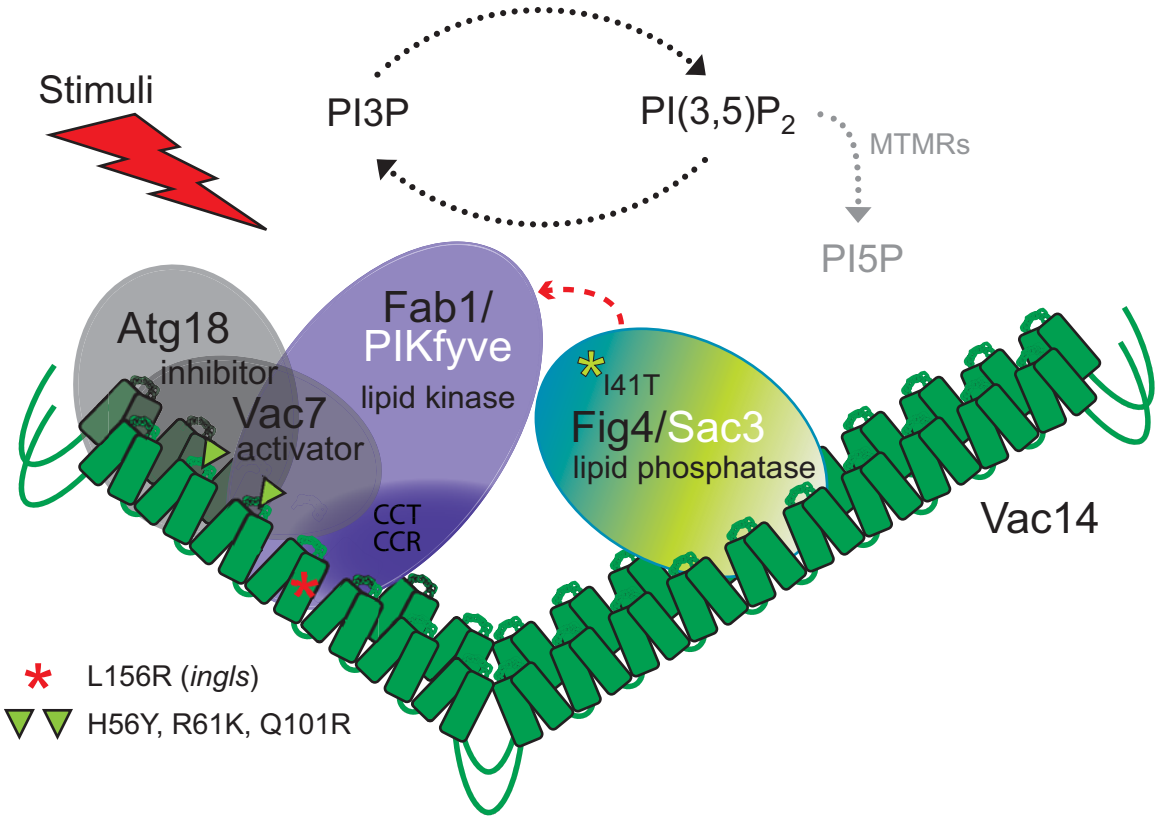

Figure 1-3. Schematic of the Fab1/PIKfyve, Vac14, Fig4/Sac3 complex
Vac14 oligomerizes with itself and nucleates the complex through direct interactions with Fab1/PIKfyve and Fig4/Sac3. In yeast, Vac14 also directly interacts with Atg18 and Vac7. The yeast Vac14 point mutants, H56Y (HEAT repeat loop 2), R61K (HEAT repeat loop 2) and Q101R (HEAT repeats loop 3), each disrupt binding of Atg18 and Vac7. Thus, Atg18 and Vac7 may bind overlapping or identical sites of Vac14 (Jin et al., 2008). The Vac14-L156R mutation, found in *ingls* mice, and corresponding mutation Vac14-L149R in yeast, disrupts Vac14 interaction with Atg18, Vac7 and Fab1. This suggests that all three proteins bind overlapping sites on Vac14. The point mutation, Fig4-I41T found in patients with CMT4J, disrupts the interaction between Fig4 and Vac14, although the major portion of human Fig4 that interacts with Vac14 resides within residues 478-907 (Ikonomov et al., 2009b). In mammalian cells, myotubularin related proteins (MTMRs) can convert $PI(3,5)P_2$ to PI5P and may provide the majority of cellular PI5P. ◊This figure is adapted from Jin et al. (2008).

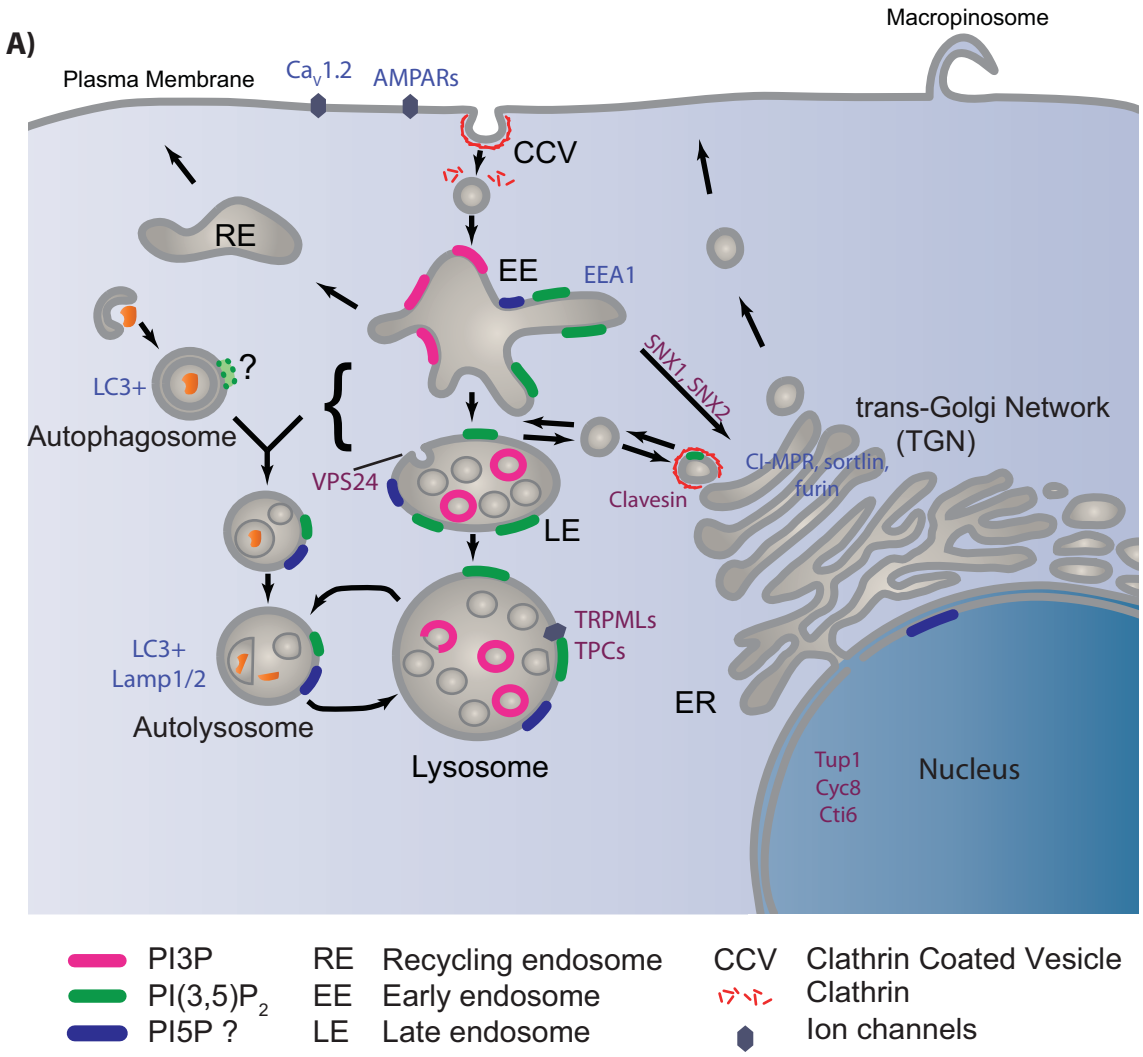
A)
Macropinosome
Plasma Membrane
$Ca_V1.2$
AMPARs
CCV
RE
EE
EEA1
LC3+
?
Autophagosome
SNX1, SNX2
trans-Golgi Network
(TGN)
VPS24
Clavesin
CI-MPR, sortlin,
furin
LE
TRPMLs
TPCs
LC3+
Lamp1/2
Autolysosome
Lysosome
ER
Tup1
Cyc8
Cti6
Nucleus
PI3P
$PI(3,5)P_2$
PI5P ?
RE Recycling endosome
EE Early endosome
LE Late endosome
CCV Clathrin Coated Vesicle
Clathrin
Ion channels

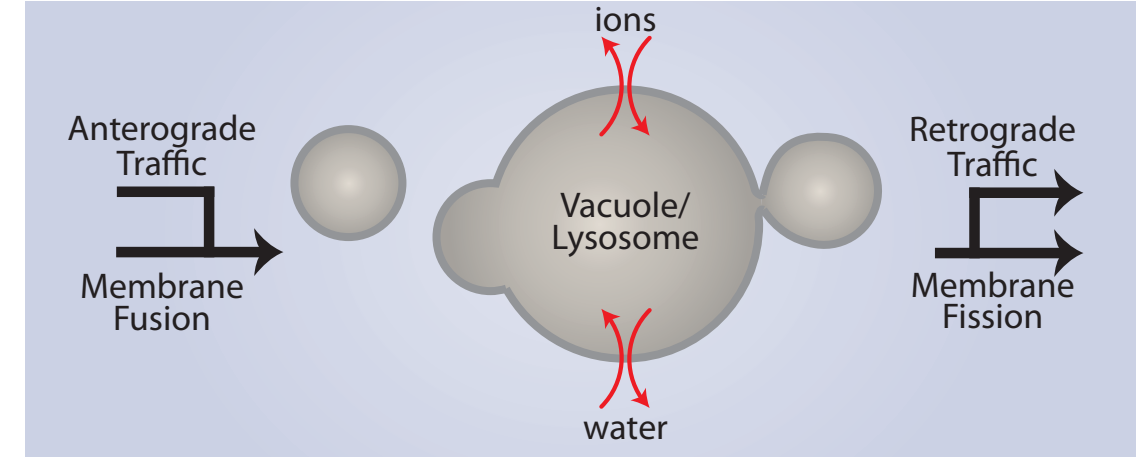
B)
ions
Anterograde
Traffic
Membrane
Fusion
Vacuole/
Lysosome
water
Retrograde
Traffic
Membrane
Fission

Figure 1-4. Cellular localization of PI(3,5)P_2
(A) Localization of PI(3,5)P_2 and PI5P inferred from the localization of PIKfyve and Vac14. PI(3,5)P_2 localizes on early endosomes, late endosomes and lysosomes. Localization of PI(3,5)P_2 on autophagosomes is less clear. PI5P may also be present at all or some of these locations. To further establish the locations of these lipids, suitable lipid probes need to be developed. PI(3,5)P_2 effectors and trafficking pathways affected in PIKfyve/Vac14/Fig4 deficient cells are also indicated. Purple: known PI(3,5)P_2 effectors. Blue: proteins affected by PI(3,5)P_2 and/or PI5P. **(B)** The size of a yeast vacuole or mammalian lysosome is dependent on ion and water homeostasis, as well as the net sum of anterograde traffic, retrograde traffic, membrane fusion and membrane fission.

Table 1. Pathways regulated by Fab1/PIKfyve

Pathways affected	Known PI(3,5)P_2 Effectors	Species and reference
PI5P biogenesis	MTMRs[†] (Zolov et al., 2012, Berger et al., 2003)	Cell culture (Zolov et al., 2012)
Vacuole fission	Atg18 (Dove et al., 2004)	*S. cerevisiae* (Bonangelino et al., 1997)
Retrograde traffic from the vacuole	Atg18 (Dove et al., 2004)	*S. cerevisiae* (Bryant et al., 1998, Dove et al., 2004)
Acidification of vacuoles or endolysosomes		*S. cerevisiae* (Yamamoto et al., 1995, Bonangelino et al., 1997); *C. elegans* (Nicot et al., 2006); *D. melanogaster (Rusten et al., 2006);* *A. thaliana* (Hirano et al., 2011);
Ion channel function	TRPML1, TRPML2, TRPML3 (Dong et al., 2010); TPC1, TPC2, TPC3 (Wang et al., 2012); RyR1, RyR2 (Touchberry et al., 2010, Silswal et al., 2011)	Cell culture and mouse (Dong et al., 2010, Touchberry et al., 2010, Silswal et al., 2011, Wang et al., 2012)
Autophagy in metazoans		*C. elegans* (Nicot et al., 2006); *D. melanogaster* (Rusten et al., 2007); Cell culture (Jefferies et al., 2008, de Lartigue et al., 2009); Mouse (Ferguson et al., 2009, Vaccari et al., 2011, Lenk et al., 2011, Katona et al., 2011)
Fluid phase endocytosis		Cell culture (Ikonomov et al., 2003, Zhang et al., 2007, de Lartigue et al., 2009); *D. melanogaster* (Rusten et al., 2006)
Sorting of cargoes at the MVB	Vps24[†] (Whitley et al., 2003)	*S. cerevisiae* (Reviewed in (Ho et al., 2012))
Traffic of cell surface receptors to lysosomes		Cell culture (de Lartigue et al., 2009); D. melanogaster (Rusten et al., 2006)
Endosome-to-TGN traffic	SNX1, SNX2 (Carlton et al., 2005)	Cell culture (Rutherford et al., 2006, Zhang et al., 2007, Ikonomov et al., 2009, de Lartigue et al., 2009,)

Glut4 translocation in response to insulin		3T3 adipocytes (Reviewed in (Shisheva, 2012))
mTORC1 translocation to the plasma membrane in response to insulin	Raptor (Bridges et al., 2012)	3T3 adipocytes (Bridges et al., 2012);
Cortical actin array dynamics	Formins (van Gisbergen et al., 2012)	*P. patens* (van Gisbergen et al., 2012)
GAL1 induction in the absence of GAL4	Tup1, Cti6 (Han and Emr, 2011)	*S. cerevisiae* (Han and Emr, 2011)
AMPA receptor and $Ca_v1.2$ trafficking		Neuron culture (Tsuruta et al., 2009, Zhang et al., 2012, Seebohm et al., 2012)
Exocytosis		Neuron culture (Osborne et al., 2008, Zhang et al., 2012)

† Potential binding of Vps24 (Narayan and Lemmon, 2006) and MTMRs (Choudhury et al., 2006) are controversial.

Table 2. Phenotypes of PI(3,5)P_2 deficiency in model organisms

Phenotypes	Species and reference
Enlarged endosomes and lysosomes	*S. cerevisiae* (Yamamoto et al., 1995, Bonangelino et al., 1997, Gary et al., 1998, Cooke et al., 1998); *S. pombe* (Morishita et al., 2002); *C. albicans* (Augsten et al., 2002); Cell culture (Ikonomov et al., 2001, Rutherford et al., 2006, Zhang et al., 2007, Chow et al., 2007, Jefferies et al., 2008, de Lartigue et al., 2009, Zolov et al., 2012); *C. elegans* (Nicot et al., 2006); *D. melanogaster* (Rusten et al., 2006); *A. thaliana* (Whitley et al., 2009) Mouse (Chow et al., 2007, Ferguson et al., 2009, Zhang et al., 2012)
Sensitivity to heat and calcium	*S. cerevisiae* (Yamamoto et al., 1995); *S. pombe* (Morishita et al., 2002)
Secretion and response to mating hormones	*S. pombe* (Morishita et al., 2002)
Hyphae formation on solid medium	*C. albicans* (Augsten et al., 2002)
Inviable pollen, slow root growth, curled leaves, dwarfed plants, abnormal flowers	*A. thaliana* (Whitley et al., 2009, Hirano et al., 2011)
Stunted growth	*P. patens* (van Gisbergen et al., 2012)
Early lethality	*C. elegans* (Nicot et al., 2006); *D. melanogaster* (Rusten et al., 2006); mouse (Zhang et al., 2007, Jin et al., 2008, Chow et al., 2007, Ikonomov et al., 2011, Zolov et al., 2012)
Dilute coat color	Mouse (Chow et al., 2007, Jin et al., 2008)
Neurodegeneration	Mouse (Bolino et al., 2004, Zhang et al., 2007, Chow et al., 2007, Jin et al., 2008, Zhang et al., 2008, Katona et al., 2011, Winters et al., 2011, Vaccari et al., 2011, Ferguson et al., 2012, Zolov et al., 2012)
Increased pre- and post-synaptic strength	Neuron culture (Zhang et al., 2012)
Myelination defects	Mouse (Bolino et al., 2004, Zhang et al., 2008, Vaccari et al., 2011, Winters et al., 2011)
Abnormalities in heart, lung, kidney, thymus, and spleen	Mouse (Chow et al., 2007, Zolov et al., 2012)

Table 3. Human disease linked to defects in $PI(3,5)P_2$

Disease	Affected Gene	Reference
Charcot Marie-Tooth type 4J (CMT4J)	Fig4 (I41T)* Fig4 (L17P)*	Chow et al., 2007, Zhang et al., 2008, Chow et al., 2009
Amyotrophic lateral sclerosis (ALS)	Fig4	Chow et al., 2009
Primary lateral sclerosis (PLS)	Fig4	Chow et al., 2009
Yunis–Varon syndrome	Fig4**	Campeau et al., 2013
Charcot Marie-Tooth type 4B1	MTMR2	Reviewed in Bolis et al., 2007
Charcot Marie-Tooth type 4B2	MTMR13	Reviewed in Bolis et al., 2007
Francois-Mouchetee Fleck Corneal Dystrophy	PIKfyve	Li et al., 2005, Kotoulas et al., 2011
Polymicrogyria with epilepsy	Fig4	Baulac et al., 2014
Chronic Fatigue Syndrome	Down regulation of Vac14	Carmel et al., 2006

*Patients are compound heterozygotes with a null allele of Fig4 and Fig4-I41T, or Fig4-L17P.

**Patients are homozygous for loss-of-function (null) alleles of Fig4

1.7 BIBLIOGRAPHY

Alghamdi TA, Ho CY, Mrakovic A, Taylor D, Mao D & Botelho RJ. 2013. Vac14 protein multimerization is a prerequisite step for Fab1 protein complex assembly and function. *The Journal of biological chemistry,* **288,** 9363-72.

Augsten M, Hubner C, Nguyen M, Kunkel W, Hartl A & Eck R. 2002. Defective Hyphal induction of a Candida albicans phosphatidylinositol 3-phosphate 5-kinase null mutant on solid media does not lead to decreased virulence. *Infect Immun,* **70,** 4462-70.

Baars TL, Petri S, Peters C & Mayer A. 2007. Role of the V-ATPase in regulation of the vacuolar fission-fusion equilibrium. *Molecular biology of the cell,* **18,** 3873-82.

Bak G, Lee EJ, Lee Y, Kato M, Segami S, Sze H, Maeshima M & Hwang JU. 2013. Rapid Structural Changes and Acidification of Guard Cell Vacuoles during Stomatal Closure Require Phosphatidylinositol 3,5-Bisphosphate. *The Plant cell,* **25,** 2202-2216.

Baulac S, Lenk GM, Dufresnois B, Bencheikh BOA, Couarch P, Renard J, Larson PA, Ferguson CJ, Noé E, Poirier K, Hubans C, Ferreira S, Guerrini R, Ouazzani R, El KH, Hachimi KHE, Meisler MH & Leguern E. 2014. Role of the phosphoinositide phosphatase FIG4 gene in familial epilepsy with polymicrogyria. *Neurology,* **82,** 1068-75.

Baskaran S, Ragusa MJ, Boura E & Hurley JH. 2012. Two-site recognition of phosphatidylinositol 3-phosphate by PROPPINs in autophagy. *Molecular cell,* **47,** 339-48.

Berwick DC, Dell GC, Welsh GI, Heesom KJ, Hers I, Fletcher LM, Cooke FT & Tavare JM. 2004. Protein kinase B phosphorylation of PIKfyve regulates the trafficking of GLUT4 vesicles. *Journal of Cell Science,* **117,** 5985-5993.

Berger P, Schaffitzel C, Berger I, Ban N & Suter U. 2003. Membrane association of myotubularin-related protein 2 is mediated by a pleckstrin homology-GRAM domain and a coiled-coil dimerization module. *Proceedings of the National Academy of Sciences of the United States of America,* **100,** 12177-82.

Bolino A, Bolis A, Previtali SC, Dina G, Bussini S, Dati G, Amadio S, Del Carro U, Mruk DD, Feltri ML, Cheng CY, Quattrini A & Wrabetz L. 2004. Disruption of Mtmr2 produces CMT4B1-like neuropathy with myelin outfolding and impaired spermatogenesis. *J Cell Biol,* **167,** 711-21.

Bolis A, Zordan P, Coviello S & Bolino A. 2007. Myotubularin-related (MTMR) phospholipid phosphatase proteins in the peripheral nervous system. *Molecular neurobiology,* **35,** 308-16.

Bonangelino CJ, Catlett NL & Weisman LS. 1997. Vac7p, a novel vacuolar protein, is required for normal vacuole inheritance and morphology. *Molecular and cellular biology,* **17,** 6847-58.

Bonangelino CJ, Nau JJ, Duex JE, Brinkman M, Wurmser AE, Gary JD, Emr SD & Weisman LS. 2002. Osmotic stress-induced increase of phosphatidylinositol 3,5-bisphosphate requires Vac14p, an activator of the lipid kinase Fab1p. *The Journal of cell biology,* **156,** 1015-28.

Botelho RJ. 2009. Changing phosphoinositides "on the fly": how trafficking vesicles avoid an identity crisis. *BioEssays : news and reviews in molecular, cellular and developmental biology,* **31,** 1127-36.

Botelho RJ, Efe JA, Teis D & Emr SD. 2008. Assembly of a Fab1 phosphoinositide kinase signaling complex requires the Fig4 phosphoinositide phosphatase. *Mol Biol Cell,* **19,** 4273-86.

Bridges D, Ma JT, Park S, Inoki K, Weisman LS & Saltiel AR. 2012. Phosphatidylinositol 3,5-bisphosphate plays a role in the activation and subcellular localization of mechanistic target of rapamycin 1. *Molecular biology of the cell,* **23,** 2955-62.

Brockerhoff H & Ballou CE. 1962. Phosphate incorporation in brain phosphionositides. *The Journal of biological chemistry,* **237,** 49-52.

Bryant NJ, Piper RC, Weisman LS & Stevens TH. 1998. Retrograde traffic out of the yeast vacuole to the TGN occurs via the prevacuolar/endosomal compartment. *J Cell Biol,* **142,** 651-63.

Burd CG & Emr SD. 1998. Phosphatidylinositol(3)-phosphate signaling mediated by specific binding to RING FYVE domains. *Molecular cell,* **2,** 157-62.

Cabezas A, Pattni K & Stenmark H. 2006. Cloning and subcellular localization of a human phosphatidylinositol 3-phosphate 5-kinase, PIKfyve/Fab1. *Gene,* **371,** 34-41.

Cai X, Xu Y, Cheung AK, Tomlinson RC, Alcazar-Roman A, Murphy L, Billich A, Zhang B, Feng Y, Klumpp M, Rondeau JM, Fazal AN, Wilson CJ, Myer V, Joberty G, Bouwmeester T, Labow MA, Finan PM, Porter JA, Ploegh HL, Baird D, De Camilli P, Tallarico JA & Huang Q. 2013. PIKfyve, a class III PI kinase, is the target of the small molecular IL-12/IL-23 inhibitor apilimod and a player in Toll-like receptor signaling. *Chemistry & biology,* **20,** 912-21.

Campeau PM, Lenk GM, Lu JT, Bae Y, Burrage L, Turnpenny P, Corona-Rivera JR, Morandi L, Mora M, Reutter H, Vulto-van Silfhout AT, Faivre L, Haan E, Gibbs RA, Meisler MH & Lee BH. 2013. Yunis-Varón syndrome is caused by mutations in FIG4 encoding a phosphoinositide phosphatase. *American Journal of Human Genetics,* **92,** 781-91.

Carlton J, Bujny M, Peter BJ, Oorschot VM, Rutherford A, Mellor H, Klumperman J, McMahon HT & Cullen PJ. 2004. Sorting nexin-1 mediates tubular endosome-to-TGN transport through coincidence sensing of high- curvature membranes and 3-phosphoinositides. *Curr Biol,* **14,** 1791-800.

Carlton JG, Bujny MV, Peter BJ, Oorschot VM, Rutherford A, Arkell RS, Klumperman J, McMahon HT & Cullen PJ. 2005. Sorting nexin-2 is associated with tubular elements of the early endosome, but is not essential for retromer-mediated endosome-to-TGN transport. *J Cell Sci,* **118,** 4527-39.

Carmel L, Efroni S, White PD, Aslakson E, Vollmer-Conna U & Rajeevan MS. 2006. Gene expression profile of empirically delineated classes of unexplained chronic fatigue. *Pharmacogenomics,* **7,** 375-386.

Carricaburu V, Lamia KA, Lo E, Favereaux L, Payrastre B, Cantley LC & Rameh LE. 2003. The phosphatidylinositol (PI)-5-phosphate 4-kinase type II enzyme controls insulin signaling by regulating PI-3,4,5-trisphosphate degradation. *Proceedings of the National Academy of Sciences of the United States of America,* **100,** 9867-72.

Chow CY, Landers JE, Bergren SK, Sapp PC, Grant AE, Jones JM, Everett L, Lenk GM, McKenna-Yasek DM, Weisman LS, Figlewicz D, Brown RH & Meisler MH. 2009. Deleterious variants of FIG4, a phosphoinositide phosphatase, in patients with ALS. *American journal of human genetics,* **84,** 85-8.

Chow CY, Zhang Y, Dowling JJ, Jin N, Adamska M, Shiga K, Szigeti K, Shy ME, Li J, Zhang X, Lupski JR, Weisman LS & Meisler MH. 2007. Mutation of FIG4 causes neurodegeneration in the pale tremor mouse and patients with CMT4J. *Nature,* **448,** 68-72.

Choudhury P, Srivastava S, Li Z, Ko K, Albaqumi M, Narayan K, Coetzee WA, Lemmon MA & Skolnik EY. 2006. Specificity of the myotubularin family of phosphatidylinositol-3-phosphatase is determined by the PH/GRAM domain. *J Biol Chem,* **281,** 31762-9.

Cooke FT, Dove SK, McEwen RK, Painter G, Holmes AB, Hall MN, Michell RH & Parker PJ. 1998. The stress-activated phosphatidylinositol 3-phosphate 5-kinase Fab1p is essential for vacuole function in S-cerevisiae. *Current Biology,* **8,** 1219-1222.

de Lartigue J, Polson H, Feldman M, Shokat K, Tooze SA, Urbe S & Clague MJ. 2009. PIKfyve regulation of endosome-linked pathways. *Traffic,* **10,** 883-93.

Dong XP, Shen D, Wang X, Dawson T, Li X, Zhang Q, Cheng X, Zhang Y, Weisman LS, Delling M & Xu H. 2010. PI(3,5)P(2) controls membrane trafficking by direct activation of mucolipin Ca(2+) release channels in the endolysosome. *Nature communications,* **1**.

Dove SK, Cooke FT, Douglas MR, Sayers LG, Parker PJ & Michell RH. 1997. Osmotic stress activates phosphatidylinositol-3,5-bisphosphate synthesis. *Nature,* **390,** 187-92.

Dove SK, Dong K, Kobayashi T, Williams FK & Michell RH. 2009. Phosphatidylinositol 3,5-bisphosphate and Fab1p/PlKfyve underPPIn endo-lysosome function. *Biochemical Journal,* **419,** 1-13.

Dove SK, McEwen RK, Mayes A, Hughes DC, Beggs JD & Michell RH. 2002. Vac14 controls PtdIns(3,5)P-2 synthesis and Fab1-dependent protein trafficking to the multivesicular body. *Current Biology,* **12,** 885-893.

Dove SK, Piper RC, McEwen RK, Yu JW, King MC, Hughes DC, Thuring J, Holmes AB, Cooke FT, Michell RH, Parker PJ & Lemmon MA. 2004. Svp1p defines a family of phosphatidylinositol 3,5-bisphosphate effectors. *Embo Journal,* **23,** 1922-1933.

Duex JE, Nau JJ, Kauffman EJ & Weisman LS. 2006a. Phosphoinositide 5-phosphatase Fig 4p is required for both acute rise and subsequent fall in stress-induced phosphatidylinositol 3,5-bisphosphate levels. *Eukaryotic cell,* **5,** 723-31.

Duex JE, Tang F & Weisman LS. 2006b. The Vac14p-Fig4p complex acts independently of Vac7p and couples PI3,5P2 synthesis and turnover. *The Journal of cell biology,* **172,** 693-704.

Efe JA, Botelho RJ & Emr SD. 2007. Atg18 regulates organelle morphology and Fab1 kinase activity independent of its membrane recruitment by phosphatidylinositol 3,5-bisphosphate. *Mol Biol Cell,* **18,** 4232-44.

Er EE, Mendoza MC, Mackey AM, Rameh LE & Blenis J. 2013. AKT Facilitates EGFR Trafficking and Degradation by Phosphorylating and Activating PIKfyve. *Science signaling,* **6,** ra45. 10.1126/scisignal.2004015.

Falkenburger BH, Jensen JB, Dickson EJ, Suh BC & Hille B. 2010. Phosphoinositides: lipid regulators of membrane proteins. *The Journal of physiology,* **588,** 3179-85.

Ferguson CJ, Lenk GM, Jones JM, Grant AE, Winters JJ, Dowling JJ, Giger RJ & Meisler MH. 2012. Neuronal expression of Fig4 is both necessary and sufficient to prevent spongiform neurodegeneration. *Human Molecular Genetics,* **21,** 3525-3534.

Ferguson CJ, Lenk GM & Meisler MH. 2009. Defective autophagy in neurons and astrocytes from mice deficient in PI(3,5)P2. *Hum Mol Genet,* **18,** 4868-78.

Gary JD, Sato TK, Stefan CJ, Bonangelino CJ, Weisman LS & Emr SD. 2002. Regulation of Fab1 phosphatidylinositol 3-phosphate 5-kinase pathway by Vac7 protein and Fig4, a polyphosphoinositide phosphatase family member. *Molecular biology of the cell,* **13,** 1238-51.

Gary JD, Wurmser AE, Bonangelino CJ, Weisman LS & Emr SD. 1998. Fab1p is essential for PtdIns(3)P 5-kinase activity and the maintenance of vacuolar size and membrane homeostasis. *The Journal of cell biology,* **143,** 65-79.

Guo JS, Ma YH, Yan Q, Wang L, Zeng YS, Wu JL & Li J. 2012. Fig4 Expression in the Rodent Nervous System and Its Potential Role in Preventing Abnormal Lysosomal Accumulation. *Journal of Neuropathology and Experimental Neurology,* **71,** 28-39.

Han BK & Emr SD. 2011. Phosphoinositide [PI(3,5)P2] lipid-dependent regulation of the general transcriptional regulator Tup1. *Genes Dev,* **25,** 984-95.

Hazeki K, Nigorikawa K, Takaba Y, Segawa T, Nukuda A, Masuda A, Ishikawa Y, Kubota K, Takasuga S & Hazeki O. 2012. Essential roles of PIKfyve and PTEN on phagosomal phosphatidylinositol 3-phosphate dynamics. *FEBS Lett,* **586,** 4010-4015.

Hirano T, Matsuzawa T, Takegawa K & Sato MH. 2011. Loss-of-Function and Gain-of-Function Mutations in FAB1A/B Impair Endomembrane Homeostasis, Conferring Pleiotropic Developmental Abnormalities in Arabidopsis. *Plant Physiology,* **155,** 797-807.

Hirano T & Sato MH. 2011. Arabidopsis FAB1A/B is possibly involved in the recycling of auxin transporters. *Plant Signal Behav,* **6,** 583-5.

Ho CY, Alghamdi TA & Botelho RJ. 2012. Phosphatidylinositol-3,5-bisphosphate: no longer the poor PIP2. *Traffic,* **13,** 1-8.

Ikonomov OC, Fligger J, Sbrissa D, Dondapati R, Mlak K, Deeb R & Shisheva A. 2009a. Kinesin Adapter JLP Links PIKfyve to Microtubule-based Endosome-to-Trans-Golgi Network Traffic of Furin. *Journal of Biological Chemistry,* **284,** 3750-3761.

Ikonomov OC, Sbrissa D, Delvecchio K, Feng HZ, Cartee GD, Jin JP & Shisheva A. 2013. Muscle-specific Pikfyve gene disruption causes glucose intolerance, insulin resistance, adiposity, and hyperinsulinemia but not muscle fiber-type switching. *American journal of physiology. Endocrinology and metabolism,* **305,** E119-31.

Ikonomov OC, Sbrissa D, Delvecchio K, Xie YF, Jin JP, Rappolee D & Shisheva A. 2011. The phosphoinositide kinase PIKfyve is vital in early embryonic development: preimplantation lethality of PIKfyve(-/-) embryos but normality of PIKfyve(+/-) mice. *Journal of Biological Chemistry,* **286,** 13404-13413. DOI

Ikonomov OC, Sbrissa D, Fenner H & Shisheva A. 2009b. PIKfyve-ArPIKfyve-Sac3 core complex: contact sites and their consequence for Sac3 phosphatase activity and endocytic membrane homeostasis. *The Journal of biological chemistry,* **284,** 35794-806.

Ikonomov OC, Sbrissa D, Fligger J, Delvecchio K & Shisheva A. 2010. ArPIKfyve regulates Sac3 protein abundance and turnover: disruption of the mechanism by Sac3I41T mutation causing Charcot-Marie-Tooth 4J disorder. *The Journal of biological chemistry,* **285,** 26760-4.

Ikonomov OC, Sbrissa D, Mlak K, Deeb R, Fligger J, Soans A, Finley RL & Shisheva A. 2003. Active PIKfyve associates with and promotes the membrane attachment of the late endosome-to-trans-Golgi network transport factor Rab9 effector p40. *Journal of Biological Chemistry,* **278,** 50863-50871.

Ikonomov OC, Sbrissa D & Shisheva A. 2001. Mammalian cell morphology and endocytic membrane homeostasis require enzymatically active phosphoinositide 6-kinase PIKfyve. *Journal of Biological Chemistry,* **276,** 26141-26147.

Ikonomov OC, Sbrissa D & Shisheva A. 2006. Localized PtdIns 3,5-P-2 synthesis to regulate early endosome dynamics and. *American Journal of Physiology-Cell Physiology,* **291,** C393-C404.

Ikonomov OC, Sbrissa D & Shisheva A. 2009c. YM201636, an inhibitor of retroviral budding and PIKfyve-catalyzed PtdIns(3,5)P-2 synthesis, halts glucose entry by insulin in adipocytes. *Biochemical and Biophysical Research Communications,* **382,** 566-570.

Jefferies HB, Cooke FT, Jat P, Boucheron C, Koizumi T, Hayakawa M, Kaizawa H, Ohishi T, Workman P, Waterfield MD & Parker PJ. 2008. A selective PIKfyve inhibitor blocks PtdIns(3,5)P(2) production and disrupts endomembrane transport and retroviral budding. *EMBO Rep,* **9,** 164-70.

Jeffries TR, Dove SK, Michell RH & Parker PJ. 2004. PtdIns-specific MPR pathway association of a novel WD40 repeat protein, WIPI49. *Molecular Biology of the Cell,* **15,** 2652-2663.

Jin N, Chow CY, Liu L, Zolov SN, Bronson R, Davisson M, Petersen JL, Zhang Y, Park S, Duex JE, Goldowitz D, Meisler MH & Weisman LS. 2008. VAC14 nucleates a protein complex essential for the acute interconversion of PI3P and PI(3,5)P(2) in yeast and mouse. *The EMBO journal,* **27,** 3221-34.

Jones DR, Foulger R, Keune WJ, Bultsma Y & Divecha N. 2012. PtdIns5P is an oxidative stress-induced second messenger that regulates PKB activation. *FASEB J,* **27,** 1644-1656.

Katoh Y, Ritter B, Gaffry T, Blondeau F, Honing S & McPherson PS. 2009. The clavesin family, neuron-specific lipid- and clathrin-binding Sec14 proteins regulating lysosomal morphology. *J Biol Chem,* **284,** 27646-54.

Katona I, Zhang X, Bai Y, Shy ME, Guo J, Yan Q, Hatfield J, Kupsky WJ & Li J. 2011. Distinct pathogenic processes between Fig4-deficient motor and sensory neurons. *Eur J Neurosci,* **33,** 1401-10.

Kerr MC, Wang JTH, Castro NA, Hamilton NA, Town L, Brown DL, Meunier FA, Brown NF, Stow JL & Teasdale RD. 2010. Inhibition of the PtdIns(5) kinase PIKfyve disrupts intracellular replication of Salmonella. *Embo Journal,* **29,** 1331-1347.

Kotoulas A, Kokotas H, Kopsidas K, Droutsas K, Grigoriadou M, Bajrami H, Schorderet DF & Petersen MB. 2011. novel PIKFYVE mutation in fleck corneal dystrophy. *Molecular Vision,* **17,** 2776-2781.

Krick R, Busse RA, Scacioc A, Stephan M, Janshoff A, Thumm M & Kuhnel K. 2012. Structural and functional characterization of the two phosphoinositide binding sites of PROPPINs, a beta-propeller protein family. *Proceedings of the National Academy of Sciences of the United States of America,* **109,** E2042-9.

Lemaire JF & McPherson PS. 2006. Binding of Vac14 to neuronal nitric oxide synthase: Characterisation of a new internal PDZ-recognition motif. *FEBS Lett,* **580,** 6948-54.

Lemmon MA. 2008. Membrane recognition by phospholipid-binding domains. *Nature reviews. Molecular cell biology,* **9,** 99-111.

Lenk GM, Ferguson CJ, Chow CY, Jin N, Jones JM, Grant AE, Zolov SN, Winters JJ, Giger RJ, Dowling JJ, Weisman LS & Meisler MH. 2011. Pathogenic mechanism of the FIG4 mutation responsible for Charcot-Marie-Tooth disease CMT4J. *PLoS genetics,* **7,** e1002104.

Li SL, Tiab L, Jiao XD, Munier FL, Zografos L, Frueh BE, Sergeev Y, Smith J, Rubin B, Meallet MA, Forster RK, Hejtmancik JF & Schorderet DF. 2005. Mutations in PIP5K3 are associated with Francois-Neetens Mouchetee fleck corneal dystrophy. *American Journal of Human Genetics,* **77,** 54-63.

Manford A, Xia TA, Saxena AK, Stefan C, Hu FH, Emr SD & Mao YX. 2010. Crystal structure of the yeast Sac1: implications for its phosphoinositide phosphatase function (vol 29, pg 1489, 2010). *EMBO J,* **29,** 1489-1498.

Martin S, Harper CB, May LM, Coulson EJ, Meunier FA & Osborne SL. 2013. Inhibition of PIKfyve by YM-201636 dysregulates autophagy and leads to apoptosis-independent neuronal cell death. *PLoS One,* **8,** e60152.

Martyn C & Li J. 2013. Fig4 deficiency: a newly emerged lysosomal storage disorder? *Progress in neurobiology,* **101-102,** 35-45.

McEwen RK, Dove SK, Cooke FT, Painter GF, Holmes AB, Shisheva A, Ohya Y, Parker PJ & Michell RH. 1999. Complementation analysis in PtdInsP kinase-deficient yeast mutants demonstrates that Schizosaccharomyces pombe and murine Fab1p homologues are phosphatidylinositol 3-phosphate 5-kinases. *Journal of Biological Chemistry,* **274,** 33905-33912.

Michell RH, Heath VL, Lemmon MA & Dove SK. 2006. Phosphatidylinositol 3,5-bisphosphate: metabolism and cellular functions. *Trends in biochemical sciences,* **31,** 52-63.

Morishita M, Morimoto F, Kitamura K, Koga T, Fukui Y, Maekawa H, Yamashita I & Shimoda C. 2002. Phosphatidylinositol 3-phosphate 5-kinase is required for the cellular response to nutritional starvation and mating pheromone signals in Schizosaccharomyces pombe. *Genes Cells,* **7,** 199-215.

Narayan K & Lemmon MA. 2006. Determining selectivity of phosphoinositide-binding domains. *Methods,* **39,** 122-33.

Nicot AS, Fares H, Payrastre B, Chisholm AD, Labouesse M & Laporte J. 2006. The phosphoinositide kinase PIKfyve/Fab1p regulates terminal lysosome maturation in Caenorhabditis elegans. *Molecular Biology of the Cell,* **17,** 3062-3074.

Norris FA, Auethavekiat V & Majerus PW. 1995. The isolation and characterization of cDNA encoding human and rat brain inositol polyphosphate 4-phosphatase. *J Biol Chem,* **270,** 16128-33.

Onishi M, Nakamura Y, Koga T, Takegawa K & Fukui Y. 2003. Isolation of suppressor mutants of phosphatidylinositol 3-phosphate 5-kinase deficient cells in Schizosaccharomyces pombe. *Bioscience, biotechnology, and biochemistry,* **67,** 1772-9.

Oppelt A, Lobert VH, Haglund K, Mackey AM, Rameh LE, Liestol K, Oliver Schink K, Marie Pedersen N, Wenzel EM, Haugsten EM, Brech A, Erik Rusten T, Stenmark H & Wesche J. 2013. Production of phosphatidylinositol 5-phosphate via PIKfyve and MTMR3 regulates cell migration. *EMBO reports,* **14,** 149-59.

Osborne SL, Wen PJ, Boucheron C, Nguyen HN, Hayakawa M, Kaizawa H, Parker PJ, Vitale N & Meunier FA. 2008. PIKfyve negatively regulates exocytosis in neurosecretory cells. *J Biol Chem,* **283,** 2804-13.

Proikas-Cezanne T, Ruckerbauer S, Stierhof YD, Berg C & Nordheim A. 2007. Human WIPI-1 puncta-formation: a novel assay to assess mammalian autophagy. *FEBS Lett,* **581,** 3396-404.

Rameh LE, Tolias KF, Duckworth BC & Cantley LC. 1997. A new pathway for synthesis of phosphatidylinositol-4,5-bisphosphate. *Nature,* **390,** 192-6.

Rudge SA, Anderson DM & Emr SD. 2004. Vacuole size control: Regulation of PtdIns(3,5)P-2 levels by the vacuole-associated Vac14-Fig4 complex, a PtdIns(3.5)P-2-specific phosphatase. *Molecular Biology of the Cell,* **15,** 24-36.

Rusten TE, Rodahl LMW, Pattni K, Englund C, Samakovlis C, Dove S, Brech A & Stenmark H. 2006. Fab1 phosphatidylinositol 3-phosphate 5-kinase controls trafficking but not silencing of endocytosed receptors. *Molecular Biology of the Cell,* **17,** 3989-4001.

Rusten TE, Vaccari T, Lindmo K, Rodahl LMW, Nezis IP, Sem-Jacobsen C, Wendler F, Vincent JP, Brech A, Bilder D & Stenmark H. 2007. ESCRTs and Fab1 regulate distinct steps of autophagy. *Current Biology,* **17,** 1817-1825.

Rutherford AC, Traer C, Wassmer T, Pattni K, Bujny MV, Carlton JG, Stenmark H & Cullen PJ. 2006. The mammalian phosphatidylinositol 3-phosphate 5-kinase (PIKfyve) regulates endosome-to-TGN retrograde transport. *J Cell Sci,* **119,** 3944-57.

Sbrissa D, Ikonomov OC, Fenner H & Shisheva A. 2008. ArPIKfyve homomeric and heteromeric interactions scaffold PIKfyve and Sac3 in a complex to promote PIKfyve activity and functionality. *Journal of molecular biology,* **384,** 766-79.

Sbrissa D, Ikonomov OC, Filios C, Delvecchio K & Shisheva A. 2012. Functional dissociation between PIKfyve-synthesized PtdIns5P and PtdIns(3,5)P-2 by means of the PIKfyve inhibitor YM201636. *American Journal of Physiology-Cell Physiology,* **303,** C436-C446.

Sbrissa D, Ikonomov OC, Fu ZY, Ijuin T, Gruenberg J, Takenawa T & Shisheva A. 2007. Core protein machinery for mammalian phosphatidylinositol 3,5-bisphosphate synthesis and turnover that regulates the progression of endosomal transport - Novel sac phosphatase joins the arpikfyve-pikfyve complex. *Journal of Biological Chemistry,* **282,** 23878-23891.

Sbrissa D, Ikonomov OC & Shisheva A. 2000. PIKfyve lipid kinase is a protein kinase: Downregulation of 5 '-phosphoinositide product formation by autophosphorylation. *Biochemistry,* **39,** 15980-15989.

Sbrissa D, Ikonomov OC, Strakova J, Dondapati R, Mlak K, Deeb R, Silver R & Shisheva A. 2004. A mammalian ortholog of Saccharomyces cerevisiae Vac14 that associates with and up-regulates PIKfyve phosphoinositide 5-kinase activity. *Mol Cell Biol,* **24,** 10437-47.

Schu PV, Takegawa K, Fry MJ, Stack JH, Waterfield MD & Emr SD. 1993. Phosphatidylinositol 3-kinase encoded by yeast VPS34 gene essential for protein sorting. *Science,* **260,** 88-91.

Seebohm G, Neumann S, Theiss C, Novkovic T, Hill EV, Tavare JM, Lang F, Hollmann M, Manahan-Vaughan D & Strutz-Seebohm N. 2012. Identification of a Novel Signaling Pathway and Its Relevance for GluA1 Recycling. *Plos One,* **7,** e33889.

Shen J, Yu W-M, Brotto M, Scherman JA, Guo C, Stoddard C, Nosek TM, Valdivia HH & Qu C-K. 2009. Deficiency of MIP/MTMR14 phosphatase induces a muscle disorder by disrupting Ca2+ homeostasis. *Nat Cell Biol,* **11,** 769-776.

Shisheva A. 2012. PIKfyve and its Lipid products in health and in sickness. *Current topics in microbiology and immunology,* **362,** 127-62.

Shisheva A, Rusin B, Ikonomov OC, DeMarco C & Sbrissa D. 2001. Localization and insulin-regulated relocation of phosphoinositide 5-kinase PIKfyve in 3T3-L1 adipocytes. *Journal of Biological Chemistry,* **276,** 11859-11869.

Silswal N, Parelkar NK, Wacker MJ, Brotto M & Andresen J. 2011. Phosphatidylinositol 3,5-bisphosphate increases intracellular free Ca2+ in arterial smooth muscle cells and elicits vasocontraction. *Am J Physiol Heart Circ Physiol,* **300,** H2016-26.

Takasuga S, Horie Y, Sasaki J, Ge-Hong Sun-Wada G, Kawamura N, Iizuka R, Mizuno K, Eguchi S, Kofuji S, Kiyotaka K, Yamazaki M, Kontani K, Harada A, Katada T, Suzuki A, Wada O, Ohnishi H & Sasaki T. 2013. Critical roles of type III phosphatidylinositol phosphate kinase in murine embryonic visceral endoderm and adult intestine. *Proceedings of the National Academy of Sciences of the United States of America,* **110,** 1726-1731.

Touchberry CD, Bales IK, Stone JK, Rohrberg TJ, Parelkar NK, Nguyen T, Fuentes O, Liu X, Qu CK, Andresen JJ, Valdivia HH, Brotto M & Wacker MJ. 2010. Phosphatidylinositol 3,5-bisphosphate (PI(3,5)P2) potentiates cardiac contractility via activation of the ryanodine receptor. *J Biol Chem,* **285,** 40312-21.

Tronchere H, Laporte J, Pendaries C, Chaussade C, Liaubet L, Pirola L, Mandel JL & Payrastre B. 2004. Production of phosphatidylinositol 5-phosphate by the phosphoinositide 3-phosphatase myotubularin in mammalian cells. *J Biol Chem,* **279,** 7304-12.

Tsuruta F, Green EM, Rousset M & Dolmetsch RE. 2009. PIKfyve regulates CaV1.2 degradation and prevents excitotoxic cell death. *J Cell Biol,* **187,** 279-94.

Vaccari I, Dina G, Tronchere H, Kaufman E, Chicanne G, Cerri F, Wrabetz L, Payrastre B, Quattrini A, Weisman LS, Meisler MH & Bolino A. 2011. Genetic interaction between MTMR2 and FIG4 phospholipid phosphatases involved in Charcot-Marie-Tooth neuropathies. *PLoS genetics,* **7**. 10.1371/journal.pgen.1002319.

van Gisbergen PA, Li M, Wu SZ & Bezanilla M. 2012. Class II formin targeting to the cell cortex by binding PI(3,5)P(2) is essential for polarized growth. *J Cell Biol,* **198,** 235-50.

Wang X, Zhang X, Dong XP, Samie M, Li X, Cheng X, Goschka A, Shen D, Zhou Y, Harlow J, Zhu MX, Clapham DE, Ren D & Xu H. 2012. TPC Proteins Are Phosphoinositide-Activated Sodium-Selective Ion Channels in Endosomes and Lysosomes. *Cell,* **151,** 372-83.

Watanabe Y, Kobayashi T, Yamamoto H, Hoshida H, Akada R, Inagaki F, Ohsumi Y & Noda NN. 2012. Structure-based analyses reveal distinct binding sites for Atg2 and phosphoinositides in Atg18. *The Journal of biological chemistry,* **287,** 31681-90.

Whiteford CC, Brearley CA & Ulug ET. 1997. Phosphatidylinositol 3,5-bisphosphate defines a novel PI 3-kinase pathway in resting mouse fibroblasts. *Biochem J,* **323 (Pt 3),** 597-601.

Whitley P, Hinz S & Doughty J. 2009. Arabidopsis FAB1/PIKfyve Proteins Are Essential for Development of Viable Pollen. *Plant Physiology,* **151,** 1812-1822.

Whitley P, Reaves BJ, Hashimoto M, Riley AM, Potter BV & Holman GD. 2003. Identification of mammalian Vps24p as an effector of phosphatidylinositol 3,5-bisphosphate-dependent endosome compartmentalization. *J Biol Chem,* **278,** 38786-95.

Winters JJ, Ferguson CJ, Lenk GM, Giger-Mateeva VI, Shrager P, Meisler MH & Giger RJ. 2011. Congenital CNS hypomyelination in the Fig4 null mouse is rescued by neuronal expression of the PI(3,5)P(2) phosphatase Fig4. *The Journal of neuroscience : the official journal of the Society for Neuroscience,* **31,** 17736-51.

Yamamoto A, Dewald DB, Boronenkov IV, Anderson RA, Emr SD & Koshland D. 1995. Novel Pi(4)P 5-Kinase Homolog, Fab1p, Essential for Normal Vacuole Function and Morphology in Yeast. *Molecular Biology of the Cell,* **6,** 525-539.

Yan Q, Guo J, Zhang X, Bai Y, Wang L & Li J. 2012. Trauma does not accelerate neuronal degeneration in Fig4 insufficient mice. *J Neurol Sci,* **312,** 102-7.

Zhou X, Wang L, Hasegawa H, Amin P, Han BX, Kaneko S, He Y & Wang F. 2010. Deletion of PIK3C3/Vps34 in sensory neurons causes rapid neurodegeneration by disrupting the endosomal but not the autophagic pathway. *Proceedings of the National Academy of Sciences of the United States of America,* **107,** 9424-9.

Zhang Y, McCartney AJ, Zolov SN, Ferguson CJ, Meisler MH, Sutton MA & Weisman LS. 2012. Modulation of synaptic function by VAC14, a protein that regulates the phosphoinositides PI(3,5)P(2) and PI(5)P. *EMBO J,* **31,** 3442-56.

Zhang Y, Zolov SN, Chow CY, Slutsky SG, Richardson SC, Piper RC, Yang B, Nau JJ, Westrick RJ, Morrison SJ, Meisler MH & Weisman LS. 2007. Loss of Vac14, a

regulator of the signaling lipid phosphatidylinositol 3,5-bisphosphate, results in neurodegeneration in mice. *Proceedings of the National Academy of Sciences of the United States of America,* **104,** 17518-23. DOI 10.1073/pnas.0702275104.Zieger M & Mayer A. 2012. Yeast vacuoles fragment in an asymmetrical two-phase process with distinct protein requirements. *Mol Biol Cell,* **23,** 3438-49.

Zolov SN, Bridges D, Zhang Y, Lee W-W, Riehle E, Verma R, Lenk GM, Converso-Baran K, Weide T, Albin RL, Saltiel AR, Meisler MH, Russell MW & Weisman LS. 2012. In vivo, Pikfyve generates PI(3,5)P2, which serves as both a signaling lipid and the major precursor for PI5P. *Proceedings of the National Academy of Sciences,* **109,** 17472-17477.

CHAPTER 2

MODULATION OF SYNAPTIC FUNCTION BY VAC14, A PROTEIN THAT REGULATES THE PHOSPHOINOSITIDES PI(3,5)P_2 AND PI(5)P

2.1 SUMMARY

[2]Normal steady state level of the signaling lipids PI(3,5)P_2 and PI(5)P requires the lipid kinase FAB1/PIKfyve and its regulators, VAC14 and FIG4. Mutations in the PIKfyve/VAC14/FIG4 pathway are associated with Charcot-Marie-Tooth syndrome and Amyotrophic Lateral Sclerosis in humans, and profound neurodegeneration in mice. Hence, tight regulation of this pathway is critical for neural function. Here, we examine the localization and physiological role of VAC14 in neurons. We report that endogenous VAC14 localizes to endocytic organelles in fibroblasts and neurons. Unexpectedly, VAC14 exhibits a pronounced synaptic localization in hippocampal neurons, suggesting a role in regulating synaptic function. Indeed, the amplitude of miniature excitatory postsynaptic currents is enhanced in both *Vac14*$^{-/-}$ and *Fig4*$^{-/-}$ neurons. Re-introduction of VAC14 in postsynaptic *Vac14*$^{-/-}$ cells reverses this effect. These changes in synaptic strength in *Vac14*$^{-/-}$ neurons are associated with enhanced surface levels of the AMPA-type glutamate receptor subunit GluA2, an effect that is due to diminished regulated

[2] This chapter was published as a research article: Zhang YL*, McCartney AJ*, Zolov SN, Ferguson CJ, Meisler MH, Sutton MA & Weisman LS. 2012. Modulation of synaptic function by VAC14, a protein that regulates the phosphoinositides PI(3,5)P2 and PI(5)P. *Embo Journal,* 31, 3442-3456. DOI 10.1038/emboj.2012.200.

endocytosis of AMPA receptors. Thus, VAC14, $PI(3,5)P_2$ and/or PI(5)P play a role in controlling postsynaptic function via regulation of endocytic cycling of AMPA receptors.

2.2 INTRODUCTION

Phosphorylated phosphoinositide lipids (PIs) reside on the cytoplasmic side of eukaryotic membranes and regulate a diverse array of cellular functions. The sn-3, 4 and 5 positions of the inositol head group have the potential to be phosphorylated in all seven combinations and each type of phosphoinositide plays unique roles in mammals. Each PI recruits a distinct set of protein effectors and regulates multiple cellular events including membrane traffic (Corvera et al., 1999, Roth, 2004), protein sorting (Saksena et al., 2007), growth factor signaling (Cantley, 2002), ion homeostasis (Balla, 2006, Dong et al., 2010), cell survival (Brunet et al., 2001) and cell motility (Yin and Janmey, 2003).

PI lipids are tightly regulated and inter-converted by an array of lipid kinases and phosphatases. A conserved protein complex including PIKfyve/FAB1/PIP5K3 (GenBank accession # NP_035216), VAC14 (NP_666328) and FIG4/SAC3 (NP_598760) is responsible for the biosynthesis and turnover of $PI(3,5)P_2$ (Jin et al., 2008, Ikonomov et al., 2009). PIKfyve is the PI(3)P 5-kinase that phosphorylates PI(3)P to form $PI(3,5)P_2$ (Gary et al., 1998), whereas FIG4 dephosphorylates $PI(3,5)P_2$ back to PI(3)P (Rudge et al., 2004, Duex et al., 2006a). The presence of both a kinase and a phosphatase in the same complex allows for tight regulation of $PI(3,5)P_2$ levels. VAC14, a HEAT repeat protein, forms a scaffold for formation of the complex and also brings in other regulatory factors (Jin et al., 2008). Loss of PIKfyve or VAC14 causes a loss of or decrease in $PI(3,5)P_2$ levels, respectively (Duex et al., 2006b, Zhang et al., 2007, Ikonomov et al., 2011). While

knockout of FIG4 might be predicted to increase PI(3,5)P_2, FIG4 also activates PIKfyve and thus, PI(3,5)P_2 is decreased in *Fig4*$^{-/-}$ fibroblasts (Chow et al., 2007) and yeast (Duex et al., 2006a). Interestingly, impairment of PIKfyve activity by either loss of VAC14 (Zhang et al., 2007) or pharmacological inhibition with YM201636 (Sbrissa et al., 2012) also causes a decrease in PI(5)P levels in mammals. Note that yeast *S. cerevisiae* does not produce PI(5)P. In mammals, the PI(5)P pool could come either from direct phosphorylation of phosphatidylinositol by PIKfyve (Sbrissa et al., 1999), or via dephosphorylation of PI(3,5)P_2 by myotubularin family phosphatases (Tronchère et al., 2004); both pathways are dependent on PIKfyve activity.

The PIKfyve/VAC14/FIG4 complex is critical for endomembrane homeostasis and has been implicated in an ever-growing list of processes. In yeast, PI(3,5)P_2 regulates vacuole fission, vacuole acidification (Bonangelino et al., 1997, Gary et al., 1998, Bonangelino et al., 2002), retrograde traffic from the vacuole (Bryant et al., 1998, Dove et al., 2004), and is involved in the assembly of transcriptional regulators (Han and Emr, 2011). In metazoans, the PIKfyve/VAC14/FIG4 pathway regulates endosome-to-trans-Golgi network retrograde transport (Rutherford et al., 2006), autophagy (Rusten et al., 2007, Ferguson et al., 2009, de Lartigue et al., 2009), exocytosis (Osborne et al., 2008), calcium channel activation (Shen et al., 2009, Dong et al., 2010) and degradation (Tsuruta et al., 2009). In plants, the PIKfyve/VAC14/FIG4 pathway is involved in endocytosis, vacuole formation, auxin transporter recycling, and pollen development (Hirano and Sato, 2011, Hirano et al., 2011). It remains to be determined which of the mammalian pathways are regulated by PI(3,5)P_2 and/or PI(5)P.

Analysis of several mouse mutants point to critical roles for the PIKfyve/VAC14/FIG4 pathway in the central and peripheral nervous systems. *Vac14* gene trap (*Vac14*$^{-/-}$) mice have half of the normal levels of PI(3,5)P_2 and PI(5)P. They develop normally, yet die perinatally with numerous neural defects including spongiform-like lesions and increased apoptosis in the brain, and intracellular vacuolation in peripheral neurons (Zhang et al., 2007, Chow et al., 2007, Jin et al., 2008, Ferguson et al., 2009, Lenk et al., 2011). *Fig4*$^{-/-}$ (Chow et al., 2007, Ferguson et al., 2009) and *Vac14*$^{L156R/L156R}$ (*ingls*) (Jin et al., 2008), mouse mutants defective in PI(3,5)P_2 and PI(5)P regulation, have similar patterns of neurodegeneration to that observed in the *Vac14*$^{-/-}$ mouse.

Importantly, human patients with minor defects in the PIKfyve/VAC14/FIG4 pathway also display severe neurological problems. Mutations in *FIG4* are responsible for human Charcot-Marie-Tooth disease type 4J (CMT4J), a recessive disorder affecting the peripheral nervous system (Chow et al., 2007, Nicholson et al., 2011). The most common CMT4J allele, I41T, destabilizes the mutant FIG4 protein and impairs its binding to VAC14 (Ikonomov et al., 2010, Lenk et al., 2011). Heterozygous *FIG4* mutations have also been identified in patients with amyotrophic lateral sclerosis (ALS) and primary lateral sclerosis (PLS), two forms of motor neuron disease (Chow et al., 2009). These observations suggest that the PIKfyve/VAC14/FIG4 pathway has specialized functions in the nervous system.

Defects in multiple neural cell types likely contribute to the pathologies observed in VAC14/FIG4 deficient mouse models. Both neurons (Zhang et al., 2007, Chow et al.,

2007, Zhang et al., 2008, Katona et al., 2011) and astrocytes (Jin et al., 2008, Ferguson et al., 2009) are affected by mutations in VAC14 or FIG4. However, expression of FIG4 in neurons, but not astrocytes, rescues the spongiform-like lesions, gliosis and early lethality in *Fig4*$^{-/-}$ mice (Ferguson et al., 2012), emphasizing the importance of the PIKfyve/VAC14/FIG4 pathway in neuronal function.

Neurons are highly polarized cells that process electrochemical signals by extending long specialized processes - axons and dendrites - to facilitate information transfer through neural circuits. Accordingly, the endosomal system in neurons has both general and specialized pathways, such as long-range trafficking along neurites (Ibáñez, 2007), as well as specialized recycling in both the pre- and postsynaptic terminals (Kennedy and Ehlers, 2006, Dittman and Ryan, 2009). These membrane events are critical for multiple aspects of neuronal function such as neurite outgrowth, neurotrophic factor signaling, and synaptic plasticity (Lasiecka and Winckler, 2011). However, the role of PIKfyve/VAC14/FIG4 in neuronal function remains unknown.

Here, we address the functional significance of PIKfyve/VAC14/FIG4 pathway in cultured neurons from the hippocampus of wild-type and *Vac14*$^{-/-}$ mice. To gain insight into the cellular distribution of PIKfyve/VAC14/FIG4 pathway, we developed an antibody to VAC14 suitable for immunofluorescence microscopy and found that endogenous VAC14 localizes to multiple organelles, consistent with multiple roles for PI(3,5)P_2 in the endomembrane system. VAC14 partially colocalizes with early endosomes, late endosomes, lysosomes and autophagosomes. In neurons, VAC14 is found in both somatodendritic regions and axons. Notably, a substantial amount of endogenous

VAC14 is present at synaptic sites, suggesting a potential role for VAC14 in the regulation of synaptic efficacy. Indeed, we find that synaptic function is altered in neurons cultured from *Vac14*$^{-/-}$ and *Fig4*$^{-/-}$ mice. Postsynaptic function and surface expression of AMPA-type glutamate receptors are both enhanced in *Vac14*$^{-/-}$ hippocampal neurons. Expression of VAC14 in *Vac14*$^{-/-}$ neurons reverses the synaptic phenotype, indicating a cell-autonomous and post-developmental role for VAC14 in regulating excitatory synaptic strength. We further show that the elevated surface AMPA receptor level in *Vac14*$^{-/-}$ neurons is due to decreased endocytosis at postsynaptic sites. Together, our results identify control of PI(3,5)P_2 and/or PI(5)P syntheses as a novel regulatory pathway at synapses that influences surface levels of glutamate receptors and synaptic function.

2.3 RESULTS

2.3.1 Vac14$^{-/-}$ hippocampal neurons exhibit vacuolation, but otherwise develop normally in culture

Consistent with its importance in the nervous system, expression of VAC14 is abundant in the brain relative to other tissues (Figure 2-1A-B). In this study, we sought molecular insights into the neuronal-specific functions of the PIKfyve/VAC14/FIG4 complex. We focused on hippocampal neurons because VAC14 expression in the hippocampus is similar to other brain regions (Figure 2- 1C) and the hippocampus is largely spared from neurodegeneration, even at the time of death in *Vac14*$^{-/-}$ and *Fig4*$^{-/-}$ animals (Chow et al., 2007, Zhang et al., 2007). Hippocampal neurons from *Vac14*$^{-/-}$

embryos remain viable for several weeks, which enabled us to examine the impact of *Vac14* deletion in these cells.

Although no spongiform lesions were observed in hippocampal regions *in vivo*, cultured *Vac14*$^{-/-}$ hippocampal neurons developed small vacuoles in the soma as early as 1 day *in vitro* (DIV) (Figure 2-2A). Similar to fibroblasts, the neuronal vacuoles are positive for the late endosome/lysosome marker LAMP1 and negative for the early endosome marker EEA1 (Figure 2-2B). Notably, at the neuron density used (2 x 10^4 per 1.91 cm^2), vacuoles are also observed in neurites by 12 DIV, suggesting that VAC14 functions in both the soma and neurites. Vacuole formation in *Vac14*$^{-/-}$ neurons appears to be activity-independent, as the degree of vacuolation in cells subject to activity blockade (1 µM TTX, 40 µM CNQX, 20 µM APV) from DIV3-DIV18 was similar to that in untreated neurons (Figure 2-2C).

The presence of vacuoles in neurons lacking VAC14 did not appear to affect axon and dendrite development in culture, as assessed using the five stage model (Dotti et al., 1988) (Figure 2-3A). *Vac14*$^{-/-}$ neurons progressed from stage I (lamellipodia) to stage IV/V (complicated networks) at a rate similar to wild-type neurons (Figure 2-3B), implying normal neurite outgrowth and differentiation.

2.3.2 Subcellular localization of VAC14 in cultured fibroblasts

To determine the sites of action of the PIKfyve/VAC14/FIG4 complex in neurons, we determined the localization of endogenous VAC14. Previous attempts to localize components of the PIKfyve complex in non-neuronal cells relied on overexpression of tagged proteins, and have produced divergent results. An earlier study indicated that

overexpressed, tagged PIKfyve is confined to late endosome/lysosome compartments (Ikonomov et al., 2001), whereas other analyses found tagged FAB1/PIKfyve primarily localized to early endosomes (Cabezas et al., 2006, Rutherford et al., 2006).

To better understand the endogenous cellular distribution of the PIKfyve/VAC14/FIG4 complex, we raised a rabbit polyclonal antibody against full length human VAC14 protein. After extensive affinity purification, we obtained a reagent that, in Western blot analysis, revealed a major band at the expected molecular weight (88 kD) in wild-type but not *Vac14*$^{-/-}$ brain (Figure 2-1A). In wild-type fibroblasts, permeabilized with saponin prior to fixation, VAC14 was present on punctate organelles distributed throughout the cytoplasm; these structures were absent from *Vac14*$^{-/-}$ fibroblast controls (Figure 2-4A). Nuclear staining was frequently observed in both wild-type and *Vac14*$^{-/-}$ cells (Figure 2-5A); thus, the antibody is not suitable to test whether VAC14 is also localized in the nucleus.

To determine the relative distribution of VAC14 on endosomal and lysosomal membranes, we performed triple labeling experiments in primary fibroblasts and determined the distribution of VAC14, EEA1 and LAMP1 (Figure 2-4B and Figure 2-5B, F). Consistent with earlier studies, EEA1 and LAMP1 labeled distinct compartments. The majority of VAC14 puncta colocalized with either EEA1 (20 ± 5%), LAMP1 (30 ± 5%), or both markers (19 ± 7%). These triple-labeled puncta likely represent intermediate endosomes. Thus, VAC14, PI(3,5)P_2, and potentially PI5P, are present in multiple locations within the endomembrane system, including early endosomes, late endosomes and lysosomes (Figure 2-6). Some VAC14 puncta (31 ± 8%) did not colocalize

with either EEA1 or LAMP1, suggesting that VAC14 may also function on other compartments.

LAMP1 is present on both late endosomes and lysosomes. To determine whether VAC14 is found on one or both of these compartments, we examined VAC14 localization relative to LBPA (late endosomes) or internalized dextran (lysosomes). Partial colocalization was observed between VAC14 (15 ± 6%) and LBPA (Figure 2-4C and Figure 2-5C, G), which indicates that some VAC14 resides on late endosomes. To determine whether lysosomes also contain VAC14, cells were incubated with a fluid phase marker, 70kD Texas Red-dextran, and then chased in the absence of dextran for twenty-four hours to allow it to reach lysosomes. Partial colocalization was observed between VAC14 (23 ± 9%) and lysosomes loaded with dextran (Figure 2-4D and Figure 2-5D, G), suggesting that some VAC14 is also localized on lysosomes. Interestingly, the limiting membrane of vacuoles in *Vac14*$^{-/-}$ fibroblasts is positive for LAMP1, but negative for LBPA (Figure 2-4E), implying that the large vacuoles derive solely from lysosomes.

In metazoans, the PIKfyve/VAC14/FIG4 pathway is thought to play a role in autophagy, either during fusion of autophagosomes with endosomes/lysosomes, or recycling of lysosomes from autolysosomes (Rusten et al., 2007, de Lartigue et al., 2009, Ferguson et al., 2009). LC3 is a common marker of autophagosomes. We transfected wild-type or *Vac14*$^{-/-}$ fibroblasts with LC3-RFP and colabeled transfected cells with anti-VAC14. VAC14 (17 ± 13%) partially colocalized with LC3 (Figure 2-4F and Figure 2-5E, G), suggesting that autophagosomes may contain PI(3,5)P_2 and/or PI(5)P. Alternatively,

these PI(3,5)P_2 and/or PI(5)P containing regions may represent the interface between autophagosomes and endosomes/lysosomes.

2.3.3 Localization of VAC14 in neurons

To determine the localization of VAC14 in neurons, we first examined its distribution in the soma. In this case, neurons were not permeabilized with saponin prior to fixation; thus, the images indicate both membrane bound and cytosolic pools of VAC14. A significant portion of the VAC14 localized to punctate structures (Figure 2-7). As in fibroblasts, VAC14 puncta colocalized with both the early endosome marker, EEA1 (Figure 2-7A), and with the late endosome/lysosome marker, LAMP2 (Figure 2-7B).

To test whether VAC14 is present in dendrites, hippocampal neurons were labeled with antibodies against VAC14 and against MAP2, a microtubule-associated protein that is highly expressed in dendrites but not axons. Notably, discrete VAC14 puncta were found in MAP2-positive dendrites (Figure 2-8A and Figure 2-9A). Moreover, another pool of VAC14 puncta was evident in MAP2-negative neurites, implying an axonal localization. To test this further, we labeled neurons with anti-VAC14 and anti-TAU-1, which preferentially labels axons in younger cultures (Horton et al., 2005). Again, VAC14 puncta were present in TAU-1 labeled axons (Figure 2-8A and Figure 2-9A), although this axonal VAC14 pool was less prominent than the dendritic pool. In neurites, VAC14 puncta partially co-localized with both EEA1 (23±12%) and LAMP1 (29±9%) (Figure 2-8B and Figure 2-9B-C), suggesting that VAC14 in neuronal processes functions in pathways that involve early and late endosomes as well as lysosomes.

2.3.4 Endogenous VAC14 localizes to synapses

Interestingly, the most striking colocalization was observed between VAC14 and synaptic markers. A substantial number of VAC14 puncta colocalized with the presynaptic terminal markers synapsin, synaptotagmin, and VAMP/synaptobrevin (Figure 2-8C and Figure 2-9D). To test whether VAC14 colocalizes with excitatory synapses, we performed triple labeling against VAC14, as well as vGlut1 (the glutamate transporter on presynaptic vesicles), and the postsynaptic scaffolding protein PSD95. VAC14 puncta colocalized extensively with vGlut1/PSD95 double-positive puncta (Figure 2-8D and Figure 2-9E), suggesting a role for VAC14 in excitatory synapse function.

2.3.5 Altered synaptic function in cultured Vac14$^{-/-}$ neurons

To examine a functional role for the PIKfyve/VAC14/FIG4 pathway at the synapse, we measured miniature excitatory postsynaptic currents (mEPSCs) in pyramidal-like neurons from *Vac14*$^{-/-}$ hippocampal cultures and corresponding wild-type controls. mEPSCs represent unitary synaptic currents mediated by the spontaneous fusion of single synaptic vesicles, and are often used to reveal functional changes in synaptic strength. Pyramidal neurons with little to no vacuolation were targeted for electrophysiology. Given the neurodegeneration observed in other regions of the brain at the time of birth, one might expect synaptic function to be diminished in *Vac14*$^{-/-}$ neurons. Surprisingly, mEPSCs from *Vac14*$^{-/-}$ neurons displayed a significant increase (24% ± 6%) in amplitude relative to wild-type mEPSCs (Figure 2-10A-B), suggesting an inhibitory role for VAC14 in synaptic function. We found no difference in mEPSC frequency or decay time in *Vac14*$^{-/-}$ mEPSCs (Figure 2-10C-E). In a parallel experiment,

we found mEPSC amplitude was similarly increased in *Fig4*$^{-/-}$ mice (Figure 2-10F-G), which also have reduced PIKfyve kinase activity. Together, these data suggest that the increase in mEPSC amplitude in both *Vac14*$^{-/-}$ and *Fig4*$^{-/-}$ neurons results from defects in the synthesis of PI(3,5)P_2 and/or PI(5)P.

Although we found no change in mEPSC frequency in either *Vac14*$^{-/-}$ (Figure 2-10C), or *Fig4*$^{-/-}$ neurons (Figure 2-10H), VAC14 is localized to axons (Figure 2-8A) and therefore is well positioned to contribute to presynaptic function. The enlargement of endocytic compartments in *Vac14*$^{-/-}$ cells (Zhang et al., 2007) also suggested that the increase in mEPSC amplitude in *Vac14*$^{-/-}$ neurons could have resulted from increased glutamate release by enlarged presynaptic vesicles (increased quantal content). To examine this possibility, we performed transmission electron microscopy on thin sections from the hippocampus and hindbrain of wild-type and *Vac14*$^{-/-}$ mice at P0. The hindbrain was used because it is the most vacuolated brain region in the *Vac14*$^{-/-}$ animal at the time of death. We found similar synaptic vesicle diameter in wild-type and *Vac14*$^{-/-}$ presynaptic terminals of both brain regions (Figure 2-11A-B).

Despite similar mEPSC frequency between *Vac14*$^{-/-}$ and wild-type neurons, we observed that the number of excitatory synapses in the first 100 µm of *Vac14*$^{-/-}$ dendrites was modestly but significantly decreased (Figure 2-11C-D). This discrepancy raised the possibility that although *Vac14*$^{-/-}$ neurons have fewer presynaptic inputs, the terminals may have elevated neurotransmitter release probability. To further examine presynaptic function, we measured the probability of synaptic vesicle release by recording postsynaptic NMDA-currents in the presence of the use-dependent NMDA

receptor antagonist, MK801 (Huettner and Bean, 1988). The degree of NMDA receptor blockade is proportional to the number of presynaptic vesicles that release glutamate in response to stimulation (Rosenmund et al., 1993). We found that *Vac14*$^{-/-}$ neurons showed greater blockade than wild-type neurons (Figure 2-11E-F) which suggests an enhancement of release probability in *Vac14*$^{-/-}$ neurons. Given that the frequency of mEPSCs was similar, the expected change in mEPSC frequency was likely masked by the decrease in synapse number. Together these results suggest that the PIKfyve/VAC14/FIG4 pathway modulates neurotransmitter release at the presynaptic terminal.

VAC14 levels are higher in dendrites than axons. To test whether increased mEPSC amplitude in *Vac14*$^{-/-}$ neurons is due to loss of VAC14 in the postsynaptic neuron, we transfected neurons with plasmids encoding Citrine-tagged human VAC14. For these experiments, we used calcium phosphate based transfection because the low transfection efficiency (~1% of cells) ensures that the few neurons that express VAC14 in *Vac14*$^{-/-}$ cultures received the excitatory synaptic contacts from neurons that lack VAC14. Thus, mEPSCs recorded from transfected neurons measure the effect of restoring VAC14 to the postsynaptic cell. We found VAC14 expression reversed the increase in mEPSC amplitude observed in *Vac14*$^{-/-}$ relative to wild-type neurons, whereas expression of Citrine alone did not (Figure 2-12). Moreover, even in wild-type neurons, overexpression of Citrine-VAC14 significantly depressed mEPSC amplitude relative to expression of untransfected neighbors, suggesting that synaptic strength is

bi-directionally regulated by the level of VAC14 in postsynaptic neurons. Together, these results strongly implicate VAC14 in the regulation of postsynaptic function.

2.3.6 Surface AMPA receptors are elevated in Vac14$^{-/-}$ neurons

Miniature EPSCs are dominated by currents through AMPARs localized on the postsynaptic membrane (Gong and De Camilli, 2008). Thus, the increase in mEPSC amplitude in *Vac14*$^{-/-}$ neurons could result from changes in the number of surface AMPA receptors. Under basal conditions, most AMPA receptors in the hippocampus are heterotetramers of the GluA2 and GluA1subunits (Lu et al., 2009). By Western blot, we found similar levels of total GluA2 between wild-type and *Vac14*$^{-/-}$ neurons (Figure 2-13). To test if the level of GluA2 at the cell surface was different, intact cultured neurons were incubated with an antibody against an extracellular epitope of GluA2 (Mouse IgG2a, MAB397, Chemicon), followed by fixation and incubation with a fluorescent secondary antibody under non-permeabilizing conditions. Surface GluA2 puncta were quantified using immunofluorescence microscopy (Figure 2-14A). In both wild-type and *Vac14*$^{-/-}$ neurons, there was a wide range in intensities of surface GluA2 puncta. However, in *Vac14*$^{-/-}$ neurons, the average and median surface GluA2 intensities were 34% and 17% higher, respectively, relative to wild-type neurons. The medians differed significantly with 95% confidence, indicated by the non-overlapping notches surrounding the medians in the box plot. Moreover, the cumulative distribution of surface GluA2 puncta intensities was right-shifted in *Vac14*$^{-/-}$ neurons (Figure 2-14B). These data indicate that surface GluA2 levels are increased in *Vac14*$^{-/-}$ neurons, which likely accounts for the increased amplitude of mEPSCs. In an independent approach, we

measured the ratio of surface to total GluA2 in dendrites. Surface GluA2 was labeled as described above. Then neurons were permeabilized and labeled with a C-terminal GluA2 antibody (Rabbit pAb, AB1768, Chemicon) to identify total GluA2. We found that the ratio of surface to total GluA2 was increased in *Vac14*$^{-/-}$ dendrites, relative to wild-type (Figure 2-14C-D). Together, these results suggest that GluA2 receptors are expressed in *Vac14*$^{-/-}$ neurons at a similar level, but accumulate on the surface.

2.3.7 Trafficking of AMPA receptors is altered in Vac14$^{-/-}$ neurons

GluA2 undergoes constant cycling between the surface and internal pools; once internalized, GluA2 may be either degraded in lysosomes or recycled back to the plasma membrane. Perturbations in endocytosis, recycling, or degradation could lead to an accumulation of surface receptors in *Vac14*$^{-/-}$ neurons. To measure the rate of endocytosis of AMPA receptors, we performed live-labeling of surface GluA2 with anti-GluA2 antibody and then stimulated endocytosis via addition of NMDA (Figure 2-15A). After 10 minutes, surface bound GluA2 antibodies were stripped by a brief wash in low pH solution, such that only internalized GluA2 antibodies were detected after fixation and permeablization. Leupeptin was present throughout to prevent lysosomal degradation. Notably, the number of internalized GluA2 puncta was decreased by 30% in dendrites in *Vac14*$^{-/-}$ neurons (Figure 2-15B, E). Total levels of internalized GluA2 puncta in the soma and dendrites were reduced to 71% and 56%, respectively, compared to wild-type (Figure 2-15C-D). These results are consistent with an endocytosis defect in *Vac14*$^{-/-}$ neurons.

To determine whether internalized GluA2 still enters the degradation pathway in *Vac14*$^{-/-}$ neurons, we further measured the proportion of internalized GluA2 puncta that colocalized with the late endosomal and lysosomal marker LAMP1 (Figure 2-16). Though fewer internalized GluA2 puncta were observed in *Vac14*$^{-/-}$neurons, a similar proportion exhibited colocalization with LAMP1 (27% in wild-type vs. 26% in *Vac14*$^{-/-}$). This suggests that the transport of AMPA receptors late in the endocytic pathway is normal in *Vac14*$^{-/-}$ neurons. In addition, we tested whether the reduction in internalized puncta was also due to enhanced recycling back to the surface. We transfected neurons at DIV12 with plasmids encoding super-ecliptic pHluroin tagged-GluA1(Kopec et al., 2006), which are strongly fluorescent when exposed to the neutral pH of the extracellular space. At DIV14, we measured the rate of internalization and recycling of pHluorin-GluA1 following NMDA stimulation (Figure 2-17). Five-minutes of NMDA stimulation markedly reduced the intensity of pHluorin-GluA1. Following wash-out, fluorescence recovered to baseline levels as internalized receptors recycled back to the plasma membrane (Figure 2-17A-D). The magnitude of NMDA-dependent internalization of GluA1 was diminished in *Vac14*$^{-/-}$ neurons (Figure 2-18E), again suggesting reduced receptor endocytosis in these neurons. To measure the rate of recycling, we calculated the time-point after NMDA stimulation at which fluorescence intensity recovered to 50% of the pre-NMDA baseline. Whereas GluA1 internalization was reduced in *Vac14*$^{-/-}$ neurons, we found no difference in the rate of recycling relative to wild-type (Figure 2-17F). These results suggest that the initial steps in AMPA receptor endocytosis, rather than postendocytic sorting, represent the most prominent trafficking defect accompanying loss of VAC14.

Together, our findings suggest that the PIKfyve/VAC14/FIG4 pathway regulates excitatory synapse function largely via modulation of AMPA receptor endocytosis (Figure 2-18).

2.4 DISCUSSION

2.4.1 VAC14 modulates synaptic activity in hippocampal neurons

VAC14 is present in neuronal dendrites and axons and exhibits extensive colocalization with synaptic markers. Thus, the PIKfyve/VAC14/FIG4 pathway likely impacts the synapse at multiple levels, including modulation of both presynaptic and postsynaptic function. Although here we focused on the postsynaptic VAC14, our results are also consistent with effects on presynaptic function. Thus, while mEPSC frequency is unaltered in *Vac14*$^{-/-}$ neurons, MK-801 use-dependent block of NMDA receptor currents is accelerated in these cells, suggesting elevated neurotransmitter release probability. Consistent with a presynaptic role for PI(3,5)P_2 and/or PI(5)P, an earlier report identified *C. elegans* FIG4 at presynaptic sites in a large scale RNAi screen (Sieburth et al., 2005). An increase in probability of presynaptic vesicle fusion with the plasma membrane fits with a previous study demonstrating enhanced granule exocytosis following knock-down of PIKfyve in cultured chromaffin and PC12 cells (Osborne et al., 2008). This pathway may be interacting directly with exocytic machinery. Alternatively, it is possible that voltage-gated calcium channels or other membrane proteins that are important for membrane excitability are more highly expressed on the surface of *Vac14*$^{-/-}$ neurons which causes increased calcium influx in response to depolarization.

The presence of VAC14, and its lipid products, in the postsynaptic terminal is consistent with earlier findings that VAC14 interacts with nNOS (Lemaire and McPherson, 2006), which interacts with the postsynaptic scaffolding protein PSD95 (Tochio et al., 2000). In addition, MTMR2, a phosphatase that acts on $PI(3,5)P_2$ *in vitro* and likely *in vivo,* also interacts with PSD95 (Lee et al., 2010). Since VAC14 levels in the somatodendritic region are significantly higher than in axons, it is likely that the PIKfyve/VAC14/FIG4 pathway controls critical aspects of postsynaptic function. Indeed, we found that genetic deletion of VAC14 is accompanied by enhanced mEPSC amplitude. Importantly, postsynaptic expression of VAC14 rescues this defect, strongly suggesting that postsynaptic loss of VAC14 is responsible for the enhanced mEPSC amplitude. Moreover, *Fig4*$^{-/-}$ neurons exhibited a similar increase in mEPSC amplitude, strengthening the argument that PIKfyve/VAC14/FIG4 pathway, and their lipid products $PI(3,5)P_2$ and/or PI(5)P, play a role in postsynaptic function.

2.4.2 AMPA receptor trafficking in Vac14$^{-/-}$ neurons

Our results further indicate that VAC14 regulates postsynaptic function through regulation of AMPA receptor trafficking. Surface levels of AMPA receptors are tightly controlled by trafficking to and from the cell interior. Consistent with increased mEPSC amplitude, steady-state levels of surface exposed AMPA receptors are elevated in *Vac14*$^{-/-}$ neurons. Using two independent methods, we found that AMPA receptor internalization following NMDA receptor activation is defective in *Vac14*$^{-/-}$ neurons. The total levels of regulated endocytosed AMPA receptors, quantified from internalized GluA2 puncta or amplitude of change in pHluorin-GluA1 fluorescence, are reduced in

Vac14$^{-/-}$ neurons, which likely accounts for the elevated surface AMPA receptor levels. This endocytosis defect is consistent with the finding that internalization of transfected GluA2 is reduced in cortical neurons after siRNA knockdown of PIKfyve (Tsuruta et al., 2009). Conversely, MTMR2 knockdown, which is predicted to increase PI(3,5)P_2 levels, enhances AMPA receptor endocytosis (Lee et al., 2010). Together, these findings suggest a new role for PI(3,5)P_2 and/or PI(5)P, and downstream effector(s), early in the endocytic pathway. Though general endocytosis could be regulated by these signaling lipids, Tsuruta et al. found that the internalization of Cav1.2, but not Kv1.2, was affected by PIKfyve knockdown (Tsuruta et al., 2009); thus the PIKfyve/VAC14/FIG4 pathway may play a more selective role in endocytosis of particular membrane proteins.

While VAC14 is localized throughout the endocytic pathway, we found that the recycling and degradative trafficking of AMPA receptors are normal in *Vac14*$^{-/-}$ neurons. Similarly, EGF receptors traffic normally to lysosomes in *Vac14*$^{-/-}$ fibroblasts (Zhang et al., 2007), and EGF receptor trafficking is also unaffected by siRNA knockdown of PIKfyve (Rutherford et al., 2006), or overexpression of a dominant-negative mutant PIKfyve (Ikonomov et al., 2003), although EGF receptor degradation is slowed when a PIKfyve inhibitor is used (de Lartigue et al., 2009). Importantly, since *Vac14*$^{-/-}$ cells have half of the normal levels of PI(3,5)P_2 and PI(5)P, it remains possible that different trafficking steps have distinct sensitivities to the extent of loss of PI(3,5)P_2 and/or PI(5)P. Future work is needed to determine if AMPA receptor trafficking late in the endocytic pathway are affected if the PIKfyve/VAC14/FIG4 pathway is inhibited further.

2.4.3 Potential roles of VAC14 in learning and memory

AMPA receptor expression at synapses is regulated to modify synaptic efficacy in the context of long-term potentiation (LTP) and long-term depression (LTD) (Song and Huganir, 2002), as well as homeostatic control of synaptic function driven by persistent changes in neuronal activity (Turrigiano, 2008). Rab5, which likely acts in pathways that are also regulated by PIKfyve (Jefferies et al., 2008), is similarly involved in postsynaptic glutamate receptor trafficking and is required for LTD (Brown et al., 2005), raising the possibility that dynamic control of $PI(3,5)P_2$ and/or PI(5)P synthesis contributes to these forms of synaptic plasticity as well. It is now of interest to assess whether, in addition to the more severe neurophysiological outcomes that accompany PIKfyve/VAC14/FIG4-deficiency, perturbations of the $PI(3,5)P_2$ and/or PI(5)P-related signaling pathways underlie defects in learning and memory. The *Fig4-I41T* Tg705 transgenic line which survives to 3 months of age with a reduced extent of spongiform degeneration could be useful for this purpose (Lenk et al., 2011).

2.4.4 Excitotoxicity in $Vac14^{-/-}$ neurons

Excitotoxicity has been implicated in many acute and chronic neurological disease such as stroke (Rothman and Olney, 1986) and ALS (Rothstein et al., 1992, Beal, 1992, Martin, 2010). The increased synaptic efficacy in cultured *Vac14*$^{-/-}$ neurons also raises the question of whether excitotoxicity contributes to the neurodegeneration phenotypes observed in VAC14/FIG4 deficient mouse models. Consistent with this idea, PIKfyve overexpression has been shown to protect cultured neurons against excitotoxicity (Tsuruta et al., 2009). In this case, it was postulated that an increase in

PIKfyve activity led to down-regulation of voltage-gated calcium channels and of GluA2, and possibly other as yet undetermined channels and transporters.

2.4.5 Endogenous VAC14 localizes to multiple compartments in the endomembrane system

A common view in recently published reviews is that PI(3,5)P_2 is confined to late endosomes, and has little overlap with its precursor, PI(3)P, which is viewed as a phosphoinositide lipid confined to early endosomes. However, in fibroblasts, using an antibody to endogenous VAC14, we found that VAC14 was equally distributed between early and late endosomes as well as lysosomes, with some localization to autophagosomes. Assuming that the location of VAC14 on membranes reflects the distribution of PI(3,5)P_2 and/or PI(5)P, we predict that these lipids may regulate pathways that emanate from each of these organelles. VAC14 also localizes to punctate spots that contain neither EEA1 nor LAMP1, which suggests that there are as yet undetermined organelles that contain PI(3,5)P_2 and PI(5)P. We also found that AMPA receptor internalization and evoked presynaptic vesicle release are altered in the absence of VAC14, which suggest novel roles for PIKfyve/VAC14/FIG4, or their downstream effectors, near the plasma membrane. At present, it remains to be determined whether these are specific to neurons or particular neuronal compartments.

In summary, this chapter describes a critical new role for VAC14 and, by implication, PI(3,5)P_2 and/or PI(5)P in regulating synaptic function in neurons. Future work will elucidate specific molecular pathways controlled by PI(3,5)P_2 and/or PI(5)P and may provide insights into the treatment of human neuropathies that can be mitigated

via regulation of these lipids. Thus development of drugs designed to modulate the levels of these lipids might lead to new therapies for several types of neurological disorders where the PIKfyve/VAC14/FIG4 pathway is altered.

2.5 EXPERIMENTAL PROCEEDURES

2.5.1 Ethics Statement

All animal use was performed in compliance with guidelines of the University Committee on Use and Care of Animals of the University of Michigan and National Institutes of Health.

2.5.2 Electrophysiology

Whole-cell patch clamp recordings were performed with an Axopatch 200B amplifier from 13-15 DIV cultured hippocampal pyramidal-like neurons bathed in an extracellular solution containing 119 mM NaCl, 5 mM KCl, 2 mM $CaCl_2$, 2 mM $MgCl_2$, 30 mM glucose, 10 mM HEPES (pH 7.4) plus 1 µM TTX and 10 µM bicuculline to isolate glutamatergic mEPSCs. Internal pipette solution contained 100 mM cesium gluconate, 0.2 mM EGTA, 5 mM $MgCl_2$, 40 mM HEPES, 2 mM Mg-ATP, 0.3 mM Li-GTP, 1 mM QX-314 (pH 7.2). Pipette resistance ranged from 3-5 MΩ. Neurons with a pyramidal-like morphology were targeted for analysis. For *Vac14*$^{-/-}$ neurons, pyramidal-like neurons with few to no vacuoles were targeted for analysis. Neurons were voltage clamped at -70 mV, and series resistance was not compensated. mEPSC amplitude and frequency were analyzed offline using Minianalysis (Synaptosoft). Average traces and statistical analysis was performed in Matlab (Mathworks). Statistical differences between control and experimental conditions were determined by ANOVA and Tukey-Kramer test.

In order to measure probability of evoked synaptic vesicle release in presynaptic terminals forming synapses onto wild-type or *Vac14*$^{-/-}$ neurons, a low transfection strategy (Cal Phos kit, Clonetech) was used to limit expression to a small fraction of the cells. Twenty-four hours after transfection, warm (37°C), 0 Mg^{2+} solution was applied to the bath: 125 mM NaCl, 2.5 mM KCl, 5 mM HEPES, 2 mM Ca-Cl_2, 33 mM D-Glucose, pH 7.4). AMPA receptor antagonist, CNQX (20 µM), and $GABA_A$ receptor antagonist, Bicuculline (10 µM), were included to isolate NMDA receptor currents. Neurons were voltage-clamped at -70 mV and evoked excitatory postsynaptic currents were measured by positioning a stimulating electrode close to the neuron. Once a stable response was obtained, MK801 (20 µM), a use dependent antagonist for NMDA receptors, was applied to the bath for 5 minutes without stimulation. Following wash-in, 200 stimulations at 0.33 Hz were delivered in the presence of MK801. The peak of the NMDA receptor current was measured for each and normalized to the first response following MK801 wash in.

2.5.3 Endocytosis assay

Neurons were treated with 20 µM leupeptin for 30 minutes before live labeling with mouse GluA2 antibodies diluted in normal medium with leupeptin for 15 minutes. After washing with neurobasal medium, neurons were incubated in normal medium supplemented with 50 µM NMDA and 20 µM leupeptin for 10 minutes. Endocytosis was stopped by washing in cold 1x PBS with 0.1 mM $CaCl_2$ and 1 mM $MgCl_2$. Surface bound GluA2 antibodies were stripped with 0.5M NaCl/0.2M Acetic acid for 4 minutes on ice. Neurons were fixed in 2% paraformaldehyde and 2% sucrose for 15 minutes and

permeabilized with 0.1% Triton X-100 for 5 minutes. After blocking with 2% BSA, neurons were incubated with Alexa 555 anti-mouse secondary antibody for 1 hour.

To examine the degradation pathway, neurons were incubated with rat anti-Lamp1 antibodies and then Alexa 488 anti-rat and Alexa 555 anti-mouse secondary antibodies.

2.5.4 Endocytosis and recycling assay

Neurons were transfected at DIV12 by Calcium Phosphate and pHluorin-GluA1 endocytosis and recycling live-imaging assays were performed 36-48 hours post-transfection. Mattek dishes were placed on the stage of the confocal microscope and perfused with normal extracellular buffer (25 mM HEPES, 120 mM NaCl, 5 mM KCl, 2 mM$CaCl_2$, 2 mM $MgCl_2$, 30 mM D-glucose, 1 µM TTX, pH 7.4). Images were acquired once per minute for (I) a 10 minute baseline, (II) after the bath was switched to NMDA stimulation buffer (25 mM HEPES, 120 mM NaCl2, 5 mM KCl, 2 mM $CaCl_2$, 0.2 mM $MgCl_2$, 30 mM D-glucose, 1 µM TTX, 20 µM NMDA, 10 µM glycine, pH 7.4) for 5 minutes to stimulate internalization, and (III), then following washout of the NMDA stimulation buffer to monitor recycling back to the cell surface. The pHluorin fluorescence was imaged at 488 nm excitation, while mCherry fluorescence was imaged at 559 nm excitation, through a 60X oil objective at a rate of 1 image per minute. Images were analyzed using ImageJ software (NIH) by straightening the primary dendrite of the neuron, starting from the soma, and calculating the fluorescence intensity relative to the average intensity of the baseline period. The degree of GluA1 endocytosis was determined by analyzing the first 1-3 mins after NMDA stimulation (max decrease in

signal) and the rate of GluA1 recycling was determined by fitting a linear curve to the time after max internalization and calculating the time-point at which 50% of fluorescence recovered. pHluorin-GluA1 was a gift of Roberto Malinow (Addgene plasmid #24000).

2.5.5 Antibodies

To generate polyclonal rabbit VAC14 antibody, full length human *VAC14* cDNA was cloned into pMALc2H$_{10}$T (Kristelly et al., 2004). Recombinant MBP-10x His tagged VAC14 protein was purified from E. coli (Rosetta) using Ni-NTA agarose (Qiagen, 30210). The MBP-10x His tag was cleaved with AcTEV proteases (Invitrogen, 12575-015) and the tag removed via Ni-NTA agarose. 0.1% Triton X-100 was added to stabilize VAC14. Purified protein was injected into a rabbit. Serum was affinity purified by enrichment of the IgG fractions with protein A Sepharose-4B (Sigma, P9424). Nonspecific IgGs were depleted on a total *Vac14*$^{-/-}$ column made from Actigel resin (Sterogene Bioseparations Inc., 2731). VAC14 specific IgGs were purified on an affinity column with VAC14 protein conjugated to Actigel. Antibodies were eluted with a decreasing pH gradient: 0.1 M citrate (pH5.0, 4.5, 4.0, 3.5, 3.0) and 0.2 M glycine (pH 2.8). Eluted fractions were analyzed by western blot and pooled. The best fractions were eluted at pH 3.0.

Chicken anti-EEA1 was a gift from Dr. Silvia Corvera (University of Massachusetts Medical School, Worcester, MA). Commercial antibodies: GAPDH antibody (Ambion, AM4300); surface GluA2 antibody (Chemicon, MAB397); C-terminal GluA2 antibody (Rabbit pAb, AB1768, Chemicon); LAMP-1 antibody (University of Iowa Hybridoma Bank, 1D4B); LAMP-2 antibody (University of Iowa Hybridoma Bank, ABL-93); LBPA antibody

(Echelon Biosciences, Z-SLBPA); MAP2 antibodies (Santa Cruz, sc-32791, Millipore, AB5622, Sigma-Aldrich, M4403); PSD95 antibody (Thermoscientific, MA1-045); synapsin antibody (Synaptic Systems, 106004), synaptobrevin antibody (Calbiochem, NB07); synaptotagmin antibody (Calbiochem, 573824); TAU-1 antibody (Chemicon, MAB3420); vGlut1 antibody (Millipore, AB5905). All secondary antibodies are from Molecular Probes (Invitrogen, Carlsbad, CA).

2.5.6 Cell culture

Hippocampal neurons were cultured from E14-18 embryos from matings between *Vac14*$^{+/-}$ and *Vac14*$^{+/-}$ mice (C57BL/6J □ 129/Ola mixed background). Culture medium included neurobasal medium (Invitrogen, 10888022), 1x B27 supplement (Invitrogen, 17504-044), 2 mM L-glutamine (Invitrogen, 25030-081) and 1x antibiotics/antimycotics (Invitrogen, 15240-062). Hippocampi were dissected and digested in 0.25% trypsin (Invitrogen, 25200) for 15 minutes; the reaction was stopped with 0.5 mg/ml soybean trypsin inhibitor (Invitrogen, 17075-029) in PBS. Tissues were triturated in culture medium ~10-15 times. Cells were counted and plated on poly-D-lysine (Sigma P0899) coated coverslips or Mattek dishes (Mattek Corporation, P35G-0-14-C). For experiments requiring distinct single cells, 5, 000 – 20, 000 cells were seeded per 12 mm coverslip (Fisher Scientific, 12-545-82). For electrophysiology experiments, 65 000 cells were seeded per Mattek dish. Media were changed every two days until day 10.

Mouse primary fibroblasts were cultured from P0 pups from matings between *Vac14*$^{+/-}$ and *Vac14*$^{+/-}$ mice as described (Zhang et al., 2007).

2.5.7 Immunofluorescence microscopy

A large fraction of VAC14 protein is cytosolic in mammalian cells. To localize membrane bound VAC14, mouse fibroblasts were treated with 0.05% saponin for 1 minute before fixation. Localization of proteins in neurons was performed without this step. Unless noted elsewhere, cells were fixed in 4% paraformaldehyde for 15 minutes. Cells were blocked in filtered 2% goat serum/2% donkey serum/5% BSA/PBS/0.1% saponin for 1 hour, incubated with primary and then secondary antibodies for 1 hour each and mounted with Prolong Gold Antifade reagent (Invitrogen, P36930). *Vac14*$^{-/-}$ fibroblasts or neurons were used as negative controls in all immunofluorescence experiments using anti-VAC14 antibody. Images were taken on an inverted Olympus FV1000 laser scanning confocal microscope or a Zeiss 510 laser scanning confocal microscope.

For PSD95 experiments, neurons were fixed with 2% paraformaldehyde/2% sucrose for 15 minutes and permeabilized with 0.1% Triton X-100 for 10 minutes.

To label surface GluA2, mouse GluA2 antibody (IgG2a) was diluted and applied onto live neurons for 15 minutes. Neurons were washed with cold PBS containing 1 mM $MgCl_2$ and 0.1 mM $CaCl_2$, fixed in 4% paraformaldehyde/4% sucrose, blocked with 2% BSA for 20 minutes and incubated with fluorescent antibody (Goat α M-488). Quantitation of GluA2 puncta was done in IMAGE J. Dendrites were straightened and intensity of individual puncta analyzed using modified IMAGEJ particle analysis macros. All intensities are normalized to the mean of the wild-type. To label total GluA2 and Map2, following surface GluA2 labeling, neurons were permeabilized with 0.1% TritonX-

100 and incubated with rabbit GluA2 and MAP2 (IgG1, Sigma-Aldrich) antibodies for 1 hour at room temperature, and then incubated with appropriate fluorescent secondary antibodies (Goat α IgG2a-488, Goat α IgG_1-555, Goat α Rabbit-647).

To label lysosomes, mouse primary fibroblasts were incubated with 1 mg/ml Texas red Dextran (Invitrogen D1864, Mw 70, 000) for 1 hour and chased in normal medium for 24 hours before fixation.

2.5.8 Western blot analysis

Tissues or brain regions were dissected from P0 pups and homogenized in RIPA buffer (50 mM Tris, pH 7.4; 150 mM NaCl; 1 mM EDTA; 1% deoxycholic acid; 1% NP-40; 0.1% SDS; 10 mM NaF; 1 mM Na_3VO4; 1x protease inhibitor cocktail (Sigma P8215)). Protein concentrations were determined by BCA assay (Thermoscientific 23228). Equal amount of total protein (15 µg) were separated by SDS-PAGE, transferred to nitrocellulose membrane and blotted with anti-VAC14 (1:2000) or anti-GAPDH (1: 300, 000). Quantitation was done with IMAGE J's Gel Analyzer function. All lanes are normalized to the first lane.

2.5.9 Transfection

Neurons were transfected with 0.5-1 µg *Citrine* or *VAC14-Citrine* plasmid (Zhang et al., 2007) with the CalPhos Transfection kit (CloneTech; Mountain View, CA). Experiments were performed 24-48 hours after transfection.

2.5.10 Electron microscopy

Brain tissue from P0 pups was fixed in 2.5 % glutaraldehyde in 0.1 M Sorensen's buffer for one hour and post-fixed for one hour in 1% osmium tetroxide in the same buffer. Samples were rinsed in double distilled water to remove phosphate and then en bloc stained with aqueous 3% uranyl acetate for one hour. Samples were dehydrated in ascending concentrations of ethanol, treated with propylene oxide, and embedded in Epon epoxy resin. Semi-thin sections were stained with toluidine blue for tissue identification. Ultra-thin sections (70 nm) of the mid and hind brain were post stained with uranyl acetate and lead citrate. Samples were examined with a Philips CM100 electron microscope at 60 KV, images were captured with a Hamamatsu ORCA-HR digital camera system, and AMT software (Advanced Microscopy Techniques Corp., Danvers, MA).

2.5.11 Image Quantitation

To quantify VAC14 colocalization with various endocytic and autophagic markers, Puncta Analyzer plugin (gift from Dr. Cagla Eroglu) (Ippolito and Eroglu, 2010) for ImageJ was used. This plugin identifies and counts the numbers of green (VAC14) and red (EEA1, LAMP1, LBPA or LC3) puncta at user-defined thresholds and calculates the number of colocalizing puncta. It also labels colocalized puncta after the analysis so that the result can be validated. Before processing, the nonspecific nuclear staining in the VAC14 channel, if present, was removed. Rolling ball radius method was used to subtract the background. In the VAC14/EEA1/LAMP1 triple labeling experiment, due to the presence of triple-labeled puncta, more calculations were performed as follows.

After the routine analysis where the number of VAC14 that colocalized with EEA1 (N_{EEA1}) and LAMP1($N_{LAMP1)}$ are measured, thresholded LAMP1 and EEA1 channels were mathematically added to create one single channel. This way, the number of VAC14 puncta that colocalized with either EEA1 or LAMP1 (N_e) could be measured. The number of VAC14 puncta that colocalized with neither marker (N_n) was calculated by: N_n = total VAC14 – N_e. The number of VAC14 puncta that colocalized with both LAMP1 and EEA1 (N_b) was calculated by: $Nb = N_{EEA1} + N_{LAMP1} – N_e$. The number of VAC14 puncta that colocalized with only EEA1 was calculated by: $N_{EEA1}' = N_{EEA1} – N_b$. The number of VAC14 puncta that colocalized with only LAMP1 was calculated by: $N_{LAMP1}' = N_{LAMP1} – N_b$.

To quantify surface GluA2 puncta with ImageJ, a user written macro was used. Dendrites were straightened with ImageJ's Straighten plugin. Straightened dendrite images were made binary with user-defined threshold and then treated with the watershed filter. Puncta were identified by IMAGEJ's "analyze particles..." command. The integrated intensity values were calculated from the original pixels that lie within each punctate region. This macro is available upon request.

To quantify total internalized GluA2, region of interests (soma or dendrites) were measured directly with ImageJ. Soma were defined with freehand selections. Apical dendrites were straightened and a fixed length (35 µm) was used. Area and integrated intensity were measured with IMAGEJ. Intensity values were normalized to the area.

2.6 ACKNOWLEDGMENTS

We thank Dr. Silvia Corvera for the EEA1 antibody, Dr. John Tesmer for the pMALc2H_{10}T vector, Dr. Roberto Malinow and Addgene for the pHlorin-GluA1 plasmid,

Dr. Zhaohui Xu for the Rosetta strain, Cynthia J.L. Carruthers for conditioned media, Amanda S. Perez for help with IMAGE J, Dotty Sorenson for assistance with the EM. We thank the Microscopy Image Analysis Laboratory for technical assistance. This work was supported by NIH grants R01-NS064015 to LSW, RO1-MH085798 to MAS and R01-GM24872 to MHM. AJM was supported in part by NRSA F31NS074740-01. This work utilized the Microscopy Image Analysis Laboratory of the Michigan Diabetes Research and Training Center funded by K020572 from the National Institute of Diabetes and Digestive and Kidney Diseases.

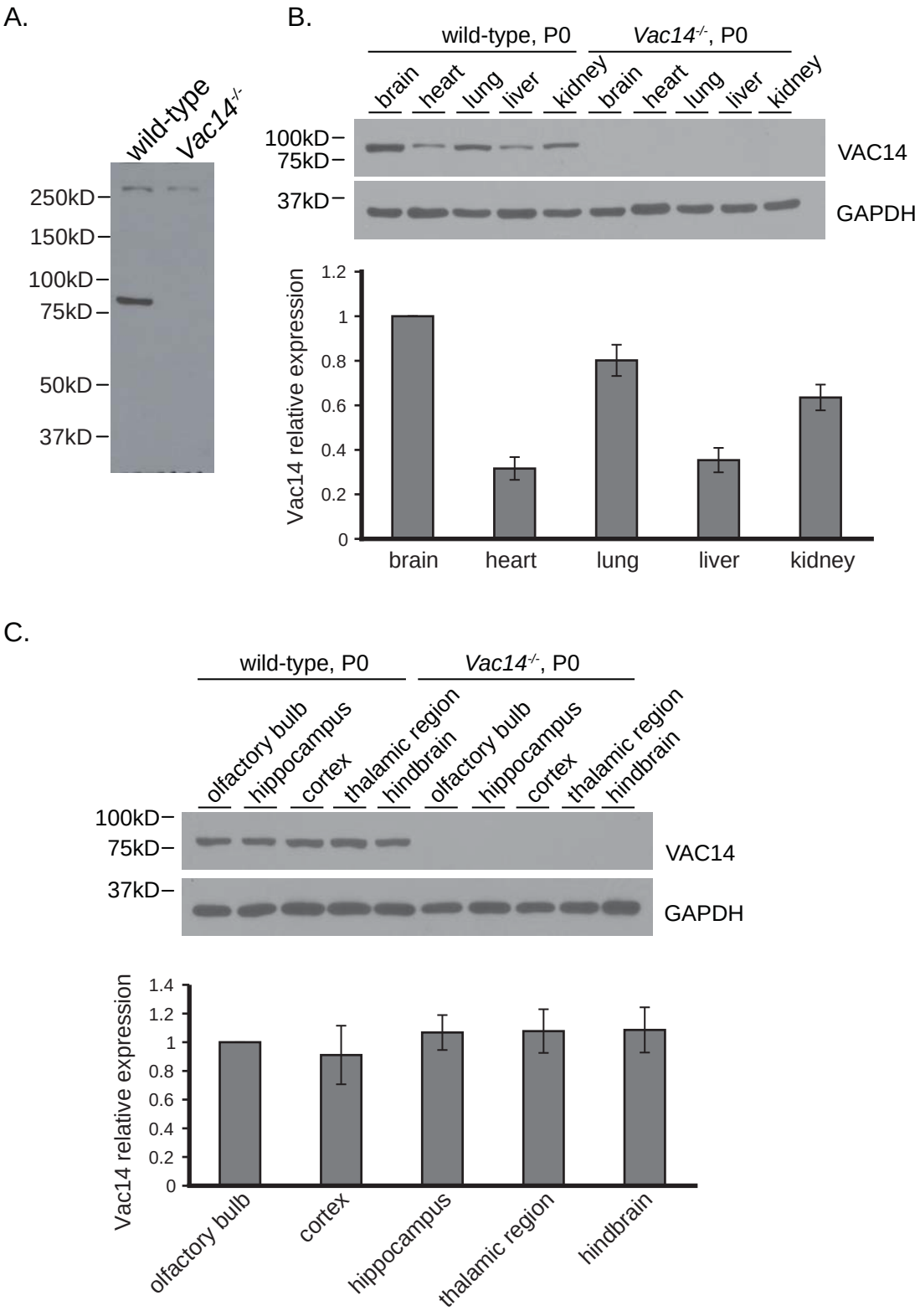
A.
wild-type
Vac14-/-
250kD
150kD
100kD
75kD
50kD
37kD
B.
wild-type, P0
Vac14-/-, P0
brain
heart
lung
liver
kidney
100kD
75kD
37kD
VAC14
GAPDH
Vac14 relative expression
1.2
1
0.8
0.6
0.4
0.2
0
C.
wild-type, P0
Vac14-/-, P0
olfactory bulb
hippocampus
cortex
thalamic region
hindbrain
100kD
75kD
37kD
VAC14
GAPDH
Vac14 relative expression
1.4
1.2
1
0.8
0.6
0.4
0.2
0

Figure 2-1. VAC14 is widely distributed in all tissues and brain regions tested
(A) Polyclonal rabbit anti-VAC14 antibody specifically recognizes VAC14 on western blots. Brain extracts from P0 wild-type and $Vac14^{-/-}$ pups were homogenized and detected by western blot analysis using anti-VAC14. **(B)** VAC14 is expressed in all tissues tested. Brain, heart, lung, liver and kidney were dissected from P0 pups. Western blots were probed with affinity purified rabbit anti-VAC14 antibody. **(C)** VAC14 is found in all tested regions of the brain. (B-C) $Vac14^{-/-}$ litter mates indicate the absence of VAC14 in all $Vac14^{-/-}$ tissues. Blots shown are representative of 3 independent experiments. VAC14 expression levels were quantified using the ratio of VAC14/GAPDH band densities and normalized to the first lane. Error bars, STD. ◊Data were collected and analyzed by Yanling Zhang.

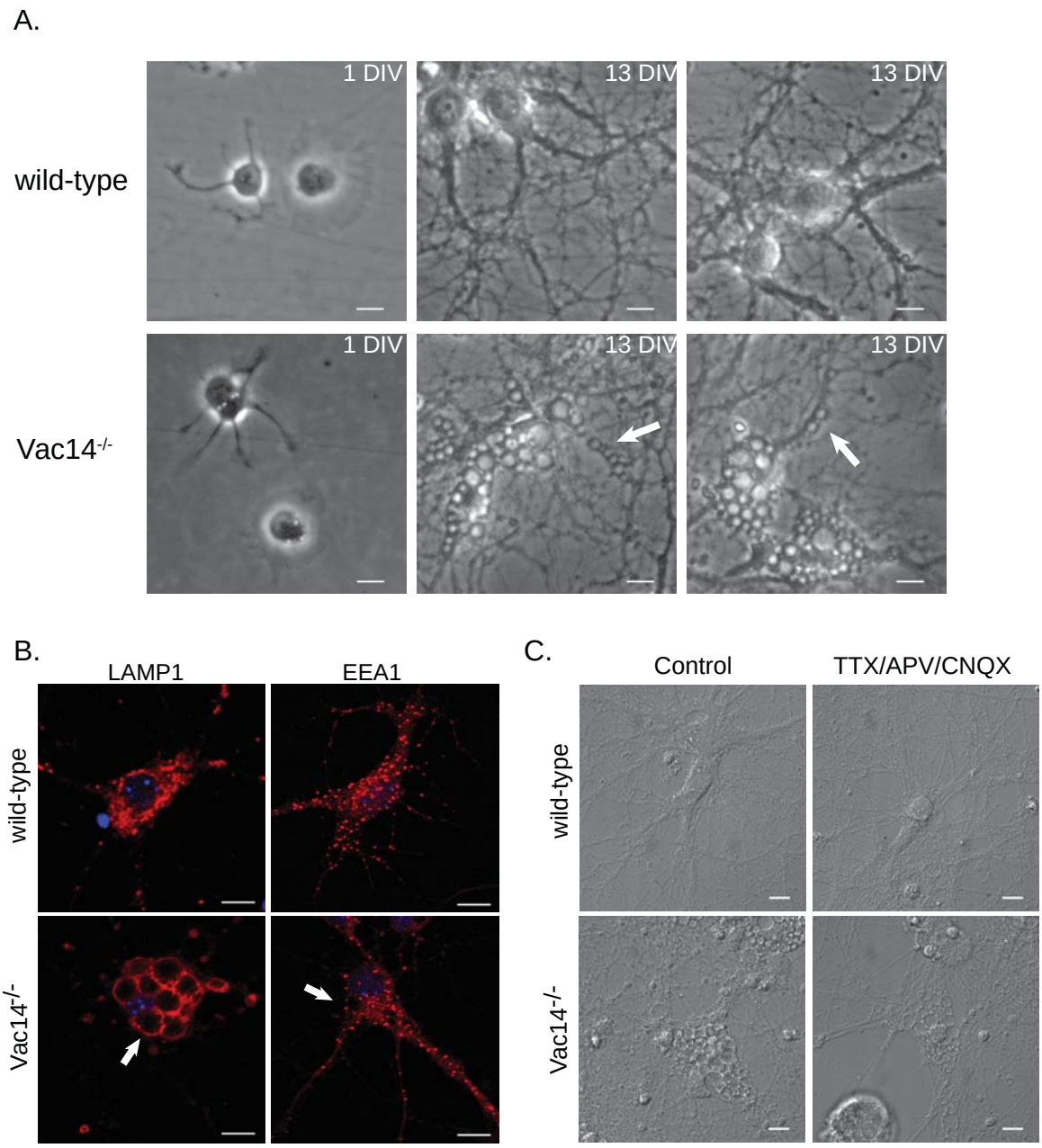

Figure 2-2. Vacuoles in cultured Vac14$^{-/-}$ hippocampal neurons
(A) Vac14$^{-/-}$ neurons form vacuoles as early as 1 DIV. Starting from 12 DIV, vacuoles were frequently observed in both the soma and the neurites (arrows). **(B)** Wild-type and Vac14$^{-/-}$ neurons were fixed and labeled with LAMP1 or EEA1. Vacuoles in Vac14$^{-/-}$ neurons (arrows) are positive for LAMP1 (late endosomal and lysosomal marker) but not EEA1 (early endosomal marker). **(C)** Vacuolation in neurons is not rescued by suppressing neuronal activities. Hippocampal neurons from wild type or Vac14$^{-/-}$ embryos were treated with 2 µM TTX, 20 µM APV and 40 µM CNQX starting from 3 DIV. Media were changed every other day in both drug treated and control dishes. Neurons were imaged at 18 DIV. (A-C) Bar = 10 µm. ◊ Data were collected by Yanling Zhang.

A.

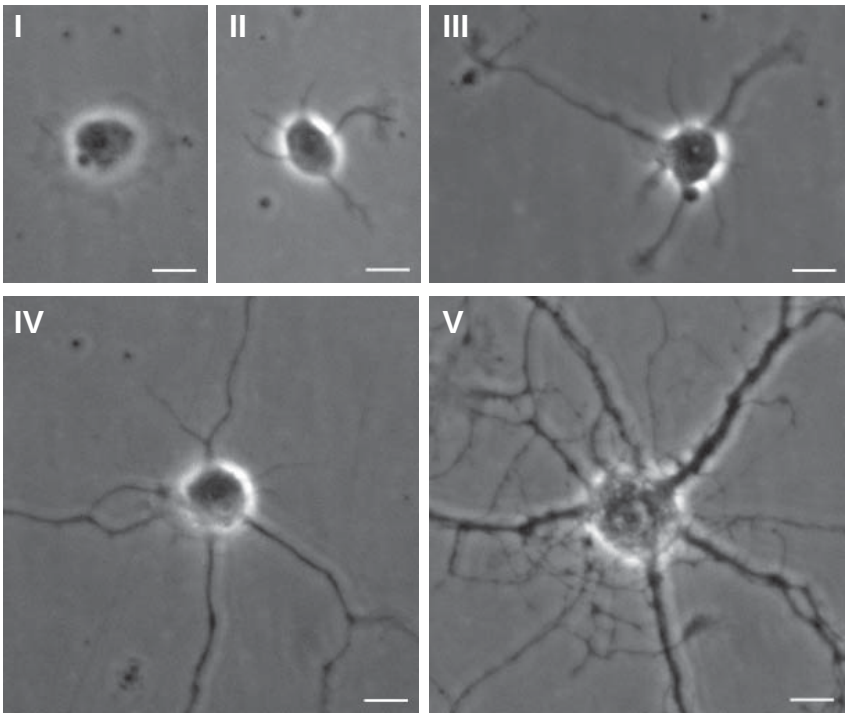

B.

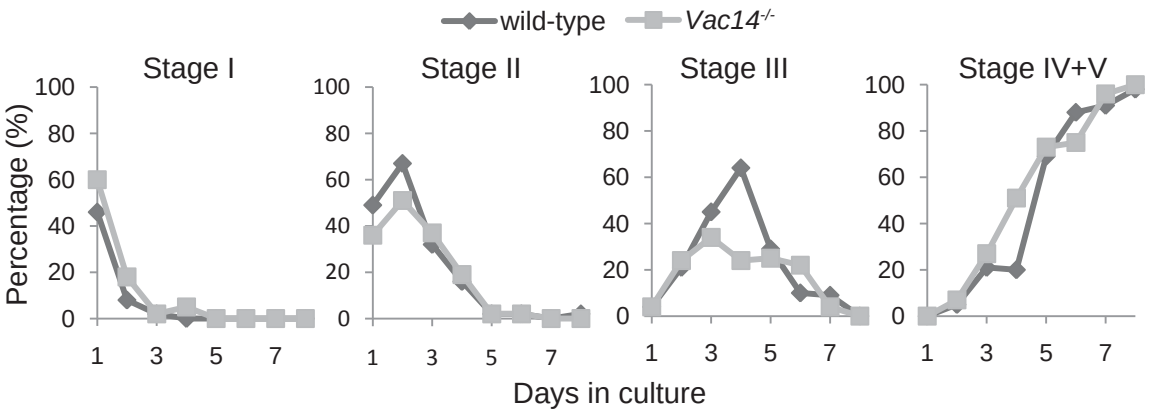

Figure 2-3. Vac14$^{-/-}$ neurons form vacuoles in culture, yet arborization is similar to wild-type neurons

(A) Examples of Stage I-V hippocampal neurons. Hippocampal neurons start out as fibroblast-like lamellipodia (Stage I). Then several short neurites emerge (Stage II). One extends further than the others and commits to the fate of an axon (Stage III). The other neurites (dendrites) extend further and form complicated networks (Stage IV &V). Bar = 10 µm. **(B)** Vac14$^{-/-}$ neurons undergo normal arborization. Cultured wild-type and Vac14$^{-/-}$ neurons were plated at a density that allowed visualization of single neurons (5, 000 to 10, 000 per 1.91 cm^2), and randomly selected neurons were imaged every 24h by phase contrast microscope. The numbers of neurons at different stages were counted. N = 50-80 neurons for each. Similar results were obtained in three independent experiments. ◊Data were collected and analyzed by Yanling Zhang.

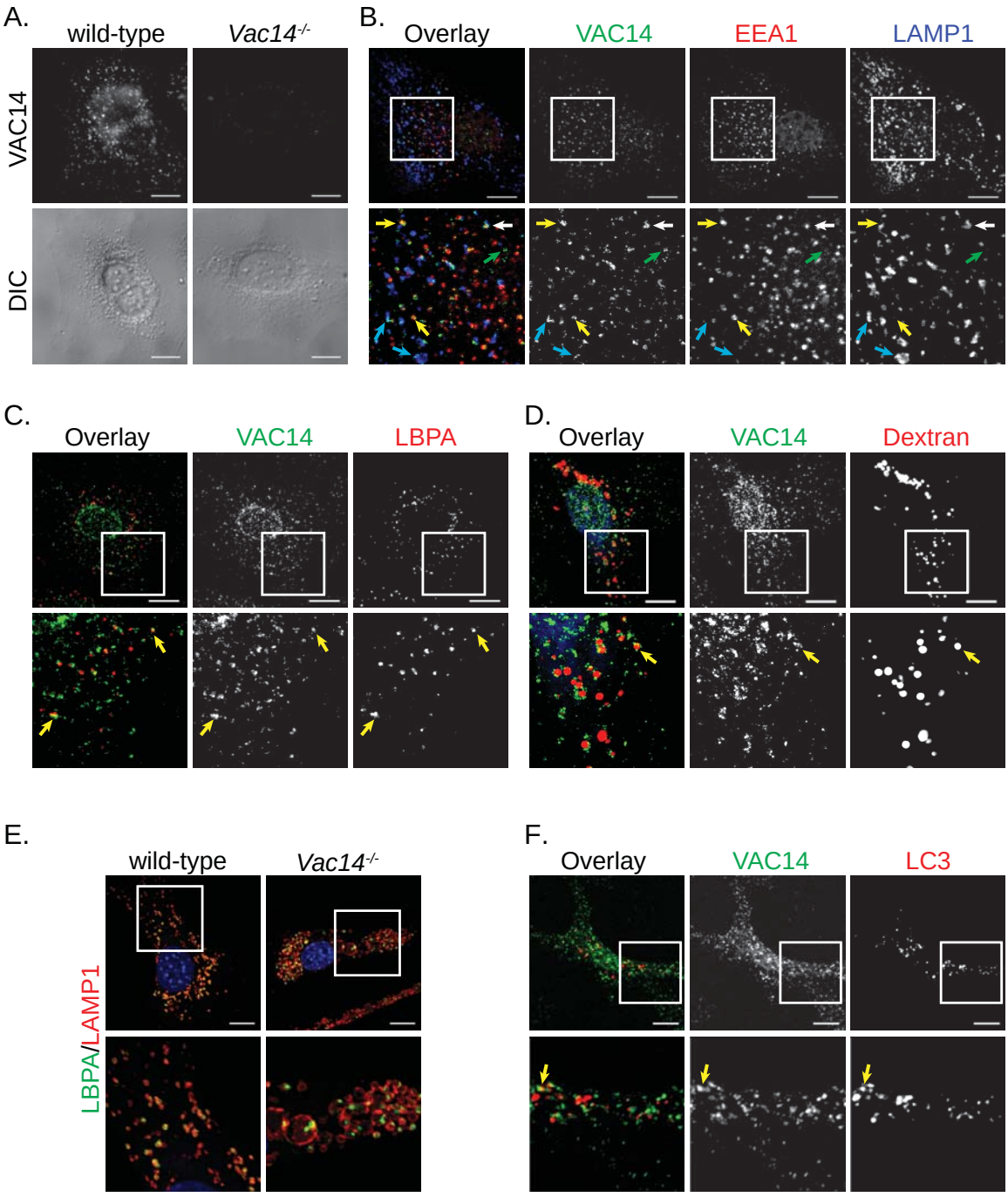

Figure 2-4. Endogenous VAC14 partially colocalizes with multiple endocytic organelles
(A) Polyclonal VAC14 antibody recognizes punctate structures in wild-type cells. Fibroblasts were permeabilized with saponin followed by fixation and labeled with anti-VAC14 antibody. Bottom panels, DIC images. **(B)** In fibroblasts, endogenous VAC14 colocalizes with both EEA1 and LAMP1. Wild-type fibroblasts were triple labeled with rabbit anti-VAC14, chicken anti-EEA1 and rat anti-LAMP1. The majority of VAC14 colocalized with either EEA1 (yellow arrows) or LAMP1 (turquoise arrows). Some VAC14 colocalized with both (white arrows) or neither (green arrow) markers. **(C)** VAC14

partially colocalizes with the late endosome marker LBPA (arrow). Fibroblasts are double labeled with rabbit anti-VAC14 and mouse anti-LBPA. **(D)** VAC14 partially colocalizes with lysosomes (arrow). To label lysosomes, prior to fixation, fibroblasts were pulsed with Texas Red-Dextran (MW 70kD) for 1 hour and chased in the absence of dextran for 24 hours. **(E)** The limiting membrane of vacuoles in $Vac14^{-/-}$ cells is positive for LAMP1 while negative for LBPA (arrow), suggesting a lysosomal origin. $Vac14^{-/-}$ fibroblasts were double labeled with rat anti-LAMP1 and mouse anti-LBPA. (D-E) DAPI (blue) was used to label the nuclei. **(F)** VAC14 partially colocalizes with LC3-RFP puncta (arrows). Fibroblasts transfected with LC3-RFP were fixed and labeled with anti-VAC14. (A-F) Bar = 10 µm. ◊Data in A-E were collected and analyzed by Yanling Zhang. Data in F were collected and analyzed by Cole Ferguson.

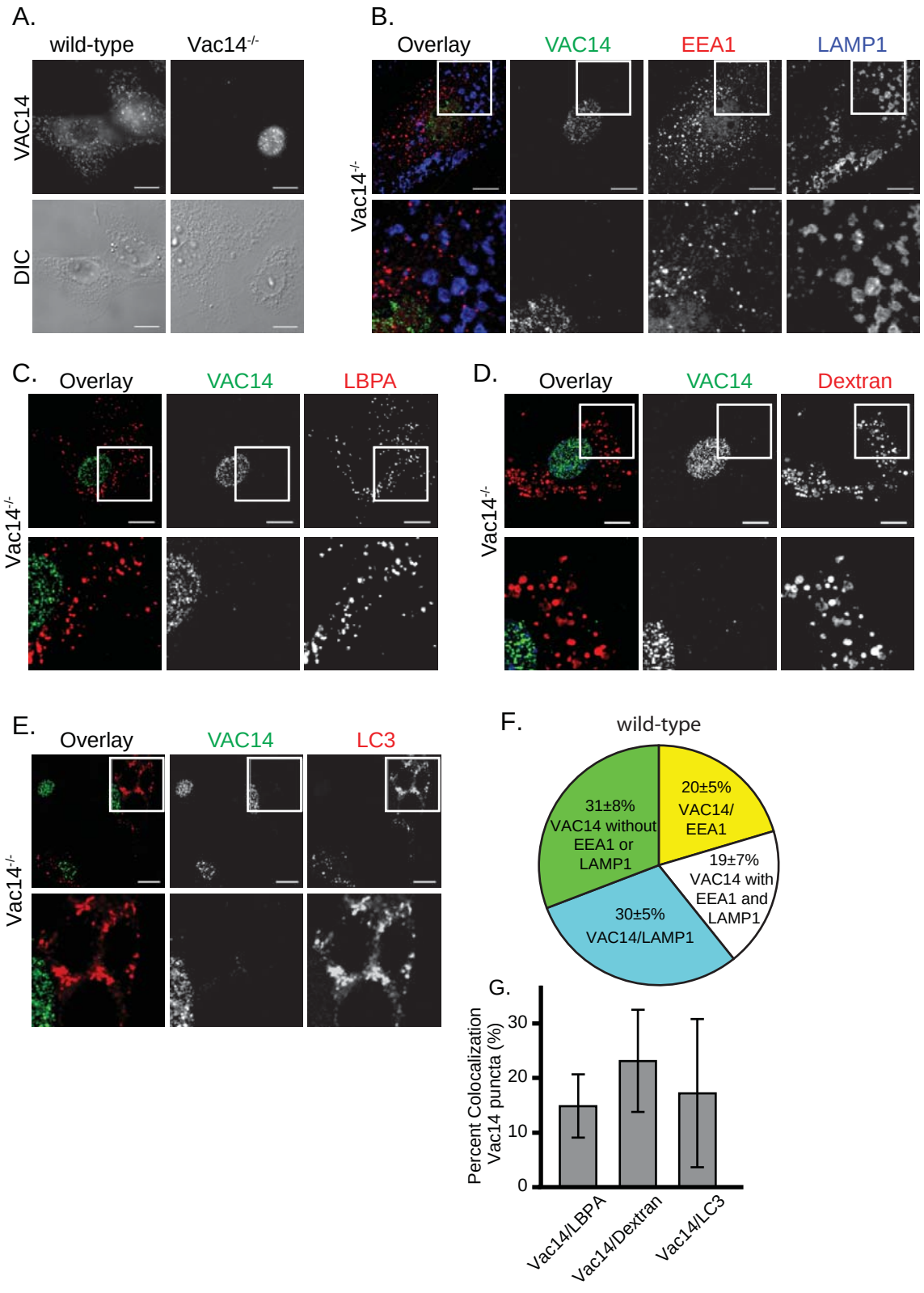
A.
wild-type
Vac14-/-
VAC14
DIC
B.
Overlay
VAC14
EEA1
LAMP1
Vac14-/-
C.
Overlay
VAC14
LBPA
Vac14-/-
D.
Overlay
VAC14
Dextran
Vac14-/-
E.
Overlay
VAC14
LC3
Vac14-/-
F.
wild-type
20±5%
VAC14/
EEA1
19±7%
VAC14 with
EEA1 and
LAMP1
30±5%
VAC14/LAMP1
31±8%
VAC14 without
EEA1 or
LAMP1
G.
Percent Colocalization
Vac14 puncta (%)
0
10
20
30
Vac14/LBPA
Vac14/Dextran
Vac14/LC3

Figure 2-5. Polyclonal rabbit anti-VAC14 antibody specifically recognizes VAC14 in fixed cells

(A) Immunofluorescence with anti-VAC14. Puncta in the cytoplasm were seen in wild-type cells but not $Vac14^{-/-}$ cells. Nonspecific nuclear staining was frequently present in cells cultured from both wild-type and $Vac14^{-/-}$ mutant mice. Bottom panels, DIC images. **(B, C, D, E)** $Vac14^{-/-}$ controls for Figure 2-8 B, C, D, F, respectively. Bar = 10 µm. **(F-G)** Quantification of VAC14 colocalization with endocytic and autophagic markers. **(F)** Percentages of VAC14 puncta that colocalized with EEA1, LAMP1, neither marker or both markers were quantified from triple labeling of VAC14/EEA1/LAMP1 immunofluorescence (N = 11 cells). Error, STD. **(G)** Percentages of VAC14 puncta that colocalized with LBPA, Dextran or LC3 were quantified from double labeling of VAC14 and the marker of interest (N= 7 for LBPA, 16 for Dextran, 15 for LC3). Error bars, STD. ◊Data in A-D were collected and analyzed by Yanling Zhang. Data in E were collected and analyzed by Cole Ferguson

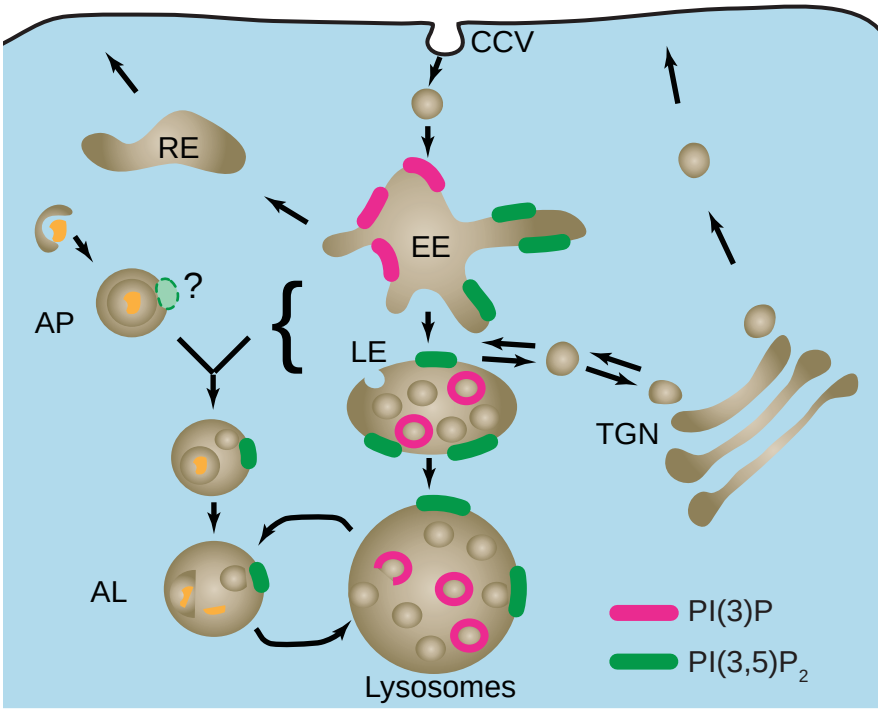

Figure 2-6. VAC14 distribution in the endomembrane system
Diagram of proposed PI(3,5)P_2¬ distribution in the endomembrane system. Based on the localization of endogenous VAC14, PI(3,5)P_2 localizes on early endosomes, late endosomes, lysosomes, and possibly autophagosomes. CCV, clathrin coated vesicles; EE, early endosomes; LE, late endosomes, RE, recycling endosomes; AP, autophagosomes; AL, autolysosomes; TGN, trans-Golgi network.

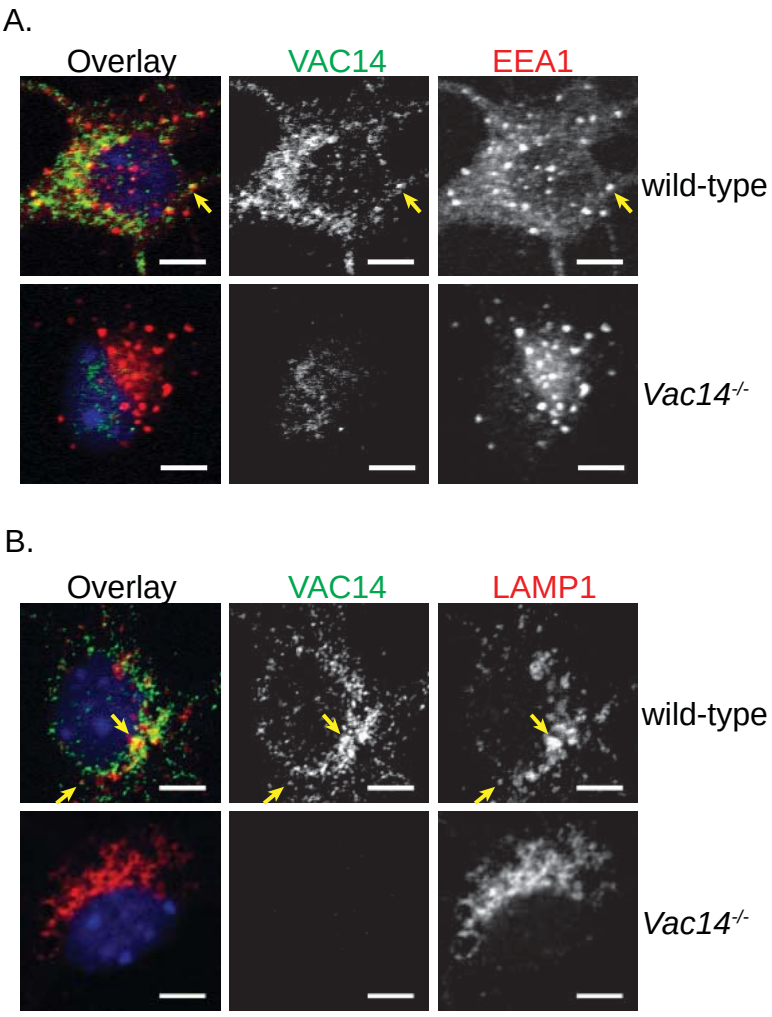

Figure 2-7. VAC14 partially colocalizes with EEA1 or LAMP2 in the soma
Wild-type and Vac14$^{-/-}$ neurons were double labeled with rabbit anti-VAC14 and chicken anti-EEA1 (A) or rat anti-LAMP1 (B). Arrows; colocalization between VAC14 and EEA1 or LAMP2. Bar = 5 µm. ◊Data in A and B were collected and analyzed by Yanling Zhang.

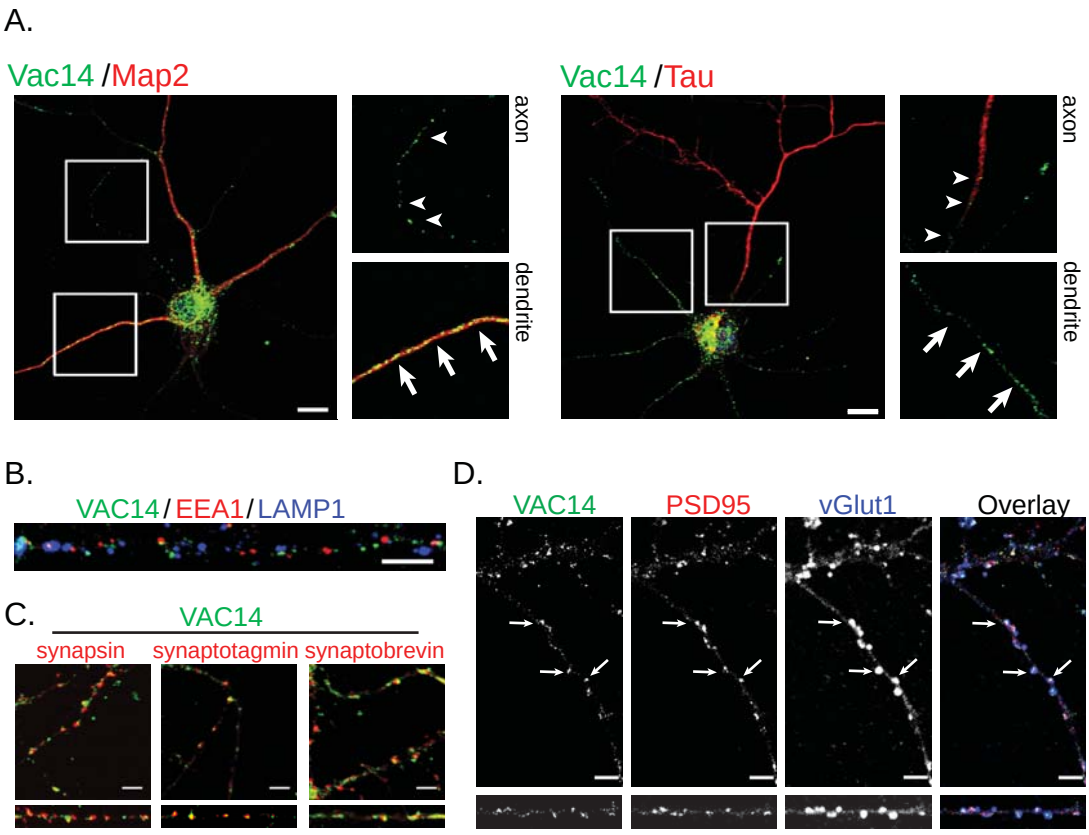

Figure 2-8. VAC14 is found in both dendrites and axons, and colocalized with endocytic and synaptic markers in hippocampal neurons

(A) Wild-type and Vac14$^{-/-}$ neurons were double labeled with rabbit anti-VAC14 and mouse anti-MAP2 (dendrites) or mouse anti-TAU-1 (axons). Arrows indicate the localization of VAC14 on dendrites (MAP2 positive and TAU negative neurites). Arrowheads indicate the localization of VAC14 on axons (MAP2 negative and TAU-1 positive neurites). Bar = 10 µm. **(B)** VAC14 partially colocalizes with EEA1 or LAMP1 in the neurites (arrows). Wild-type and Vac14$^{-/-}$ neurons were triple labeled with rabbit anti-VAC14, chicken anti-EEA1 and rat anti-LAMP1. Bar = 5 µm. **(C)** VAC14 displays significant colocalization with several synaptic markers: synapsin, synaptotagmin and synaptobrevin. Wild-type and Vac14$^{-/-}$ neurons were double labeled with rabbit anti-VAC14 and guinea pig anti-synapsin, mouse anti-synaptotagmin or mouse anti-synaptobrevin. Bar = 5 µm. **(D)** VAC14 partially localizes at excitatory synapses (labeled with both the synaptic vesicle glutamate transporter vGlut1, and postsynaptic marker PSD95). Wild-type and Vac14$^{-/-}$ neurons were labeled with rabbit anti-VAC14, mouse anti-PSD95 and guinea pig anti-vGlut1. Arrows indicate examples of colocalization. (C and D) Lower panels show straightened dendrites from corresponding top panels. Bar = 5 µm. ◊Data in A-D were collected by Yanling Zhang.

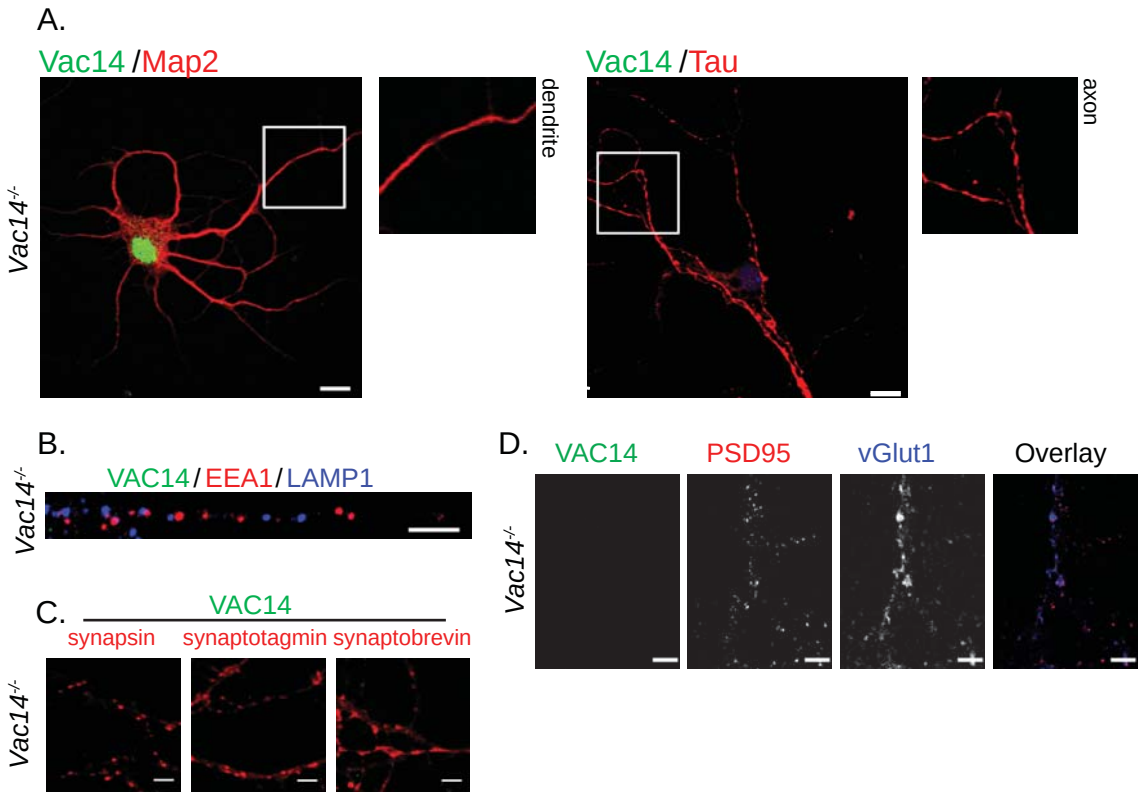

Figure 2-9. Polyclonal rabbit anti-VAC14 antibody specifically recognizes VAC14 in fixed neurons

(A-B) Vac14$^{-/-}$ controls for Figure 2-8(A-B) respectively. **(C)** Quantification of VAC14 puncta colocalization with endocytic markers in neurites. Percentages of VAC14 puncta that colocalized with EEA1 and LAMP1 were quantified from triple labeling of VAC14/ EEA1/LAMP1 immunofluorescence (N = 12 neurites). Error, STD. **(D-E)** Vac14$^{-/-}$ controls for Figure 2-8(C-D), respectively. (A) Bar = 10 µm. (B, D, E) Bar = 5 µm. ◊Data in A-D were collected by Yanling Zhang.

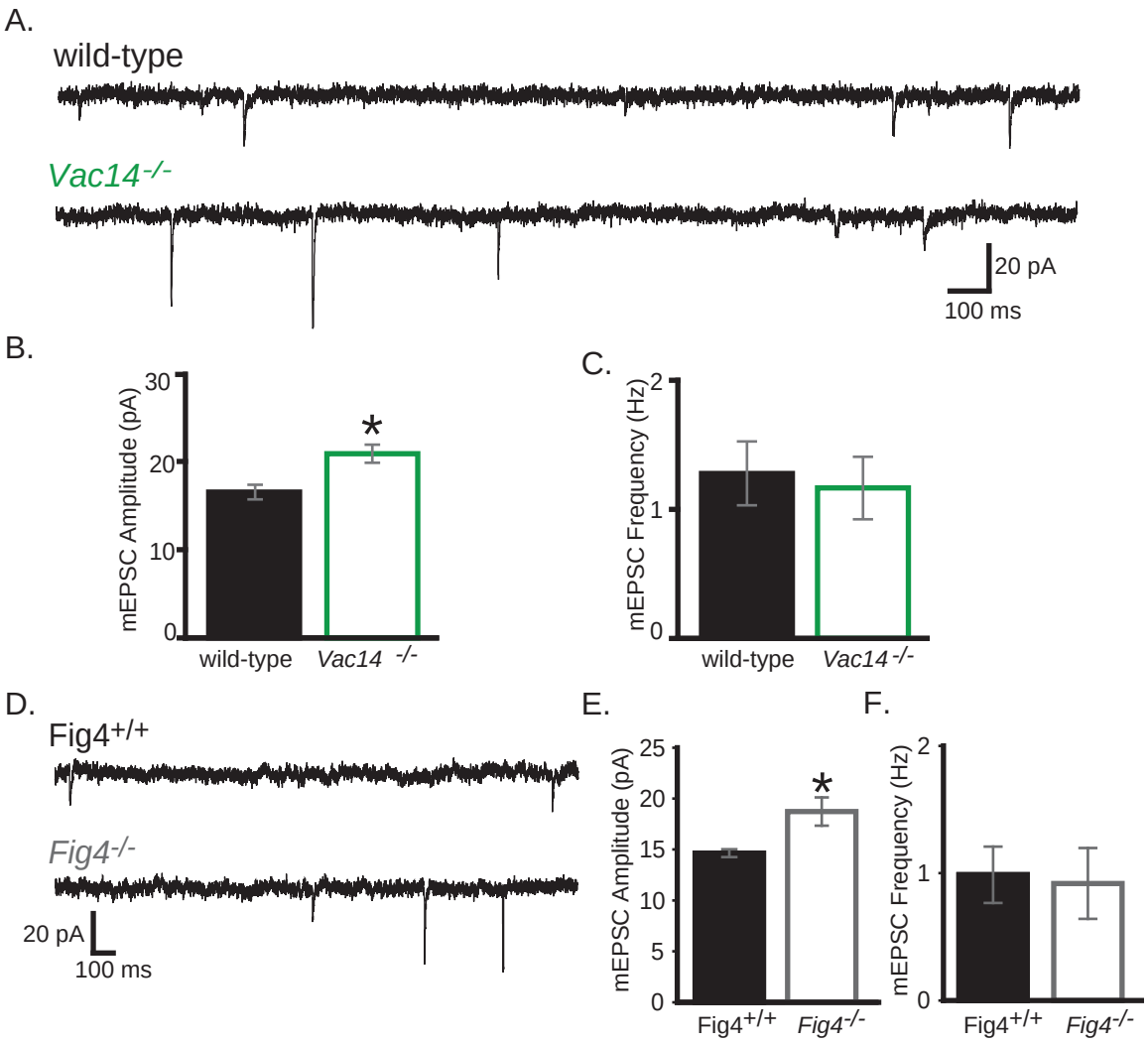

Figure 2-10. Loss of VAC14 or FIG4 leads to an increase in excitatory synaptic function **(A)** Representative mEPSC recordings of wild-type (N=32) and Vac14$^{-/-}$ neurons (N=32). **(B)** Mean mEPSC amplitude in Vac14$^{-/-}$ neurons is larger than wild-type neurons, 20.86±1.03 pA vs. 16.83±0.91 pA, respectively. *p = 0.0045, t-test. **(C)** Mean mEPSC frequency is similar in wild-type (1.21±0.26 Hz) and Vac14$^{-/-}$ (1.16±0.24 Hz) neurons. **(D-E)** Summary of mEPSC kinetics in wild-type and Vac14$^{-/-}$ neurons. **(D)** Individual mEPSCs overlaid. Thick lines show the mean trace. Dashed line is aligned to the mean peak inward current of Vac14$^{-/-}$ mEPSC. Scaled overlay shows similar kinetics between wild-type and Vac14$^{-/-}$ mEPSCs. **(E)** Mean mEPSC decay is similar between wild-type (3.80±0.15 ms) and Vac14$^{-/-}$ (3.69±0.14 ms). **(F)** Representative mEPSC traces of wild-type (Fig4$^{+/+}$) (N=12) and Fig4$^{-/-}$ neurons (N=14). **(G)** Mean mEPSC amplitude in Fig4$^{-/-}$ neurons is larger than Fig4$^{+/+}$ neurons (14.64±0.39 pA vs. 18.73±1.38 pA, respectively. *p =0.0164, t-test). **(H)** Mean mEPSC frequency is similar in Fig4$^{+/+}$ and Fig4$^{-/-}$ (0.99±0.22 Hz vs. 0.92±0.28 Hz, respectively. p = 0.8542, t-test). Error bars are standard error of the mean (SEM).

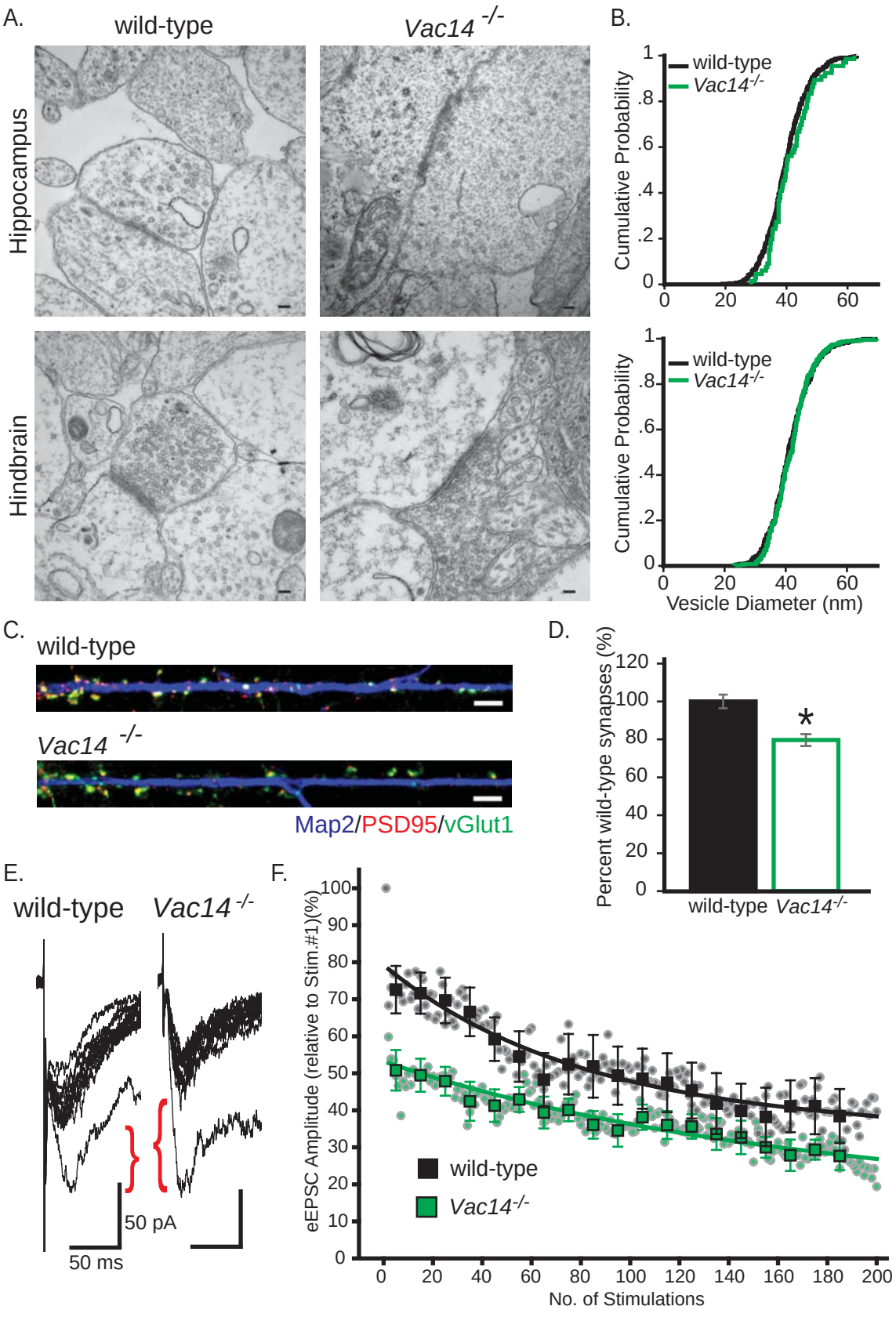
A.
wild-type
Vac14 -/-
Hippocampus
Hindbrain
B.
wild-type
Vac14-/-
Cumulative Probability
Vesicle Diameter (nm)
C.
wild-type
Vac14 -/-
Map2/PSD95/vGlut1
D.
Percent wild-type synapses (%)
wild-type Vac14-/-
E.
wild-type Vac14 -/-
50 pA
50 ms
F.
eEPSC Amplitude (relative to Stim.#1)(%)
No. of Stimulations
wild-type
Vac14-/-

Figure 2-11. Presynaptic probability of release is enhanced in Vac14$^{-/-}$ neurons
(A-B) Synaptic vesicles from Vac14$^{-/-}$ are not larger than synaptic vesicles observed in brains from wild-type. (A) Electron microscopy of excitatory synapses, evident by the thickening of the postsynaptic membrane, in wild-type and Vac14$^{-/-}$ hippocampus and hindbrain. Bar = 100 nm. **(B)** Quantification of the diameter of synaptic vesicles. Cumulative probability distribution of synaptic vesicle diameter. No significance difference was found between wild-type and Vac14$^{-/-}$ by a two-sample Kolmogorov-Smirnov test (kstest2, Matlab) (hippocampus, p=0.32; hindbrain, p=0.46). Three wild-type and three Vac14$^{-/-}$ animals were analyzed. Hindbrain: N = 567 vesicles from 33 terminals for wild-type and 388 vesicles from 29 terminals for Vac14$^{-/-}$. Hippocampus: N = 433 vesicles from 33 terminals for wild-type and 66 vesicles from 15 terminals for Vac14$^{-/-}$. **(C-D)** The number of synapses is decreased in Vac14$^{-/-}$ neurons. **(C)** Wild-type and Vac14$^{-/-}$ hippocampal neurons were triple labeled with rabbit anti-MAP2 (blue), mouse anti-PSD95 (red) and guinea pig anti-vGlut (green). Examples of straightened dendrites are shown. Bar = 5 µm. **(D)** Quantitation of the number of synapses on the first 100 µm of dendrites starting from the soma. The numbers of synapses were normalized to the average of wild-type. Vac14$^{-/-}$ neurons had fewer synapses (N = 91 for wild-type and 71 for Vac14$^{-/-}$) (*p = 1.7 x 10-4, t-test). Error bars, SEM. **(E-F)** Presynaptic probability of release is increased in Vac14-/- neurons. NMDA currents were pharmacologically isolated from AMPA and $GABA_A$ mediated currents and recorded at -70 mV (solution contained 0 Mg^{2+}). An extracellular stimulating electrode was placed locally and used to stimulate vesicle release in afferent axons. Once a stable response was obtained, 20 µM MK801, an open-channel blocker of NMDA receptors, was added to the bath for 5 mins without stimulation. Then 200 stimulations were delivered and amplitude of the current measured (mean amplitude is shown by filled circles). In the presence of MK-801, the current is progressively blocked. The data for each genotype were fitted with a double exponential curve. The rate of progressive blockade of NMDA current was significantly greater in Vac14$^{-/-}$ neurons; mean amplitude of the 2-11 stimulations is significantly lower in Vac14$^{-/-}$ neurons. *p=0.0217, Anova1 (Matlab). ◊Data in A were collected by Yanling Zhang and Sergey Zolov. Data in C and D were collected by Yanling Zhang.

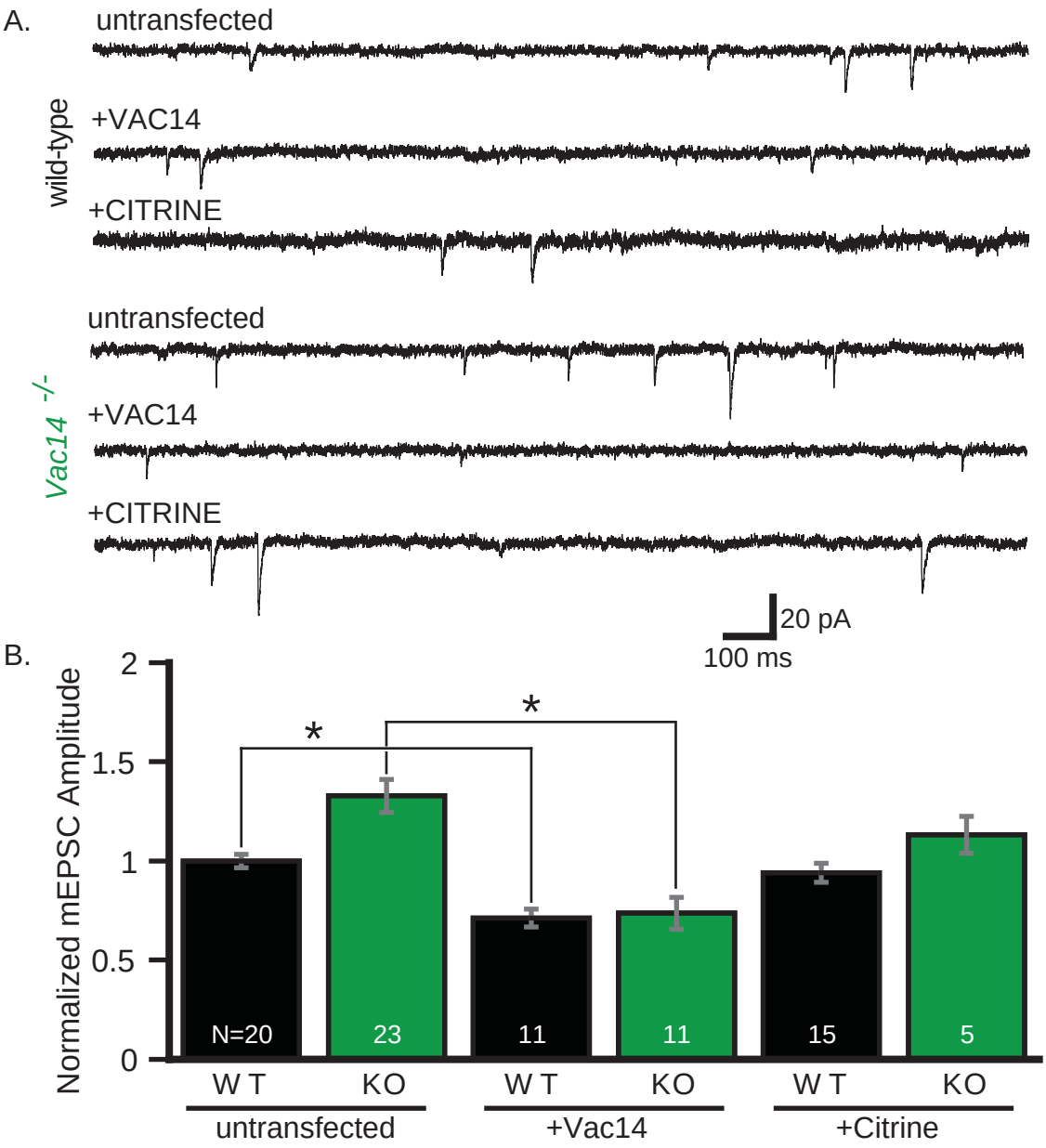

Figure 2-12. Restoration of VAC14 eliminates the increase in mEPSC amplitude in Vac14$^{-/-}$ neurons

(A) Examples of mEPSC recordings of wild-type and Vac14$^{-/-}$ neurons that were sham-transfected, expressed VAC14-Citrine or Citrine alone. **(B)** Quantification of mEPSC amplitude normalized to sham-transfected wild-type neurons shows that there is an inverse relationship between level of VAC14 expression and mEPSC amplitude. In wild-type neurons, VAC14 overexpression decreases amplitude. The increase in mEPSC amplitude in Vac14$^{-/-}$ neurons is reduced by reintroduction of VAC14. Neurons transfected with Citrine were similar to untransfected wild-type. One-way ANOVA test was used to compare mEPSC amplitudes (p=8.27e-9). *Individual comparisons were determined using the Tukey-Kramer post hoc. WT, wild-type; KO, Vac14-/-; Cit, Citrine. Error bars, SEM.

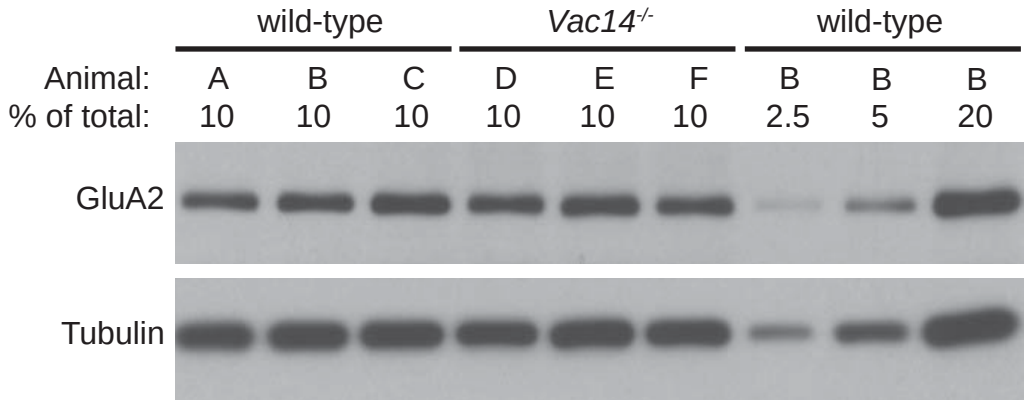

Figure 2-13. Total expression of GluA2 is similar
Cultured hippocampal neurons at 14 DIV were collected, lysed and total protein separated by SDS-PAGE. To confirm linearity of the assay, a series of dilutions of WT animal B was run on the same gel. Membranes were probed with anti-GluA2 and anti-tubulin antibodies.

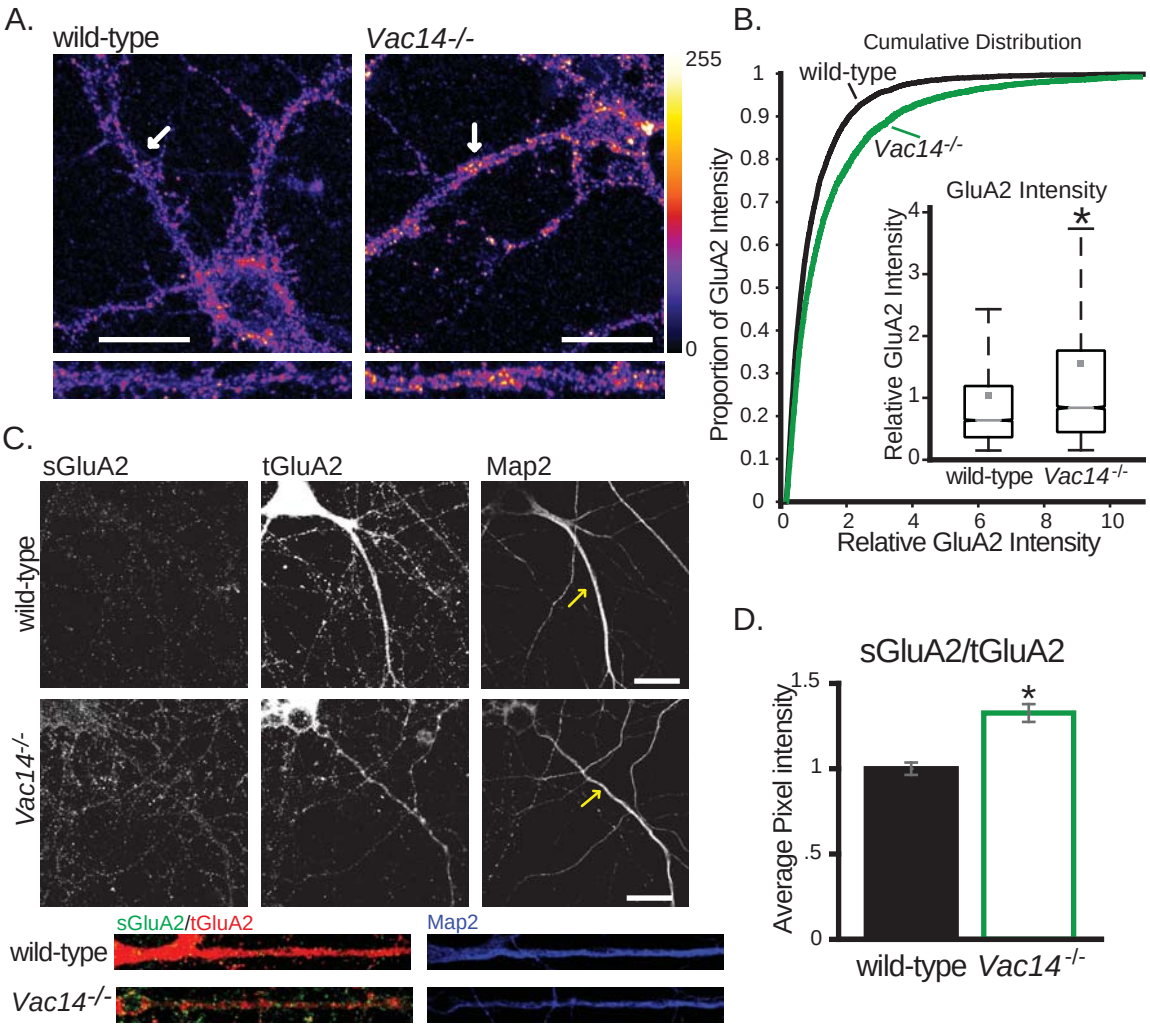

Figure 2-14. Surface GluA2 levels increase in Vac14$^{-/-}$ neurons

(A) Surface GluA2 was labeled by incubation of intact neurons with mouse anti-GluA2 antibody. Arrows highlight the dendrite used for analysis (enlarged in lower panels). Intensity presented in the "fire" LUT color scheme. **(B)** Quantitation of the intensity of GluA2 puncta, normalized to the wild-type mean. The relative intensity values from wild-type and Vac14$^{-/-}$ neurons are presented as a cumulative distribution. A Kolmogorov-Smirnov test demonstrates that the data sets differ significantly (p = 1.1e-34). The median of each data set also differ significantly (box plot in insert). Box, interquartile range; line, median; square, mean; non-overlapping notches indicate that the two medians are statistically different at the 5% significance level; whiskers, minimum and maximum of the data within 1.5 times the length of the box. N = 5272 for wild-type and 4756 for Vac14$^{-/-}$. Error bars, SEM. (C) Surface GluA2 subunits accumulate on the surface of Vac14$^{-/-}$ dendrites. Top panel shows wild-type surface GluA2, total GluA2, and dendritic marker, MAP2. Middle shows the same staining in Vac14$^{-/-}$ neurons. Yellow arrow highlights the dendrite used for analysis. Bottom shows the merged image of the straightened dendrite (left) and MAP2 (right). (D) The ratio of surface to total GluA2 is increased in Vac14$^{-/-}$ dendrites (1.32±0.052) relative to wild-type (1.0±0.0364). * p = 6.836*10-7, two-sample t-test. Scale bar = 10 µm. Error bars = SEM.

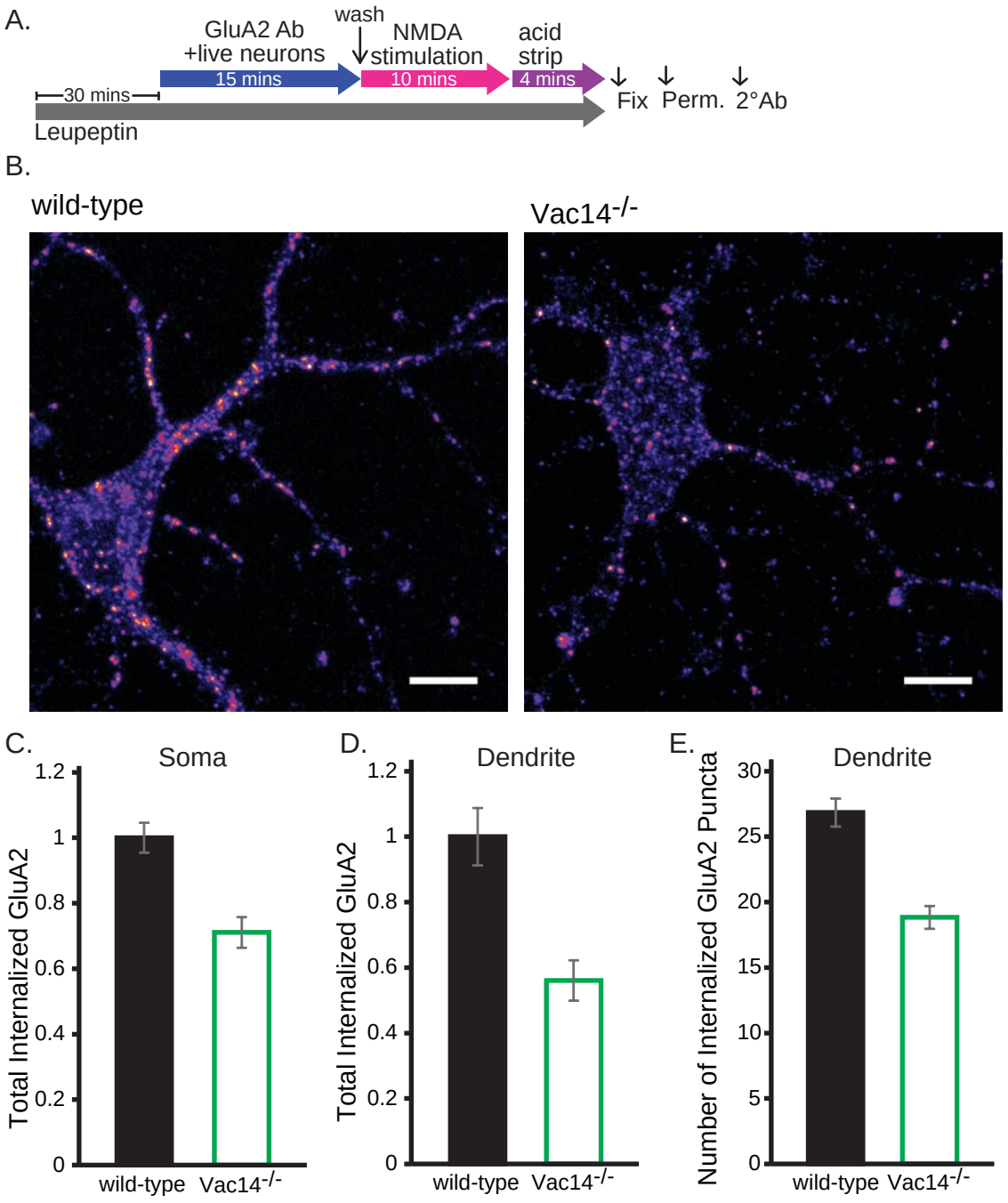

Figure 2-15. GluA2 endocytosis is reduced in Vac14$^{-/-}$ hippocampal neurons
(A) Diagram of experimental procedures. Wild-type or Vac14$^{-/-}$ hippocampal neurons embryos were treated with lysosomal inhibitor leupeptin before live labeled with mouse GluA2 antibodies. Endocytosis was stimulated with 50 µM NMDA for 10 minutes. Surface bound GluA2 antibodies were acid stripped. Neurons were then fixed and labeled with Alexa 555 anti-mouse IgG. **(B)** Example of internalized GluA2. Intensity presented in the "fire" LUT color scheme. Bar = 10 µm. **(C)** Total internalized GluA2 in the soma was decreased in Vac14$^{-/-}$ neurons (N= 55 for wild-type and 42 for Vac14$^{-/-}$. p = 2.73 x 10-5. t-test.) **(D)** Total internalized GluA2 in the dendrites was decreased in Vac14$^{-/-}$ neurons

(N= 57 for wild-type and 61 for Vac14$^{-/-}$. p = 8.33 x 10-5. t-test). **(E)** The number of internalized GluA2 was decreased in Vac14$^{-/-}$ neurons (N= 57 for wild-type and 61 for Vac14$^{-/-}$. p = 5.91 x 10-8. t-test.). A fixed length (35 µm from the soma) was used for dendrites in (D) and (E). Error bars, SEM. ◊Data were collected by Yanling Zhang.

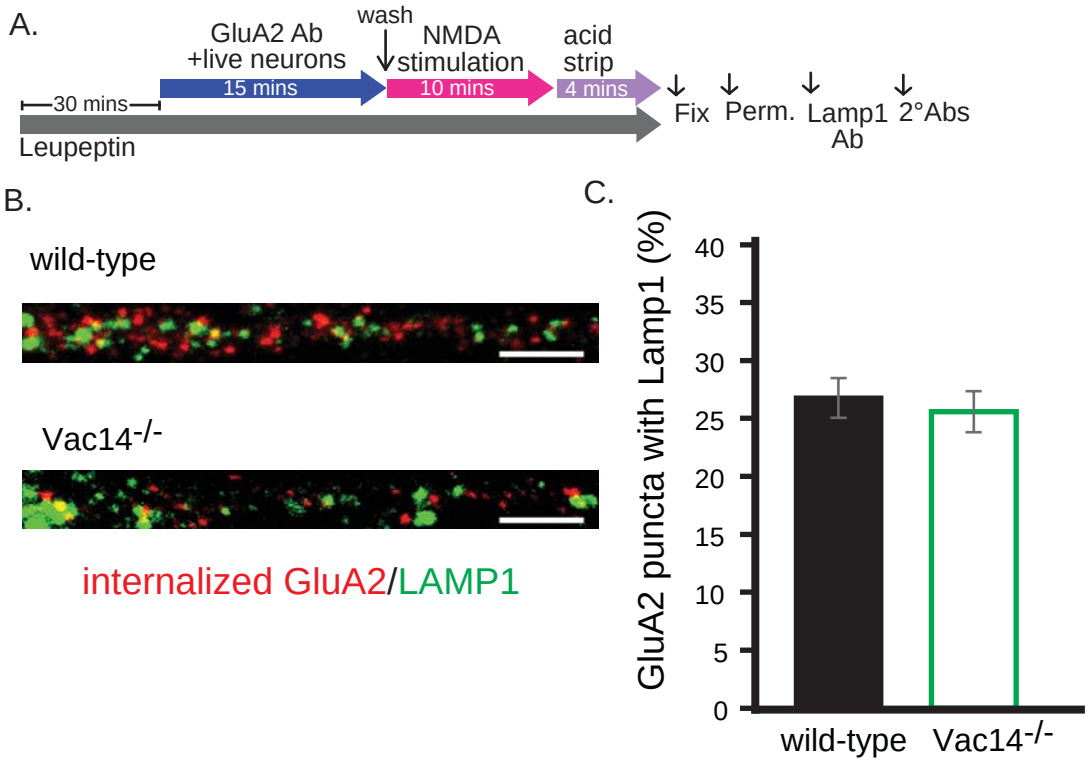

Figure 2-16. Internalized GluA2 enters the degradation pathway normally in Vac14$^{-/-}$
A-B) Hippocampal neurons from wild type or Vac14$^{-/-}$ embryos were treated with lysosomal inhibitor leupeptin before live labeled with GluA2 antibodies. Endocytosis was stimulated with 50 µM NMDA for 10 minutes. Surface bound GluA2 antibodies were acid stripped. Neurons were then fixed and labeled with LAMP1 antibodies. C) The percentage of internalized GluA2 puncta that colocalized with LAMP1 was calculated from a fixed length of apical dendrites (the first 35 µm dendrites from soma) (N = 57 for wildtype and 61 for Vac14$^{-/-}$. p = 0.63. t-test). Bars, 5 µm. ◊Data were collected by Yanling Zhang.

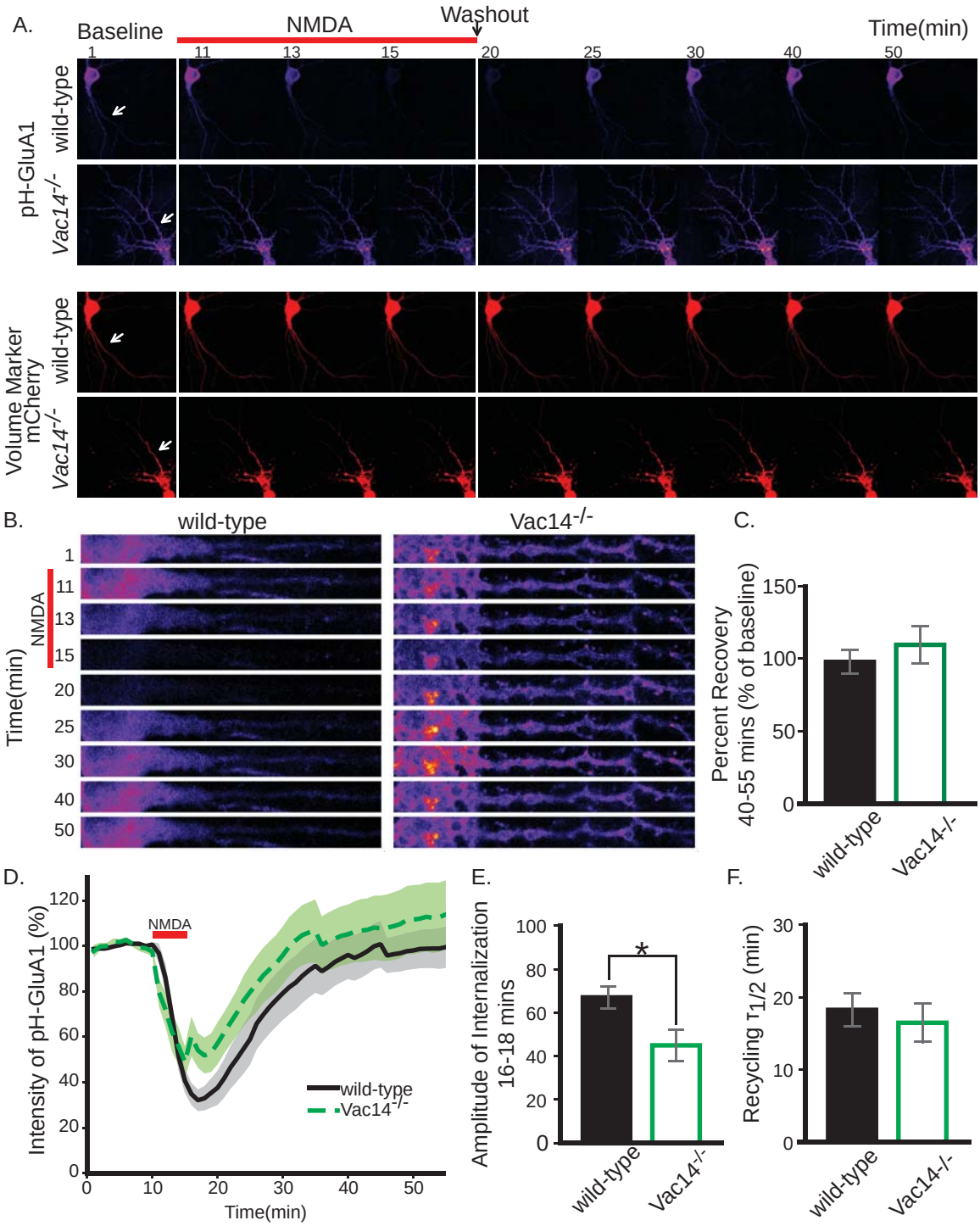

Figure 2-17. Endocytosis of AMPA receptors is reduced in Vac14$^{-/-}$ neurons
Cultured hippocampal neurons were transfected with pH-GluA1and mCherry at DIV12. At DIV14, neurons were stimulated with 20 µM NMDA for 5 mins and pH-GluA1 intensity was monitored. **(A)** Representative full-frame images of wild-type and Vac14$^{-/-}$ neurons during baseline (0-10 mins), NMDA stimulation (11-15 mins), and recovery after wash out (16-55 mins). **(B)** Changes in pH-GluA1 fluorescence were calculated from straightened dendrites isolated from full-frame images. **(C)** Wild-type and Vac14^{-}

$^{/-}$ neurons recovered back to baseline levels similarly. **(D)** Average time-course for percent change in pH-GluA1 fluorescence, normalized to average baseline intensity. **(E)** Amplitude of change in fluorescence after wash-out of NMDA is decreased in Vac14$^{-/-}$ neurons compared to wild-type (wild-type, 66.72±4.93%; Vac14$^{-/-}$ 44.68±7.10%). **(F)** t1/2 recycling rate after NMDA washout is normal. *p=.0224, t-test, n=11-14. Error bars, SEM.

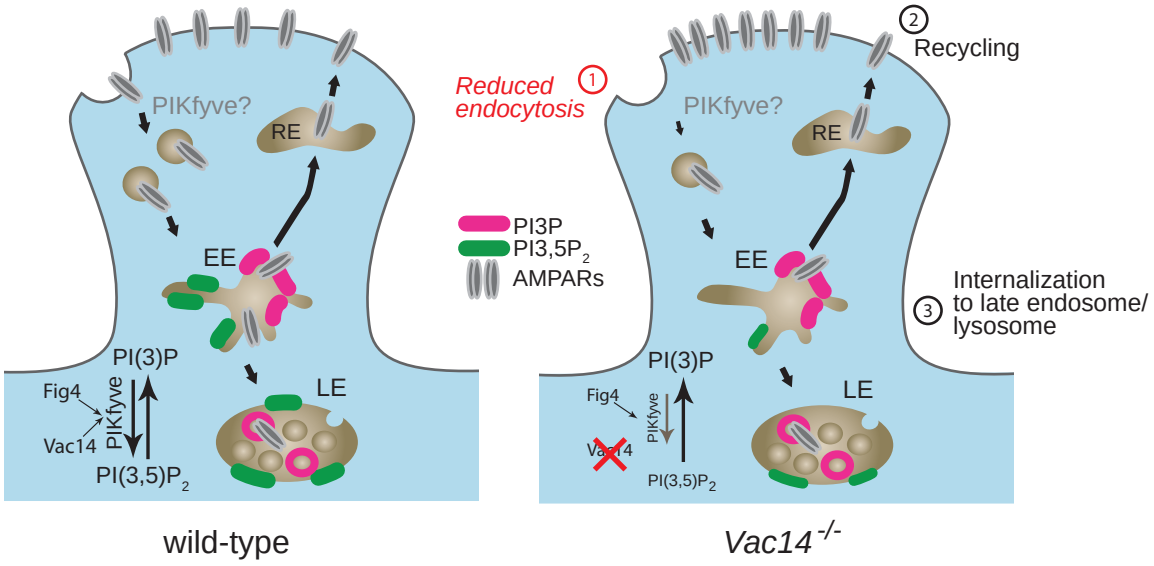

Figure 2-18. Model of trafficking defects that promote the elevation of surface AMPA receptors in Vac14$^{-/-}$ neurons

Endocytosis of surface GluA2 may be reduced in Vac14$^{-/-}$ compared with wild-type neurons (1), while recycling of internal GluA2 to the cell surface (2) and membrane transport late in the endocytic pathway (3) are normal in Vac14$^{-/-}$ neurons. Note that, in the absence of VAC14, FIG4 is destabilized (Lenk et al., 2011). V, endocytic vesicles; EE, early endosomes; LE, late endosomes; RE, recycling endosomes.

2.7 BIBLIOGRAPHY

Balla T. 2006. Phosphoinositide-derived messengers in endocrine signaling. *Journal of Endocrinology,* **188,** 135-153.

Beal MF. 1992. Mechanisms of excitotoxicity in neurologic diseases. *The FASEB Journal: Official Publication of the Federation of American Societies for Experimental Biology,* **6,** 3338-3344.

Bonangelino CJ, Catlett NL & Weisman LS. 1997. Vac7p, a novel vacuolar protein, is required for normal vacuole inheritance and morphology. *Molecular and cellular biology,* **17,** 6847-58.

Bonangelino CJ, Nau JJ, Duex JE, Brinkman M, Wurmser AE, Gary JD, Emr SD & Weisman LS. 2002. Osmotic stress-induced increase of phosphatidylinositol 3,5-bisphosphate requires Vac14p, an activator of the lipid kinase Fab1p. *The Journal of Cell Biology,* **156,** 1015-1028.

Brown TC, Tran IC, Backos DS & Esteban JA. 2005. NMDA receptor-dependent activation of the small GTPase Rab5 drives the removal of synaptic AMPA receptors during hippocampal LTD. *Neuron,* **45,** 81-94.

Brunet A, Datta SR & Greenberg ME. 2001. Transcription-dependent and -independent control of neuronal survival by the PI3K-Akt signaling pathway. *Current Opinion in Neurobiology,* **11,** 297-305.

Bryant NJ, Piper RC, Weisman LS & Stevens TH. 1998. Retrograde traffic out of the yeast vacuole to the TGN occurs via the prevacuolar/endosomal compartment. *The Journal of Cell Biology,* **142,** 651-663.

Cabezas A, Pattni K & Stenmark H. 2006. Cloning and subcellular localization of a human phosphatidylinositol 3-phosphate 5-kinase, PIKfyve/Fab1. *Gene,* **371,** 34-41.

Cantley LC. 2002. The Phosphoinositide 3-Kinase Pathway. *Science,* **296,** 1655-1657.

Chow CY, Landers JE, Bergren SK, Sapp PC, Grant AE, Jones JM, Everett L, Lenk GM, McKenna-Yasek DM, Weisman LS, Figlewicz D, Brown RH & Meisler MH. 2009. Deleterious variants of FIG4, a phosphoinositide phosphatase, in patients with ALS. *American Journal of Human Genetics,* **84,** 85-88.

Chow CY, Zhang Y, Dowling JJ, Jin N, Adamska M, Shiga K, Szigeti K, Shy ME, Li J, Zhang X, Lupski JR, Weisman LS & Meisler MH. 2007. Mutation of FIG4 causes neurodegeneration in the pale tremor mouse and patients with CMT4J. *Nature,* **448,** 68-72.

Corvera S, D'Arrigo A & Stenmark H. 1999. Phosphoinositides in membrane traffic. *Current Opinion in Cell Biology,* **11,** 460-465.

de Lartigue J, Polson H, Feldman M, Shokat K, Tooze SA, Urbé S & Clague MJ. 2009. PIKfyve regulation of endosome-linked pathways. *Traffic (Copenhagen, Denmark),* **10,** 883-893.

Dittman J & Ryan TA. 2009. Molecular circuitry of endocytosis at nerve terminals. *Annual Review of Cell and Developmental Biology,* **25,** 133-160.

Dong X-p, Shen D, Wang X, Dawson T, Li X, Zhang Q, Cheng X, Zhang Y, Weisman LS, Delling M & Xu H. 2010. PI(3,5)P2 Controls Membrane Traffic by Direct Activation of Mucolipin Ca2+ Release Channels in the Endolysosome. *Nature communications,* **1**.

Dotti CG, Sullivan CA & Banker GA. 1988. The establishment of polarity by hippocampal neurons in culture. *J. Neurosci.,* **8,** 1454-1468.

Dove SK, Piper RC, McEwen RK, Yu JW, King MC, Hughes DC, Thuring J, Holmes AB, Cooke FT, Michell RH, Parker PJ & Lemmon MA. 2004. Svp1p defines a family of phosphatidylinositol 3,5-bisphosphate effectors. *The EMBO Journal,* **23,** 1922-1933.

Duex JE, Nau JJ, Kauffman EJ & Weisman LS. 2006a. Phosphoinositide 5-phosphatase Fig 4p is required for both acute rise and subsequent fall in stress-induced phosphatidylinositol 3,5-bisphosphate levels. *Eukaryotic Cell,* **5,** 723-731.

Duex JE, Tang F & Weisman LS. 2006b. The Vac14p-Fig4p complex acts independently of Vac7p and couples PI3,5P2 synthesis and turnover. *The Journal of Cell Biology,* **172,** 693-704.

Ferguson CJ, Lenk GM, Jones JM, Grant AE, Winters JJ, Dowling JJ, Giger RJ & Meisler MH. 2012. Neuronal expression of Fig4 is necessary and sufficient to prevent spongiform neurodegeneration. *Human molecular genetics*.

Ferguson CJ, Lenk GM & Meisler MH. 2009. Defective autophagy in neurons and astrocytes from mice deficient in PI(3,5)P2. *Human Molecular Genetics,* **18,** 4868-4878.

Gary JD, Wurmser AE, Bonangelino CJ, Weisman LS & Emr SD. 1998. Fab1p is essential for PtdIns(3)P 5-kinase activity and the maintenance of vacuolar size and membrane homeostasis. *The Journal of cell biology,* **143,** 65-79.

Gong L-W & De Camilli P. 2008. Regulation of postsynaptic AMPA responses by synaptojanin 1. *Proceedings of the National Academy of Sciences,* **105,** 17561-17566.

Han B-K & Emr SD. 2011. Phosphoinositide [PI(3,5)P2] lipid-dependent regulation of the general transcriptional regulator Tup1. *Genes & Development,* **25,** 984-995.

Hirano T, Matsuzawa T, Takegawa K & Sato MH. 2011. Loss-of-function and gain-of-function mutations in FAB1A/B impair endomembrane homeostasis, conferring pleiotropic developmental abnormalities in arabidopsis. *Plant Physiology,* **155,** 797-807.

Hirano T & Sato MH. 2011. Arabidopsis FAB1A/B is possibly involved in the recycling of auxin transporters. *Plant Signaling & Behavior,* **6**.

Horton AC, Rácz B, Monson EE, Lin AL, Weinberg RJ & Ehlers MD. 2005. Polarized Secretory Trafficking Directs Cargo for Asymmetric Dendrite Growth and Morphogenesis. *Neuron,* **48,** 757-771.

Huettner JE & Bean BP. 1988. Block of N-methyl-D-aspartate-activated current by the anticonvulsant MK-801: selective binding to open channels. *Proceedings of the National Academy of Sciences of the United States of America,* **85,** 1307-11.

Ibáñez CF. 2007. Message in a bottle: long-range retrograde signaling in the nervous system. *Trends in Cell Biology,* **17,** 519-528.

Ikonomov OC, Sbrissa D, Delvecchio K, Xie Y, Jin J-P, Rappolee D & Shisheva A. 2011. The phosphoinositide kinase PIKfyve is vital in early embryonic development: Preimplantation lethality of PIKfyve-/- embryos but normality of PIKfyve+/- mice. *The Journal of Biological Chemistry*.

Ikonomov OC, Sbrissa D, Fenner H & Shisheva A. 2009. PIKfyve-ArPIKfyve-Sac3 core complex: contact sites and their consequence for Sac3 phosphatase activity and endocytic membrane homeostasis. *The Journal of Biological Chemistry,* **284,** 35794-35806.

Ikonomov OC, Sbrissa D, Fligger J, Delvecchio K & Shisheva A. 2010. ArPIKfyve regulates Sac3 protein abundance and turnover: disruption of the mechanism by Sac3I41T mutation causing Charcot-Marie-Tooth 4J disorder. *The Journal of Biological Chemistry,* **285,** 26760-26764.

Ikonomov OC, Sbrissa D, Foti M, Carpentier J-L & Shisheva A. 2003. PIKfyve controls fluid phase endocytosis but not recycling/degradation of endocytosed receptors or sorting of procathepsin D by regulating multivesicular body morphogenesis. *Molecular Biology of the Cell,* **14,** 4581-4591.

Ikonomov OC, Sbrissa D & Shisheva A. 2001. Mammalian cell morphology and endocytic membrane homeostasis require enzymatically active phosphoinositide 5-kinase PIKfyve. *The Journal of Biological Chemistry,* **276,** 26141-26147.

Ippolito DM & Eroglu C. 2010. Quantifying synapses: an immunocytochemistry-based assay to quantify synapse number. *Journal of Visualized Experiments: JoVE*.

Jefferies HBJ, Cooke FT, Jat P, Boucheron C, Koizumi T, Hayakawa M, Kaizawa H, Ohishi T, Workman P, Waterfield MD & Parker PJ. 2008. A selective PIKfyve inhibitor blocks PtdIns(3,5)P(2) production and disrupts endomembrane transport and retroviral budding. *EMBO Reports,* **9,** 164-170.

Jin N, Chow CY, Liu L, Zolov SN, Bronson R, Davisson M, Petersen JL, Zhang Y, Park S, Duex JE, Goldowitz D, Meisler MH & Weisman LS. 2008. VAC14 nucleates a protein complex essential for the acute interconversion of PI3P and PI(3,5)P(2) in yeast and mouse. *The EMBO Journal,* **27,** 3221-3234.

Katona I, Zhang X, Bai Y, Shy ME, Guo J, Yan Q, Hatfield J, Kupsky WJ & Li J. 2011. Distinct pathogenic processes between Fig4-deficient motor and sensory neurons. *The European Journal of Neuroscience*.

Kennedy MJ & Ehlers MD. 2006. Organelles and trafficking machinery for postsynaptic plasticity. *Annual Review of Neuroscience,* **29,** 325-362.

Kopec CD, Li B, Wei W, Boehm J & Malinow R. 2006. Glutamate receptor exocytosis and spine enlargement during chemically induced long-term potentiation. *The Journal of neuroscience: the official journal of the Society for Neuroscience,* **26,** 2000-2009.

Kristelly R, Gao G & Tesmer JJG. 2004. Structural Determinants of RhoA Binding and Nucleotide Exchange in Leukemia-associated Rho Guanine-Nucleotide Exchange Factor. *Journal of Biological Chemistry,* **279,** 47352-47362.

Lasiecka ZM & Winckler B. 2011. Mechanisms of polarized membrane trafficking in neurons - Focusing in on endosomes. *Molecular and Cellular Neurosciences*.

Lee HW, Kim Y, Han K, Kim H & Kim E. 2010. The Phosphoinositide 3-Phosphatase MTMR2 Interacts with PSD-95 and Maintains Excitatory Synapses by Modulating Endosomal Traffic. *J. Neurosci.,* **30,** 5508-5518.

Lemaire J-F & McPherson PS. 2006. Binding of Vac14 to neuronal nitric oxide synthase: Characterisation of a new internal PDZ-recognition motif. *FEBS Letters,* **580,** 6948-6954.

Lenk GM, Ferguson CJ, Chow CY, Jin N, Jones JM, Grant AE, Zolov SN, Winters JJ, Giger RJ, Dowling JJ, Weisman LS & Meisler MH. 2011. Pathogenic Mechanism of the FIG4 Mutation Responsible for Charcot-Marie-Tooth Disease CMT4J. *PLoS Genetics,* **7,** e1002104-e1002104.

Lu W, Shi Y, Jackson AC, Bjorgan K, During MJ, Sprengel R, Seeburg PH & Nicoll RA. 2009. Subunit composition of synaptic AMPA receptors revealed by a single-cell genetic approach. *Neuron,* **62,** 254-268.

Martin LJ. 2010. Mitochondrial and Cell Death Mechanisms in Neurodegenerative Diseases. *Pharmaceuticals (Basel, Switzerland),* **3,** 839-915.

Nicholson G, Lenk GM, Reddel SW, Grant AE, Towne CF, Ferguson CJ, Simpson E, Scheuerle A, Yasick M, Hoffman S, Blouin R, Brandt C, Coppola G, Biesecker LG, Batish SD & Meisler MH. 2011. Distinctive genetic and clinical features of CMT4J: a severe neuropathy caused by mutations in the PI(3,5)P2 phosphatase FIG4. *Brain: A Journal of Neurology,* **134,** 1959-1971.

Osborne SL, Wen PJ, Boucheron C, Nguyen HN, Hayakawa M, Kaizawa H, Parker PJ, Vitale N & Meunier FA. 2008. PIKfyve negatively regulates exocytosis in neurosecretory cells. *The Journal of Biological Chemistry,* **283,** 2804-2813.

Rosenmund C, Clements JD & Westbrook GL. 1993. Nonuniform probability of glutamate release at a hippocampal synapse. *Science (New York, N.Y.),* **262,** 754-757.

Roth MG. 2004. Phosphoinositides in constitutive membrane traffic. *Physiological Reviews,* **84,** 699-730.

Rothman SM & Olney JW. 1986. Glutamate and the pathophysiology of hypoxic--ischemic brain damage. *Annals of Neurology,* **19,** 105-111.

Rothstein JD, Martin LJ & Kuncl RW. 1992. Decreased glutamate transport by the brain and spinal cord in amyotrophic lateral sclerosis. *The New England Journal of Medicine,* **326,** 1464-1468.

Rudge SA, Anderson DM & Emr SD. 2004. Vacuole size control: regulation of PtdIns(3,5)P2 levels by the vacuole-associated Vac14-Fig4 complex, a PtdIns(3,5)P2-specific phosphatase. *Molecular Biology of the Cell,* **15,** 24-36.

Rusten TE, Vaccari T, Lindmo K, Rodahl LMW, Nezis IP, Sem-Jacobsen C, Wendler F, Vincent J-P, Brech A, Bilder D & Stenmark H. 2007. ESCRTs and Fab1 regulate distinct steps of autophagy. *Current Biology: CB,* **17,** 1817-1825.

Rutherford AC, Traer C, Wassmer T, Pattni K, Bujny MV, Carlton JG, Stenmark H & Cullen PJ. 2006. The mammalian phosphatidylinositol 3-phosphate 5-kinase (PIKfyve) regulates endosome-to-TGN retrograde transport. *Journal of Cell Science,* **119,** 3944-3957.

Saksena S, Sun J, Chu T & Emr SD. 2007. ESCRTing proteins in the endocytic pathway. *Trends in Biochemical Sciences,* **32,** 561-573.

Sbrissa D, Ikonomov OC, Filios C, Delvecchio K & Shisheva A. 2012. Functional dissociation between PIKfyve-synthesized PtdIns5P and PtdIns(3,5)P2 by means of the PIKfyve inhibitor YM201636. *American journal of physiology. Cell physiology*.

Sbrissa D, Ikonomov OC & Shisheva A. 1999. PIKfyve, a mammalian ortholog of yeast Fab1p lipid kinase, synthesizes 5-phosphoinositides. Effect of insulin. *The Journal of Biological Chemistry,* **274,** 21589-21597.

Shen J, Yu W-M, Brotto M, Scherman JA, Guo C, Stoddard C, Nosek TM, Valdivia HH & Qu C-K. 2009. Deficiency of MIP/MTMR14 phosphatase induces a muscle disorder by disrupting Ca(2+) homeostasis. *Nature Cell Biology,* **11,** 769-776.

Sieburth D, Ch'ng Q, Dybbs M, Tavazoie M, Kennedy S, Wang D, Dupuy D, Rual J-F, Hill DE, Vidal M, Ruvkun G & Kaplan JM. 2005. Systematic analysis of genes required for synapse structure and function. *Nature,* **436,** 510-517.

Song I & Huganir RL. 2002. Regulation of AMPA receptors during synaptic plasticity. *Trends in Neurosciences,* **25,** 578-588.

Tochio H, Mok YK, Zhang Q, Kan HM, Bredt DS & Zhang M. 2000. Formation of nNOS/PSD-95 PDZ dimer requires a preformed beta-finger structure from the nNOS PDZ domain. *Journal of Molecular Biology,* **303,** 359-370.

Tronchère H, Laporte J, Pendaries C, Chaussade C, Liaubet L, Pirola L, Mandel JL & Payrastre B. 2004. Production of Phosphatidylinositol 5-Phosphate by the Phosphoinositide 3-Phosphatase Myotubularin in Mammalian Cells. *Journal of Biological Chemistry,* **279,** 7304-7312.

Tsuruta F, Green EM, Rousset M & Dolmetsch RE. 2009. PIKfyve regulates CaV1.2 degradation and prevents excitotoxic cell death. *J Cell Biol,* **187,** 279-294.

Turrigiano GG. 2008. The self-tuning neuron: synaptic scaling of excitatory synapses. *Cell,* **135,** 422-435.

Yin HL & Janmey PA. 2003. Phosphoinositide regulation of the actin cytoskeleton. *Annual Review of Physiology,* **65,** 761-789.

Zhang X, Chow CY, Sahenk Z, Shy ME, Meisler MH & Li J. 2008. Mutation of FIG4 causes a rapidly progressive, asymmetric neuronal degeneration. *Brain: A Journal of Neurology,* **131,** 1990-2001.

Zhang Y, Zolov SN, Chow CY, Slutsky SG, Richardson SC, Piper RC, Yang B, Nau JJ, Westrick RJ, Morrison SJ, Meisler MH & Weisman LS. 2007. Loss of Vac14, a regulator of the signaling lipid phosphatidylinositol 3,5-bisphosphate, results in neurodegeneration in mice. *Proceedings of the National Academy of Sciences of the United States of America,* **104,** 17518-17523.

CHAPTER 3

ACTIVITY-DEPENDENT PI(3,5)P_2 SYNTHESIS CONTROLS AMPA RECEPTOR TRAFFICKING DURING SYNAPTIC DEPRESSION

3.1 SUMMARY

Dynamic regulation of phosphoinositide lipids (PIPs) is crucial for diverse cellular functions and, in neurons, is particularly important for controlling membrane trafficking at the synapse. Indeed, multiple neurological disorders are linked to mutations in PIP-related genes, suggesting that these signaling lipids are crucial for neuronal function. However, the regulation of PIPs in neurons remains poorly understood. In particular, little is known about PI(3,5)P_2, which is implicated in epilepsy, severe neuropathy and neurodegeneration. Notably, the PI(3,5)P_2 synthesis complex is highly enriched at synapses, raising the possibility that the dynamic regulation of synaptic PI(3,5)P_2 levels has a major impact on synaptic function and plasticity. Here, we present novel methods to detect and control PI(3,5)P_2 synthesis in neurons. We observe activity-dependent regulation of multiple PIPs and, surprisingly, PI(3,5)P_2 was among the most dynamic. Elevation of PI(3,5)P_2 occurs during two distinct forms of synaptic depression, and manipulation of PI(3,5)P_2 levels is sufficient to bidirectionally control synapse strength. Moreover, blocking PI(3,5)P_2 synthesis prevents or reverses synaptic depression, in part, by altering AMPA-type glutamate receptor trafficking. Taken together, our results identify the activity-dependent synthesis of PI(3,5)P_2 as a novel mechanism for

regulating synapse strength and suggest that synaptic dysfunction may contribute to the pathogenesis of neurological diseases arising from loss of dynamic PI(3,5)P_2 regulation.

3.2 INTRODUCTION

Phosphorylated phosphoinositide lipids (PIPs) are minor components of the cytosolic side of membranes and key regulators of diverse cellular processes including cell signaling, membrane trafficking, cytoskeletal rearrangements, ion homeostasis and organelle biogenesis (reviewed in (Yin and Janmey, 2003, Di Paolo and De Camilli, 2006, Balla, 2013)). Seven interconvertible PIP species, each with unique roles, are synthesized and turned over through specific sets of highly regulated lipid kinases and phosphatases. Through binding of downstream protein effectors, PIP signaling is thought to assemble complex protein machines at specific membrane subdomains, which enables PIPs to have tight control of cellular processes in space and time. Such precision is likely critical for complex cellular functions, including regulation of synaptic strength in the central nervous system.

Defects in PIP biosynthesis and signaling are implicated in multiple neurological disorders, including Down syndrome (Arai et al., 2002, Cossec et al., 2012), Alzheimer's disease (Stokes and Hawthorne, 1987, Zubenko et al., 1999, Harold et al., 2009, Naj et al., 2011), epilepsy (Krebs et al., 2013, Baulac et al., 2014), schizophrenia (Jungerius et al., 2008, Vorstman et al., 2009), and neuropathies (Bolino et al., 2000, Houlden et al., 2001, Azzedine et al., 2003, Senderek et al., 2003, Chow et al., 2007, Nicholson et al., 2011). Even perturbations of a low abundant PIP - PI(3,5)P_2 - have profound effects on human physiology. For example, mutations in *FIG4*, a positive regulator of PI(3,5)P_2, are

known to cause at least four human diseases. Homozygous null mutations in *FIG4* cause Yunis-Varon syndrome, an autosomal-recessive disorder that affects multiple systems and causes infantile death (Campeau et al., 2013). Partial loss of function mutations cause a severe peripheral neuropathy, Charcot Marie-Tooth type 4J (CMT4J) (Chow et al., 2007, Nicholson et al., 2011). Heterozygous point mutations may be a risk factor for amyotrophic lateral sclerosis (ALS) and primary lateral sclerosis (PLS) (Chow et al., 2009). Recently, a homozygous missense mutation in *FIG4* was identified as the causal gene in a consanguineous Moroccan family with multiple neurological disorders including temporo-occipital polymicrogryria, epilepsy and psychiatric indications (Baulac et al., 2014).

Impairments in the highly conserved PI(3,5)P_2 synthesis complex are linked to pleiotropic defects (reviewed in (McCartney et al., 2014)). This complex includes the lipid kinase, Fab1 (PIKfyve, in mammals) (Yamamoto et al., 1995, Gary et al., 1998, Cooke et al., 1998, Zolov et al., 2012), the lipid phosphatase, Fig4, and scaffolding protein, Vac14 (Rudge et al., 2004, Chow et al., 2007, Zhang et al., 2007, Jin et al., 2008, Botelho et al., 2008, Ikonomov et al., 2009). Fab1/PIKfyve is the sole kinase responsible for the synthesis of PI(3,5)P_2 from PI3P. In mammalian cells, the pools of PI3P that are converted to PI(3,5)P_2 have not been resolved and may include PI3P synthesized from PI by the Class III PI 3-kinase, VSP34 (Whiteford et al., 1997), the Class II PI 3-kinase, C2α (Bridges et al., 2012), or both. The lipid phosphatase, Fig4, can convert PI(3,5)P_2 to PI3P *in vitro* (Rudge et al., 2004), yet also functions as a positive regulator of Fab1/PIKfyve. Genetic loss of Fig4 decreases the levels of PI(3,5)P_2 by 50% (Chow et al., 2007). Mice

lacking Fig4 die early and have profound neurodegeneration (Chow et al., 2007). Moreover, the loss of PIKfyve in mice results in embryonic lethality as early as E3.5 (Ikonomov et al., 2011) or E8.5 (Takasuga et al., 2013). Further analysis of multiple organs *in vivo* in mouse models with reduced $PI(3,5)P_2$ levels revealed widespread defects beyond the nervous system, indicating that $PI(3,5)P_2$ is likely important for most cell types (Chow et al., 2007, Zolov et al., 2012, Takasuga et al., 2013).

The dynamic regulation of $PI(3,5)P_2$ levels in response to extracellular stimuli is likely critical for neural function, though upstream activators of the $PI(3,5)P_2$ synthesis complex and downstream targets of $PI(3,5)P_2$ are largely unknown. One stimulus, hyperosmotic stress in yeast, is known to evoke a transient elevation and subsequent turnover of $PI(3,5)P_2$ levels (Dove et al., 1997, Duex et al., 2006). Diverse external cues, such as hormones, growth factors or neurotransmitters, are likely to induce dynamic regulation of $PI(3,5)P_2$ levels in multicellular organisms as well. In support of this hypothesis, analysis of the CMT4J disease mutation, Fig4-I>T, which is in a residue conserved with yeast Fig4, showed a specific impairment in stimulus induced increases in $PI(3,5)P_2$ without any effect on basal $PI(3,5)P_2$ levels in yeast (Chow et al., 2007). Thus, even subtle problems in the dynamic activation of the complex is likely critical for neural function.

At the synapse, signaling lipids play essential roles in presynaptic and postsynaptic function. Notably, $PI(4,5)P_2$-mediated regulation of endocytosis, exocytosis, actin dynamics and ion channel function are essential for neurotransmission (McPherson et al., 1996, Cremona et al., 1999, Haffner et al., 2000, Wenk et al., 2001, Kim et al., 2002,

Di Paolo et al., 2004, Irie et al., 2005, Saheki and De Camilli, 2012 Mani et al., 2007, Gong and De Camilli, 2008). The low abundant lipid PI(3,4,5)P_3 clusters membrane proteins both presynaptically (Khuong et al., 2013) and postsynaptically (Arendt et al., 2010), and postsynaptic strength is diminished by increased turnover of PI(3,4,5)P_3 by the lipid 3-phosphatase PTEN (Jurado et al., 2010). Moreover, the number of excitatory synapses is reduced in neurons lacking either MTMR2, a 3-phosphatase that acts on PI3P and PI(3,5)P_2 (Lee et al., 2010), or Vac14, a positive regulator of PI(3,5)P_2 synthesis(Zhang et al., 2012). Collectively, these results implicate multiple PIPs in regulation of synapse strength and emphasize the importance of developing strategies to detect and control each of these low abundant signaling lipids.

To determine the signaling lipids that are dynamically regulated by neural activity, we developed methods to measure the activity-dependent regulation of each PIP species in cultured hippocampal neurons. We identified multiple activity-dependent changes in PIP levels in response to either acute or sustained changes in neuronal activity. Notably, levels of PI(3,5)P_2 are highly dynamic and increase in response to conditions that drive NMDA receptor (NMDAR)-dependent long-term depression (LTD) or homeostatic synaptic weakening. A causal role for PI(3,5)P_2 dynamics in these processes was also identified. Increasing PI(3,5)P_2 levels using a dominant-active PIKfyve mutant (PIKfyve^{KYA}) is sufficient to weaken postsynaptic strength and homeostatic weakening is lost in neurons where PI(3,5)P_2 synthesis is diminished. Moreover, acute inhibition of PIKfyve rapidly reverses established homeostatic weakening. Roles for PI(3,5)P_2 synthesis in the regulation of synaptic plasticity derive in part from PI(3,5)P_2-

dependent trafficking of AMPA-type glutamate receptors to and from the plasma membrane. Together these findings demonstrate a critical role for $PI(3,5)P_2$ dynamics in maintaining changes in synaptic strength.

3.3 RESULTS

3.3.1 Homeostatic down regulation of synapse strength is lost in neurons defective in $PI(3,5)P_2$ synthesis

We previously found that loss of Vac14 leads to increased excitatory synapse strength in cultured hippocampal neurons and that this increase could be rescued by reintroduction of Vac14 into the knockout neurons (Zhang et al., 2012). These results raise the question of whether Vac14 and/or $PI(3,5)P_2$ signaling is involved in activity-dependent changes to synapse strength. To address this question, we focused initially on homeostatic synaptic plasticity, where neurons adapt to persistent changes in network activity through compensatory changes in synapse function that maintain levels of activity in a stable range (Davis, 2013). Given the basal increase in synapse strength in Vac14 KO neurons, we hypothesized that Vac14 is required for homeostatic synaptic plasticity. We first tested whether $Vac14^{-/-}$ on C57BL/6J background shares the elevation in synapse strength found previously on a "mixed" background (strain 129 and C57BL/6J) (Zhang et al., 2012). Then, we induced prolonged increases or decreases in the level of neural activity and monitored how synapses adapt to the change by measuring the amplitude of miniature excitatory postsynaptic currents (mEPSCs).

Consistent with our previous observations, the amplitude of in mEPSCs is increased in $Vac14^{-/-}$ relative to wild-type neurons in a C57BL/6J background (Figure 3-

1A-C). To test whether homeostatic plasticity was altered in Vac14$^{-/-}$ neurons, we incubated neurons with 2 µM tetrodotoxin (TTX) or 50 µM bicuculline (Bic) for 24 h to suppress or elevate activity, respectively. As expected, wild-type neurons exhibited a homeostatic increase in mEPSC amplitude following chronic activity deprivation with TTX. Vac14$^{-/-}$ neurons, despite larger basal mEPSC amplitudes, exhibited homeostatic synaptic strengthening that was indistinguishable from wild-type neurons (Figure 3- 1B and 1D). On the other hand, whereas chronically increasing network activity induced a significant decrease in mEPSC amplitude in wild-type neurons, Vac14$^{-/-}$ neurons failed to homeostatically downscale synaptic strength (Figure 3- 1B and 1D). Together these data suggest that Vac14 is required for homeostatic downscaling, but not for homeostatic upscaling. This fits with multiple studies that suggest that these two processes are controlled by independent mechanisms (reviewed in (Turrigiano, 2012, Chen et al., 2014, Pribiag and Stellwagen, 2014, Thalhammer and Cingolani, 2014, Lee et al., 2014, Siddoway et al., 2014)). Moreover, these data suggest that elevated mEPSC amplitude in Vac14$^{-/-}$ neurons may, in part, be due to defects in homeostatic downscaling in the face of hyperactivity.

3.3.2 PI(3,5)P_2 synthesis is required for maintenance of postsynaptic strength in cultured hippocampal neurons

Vac14 has no known functions outside of its role in the PI(3,5)P_2 synthesis complex. To directly test whether Vac14 impacts synapse strength directly through the synthesis of PI(3,5)P_2, we used wild-type mouse hippocampal cultured neurons and targeted the lipid kinase PIKfyve for RNAi knock-down using a lentiviral vector to express

a PIKfyve-targeting shRNA. One week after infection with PIKfyve shRNA, small vacuoles were apparent in pyramidal-like neurons, a phenotypic hallmark of decreased PI(3,5)P_2 levels in cells (Yamamoto et al., 1995, Bonangelino et al., 1997, Ikonomov et al., 2001, Zhang et al., 2007, Jefferies et al., 2008, Takasuga et al., 2013). Notably, the amplitude of mEPSCs in PIKfyve shRNA transduced neurons, compared with control or sham treated neurons, was significantly higher (Figure 3- 1 E and 1F). Thus, PIKfyve knockdown recapitulates the effect of genetic deletion of Vac14 on mEPSC amplitude suggesting that Vac14 acts through PIKfyve to regulate synapse strength. Together, these data suggest that PI(3,5)P_2 functions as a negative regulator of synaptic strength and raises the question of whether increasing PI(3,5)P_2 levels has the opposite effect.

3.3.3 Increasing PI(3,5)P_2 levels causes synaptic depression in cultured hippocampal neurons

A common approach for increasing the levels of specific metabolites in cells is to overexpress the enzyme required for their synthesis. However, in yeast, overexpression of Fab1 (homolog of mammalian PIKfyve) does not increase PI(3,5)P_2 levels (Gary et al., 1998). To measure the impact on PIP levels of overexpressing PIKfyve, we generated two doxycycline inducible stable cells line using the Flp-In™ T-Rex™-293 system (Invitrogen) with 3XFLAG-Citrine-PIKfyve or a 3XFLAG control. After 24 h of induction, 3XFLAG-Citrine-PIKfyve is expressed approximately 16-fold above the levels of endogenous PIKfyve (Figure 3- 2A). Despite this strong overexpression, we found no change in the levels of any PIP species, including PI(3,5)P_2 (Figure 3- 2B). Thus, overexpressing PIKfyve alone is insufficient to increase PI(3,5)P_2 levels.

We had previously identified dominant mutations in yeast Fab1 that resulted in a several fold elevation in PI(3,5)P_2 (Duex et al., 2006). Two of these mutants, Fab1-E1822K,N1832Y and Fab1-E1822V,F1833L,T2250, were mutated in conserved residues (Figure 3- 2C), which suggested that a dominant active mammalian PIKfyve could be generated. Indeed, we generated and tested the PIKfyve^{KYA} (E1620K, N1630Y, S2068A) dominant active mutant and found induction of this mutant protein to levels 4-fold above endogenous PIKfyve increased PI(3,5)P_2 approximately 4-fold (Figure 3- 2B). Consistent with a precursor-product relationship, the dominant active mutant also increased the levels of PI5P 2-fold (Figure 3- 2B). To test the impact of increasing the levels of PI(3,5)P_2 on synapse function, we transfected postnatal rat cultured hippocampal neurons with dominant active Citrine-PIKfyve^{KYA} or, as a control, wild-type Citrine-PIKfyve. We compared the amplitude of mEPSCs in transfected neurons to nontransfected neighbors. In Citrine-PIKfyve^{KYA} neurons, the average amplitude of mEPSCs is reduced compared to both neighboring non-transfected neurons in the same culture and wild-type Citrine-PIKfvye expressing neurons in sister cultures (Figure 3- 2D and 2E). Taken together, our data suggest that PIKfyve activity is inversely correlated with postsynaptic strength. That basal synapse function did not change with overexpression of wild-type PIKfyve alone suggests that PI(3,5)P_2 rather than PIKfyve protein levels are important for modulating the strength of synapses.

3.3.4 PIP levels are dynamic in neurons

3.3.4.1 Detection of PIP species in cultured neurons

Little is known about the physiological processes that cause dynamic changes in $PI(3,5)P_2$ levels in mammalian cells. The link between defects in dynamic changes in $PI(3,5)P_2$ synthesis and neurological disease highlight the importance of developing methods to probe dynamic changes in PIP levels in neurons. To this end, we adapted methods designed for fibroblasts, to detect PIP species in post-mitotic cells. Briefly, cultured rat hippocampal neurons were metabolically labeled with myo-[2-^{3}H]-inositol for 24 h. Cells were precipitated by perchloric acid and the resultant precipitate treated with weak base to deacylate lipids. Following deacylation, water soluble glycerol-inositol poly-phosphates were separated by chromatography on an ion exchange column. In cultured hippocampal neurons (DIV 21), peaks representing all seven PIP species were observed, including $PI(3,5)P_2$ and PI5P. We do not report the levels of $PI(3,4)P_2$, which was observed in some samples but was often below detection levels (<0.01% of PI). Compared to mouse embryonic fibroblasts (MEF) cells (Zolov et al., 2012) neurons have 5-fold more PI4P, 3-fold more $PI(4,5)P_2$, slightly more $PI(3,4,5)P_3$ and half the levels of $PI(3,5)P_2$ (Figure 3- 3-figure supplement 1). The high levels of PI4P and $PI(4,5)P_2$ are likely due to the extensive plasma membrane, endoplasmic reticulum (ER) and abundance of somatic and dendritic Golgi in neurons.

3.3.4.2 PIPs are dynamically regulated by neuronal activity

To identify PIP species that dynamically respond to neural activity and test for activity-dependent synthesis of $PI(3,5)P_2$, we compared PIP levels in spontaneously

active neuronal cultures to those where we acutely increased or decreased network activity. Specifically, we applied 2 μM TTX for 10 min to block action potentials, 50 μM bicuculline for 1 min to enhance firing by removing inhibitory tone or 20 μM NMDA for 1 min to strongly activate NMDARs and drive glutamate receptor endocytosis (Figure 3-3A). Most PIP species did not change significantly in response to acute changes in activity (Figure 3- 3B). However, the levels of $PI(3,5)P_2$ significantly increased with 1 min 20 μM NMDA stimulation.

In addition, we tested activity-dependent changes in PIPs over longer time-scales using stimuli that are known to engage homeostatic synaptic control mechanisms. We reasoned that similar to synapse strength, PIPs involved in homeostatic synaptic plasticity might be bidirectionally regulated by chronic activity suppression or hyperactivation. However, we found no bidirectional changes in PIPs (Figure 3- 4B). Instead, we observed three significant unidirectional changes in PIPs. Following 24 h activity suppression with TTX, the levels of both PI4P and $PI(4,5)P_2$ decreased, but neither of these significantly increased during chronic activity elevation with bicuculline. By contrast, the most dramatic change observed was in the levels of $PI(3,5)P_2$, which significantly increased during chronic network hyperactivation, but did not significantly change during chronic activity suppression (Figure 3- 4B). These results, combined with the finding that defects in $PI(3,5)P_2$ synthesis disrupt homeostatic downscaling but not upscaling, are consistent with a selective role for $PI(3,5)P_2$ in homeostatic synaptic weakening. The changes in PI4P and $PI(4,5)P_2$ are potentially interesting as well, and

analysis of these species in future studies may shed additional light on mechanisms governing homeostatic synaptic strengthening.

To independently test for changes in $PI(3,5)P_2$ and determine whether there were specific subcellular locations where its synthesis occurs during homeostatic down-scaling, we monitored a fluorescent probe for $PI(3,5)P_2$ under periods of normal or hyperactive network activity. The reporter - mCherry-ML1N*2 - is mCherry fused to a tandem duplication of the $PI(3,5)P_2$ binding domain of TRPML1 and has been previously validated (Li et al., 2013). We found that relative to conditions of basal neural activity chronic hyperactivity induced by bicuculline produced a robust increase in dendritic reporter intensity (Figure 3- 4C). To normalize for differences in expression levels, we analyzed the average intensity of mCherry-ML1N*2 in the dendrite relative to the soma and found network hyperactivation increased this ratio (Figure 3- 4D). These data are consistent with the increased $PI(3,5)P_2$ levels detected by HPLC following homeostatic synaptic weakening (Figure 3- 4B) and suggest that a component of the rise in $PI(3,5)P_2$ level is due to new synthesis in dendrites during synaptic depression.

Together, these data suggest that an increase in $PI(3,5)P_2$ synthesis accompanies conditions that lead to depression of synaptic strength. To test this relationship further, we examined PIP levels during another form of functional synapse weakening, NMDAR-dependent chemical long term-depression (cLTD), using an established NMDAR-cLTD induction protocol (Lee et al., 1998, Fernandez-Monreal et al., 2012). We analyzed PIP levels at time-points during the stimulus (30 sec, 1 min, 2 min, 3 min, 5 min) and after cLTD induction (15 and 35 min) (Figure 3- 5A). The levels of PIPs in treated neurons were

compared to the average levels of unstimulated sister cultures at the 0 time point (Figure 3- 5B) and neurons that were sham stimulated (no NMDA, 35 min) (Figure 3- 5C). We found dynamic changes in the levels of multiple PIPs (Figure 3- 5C). Most of the changes occurred during the NMDA stimulation. At the latest time point examined the levels of each PIP were similar to sham stimulated at the 30 minute time point, except for elevated PI(3,4,5)P_3. PI(3,4,5)P_3 rapidly increases almost 50% within 30 seconds of the cLTD stimulus, which was then sustained at the 30 minute time point. Two of the most abundant PIPs, PI4P and PI(4,5)P_2 show transient increases and decreases during NMDA stimulation but not in a consistent direction. Interestingly, the 20-25% decrease in PI(4,5)P_2 levels at 10 min relative to unstimulated or sham samples is consistent with regulation of PI(4,5)P_2 formation in response to NMDAR activation (Horne and Dell'Acqua, 2007, Unoki et al., 2012). Note that for PIPs that are generated in multiple neuronal locations, measurements of total PIP levels may not be sufficient to detect important location-specific changes.

Importantly, among all the PIP species, PI(3,5)P_2 had the most dynamic response during cLTD induction (Figure 3- 3C). During the induction period, PI(3,5)P_2 rapidly rose in the first 3 min and then returned to baseline levels within 5 min. At 10 min post induction, PI(3,5)P_2 levels decreased to below basal levels. Consistent with a transient elevation in PI(3,5)P_2 levels, PI3P levels were stable for 1 min, then dropped by ~20% and remained reduced for 2-10 min. We also observed a depression in PI5P levels concomitant with the increase in PI(3,5)P_2 levels. This may be due to transient uncoupling of the 3-phosphatase that normally converts PI(3,5)P_2 to PI5P. Together, our

results demonstrate that induction of cLTD regulates multiple PIPs and supports the hypothesis that dynamic PIP metabolism is critical for synaptic depression.

3.3.5 PIKfyve inhibition blocks induction of chemical LTD

Given that transient elevation in the levels of $PI(3,5)P_2$ accompanies the induction of cLTD (Figure 3- 5), we tested a causal role for $PI(3,5)P_2$ dynamic synthesis by inhibiting PIKfyve during cLTD induction. We utilized two PIKfyve inhibitors: YM201636 (Jefferies et al., 2008) and apilimod (Cai et al., 2013), which rapidly and specifically block PIKfyve activity. Similar to YM201636 (Zolov et al., 2012), 1 μM apilimod decreases $PI(3,5)P_2$ levels by more than 50% in 2.5 min and 70% by 5 min (Figure 3- 6-figure supplement 2A). Neurons were treated with YM201636 (2 μM) or apilimod (1 μM) for 2.5 min before and during the 5 min cLTD stimulus (7.5 min total). Neurons were then returned to media without PIKfyve inhibitors for an additional 30 min prior to electrophysiological recordings. As expected, mEPSC amplitude was decreased after the cLTD stimulus in the absence of PIKfyve inhibitors (Figure 3- 6A and 6B). By contrast, the presence of either YM201636 or apilimod during the 5 min cLTD stimulus prevented induction of enduring synaptic depression (Figure 3- 6A and 6B). Thus, synthesis of $PI(3,5)P_2$ during induction of LTD is necessary for the sustained depression of synaptic strength.

3.3.6 Acute PIKfyve inhibition reverses established homeostatic changes in synaptic strength

Unlike cLTD induction, homeostatic downscaling is associated with a persistent increase in $PI(3,5)P_2$ levels (Figure 3- 4B and 4C) at a time in which compensatory

synaptic adaptations have already been established (O'Brien et al., 1998, Turrigiano et al., 1998, Maffei and Turrigiano, 2008, Yu and Goda, 2009, Jakawich et al., 2010). Given that Vac14$^{-/-}$ neurons fail to express homeostatic synaptic scaling in response to hyper-excitation (Figure 3- 1B and 1D) and that elevation of PI(3,5)P_2 levels leads to reductions in excitatory synaptic strength (Figure 3- 2D and 2E), we hypothesized that the changes in PI(3,5)P_2 following chronic hyperactivity play a direct role in maintaining synaptic depression. If so, then acute blockade of PI(3,5)P_2 synthesis may be sufficient to rapidly reverse homeostatic downscaling after it has been established. To test this prediction, we acutely blocked PI(3,5)P_2 production (1 μM apilimod or 2 μM YM201636) in cultured rat hippocampal neurons for 1 h. Under control conditions, neither inhibitor significantly increased mEPSC amplitude (Figure 3- 6C and 6D). Thus, acute inhibition of PIKfyve activity may not be sufficient to impact synaptic AMPA receptors under basal activity conditions. Notably, however, when neurons were treated for the previous 24 h with bicuculline to induce homeostatic synaptic weakening, PIKfyve inhibition completely reversed down-scaling of mEPSC amplitude within 60 min (Figure 3- 6C and 6D). Together, these data suggest that the maintenance of synaptic adaptations induced by network hyperactivity requires PIKfyve activity.

The trafficking of AMPA-type glutamate receptors (AMPARs) is critical for many enduring forms of synaptic plasticity (Malinow and Malenka, 2002, Anggono and Huganir, 2012, Henley and Wilkinson, 2013), and multiple groups (including ours) have found that AMPAR trafficking is sensitive to PIKfyve activity (Tsuruta et al., 2009, Zhang et al., 2012, Seebohm et al., 2012). A signature of homeostatic synaptic plasticity

induced by chronic changes in network activity is the bi-directional regulation of surface AMPAR expression, where chronic network hyperactivity drives reduced surface expression of the AMPAR subunits GluA1 and GluA2 (O'Brien et al., 1998, Cingolani et al., 2008, Jakawich et al., 2010, Hu et al., 2010, Evers et al., 2010, Lee et al., 2011). Therefore, we tested whether PIKfyve inhibition reverses homeostatic down scaling by impacting the surface levels of AMPA receptors. Surface GluA2 (sGluA2) subunits were detected with an amino-terminal antibody under non-permeabilization conditions followed by permeabilization and detection of the excitatory synaptic scaffolding molecule PSD95. Consistent with previous reports, we found that sGluA2 expression is significantly reduced during homeostatic downscaling induced by 24 h bicuculline treatment (Figure 3- 6E & 6F). We also found that this period of hyperactivity did not impact the total levels of PSD95 (Figure 3- 6-figure supplement 2B), which is also consistent with previous results from hippocampal neurons ((Jakawich et al., 2010) but see (Sun and Turrigiano, 2011)). Notably, sGluA2 expression in bicuculline-treated neurons was rapidly restored to baseline levels by PIKfyve inhibition for 60 min with either YM201636 or apilimod (Figure 3- 6E and 6F). Under basal activity conditions, the same course of apilimod treatment did not alter sGluA2 expression (Figure 3- 6-figure supplement 2C), demonstrating that the restoration of sGluA2 levels by PIKfyve inhibition, in this case, is specific for homeostatic downscaling. However, we did observe that 60 min YM201636 treatment was effective in increasing sGluA2 in control neurons, suggesting that 60 min of PIKfyve inhibition can favor enhanced surface expression of AMPARs under basal levels of activity. Together, these results suggest that the increase

in $PI(3,5)P_2$ levels during homeostatic downscaling plays a direct role in maintaining weakened synaptic strength via effects on surface AMPAR dynamics. In addition, these findings suggest that the increase in postsynaptic strength observed in mouse models with diminished $PI(3,5)P_2$ levels, such as the $Vac14^{-/-}$ mouse (Zhang et al., 2012) (Figure 3- 1C), may be due in part to a persistent inability to homeostatically adjust synaptic strength during periods of hyperactivity.

3.3.7 AMPA receptor trafficking at the plasma membrane is sensitive to PIKfyve activity

Fluorescence recovery of pHluorin-GluA2(Q) is enhanced by PIKfyve inhibition

The results described above reveal a direct relationship between PIKfyve activity and AMPAR trafficking in synaptic plasticity. This raises the question of what specific GluA2 trafficking steps are controlled by PIKfyve activity. To gain insight into this question we screened for an impact of PIKfyve inhibition on AMPA receptor trafficking in neurons by exogenously expressing AMPA receptor subunits tagged with the pH-sensitive GFP variant pHluorin, pH-GluA1 or pH-GluA2(Q). pHluorin is fluorescent at neutral pH and is quenched in acidic environments. Thus, changes in the abundance of surface exposed pH-GluAs can be detected as a change in fluorescence intensity. Note, we used pH-GluA2(Q) to minimize contamination from the ER (Rathje et al., 2013).

Initially, we tested the effect of acute PIKfyve inhibition on steady-state fluorescence and found no change compared to baseline levels (data not shown). To widen the scope of this analysis, neurons were treated for 1 h with YM201636 or apilimod and then stimulated with 20 µM NMDA to drive endocytosis of AMPA

receptors in the continuous presence of inhibitors. Of note, this NMDA stimulation does not lead to persistent loss of AMPARs as in the case of cLTD, but rather drives a transient loss of surface receptors through endocytosis that is restored over time by recycling back to the plasma membrane. Indeed, while 5 min of NMDA stimulation strongly decreased pHluorin fluorescence by approximately 60%, surface fluorescence slowly reappeared over the next 45 min due to recycling of AMPARs back to the cell surface (Figure 3- 7A and 7B). We found that PIKfyve inhibition with either YM201636 or apilimod specifically enhanced the recovery rate of pH-GluA2(Q) fluorescence, yet these inhibitors had no detectable impact on the dynamics of pH-GluA1 (Figure 3- 7C and 7D). Subunit specific trafficking of AMPA receptors has been previously observed in a variety of contexts by multiple groups (Man et al., 2000, Shi et al., 2001, Lee et al., 2004, Shepherd et al., 2006, Cingolani et al., 2008, Anggono et al., 2011). Of particular relevance, there is evidence that the coordinate loss of surface GluA1 and GluA2 during slow homeostatic downscaling requires subunit-specific trafficking events controlled by the GluA2 subunit (Gainey et al., 2009, Goold and Nicoll, 2010). Thus, our results are consistent with the idea that PIKfyve activity selectively impacts the GluA2 subunit to control the surface expression of AMPARs.

3.3.7.1 PIKfyve inhibition favors surface expression of endogenous GluA2 containing AMPARs

To determine whether the effects of PIKfyve inhibition on pH-GluA2 (Q) dynamics reflect a role for PIKfyve in native AMPAR trafficking, we measured surface expression of endogenous GluA2 using immunocytochemistry. Using NMDA stimulation

to drive AMPA receptor endocytosis, we determined the ratio of surface to internal GluA2 using an amino-terminal antibody without or with permeabilization, respectively. In control neurons, NMDA stimulation for 5 min reduced the ratio of surface to internal GluA2, but pretreatment with apilimod for 1 h blocked this NMDA-induced decrease in sGluA2 (Figure 3- 7E and 7F). Thus, PIKfyve activity may be required for GluA2 endocytosis. Alternatively, given that this NMDA regimen induces only a transient loss of surface AMPARs, these effects could reflect a situation where inhibition of PIKfyve results in a more rapid return of internalized receptors to the surface.

To determine whether PIKfyve activity has additional roles in GluA2 trafficking beyond the acute response to NMDA stimulation, we limited PIKfyve inhibition to time points after NMDAR activation. Neurons were first stimulated with NMDA for 5 min without PIKfyve inhibition and then incubated with 1 μM apilimod for 10 or 30 min. In control neurons, the intensity of sGluA2 after NMDA stimulation compared to unstimulated sister cultures was still decreased at the 10 min time point but returned to basal levels by 30 min (Figure 3- 7G and 7H). By contrast, inhibition of PIKfyve after NMDA stimulation resulted in the rapid return of sGluA2 to baseline levels within 10 min and sGluA2 expression remained stable at the 30 min time point. Together, these results suggest that a target of PIKfyve activity is the GluA2 subunit of AMPA receptors and that PIKfyve inhibition impacts multiple AMPAR trafficking steps, which collectively result in enrichment of AMPARs on the cell surface. Thus, PIKfyve activity is important for GluA2 trafficking during NMDA stimulation and then continues to play a critical role in the

subsequent membrane trafficking of AMPARs during the recycling of internalized receptor pools.

3.4 DISCUSSION

Phosphoinositide lipids play crucial roles in membrane trafficking and cell signaling in eukaryotic cells, but many of the pathways that are regulated by these lipids are unknown. Moreover, in many cases, little is known about the upstream regulators that signal dynamic changes in these lipids. This is especially true in neurons, where activity-dependent regulation of PIP lipids has remained poorly understood. In this work, we examined the dynamic regulation of PIPs in neurons in response to both acute and chronic changes in activity. Many of the PIPs exhibited activity-dependent regulation in response to driving NMDAR activation or modulating network activity. Notably, $PI(3,5)P_2$ was among the most dynamic. $PI(3,5)P_2$ was rapidly synthesized during induction of cLTD and was the only PIP to significantly increase during homeostatic synaptic depression. Intriguingly, $PI(3,5)P_2$ accumulates on the same timescale that synapses become weakened and even transient disruption of $PI(3,5)P_2$ synthesis disrupts synaptic depression. In mammalian cells, PI5P is likely synthesized from $PI(3,5)P_2$ (Zolov et al., 2012). Thus, it is notable that PI5P levels did not change during either cLTD or homeostatic downscaling. Therefore, the impact on synaptic receptors due to loss of PIKfyve activity is likely due to the loss of $PI(3,5)P_2$ synthesis rather than through effects on PI5P. While future studies are required to delineate the precise mechanism by which PIKfyve is activated by neural activity, our results suggest that this process occurs close to synaptic regions in dendrites.

Upstream activators of PIKfyve are largely unknown. In yeast, dynamic synthesis and turnover of $PI(3,5)P_2$ is induced by hyperosmotic stimulation (Dove et al., 1997, Duex et al., 2006), but the conditions that drive $PI(3,5)P_2$ dynamics in mammalian cells are poorly understood. Our results establish that, in neurons, $PI(3,5)P_2$ synthesis is regulated by neuronal activity. Hyperactivation of network activity for 24 h with bicuculline increased $PI(3,5)P_2$ levels approximately 1.6-fold. This increase is similar to increases in $PI(3,5)P_2$ levels in mammalian cells via induction by epidermal growth factor (1.5 fold (Tsujita et al., 2004)), interleukin 2 (1.75 fold (Jones et al., 1999)) and insulin (2-fold (Bridges et al., 2012)). Interestingly, similar to chronic hyperactivity, insulin stimulation of neurons causes synaptic weakening (Man et al., 2000), raising the possibility that enhanced $PI(3,5)P_2$ synthesis contributes to this effect.

The pleiotropic effects caused by defects in $PI(3,5)P_2$ synthesis (reviewed in (McCartney et al., 2014)) suggest that multiple pathways are regulated by this signaling lipid. Here, we found that the GluA2 subunit of AMPA receptors is a target of $PI(3,5)P_2$-dependent regulation. Interestingly, an instructive role for the GluA2 subunit has been demonstrated for homeostatic plasticity induced by chronic changes in activity (Cingolani et al., 2008, Gainey et al., 2009, Goold and Nicoll, 2010, Evers et al., 2010, Pozo et al., 2012, Lambo and Turrigiano, 2013), providing a further link between $PI(3,5)P_2$ dynamics during sustained activity changes and the regulation of AMPA receptor expression at the cell surface. Trafficking and surface expression of AMPA receptors can be modulated by multiple cellular processes including, lateral diffusion (reviewed in (Opazo et al., 2012)), constitutive cycling, regulated endocytosis and

exocytosis, and intracellular trafficking (reviewed in (Esteban, 2008, Anggono and Huganir, 2012, Henley and Wilkinson, 2013)). We found that acute PIKfyve inhibition during NMDA stimulation blocks the decrease in GluA2 surface levels. Additionally, PIKfyve inhibition immediately following NMDA stimulation hastens the recovery of surface GluA2 levels to baseline levels. These results are consistent with multiple steps requiring PIKfyve activity. These effects on GluA2 are consistent with previous observations that $Vac14^{-/-}$ neurons have increased surface exposed GluA2 and defects in the trafficking of both GluA1 and GluA2 (Zhang et al., 2012). One notable difference, however, is that acute loss of $PI(3,5)P_2$ synthesis appears to target GluA2 subunits selectively, whereas prolonged loss of $PI(3,5)P_2$ has effects on both GluA1 and GluA2 trafficking. This latter effect may reflect a compensatory effect of prolonged inability to synthesize $PI(3,5)P_2$.

Functional changes during homeostasis are mediated by addition and removal of synaptic AMPA receptors. Here we show that increased synthesis of $PI(3,5)P_2$ functions to reduce cell surface AMPA receptors. Moreover, we show that this regulation is specific for homeostatic downscaling, a uni-directional role that is consistent with a growing literature suggesting that distinct mechanisms underlie homeostatic strengthening and weakening of synapses (reviewed in (Turrigiano, 2012, Siddoway et al., 2014)). In the future, it will be important to integrate this aspect of homeostatic control with other known molecular pathways. Known pathways that regulate homeostatic synaptic weakening (reviewed in (Turrigiano, 2012, Pozo and Goda, 2010, Vitureira et al., 2012, Siddoway et al., 2014)) are candidates for either being regulated

by $PI(3,5)P_2$ or regulating $PI(3,5)P_2$ levels. These include post-synaptic density 95 (PSD-95) (Sun and Turrigiano, 2011, Tatavarty et al., 2013), Polo-like kinase 2 (Plk2) (Seeburg et al., 2008, Seeburg and Sheng, 2008, Lee et al., 2011, Evers et al., 2010) and cyclin-dependent kinase 5 (CDK5) (Seeburg et al., 2008). In addition, calcium influx through L-type voltage-gated calcium channels has been mechanistically linked to homeostatic synaptic plasticity (Pak and Sheng, 2003, Thiagarajan et al., 2005, Goold and Nicoll, 2010, Henry et al., 2012, Siddoway et al., 2013) and some L-type calcium channels have been shown to interact with PIKfyve (Tsuruta et al., 2009). Thus, PIKfyve is well positioned to be responsive to activity-dependent calcium influx. Finally, Vac14 contains a PDZ interaction domain, which interacts with nitric oxide synthase (nNOS) *in vitro* (Lemaire and McPherson, 2006), another modulator of synapse strength (Hardingham et al., 2013).

In addition to a focus on $PI(3,5)P_2$ dynamics, it will be important to determine how other PIP signaling pathways impact synapse function and whether there is critical cross-talk between pathways regulated by $PI(3,5)P_2$ and other PIP pathways. Indeed, clathrin-mediated endocytosis of AMPA receptors, which is regulated by $PI(4,5)P_2$ and the 5-phosphatase, synaptojanin (Irie et al., 2005, Gong and De Camilli, 2008), is critical for internalization of AMPA receptors during synaptic depression (Unoki et al., 2012). In addition, dynamic changes in the metabolism of $PI(4,5)P_2$ (Horne and Dell'Acqua, 2007, Unoki et al., 2012) and $PI(3,4,5)P_3$ (Jurado et al., 2010, Kim et al., 2011, Takeuchi et al., 2013) are critical for LTD and other forms of synaptic plasticity (reviewed in (Knafo and Esteban, 2012)). Our direct detection of $PI(3,4,5)P_3$ levels under basal conditions is also

consistent with the hypothesis that PI(3,4,5)P_3 is required continuously for maintaining synaptic AMPARs (Arendt et al., 2010) and AMPA receptor trafficking (Qin et al., 2005). Collectively, these results illustrate the complexity and importance of PIP signaling in neurons and raise the possibility that therapies targeted at PIP metabolism and signaling may be beneficial for treatment of neurological disorders characterized by aberrant synapse function.

3.5 EXPERIMENTAL PROCEEDURES

All experiments with animals were performed in compliance with guidelines of the University Committee on Use and Care of Animals of the University of Michigan and National Institutes of Health.

3.5.1 Cell Culture

For dissociated postnatal (P1-2) rat and wild type mouse (C57BL/6J) hippocampal cultures for electrophysiology and immunofluorescence, cells were plated at a density of 230-460 per mm^2 in poly-D-lysine-coated glass-bottom petri dishes (Mattek) as previously described (Sutton et al., 2006) and maintained for at least 21-24 DIV at 37 ºC in growth medium [Neurobasal A (Invitrogen 10888022) supplemented with B27 (Invitrogen 17504044) and Glutamax (Invitrogen 35050061)] prior to use. For inositol labeling and measurement of phosphoinositides, rat hippocampal neurons were plated on 35 mm dishes. For wild-type and Vac14$^{-/-}$ experiments, E18 embryos from crosses of Vac14+/- heterozygous mice (C57BL/6J) were genotyped and dissociated hippocampal cultures were prepared similarly except the culture medium was Neurobasal (Invitrogen 21103049).

3.5.2 Electrophysiology

Whole-cell patch-clamp recordings of mEPSCs were made with an Axopatch 200B amplifier from cultured hippocampal neurons bathed in HEPES-buffered saline (HBS; 119 mM NaCl, 5 mM KCl, 2 mM $CaCl_2$, 2 mM $MgCl_2$, 30 mM glucose, 10 mM HEPES, pH 7.4) plus 1 µM TTX and 10 µM bicuculline. The pipette internal solution contained 100 mM cesium gluconate, 0.2 mM EGTA, 5 mM MgCl2, 40 mM HEPES, 2 mM Mg-ATP, 0.3 mM Li-GTP, 1 mM QX314, pH 7.2 and had a resistance of 3-5 MΩ. mEPSCs were analyzed off-line using MiniAnalysis (Synaptosoft) and custom MATLAB (Mathworks) scripts.

3.5.3 Lentivirus shRNA Knockdown of Mouse PIKfyve

For knockdown of mouse PIKfyve, MISSION shRNA lentiviral plasmid pLKO.1-puro with shRNA CCGGGCCAGTCGTAACATATTCTTACTCGAGTAAGAATATGTTACGACTGGCTTTTT (Sigma-Aldrich; number: TRCN0000025096 and clone ID: NM_011086.1–949s1c1) containing 811–831 nucleotides of mouse PIKfyve cDNA (underlined) was used as described in (Zolov et al., 2012) at a MOI of 5, without polybrene. As a control, MISSION nontarget shRNA lentiviral control vector SHC002 with nonhuman or mouse shRNA was used at a MOI of 5. Neurons were incubated with virus for 1 h and virus containing medium was replaced with saved conditioned medium. Experiments were performed after 1 week of lentivirus transduction.

3.5.4 Elevation of $PI(3,5)P_2$ levels with $PIKfyve^{KYA}$ mutation

Flp-In T-Rex 293 Cells (Life Technologies R780-07) were transfected with pcDNA5-FRT vectors that carry 3XFLAG, 3XFLAG-Citrine-PIKfyve (human) or 3xFLAG-

Citrine-PIKfyve^{KYA}. Stable clones were selected according to the manual. Stably transfected cells were maintained in DMEM supplemented with 10% FBS, 1x Pen/Strep/Glutamate, 15 μg/mL Blasticidin S HCl (Life Technologies A11139) and 0.4 mg/mL Hygromycin B (Life Technologies 10687). For Western blots, cells were induced with 100 ng/mL doxycycline (Sigma D9891) for 8 or 24 hours and then harvested in RIPA buffer (50mM Tris, pH 7.4, 150mM NaCl, 1mM EDTA, 1% deoxycholic acid, 1% NP-40, 0.1% SDS, 10mM NaF, 1mM Na_3VO_4 and 1x protease inhibitor cocktail (Roche 04693116001). Antibodies used were mouse anti-FLAG (Sigma F3165, 1:1000), rabbit anti hFab1 (raised in house, 1:1000 (Zhang et al., 2007)), and mouse anti-GAPDH (Ambion AM4300, 1:50,000). For lipid determination, cells were labeled as described for fibroblasts (see below) except that 100 ng/mL doxycycline was added 24 hours before the extraction.

The sequences of the final clones used to make the Flip-in cell lines were verified as follows. Genomic DNA was prepared from Flip-in cell lines using the Qiagen DNeasy Blood and Tissue Kit. Citrine-PIKfyve and Citrine-PIKfyve^{KYA} were PCR-amplified from genomic DNA using Thermo Scientific Phusion Polymerase. Full PCR coverage of the gene was obtained with 5 primer pairs:

Pair 1: Fwd - CGCAAATGGGCGGTAGGCGTG, Rev - TAAAAGGGGGCTCATCTTGA,

Pair 2: Fwd - CTGGTGAACCGCATCGAG, Rev - AGCCTCCTCTTAGCTTGATTG,

Pair 3: Fwd - TGGTTGTCAATGGCTTTGTT, Rev - TCCTGCAACCTGTTATTCCA,

Pair 4: Fwd - GCACCAGTATACTCGCAGAGC, Rev - TGTCCCATGTAAATGTTCG,

Pair 5: Fwd – CGTCTGGAAGTCCAGTCCTT, Rev - GCTGGTTCTTTCCGCCTCAGAAG.

The absence of point mutations was confirmed by Sanger sequencing of PCR products by the University of Michigan Sequencing Core. Full sequence coverage was achieved using the following sequencing primers:

Fwd1 - CTGGTGAACCGCATCGAG,

Fwd2 - AATGATTTGCCTCGATCTCC,

Fwd4 - TCCTCAAATACTCCTCTTTCAACA,

Fwd6 - TTTGATTTCTGACACTGGAGGA,

Fwd7 - TGGTTGTCAATGGCTTTGTT,

Fwd8 - TGCAGATATTTCAGTTGCCT,

Fwd9 - AGGCTGTTGCCTCTGTGAAG,

Fwd11 - CACCAGAGACTTTGTGTGCTCT,

Fwd12 - GCACCAGTATACTCGCAGAGC,

Fwd14 - GGATCCACAGACAGCCAAGT,

Fwd16 - CGTCTGGAAGTCCAGTCCTT,

Rev1 - TGTGGCTGTTGTAGTTGTACTCC,

Rev2 - TAAAAGGGGGCTCATCTTGA,

Rev3 - TGTCTGCGCCTAAAGGTTGT,

Rev8 - AGCCTCCTCTTAGCTTGATTG,

Rev13 - TCCTGCAACCTGTTATTCCA.

The PIKfyve clone used to make the Flip-In cell line 3XFLAG-Citrine-PIKfyve is 100% identical to the GenBank sequence AAR19397. The only mutations in the Flip-In cell line 3XFLAG-Citrine-PIKfyve^{KYA} are E1620K, N1630Y, and S2068A.

3.5.5 Transfection

Neurons were transfected with 2 μg Citrine-PIKfyve WT or Citrine-PIKfyve^{KYA} plasmid and 1 μg mCherry plasmid with a modified CalPhos Transfection kit (CloneTech) protocol. After incubation with DNA, cells were briefly incubated in a 10% CO_2 incubator and DNA-containing medium discarded. Experiments were performed 1 week after transfection. For pHluorin-GluA live endocytosis assay, neurons were transfected with 1 μg SEP-GluA2(R607Q) (Addgene plasmid #24002) or 1 μg SEP-GluA1 (Addgene plasmid #24000) and 1 μg mCherry at DIV20. Experiments were performed 24-48 h later.

3.5.6 Inositol Labeling and Measurement of Phosphorylated Phosphoinositide Lipids

Mouse primary fibroblasts from C57BL/6J mice were cultured in DMEM (Life Technologies 11965) supplemented with 15% FBS (Life Technologies 16000) and 1x Pen/Strep/Glutamate (Life Technologies 10378). After reaching 60% confluence, fibroblasts were washed with PBS and custom inositol-free DMEM (Life Technologies, Cat. No. 11965092), 10 μCi/mL of myo-[2-^{3}H] inositol (Perkin Elmer, Cat. No. NET1156005MC), 10% dialyzed FBS (Life Technologies 26400), 20 mM HEPES, pH 7.2 - 7.5 (Life Technologies 15630), 5 μg/mL transferrin (Life Technologies 0030124SA), and 5 μg/mL insulin (Life Technologies 12585-014) for 48 hours. Toward the end of the labeling, cells were treated with 1 μM apilimod (Axon 1369, Axon Medchem BV) for 0 min, 2.5 min, 5 min, 30 min, and 120 min. Extraction and HPLC analysis were described in (Zolov et al., 2012).

Primary rat hippocampal neurons were cultured for 21 days, rinsed with custom inositol-free Neurobasal-A (Life Technologies, Cat. No. ME120164L1) and incubated for 24 h with inositol labeling medium containing inositol-free Neurobasal-A, 50 µCi/mL of myo-[2-^{3}H] inositol (Perkin Elmer, Cat. No. NET1156005MC), B27, and L-Glutamax. Myo-[2-^{3}H] inositol-labeled cells were treated as described (Zolov et al., 2012) with modifications. After 24 h, cultures were rinsed with HBS (HBS: 119 mM NaCl, 5 mM KCl, 2 mM $CaCl_2$, 2 mM $MgCl_2$, 30 mM Glucose, 10 mM HEPES, pH 7.4) and treated with 1 mL 4.5 % (vol/vol) perchloric acid for 15 min at room temperature. Cells were scraped off with a Cell lifter (Costar 3008) and harvested at 12,000 x g for 10 min at 4°C. Pellets were washed at room temperature with 1 mL 0.1 M EDTA and resuspended in 50 µL water. To deacylate lipids, samples were transferred to a glass vial, mixed with 1 mL methanol/40% methylamine/1-butanol (45.7 methanol, 10.7% methylamine, 11.4% L-butanol, vol/vol), and incubated at 55°C for 1 h. Samples were vacuum dried, resuspended in 0.5 mL water, and extracted twice with an equal volume of butanol/ethyl ether/ethyl formate (20:4:1, vol/vol). The aqueous phase was vacuum-dried and resuspended in 50 µl water. Equivalent amounts of ^{3}H for each sample were analyzed by HPLC (Shimadzu UFLC CBM-20A Lite) using an anion exchange 4.6 x 250 mm column (MAC MOD Analytical, Inc 46211505,). A gradient of 1 M $(NH_4)_2HPO_4$, pH 3.8 (pH adjusted with phosphoric acid), was used at a flow rate of 1 mL/min; 0% for 5 min; 0-2% 15 min; 2% 80 min; 2-10% 20 min; 10% 65 min; 10-80% 40 min; 80% 20 min; 80-0% 5 min (all vol/vol). Radiolabeled eluate was detected with an inline flow scintillation analyzer (Beta-RAM model 5 RHPLC Detector; LabLogic). A 1:2 proportion of eluate to

scintillant (National Diagnostics, Uniscint BD Cat. No. LS-276-20L) was used with a flow rate of 3 mL/min. Fractions were analyzed by binning counts every 6 s. The data were collected and analyzed by Laura-4 software (LabLogic).

For comparison of phosphatidylinositol polyphosphate (PI) levels, the raw counts in each peak were expressed as a percentage of total phosphatidylinositol, calculated from summation of the counts of seven detectable peaks: PI, PI3P, PI4P, PI5P, PI(3,5)P_2, PI(4,5)P_2, and PI(3,4,5)P_3. PI(3,4)P_2 was not always detected. Background was calculated from adjacent regions and subtracted from all peaks. For standards, except PI(3,4,5)P_3 and PI(3,4)P_2, extracts from yeast treated with 0.9 M NaCl for 5 min (Duex et al., 2006) were used. For PI(3,4,5)P_3 and PI(3,4)P_2 standards, radioactive products of PI 3-kinase phosphorylation of phosphoinositide substrates, PI(4,5)P_2 or PI4P, respectively, using ^{32}P were extracted, separated using thin-layer chromatography and analyzed by HPLC.

3.5.7 Immunocytochemistry

Primary antibodies used were mouse anti-GluA2 (IgG2a) (Millipore MAB 397) and rabbit anti-PSD95 (Abcam ab18258). Secondary antibodies were conjugated to Alexafluor 488 or 555 (Life Technologies). To label surface GluA2 and PSD95, neurons were incubated live with the sGluA2 antibody for 15 min at 37°C, rinsed with HBS, fixed with 2% paraformaldehyde, 2% sucrose, blocked with 2% bovine serum albumin (BSA) in phosphate-buffered saline with 1 mM $MgCl_2$ and 0.1 mM $CaCl_2$ (PBS-MC) for 16 min and incubated with fluorescent secondary antibody (Goat anti Mouse 488). Cells were then permeabilized with 0.2% Triton X-100 for 10 min and blocked before incubation with PSD95 antibody and later goat anti-rabbit 555 antibody. To label both surface GluA2 and

internal GluA2, neurons were fixed for 4 min with 4% paraformaldehyde/4 % sucrose, blocked with 2% BSA for 20 min and incubated with GluA2 antibody overnight. Cells were washed twice with PBS-MC, incubated with goat anti-mouse IgG2a – 488 for 1 h and fixed with 4% paraformaldehyde/4 % sucrose for 12 min. Then cultures were permeabilized, blocked, incubated with GluA2 antibody, rinsed and incubated with goat and mouse IgG2a-555. Images were acquired with an Olympus FV1000 confocal microscope (z-series, 0.41 µm intervals) and analyzed with ImageJ, Excel (Microsoft), and MATLAB (Mathworks).

3.5.8 Fluorescent recovery after NMDA stimulation

At DIV 21, neurons transfected with either pHluorin-GluA2(Q) or pHluorin-GluA1 plasmids were rinsed with warm extracellular imaging buffer (25 mM HEPES, 120 mM NaCl, 5 mM KCl, 1 mM $CaCl_2$, 2 mM $MgCl_2$, 30 mM D-glucose, 1 µM TTX, pH 7.4) to remove the media and then continuously perfused with warmed imaging buffer on the confocal stage. Pyramidal-like transfected neurons were analyzed. Images were acquired once per minute for (I) 12 min baseline, (II) 5 min 0.2 mM Mg^{2+} solution, (III) 5 min NMDA stimulation buffer (25 mM HEPES, 120 mM NaCl, 5 mM KCl, 1 mM $CaCl_2$, 0.2 mM $MgCl_2$, 30 mM D-glucose, 1 µM TTX, 20 µM NMDA, 10 µM glycine, pH 7.4), and (IV) NMDA wash-out and recovery for 50 min in imaging buffer. The pHluorin and mCherry fluorescence were imaged with 488 nm and 559 nm excitation, respectively, through a 60X oil objective.

3.5.9 Image Quantification

For all images, analysis was performed on images that were maximally z-projected in ImageJ (NIH). Quantification of surface GluA2 levels were analyzed by finding the average pixel intensity of the thickest primary dendrite of pyramidal-like neurons at user-defined thresholds. Experimental groups were normalized to the average control intensity. For the time course analysis of changes in surface GluA2 and internal GluA2 levels with NMDA stimulation, the soma average pixel intensity was measured for each channel and normalized to the baseline levels for each experiment group. The ratio of surface to internal intensity was subsequently calculated by dividing the surface and internal intensities.

3.5.10 Statistics

Statistical differences between experimental conditions were determined as indicated by ANOVA or Kruskal-Wallis ANOVA and Tukey-Kramer post hoc test MATLAB (Mathworks).

3.6 ACKNOWLEDGEMENTS

We thank Christian Althaus, and Cindy Carruthers for their assistance in preparing neuronal cultures. We thank Dr. Roberto Malinow and Addgene for the SEP-GluA1 and SEP-GluA2(Q) plasmids. This work was supported by NIH grants R01-NS064014 and R01-GM050403 to LSW and RO1-MH085798 to MAS. AJM was supported in part by NRSA F31NS07470 and the Rackham Predoctoral Fellowship award from the University of Michigan. BSS was supported by a postdoctoral Fellowship from the Jane Coffin Child Fund.

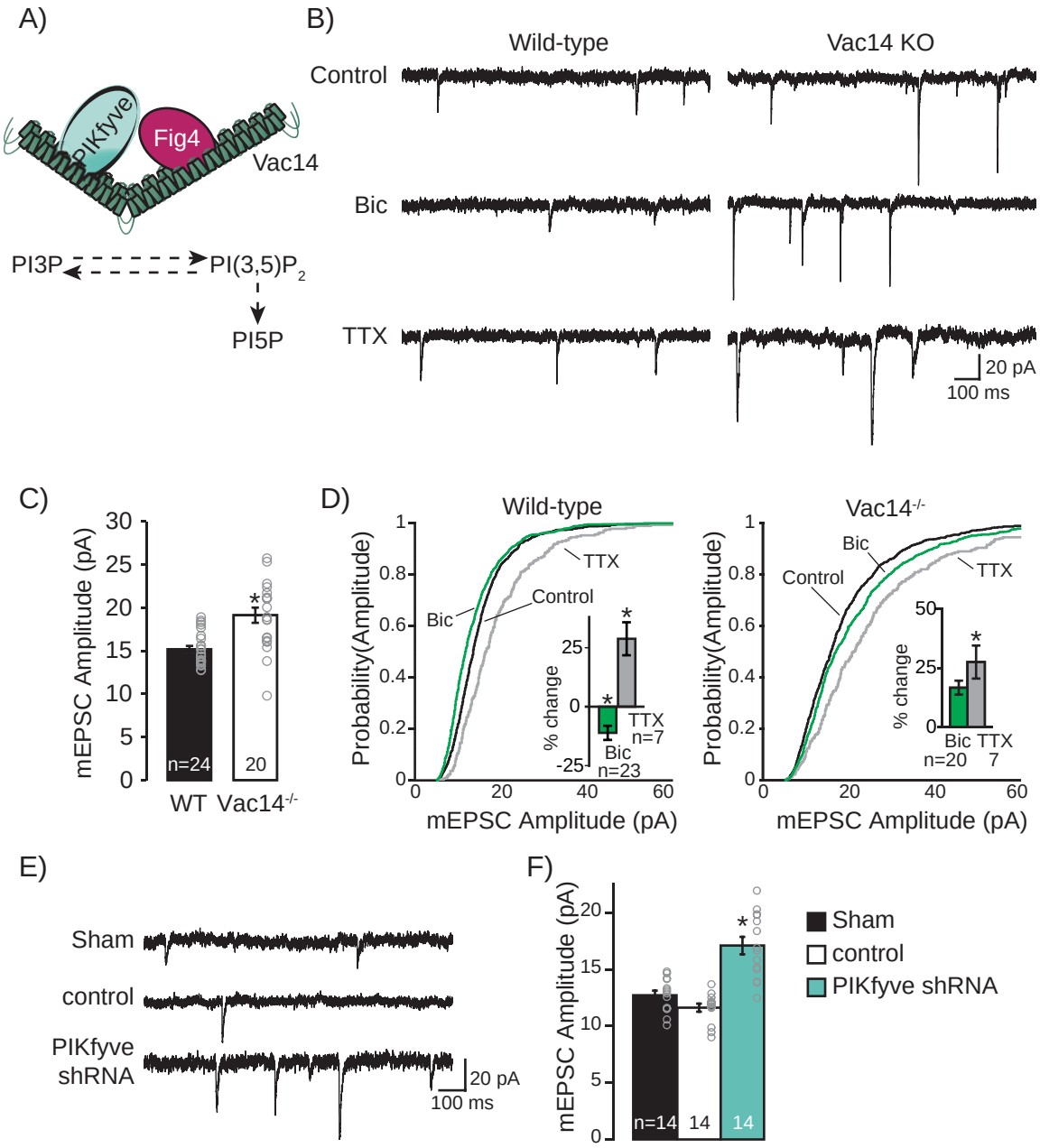

Figure 3-1. Loss of PI(3,5)P_2 synthesis increases synaptic strength and prevents homeostatic synaptic downscaling

(A) Schematic of the PI(3,5)P_2 synthesis complex. Vac14 is a scaffolding protein that interacts with PIKfyve, the sole PI3P 5-kinase, and Fig4, a PI(3,5)P_2 5-phosphatase and positive regulator of PIKfyve activity. PI(3,5)P_2 can be converted to PI3P or PI5P. In yeast, additional proteins have been identified in the complex, which regulate PIKfyve (in yeast, Fab1) activity, suggesting there are likely additional complex members in metazoans, as well. **(B)** Representative example recordings from wild-type and Vac14$^{-/-}$ mouse hippocampal cultured neurons treated for 24 h with vehicle control, 2 µM TTX or 50 µM bicuculline (Bic). **(C)** Mean (±standard error of the mean (SEM)) mEPSC amplitude in wild-type and Vac14$^{-/-}$ neurons. The amplitude of Vac14$^{-/-}$ mEPSCs is increased

relative to wild-type (wild-type: 15.16 ±0.39 pA; Vac14$^{-/-}$: 19.12±0.88 pA; t(43)=31.04, p=4.45e-31). **(D)** Cumulative distribution frequency of mEPSC amplitude from wild-type (left) and Vac14$^{-/-}$ (right) neurons treated for 24 h with vehicle control (black line), 2 µM TTX (gray line) or 50 µM Bic (green line). In wild-type neurons, the distribution of mEPSC amplitude is left-shifted following 24h bicuculline and right-shifted following 24h TTX. While Vac14$^{-/-}$ neurons normally scale-up mEPSC amplitude in response to 24 TTX, they fail to scale-down. All six distributions were compared using the one-way Kruskal-Wallis ANOVA (χ2(5, n=4016)=411.56, p=9.56e-87) and the results of Tukey-Kramer post hoc test reported here: wild-type+bicuculline is different from every group. Wild-type+TTX is different than WT. Vac14$^{-/-}$+TTX is different from every group. WT control is different from Vac14$^{-/-}$ control. Mean (±SEM) percent change in mEPSC amplitude relative to unstimulated controls of the corresponding genotype. In wild-type neurons, 24 h treatment with TTX increases mEPSC amplitude and 24 h treatment with bicuculline decreases mEPSC amplitude (wild-type, percent change from control (n=24): +TTX: 28.79±6.99%, n=7; +Bic: -11.11±2.97%, n=23; one-way ANOVA, F(2,51)=21.41, p=1.775e-7). In Vac14$^{-/-}$ neurons, 24 h treatment with TTX increases mEPSC amplitude, but 24 h treatment with bicuculline does not decrease mEPSC amplitude (Vac14$^{-/-}$, percent change from control (n=20): +TTX: 24.28±8.99%, n=7; +Bic:13.72±6.03%, n=20; one-way ANOVA, F(2,45)=4.06, p=0.02). **(E)** Representative mEPSC recordings from wild-type mouse neurons one week after lentiviral transduction with vehicle control (sham), non-targeting control shRNA or PIKfyve shRNA. **(F)** Mean (±SEM) mEPSC amplitude in neurons treated or untreated with PIKfyve shRNA for 1 week. Knocking down PIKfyve increased mEPSC amplitude (sham: 12.73±0.40 pA; control shRNA: 11.63±0.35 pA; PIKfyve shRNA: 17.11±0.77 pA; one-way ANOVA, F(2,39)=29.00; p=1.9e-8). *indicates p<0.05.

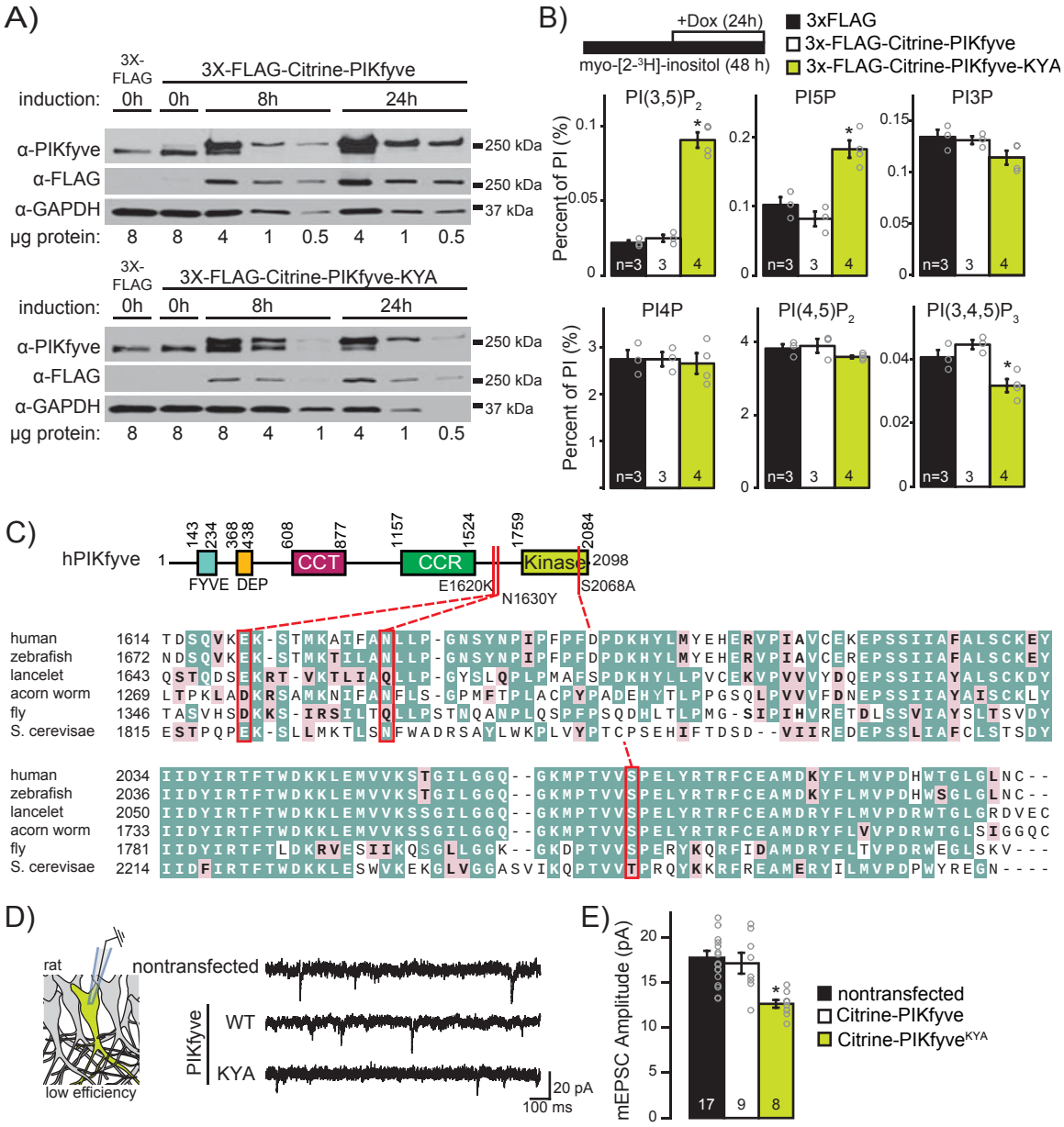

Figure 3-2. Enhancing neuronal PI(3,5)P_2 levels reduces synaptic depression
(A) Representative Western blots depicting Doxycycline dependent induction of 3X-FLAG control, 3X-FLAG-Citrine-PIKfyve (top) or 3X-FLAG-Citrine-PIKfyve^{KYA} (bottom) in stable cell lines (HEK-293). Cells were induced for 0, 8, or 24 h before lysis and analyzed by Western blot. Immunoblotting for PIKfyve with an amino-terminal PIKfyve antibody reveals two bands, which is consistent with detection of endogenous PIKfyve and 3X-FLAG-Citrine-PIKfyve or 3X-FLAG-Citrine-PIKfyve^{KYA}. **(B)** Mean (±SEM) PIP levels relative to total PI from 3xFLAG, 3X-FLAG-Citrine-PIKfyve and 3X-FLAG-Citrine-PIKfyve^{KYA} cells. Induction of 3X-FLAG-Citrine-PIKfyve^{KYA} for 24 h increases PI(3,5)P_2 and PI5P levels (PI(3,5)P_2: 3XFLAG: 0.022±0.001%, 3XFLAG-Citrine-PIKfyve: 0.025±0.002%, 3XFLAG-Citrine-PIKfyve^{KYA}: 0.093±0.005%, one-way ANOVA, F(2,7)=105.44, p=5.9e-06). (PI5P: 3XFLAG: 0.102±0.011%, 3XFLAG-Citrine-PIKfyve: 0.082±0.011%, 3XFLAG-Citrine-

PIKfyve^{KYA}: 0.185±0.012%, one-way ANOVA, F(2,7)=21.63, p=0.001). **(C)** Domain structure of human PIKfyve (reviewed in (McCartney et al., 2014)). Domains shown: FYVE (binds PI3P), DEP (function unknown), CCT (homologous to the chaperone Cpn60/TCP-1 family), CCR (conserved cysteine rich domain), and kinase (catalytic site for conversion of PI3P to PI(3,5,)P_2). Multiple alignment of human (*Homo sapiens*, AAR19397.1), fish (*Danio rerio*, NP_001120777.1), lancelet (*Branchiostoma floridae*, XP_002598618.1), acorn worm (*Saccoglossus kowalevskii*, XP_006821423.1); fly (*Drosophila pseudoobscura*, XP_001361784); yeast (*Saccharomyces cerevisiae*, BAA09258.1). PIKfyve homologues with conserved amino acids shaded in teal and conservative substitutions shaded in pink. Boxes indicate the mutated amino acids (E1620K, N1620K, S2068A) in the PIKfyveKYA mutant. **(D)** Schematic depicts a transfected neuron surrounded by nontransfected neighbors. Representative recordings from cultured rat hippocampal neurons (DIV21) transfected at DIV14 with Citrine-PIKfyve or Citrine-PIKfyve^{KYA}. Nontransfected control neurons from the same dish were also analyzed. **(E)** Mean (±SEM) mEPSC amplitude of nontransfected and transfected neurons expressing Citrine-PIKfyve or Citrine-PIKfyve^{KYA}. PIKfyve^{KYA} expression decreased mEPSC amplitude (uninfected: 17.75±0.78 pA; Citrine-PIKfyve: 17.14±1.16 pA; Citrine-PIKfyve^{KYA}: 12.65±0.43 pA; one-way ANOVA, F(2,31)=17.32, p= 0.0005). *indicates p<0.05.◊Data in A were collected by Bethany Strunk and Yanling Zhang. Data in B were collected by Sergey Zolov.

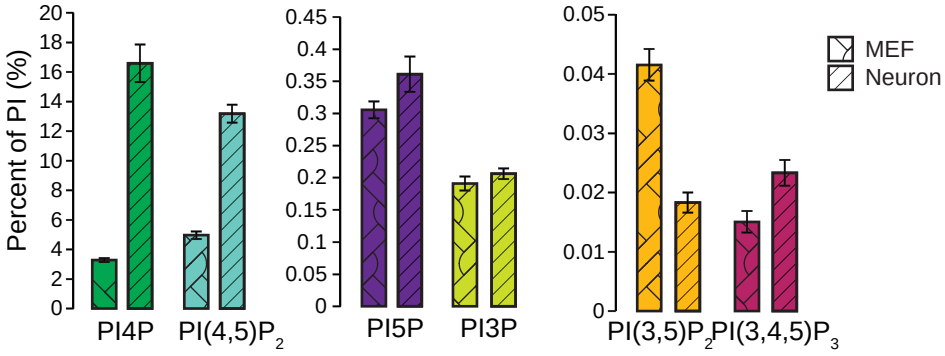

	Percent PI±sem	
	MEF (n=5)	Neuron (n=11)
PI3P	0.191 ± 0.011	0.206 ± 0.008
PI4P	3.276 ± 0.136	16.590 ± 1.274
PI5P	0.306 ± 0.013	0.361 ± 0.027
$PI(3,5)P_2$	0.042 ± 0.003	0.018 ± 0.002
$PI(4,5)P_2$	4.963 ± 0.251	13.188 ± 0.608
$PI(3,4,5)P_3$	0.015 ± 0.002	0.023 ± 0.002

Figure 3-3. Comparison of PIP levels in mouse embryonic fibroblasts and cultured hippocampal rat neurons. The values for MEF cell PIP levels are from (Zolov et al., 2012).

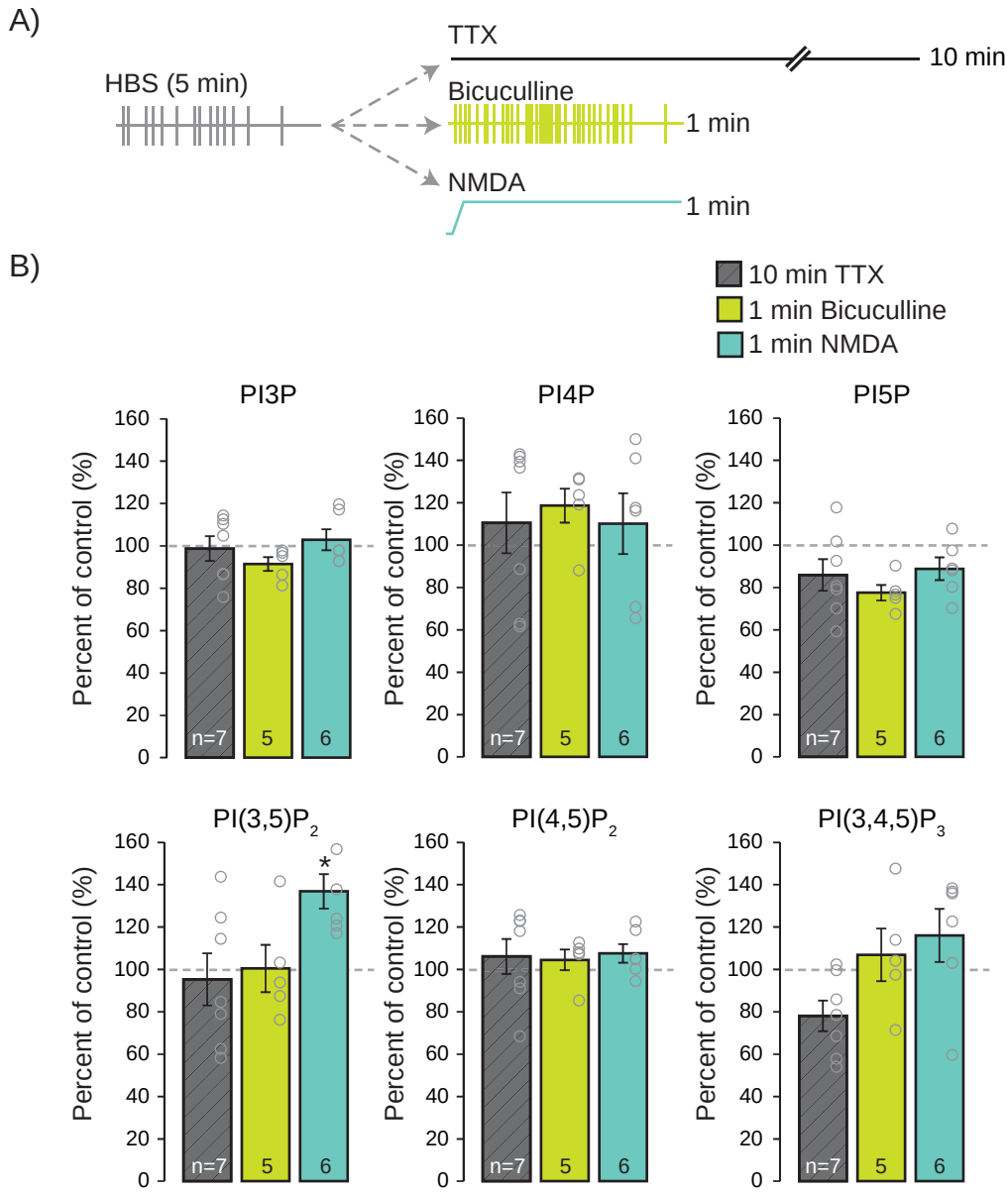

Figure 3-4. Activity-dependent regulation of neuronal phosphoinositide dynamics
(A) Schematic of experimental design. Neurons were metabolically labeled with [3H]-inositol for 24 h. The media was replaced with HBS. After 5 min, HBS was replaced with HBS+ 2 µM TTX for 10 min, 50 µM bicuculline for 1 min or 20 µM NMDA for 1 min, and then lipids were extracted. For each experiment, unstimulated controls (5 min HBS) were also collected. **(B)** Mean (±SEM) PIP level after stimulation with TTX, bicuculline or NMDA expressed as percent of control (5 min HBS). The level of $PI(3,5)P_2$ significantly increased after 1 min NMDA stimulation (Percent of control: control, 100±14.15 %, n=8; 1 min NMDA, 136.87±8.17 %, n=6, t(12)=3.06, p=0.0099). *indicates p<0.05.

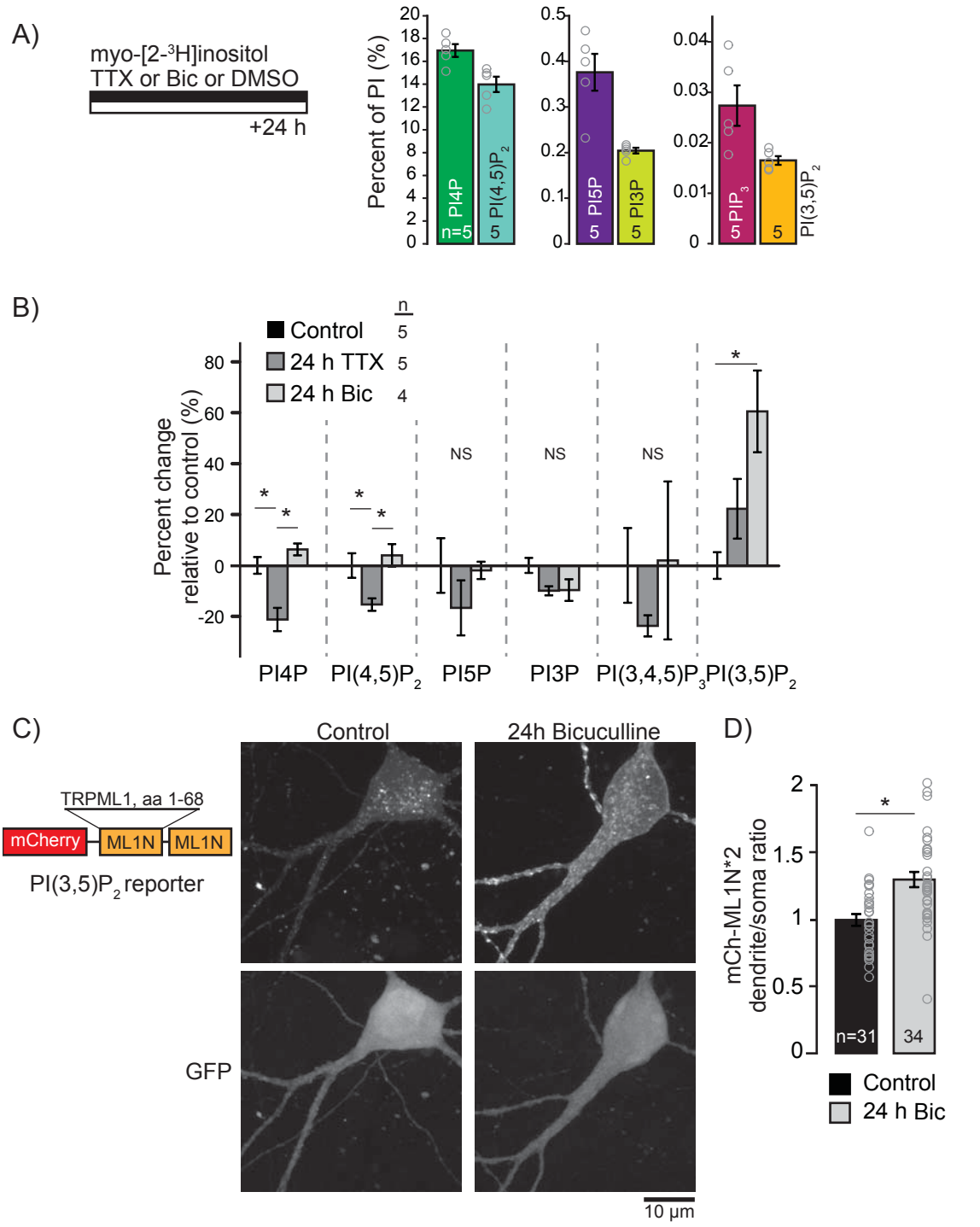

Figure 3-5. PI(3,5)P_2 synthesis accompanies homeostatic synaptic downscaling
(A) Schematic of experimental design. Neurons were metabolically labeled with [3H]-inositol for 24 h in presence of DMSO control, 2 µM TTX or 50 µM bicuculline, and lipids were extracted. The mean (±SEM) PIP level in control neurons expressed relative to PI. PIP species are plotted in order of descending abundance (PI4P: 16.95±0.56%; PI(4,5)P_2: 13.98±0.68%; PI5P: 0.38±0.04%; PI3P: 0.20±0.006%; PI(3,4,5)P_3: 0.027±0.004%; PI(3,5)P_2: 0.016±0.001%). **(B)** Mean (±SEM) percent change in PIP levels relative to

control from neurons incubated with 2 µM TTX (n=5) or 50 µM bicuculline (n=4) for 24 hr. The level of PI4P decreased after 24 h TTX (percent change:-21.26±1.77%, one-way ANOVA, $F(2,11)=15.2$, $p=0.0007$). The level of $PI(4,5)P_2$ decreased after 24h TTX (percent change:-15.34±2.45%, one-way ANOVA, $F(2,11)=6.54$, $p=0.014$). The level of PI(3,5)P2 increased after 24 h bicuculline (percent change: 60.49±16.05%, one-way ANOVA, $F(2,11)=7.13$, $p=0.01$). **(C)** Representative images of neurons expressing both the $PI(3,5)P_2$ reporter, mCherry-ML1N*2 and GFP. **(D)** Mean (±SEM) ratio of dendritic to soma mCherry-ML1N*2 fluorescence. The dendritic to soma ratio of mCherry-ML1N*2 intensity increased after 24 h bicuculline (Control: 1.0±0.04; 24 h Bic: 1.30 ±0.06; t-test, $t(63)=4.12$, $p=0.0001$). *indicates $p<0.05$.

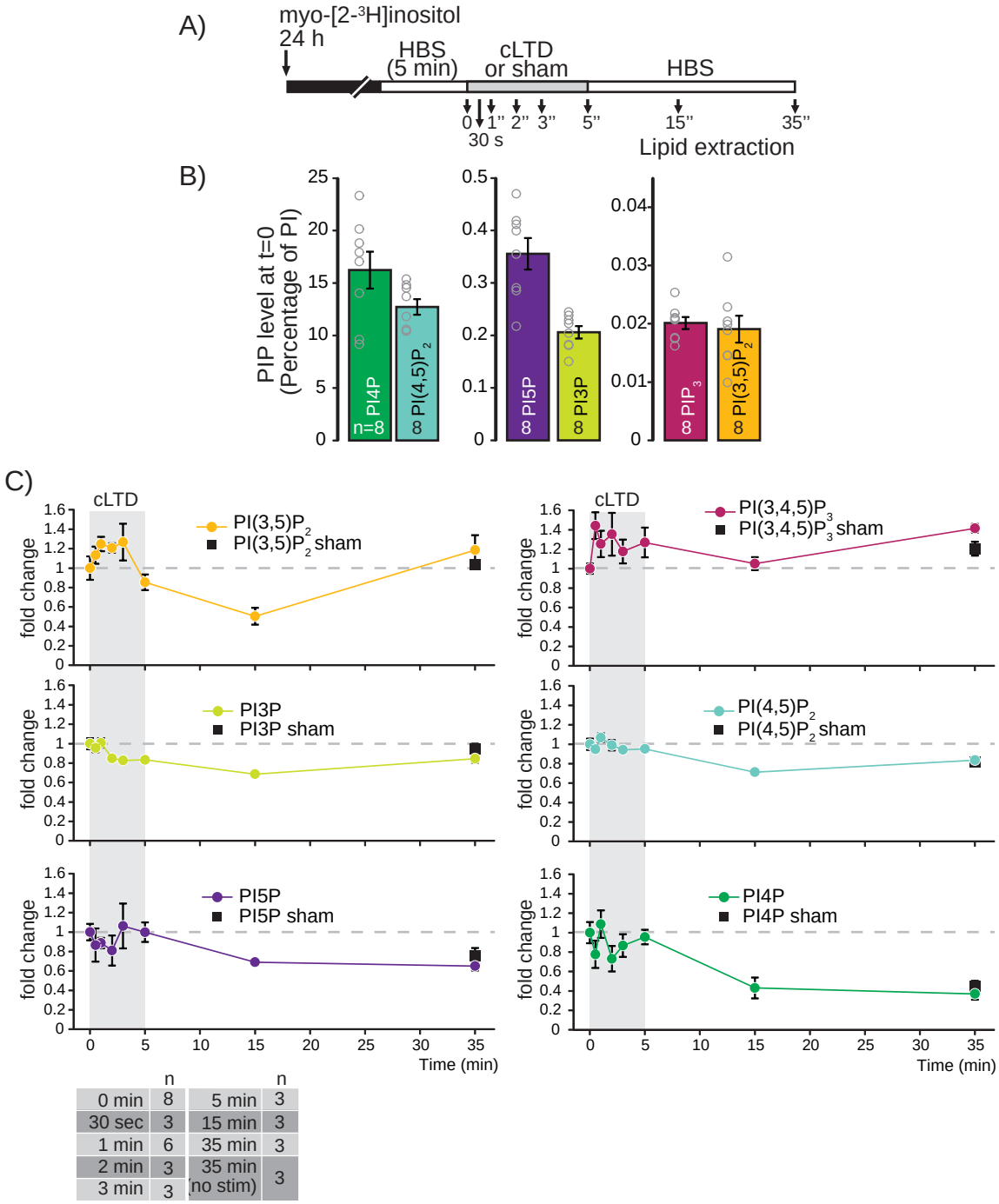

	n		n
0 min	8	5 min	3
30 sec	3	15 min	3
1 min	6	35 min	3
2 min	3	35 min (no stim)	3
3 min	3		

Figure 3-6. Rapid, but transient, PI(3,5)P_2 synthesis accompanies LTD induction
(A) Schematic of experimental design. PIP levels were analyzed after 24 h metabolic labeling, during cLTD induction (20 µM NMDA, 1 µM glycine, 0.2 mM Mg^{2+}) or after induction at the specific time points (30 sec, 1 min, 2 min, 3 min, 5 min, 15 min, or 35 min). Sham treated samples were treated identically to cLTD stimulated neurons, except NMDA and glycine were not included in the stimulus buffer. **(B)** Mean (±SEM) PIP levels at time point 0. **(C)** Mean (±SEM) levels of each PIP normalized to time point 0 (dashed line). The induction of cLTD evokes a dynamic elevation in the levels of PI(3,5)P_2 and PI(3,4,5)P_3.

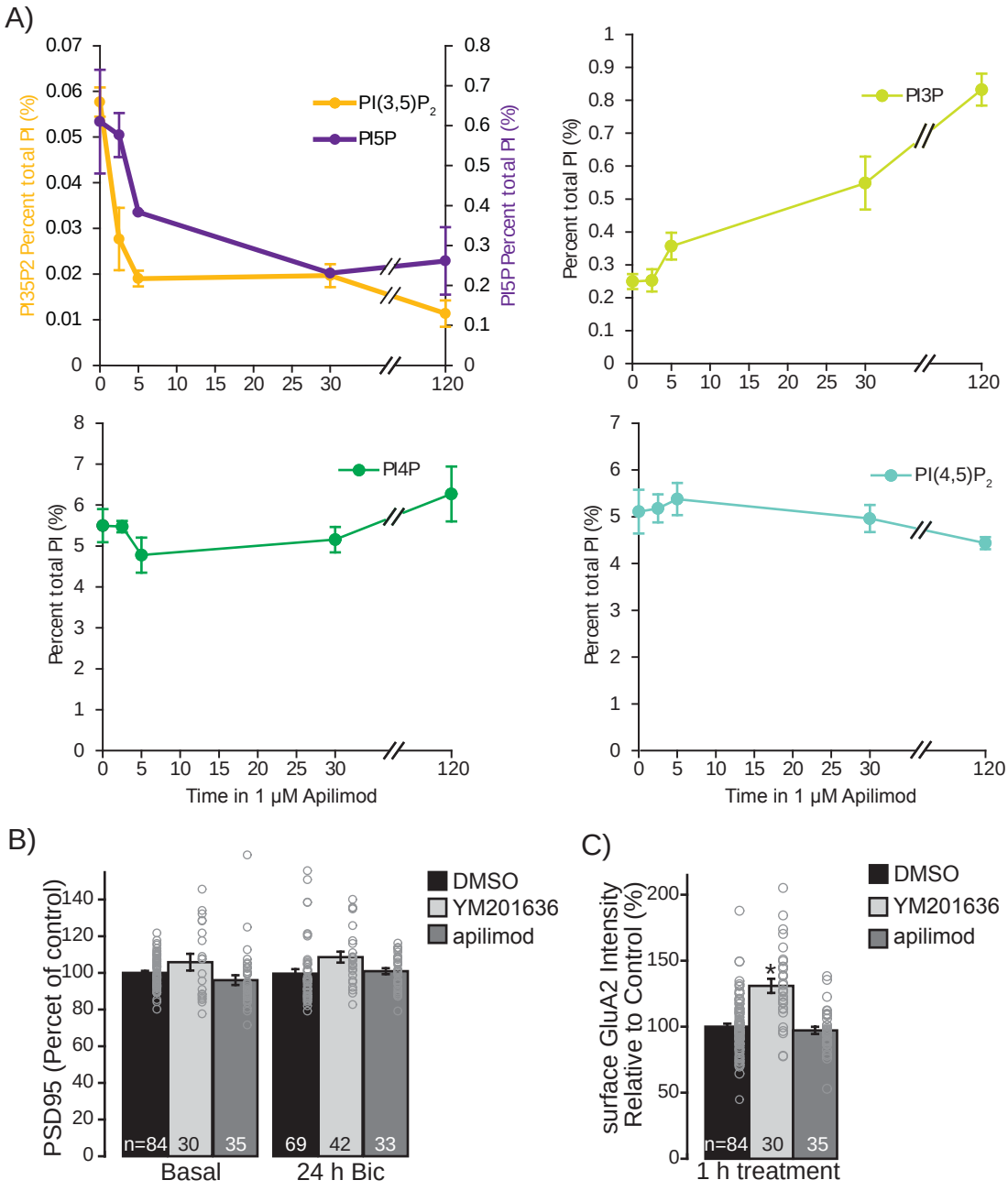

Figure 3-7. Apilimod inhibition PI(3,5)P_2 synthesis

(A) Mean (±standard deviation) PIP levels in mouse primary fibroblasts after incubation with 1 µM apilimod for the times indicated. 1 µM apilimod results in a rapid depletion of PI(3,5)P_2 and PI5P (n=3). Note, PI(3,4,5)P_3 levels were not affected by PIKfyve inhibition using 1 µM apilimod (Appendix I: Figure A-9).**(B)** Mean (±SEM) intensity of PSD-95 puncta. PSD95 intensity is not affected by 50 µM bicuculline, 1 h PIKfyve inhibition with either 2 µM YM201636 or 1 µM apilimod. **(C)** Mean (±SEM) intensity of surface GluA2 puncta. Inhibition with 2 µM YM201636, but not 1 µM apilimod, for 1 h increased the surface levels of GluA2 (control: 100±2.24%, 1 h YM201636: 130±93%, 1 h apilimod: 95.49±2.50%; one-way ANOVA, F(2,145)=26.12, p = 1.6e-10). *indicates p<0.05. ◊Data in A were collected by Yanling Zhang and Sergey Zolov.

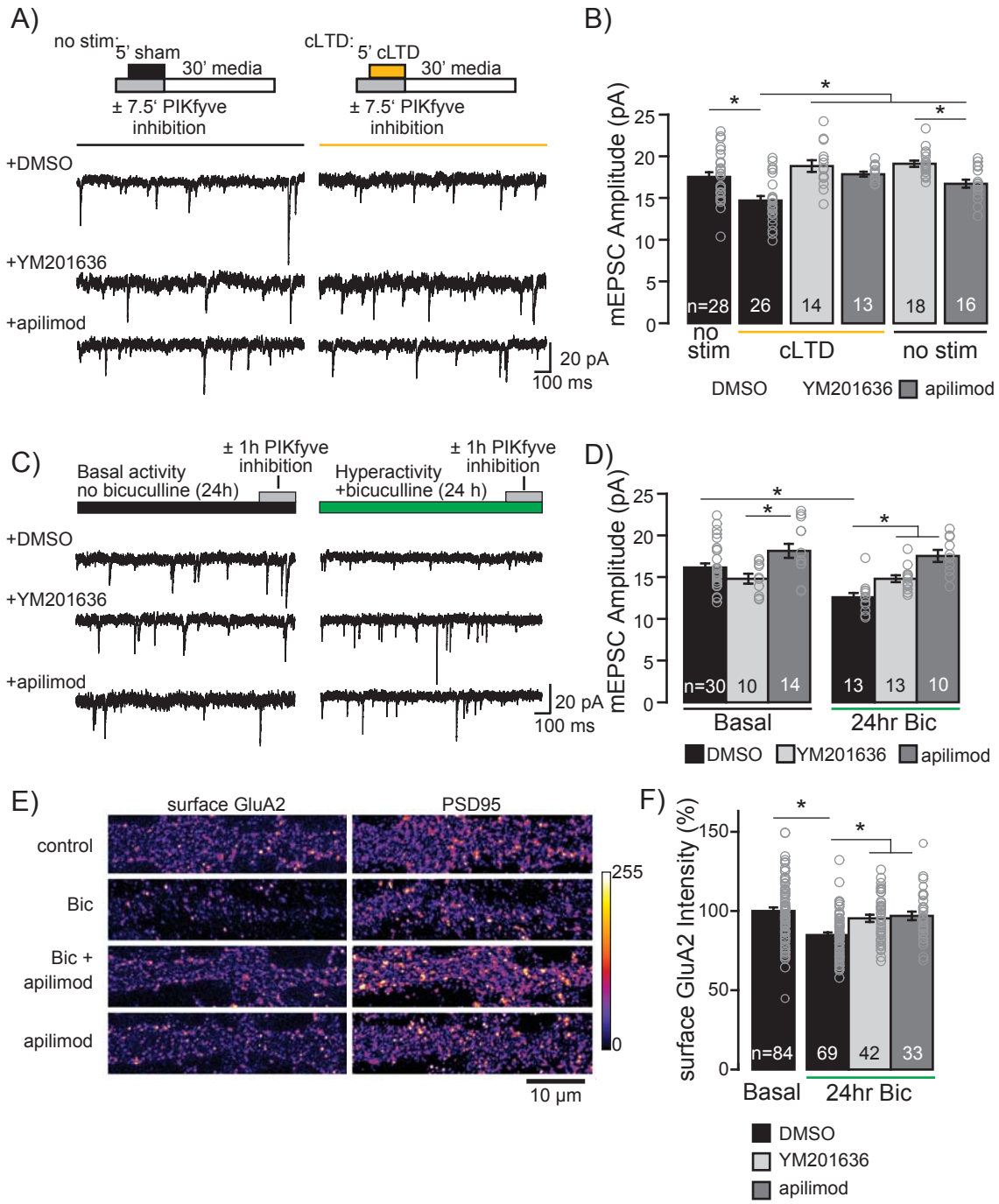

Figure 3-8. PIKfyve activity is required for synaptic depression

(A) Representative recording of mEPSCs from rat cultured hippocampal neurons that were incubated with cLTD induction, or sham solution, in the presence or absence of PIKfyve inhibitors. After stimulation, neurons were incubated with reserved conditioned media without PIKfyve inhibitors for 30 min at 37°C. **(B)** Mean (±SEM) mEPSC amplitude from neurons stimulated with sham or cLTD induction solution in the presence of absence of 1 µM apilimod or 2 µM YM201636. The induction of cLTD decreased in mEPSC amplitude. This decrease was blocked by incubation with 1 µM apilimod or 2 µM YM201636 during induction (Control: 17.52±0.55 pA ; cLTD: 14.72±0.53 pA;

cLTD+YM201636: 18.83±0.71 pA; cLTD+apilimod: 17.86±0.30 pA; 7.5min YM201636: 19.11±0.37 pA; 7.5 min apilimod: 16.72±0.48 pA; one-way ANOVA, F(5,109)=9.77, p=9.8x10-8). **(C)** Representative recordings of mEPSCs from rat cultured hippocampal neurons treated or untreated with 50 µM bicuculline for 24 h. After 23 h, the PIKfyve inhibitors, apilimod and YM201636, were added to the media of indicated dishes for 1 h. **(D)** Mean (±SEM) mEPSC amplitude. Treatment with 50 µM bicuculline for 24 h decreases mEPSC amplitude. Application of 1 µM apilimod or 2 µM YM201636 for 1 hr does not affect the amplitude of mEPSCs in control neurons not treated with bicuculline. Application of 1 µM apilimod or 2 µM YM201636 for 1 h in bicuculline treated neurons restores mEPSC amplitude to control levels (Control+DMSO: 16.15±0.49 pA ; Control+YM201636: 14.81±0.60 pA; Control+apilimod: 18.12±0.84 pA; 24h Bic+DMSO: 12.58±0.50 pA ; 24h Bic+YM201636: 14.80±0.41 pA; 24h Bic+apilimod: 17.53±0.73 pA). (one-way ANOVA, F(5,84)=9.33, p=4.3x10-7). **(E)** Representative images of surface GluA2 and PSD95 staining with or without 50 µM bicuculline for 24 h. Neurons were live labeled with an amino-terminal antibody for the GluA2 subunit and fixed. After permeabilization, neuronal cultures were stained for PSD95. **(F)** Mean (±SEM) surface GluA2 intensity quantified in the first 50 µm of dendrite relative to the average control. The abundance of sGluA2 is decreased after 24 h treatment with bicuculline. The bicuculline induced decrease is restored to control levels with 1h of PIKfyve inhibition by either 1 µM apilimod or 2 µM YM201636 (Control: 100±2.29%; 24h Bic: 83.71±1.97; 24h Bic+1h YM201636: 95.41±2.27%; 24h Bic+1h apilimod: 96.94±2.68%; one-way ANOVA, F(3,224)=11.16, p=7.48e-07). *indicates $p<0.05$.

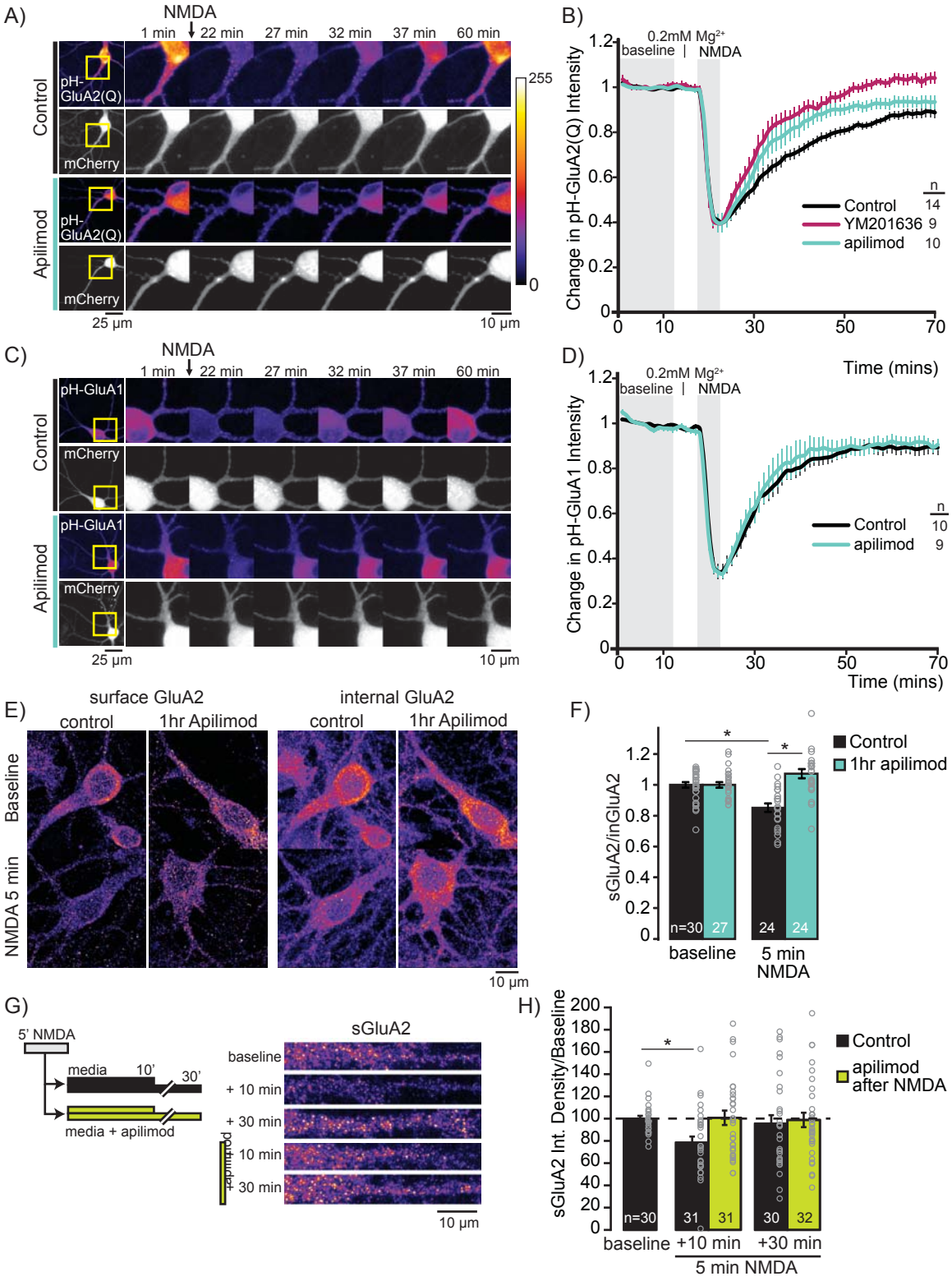

Figure 3-9. PIKfyve activity regulates AMPA receptor trafficking

(A) Representative images of neurons co-transfected with pH-GluA2(Q) and mCherry. Neurons were incubated with DMSO or PIKfyve inhibitors for 1 h prior to live-confocal imaging. During imaging all solutions were continuously perfused at 32°C. **(B)** Mean

(±SEM) intensity of pH-GluA2(Q) relative to the mean intensity of the first 10 min of imaging. Once a stable baseline was obtained, HBS (0.2 mM Mg^{2+}) was washed on for 5 min followed by 5 min stimulation with NMDA (20 µM NMDA, 10 µM Glycine, 0.2 mM Mg^{2+}). The fluorescence of pH-GluA2(Q) is quenched by NMDA stimulation. After NMDA stimulation, normal HBS was continuously perfused for the remainder of the experiment. PIKfyve inhibition by either 1 µM apilimod or 2 µM YM201636 enhances the rate of pH-GluA2(Q) fluorescence recovery. **(C)** Representative images of neurons co-transfected with pH-GluA1 and mCherry. **(D)** Mean (±SEM) intensity of pH-GluA1 relative to the mean intensity of the first 10 min of imaging. The fluorescence of pH-GluA1 is strongly quenched by NMDA stimulation, however the rate of recovery in control and PIKfyve inhibited neurons are indistinguishable. **(E)** Representative images of neurons stained for surface GluA2 (non-permeabilized) or internal GluA2 (after permeabilization) with or without 1h incubation with 1 µM apilimod. **(F)** The ratio (±SEM) of surface to internal GluA2. The surface to internal ratio is reduced by 5 min NMDA stimulation (20 µM NMDA, 10 µM Glycine, 0.2 mM Mg^{2+}) in control neurons. Incubation with 1 µM apilimod blocks the decrease in surface to internal ratio (ratio relative to average baseline: Baseline: 1.0±0.02; 5 min NMDA: 0.86±0.03; 1h apilimod: 1.0±0.02; 1h apilimod + 5 min NMDA: 1.07±0.03; one-way ANOVA, $F(3,101) = 14.68$, $p=5.26x10\text{-}8$). **(G)** Schematic of experimental design and representative images of surface GluA2 staining in dendrites. Neurons were stimulated with NMDA (20 µM NMDA, 10 µM Glycine, 0.2 mM Mg^{2+}) for 5 min and then indicated dishes were incubated with 1 µM apilimod for 10 min or 30 min at 37C. Cells were then fixed and stained for surface GluA2. **(H)** Mean (±SEM) sGluA puncta integrated density (mean intensity x puncta size). Relative to unstimulated baseline sGluA2 puncta, in control neurons NMDA stimulation transiently decreased in the integrated density of GluA2 puncta in dendrites at 10 min. When apilimod was applied after NMDA stimulation, this decrease was blocked (time after 5 min NMDA stimulation: NMDA+10min: 78.43±5.46%; NMDA+30: 95.47±7.62%; NMDA+10 w/ apilimod: 100±6.47%; NMDA+30min w/apilimod: 98.84±6.47%; Kruskal-Wallis ANOVA, $\chi2(4, 150)=12.1$, $p=0.017$). *indicates $p<0.05$.

3.7 BIBLIOGRAPHY

Anggono V, Clem RL & Huganir RL. 2011. PICK1 Loss of Function Occludes Homeostatic Synaptic Scaling. *Journal of Neuroscience,* **31,** 2188-2196.

Anggono V & Huganir RL. 2012. Regulation of AMPA receptor trafficking and synaptic plasticity. *Current opinion in neurobiology,* **22,** 461-9.

Arai Y, Ijuin T, Takenawa T, Becker LE & Takashima S. 2002. Excessive expression of synaptojanin in brains with Down syndrome. *Brain & development,* **24,** 67-72.

Arendt KL, Royo M, Fernandez-Monreal M, Knafo S, Petrok CN, Martens JR & Esteban JA. 2010. PIP3 controls synaptic function by maintaining AMPA receptor clustering at the postsynaptic membrane. *Nature neuroscience,* **13,** 36-44.

Azzedine H, Bolino A, Taïeb T, Birouk N, Di Duca M, Bouhouche A, Benamou S, Mrabet A, Hammadouche T, Chkili T, Gouider R, Ravazzolo R, Brice A, Laporte J & LeGuern E. 2003. Mutations in MTMR13, a New Pseudophosphatase Homologue of MTMR2 and Sbf1, in Two Families with an Autosomal Recessive Demyelinating Form of Charcot-Marie-Tooth Disease Associated with Early-Onset Glaucoma. *The American Journal of Human Genetics,* **72,** 1141-1153.

Balla T. 2013. Phosphoinositides: tiny lipids with giant impact on cell regulation. *Physiological reviews,* **93,** 1019-137.

Baulac S, Lenk GM, Dufresnois B, Bencheikh BOA, Couarch P, Renard J, Larson PA, Ferguson CJ, Noé E, Poirier K, Hubans C, Ferreira S, Guerrini R, Ouazzani R, El KH, Hachimi KHE, Meisler MH & Leguern E. 2014. Role of the phosphoinositide phosphatase FIG4 gene in familial epilepsy with polymicrogyria. *Neurology,* **82,** 1068-75.

Bolino A, Muglia M, Conforti FL, LeGuern E, Salih MAM, Georgiou DM, Christodoulou K, Hausmanowa-Petrusewicz I, Mandich P, Schenone A, Gambardella A, Bono F, Quattrone A, Devoto M & Monaco AP. 2000. Charcot-Marie-Tooth type 4B is caused by mutations in the gene encoding myotubularin-related protein-2. *Nature Genetics,* **25,** 17-19.

Bonangelino CJ, Catlett NL & Weisman LS. 1997. Vac7p, a novel vacuolar protein, is required for normal vacuole inheritance and morphology. *Molecular and cellular biology,* **17,** 6847-58.

Botelho RJ, Efe JA, Teis D & Emr SD. 2008. Assembly of a Fab1 phosphoinositide kinase signaling complex requires the Fig4 phosphoinositide phosphatase. *Mol Biol Cell,* **19,** 4273-86.

Bridges D, Ma JT, Park S, Inoki K, Weisman LS & Saltiel AR. 2012. Phosphatidylinositol 3,5-bisphosphate plays a role in the activation and subcellular localization of mechanistic target of rapamycin 1. *Molecular biology of the cell,* **23,** 2955-62.

Cai X, Xu Y, Cheung AK, Tomlinson RC, Alcazar-Roman A, Murphy L, Billich A, Zhang B, Feng Y, Klumpp M, Rondeau JM, Fazal AN, Wilson CJ, Myer V, Joberty G, Bouwmeester T, Labow MA, Finan PM, Porter JA, Ploegh HL, Baird D, De Camilli P, Tallarico JA & Huang Q. 2013. PIKfyve, a class III PI kinase, is the target of the small molecular IL-12/IL-23 inhibitor apilimod and a player in Toll-like receptor signaling. *Chemistry & biology,* **20,** 912-21.

Campeau PM, Lenk GM, Lu JT, Bae Y, Burrage L, Turnpenny P, Roman Corona-Rivera J, Morandi L, Mora M, Reutter H, Vulto-van Silfhout AT, Faivre L, Haan E, Gibbs RA, Meisler MH & Lee BH. 2013. Yunis-Varon syndrome is caused by mutations in FIG4, encoding a phosphoinositide phosphatase. *American journal of human genetics,* **92,** 781-91.

Chen L, Lau AG & Sarti F. 2014. Synaptic retinoic acid signaling and homeostatic synaptic plasticity. *Neuropharmacology,* **78,** 3-12.

Chow CY, Landers JE, Bergren SK, Sapp PC, Grant AE, Jones JM, Everett L, Lenk GM, McKenna-Yasek DM, Weisman LS, Figlewicz D, Brown RH & Meisler MH. 2009. Deleterious variants of FIG4, a phosphoinositide phosphatase, in patients with ALS. *American journal of human genetics,* **84,** 85-8.

Chow CY, Zhang Y, Dowling JJ, Jin N, Adamska M, Shiga K, Szigeti K, Shy ME, Li J, Zhang X, Lupski JR, Weisman LS & Meisler MH. 2007. Mutation of FIG4 causes neurodegeneration in the pale tremor mouse and patients with CMT4J. *Nature,* **448,** 68-72.

Cingolani LA, Thalhammer A, Yu LM, Catalano M, Ramos T, Colicos MA & Goda Y. 2008. Activity-dependent regulation of synaptic AMPA receptor composition and abundance by beta3 integrins. *Neuron,* **58,** 749-62.

Cooke FT, Dove SK, McEwen RK, Painter G, Holmes AB, Hall MN, Michell RH & Parker PJ. 1998. The stress-activated phosphatidylinositol 3-phosphate 5-kinase Fab1p is essential for vacuole function in S-cerevisiae. *Current Biology,* **8,** 1219-1222.

Cossec JC, Lavaur J, Berman DE, Rivals I, Hoischen A, Stora S, Ripoll C, Mircher C, Grattau Y, Olivomarin JC, de Chaumont F, Lecourtois M, Antonarakis SE, Veltman JA, Delabar JM, Duyckaerts C, Di Paolo G & Potier MC. 2012. Trisomy for synaptojanin1 in Down syndrome is functionally linked to the enlargement of early endosomes. *Human molecular genetics,* **21,** 3156-72.

Cremona O, Di Paolo G, Wenk MR, Luthi A, Kim WT, Takei K, Daniell L, Nemoto Y, Shears SB, Flavell RA, McCormick DA & De Camilli P. 1999. Essential role of phosphoinositide metabolism in synaptic vesicle recycling. *Cell,* **99,** 179-88.

Davis GW. 2013. Homeostatic signaling and the stabilization of neural function. *Neuron,* **80,** 718-28.

Di Paolo G & De Camilli P. 2006. Phosphoinositides in cell regulation and membrane dynamics. *Nature,* **443,** 651-657.

Di Paolo G, Moskowitz HS, Gipson K, Wenk MR, Voronov S, Obayashi M, Flavell R, Fitzsimonds RM, Ryan TA & De Camilli P. 2004. Impaired PtdIns(4,5)P-2 synthesis in nerve terminals produces defects in synaptic vesicle trafficking. *Nature,* **431,** 415-422.

Dove SK, Cooke FT, Douglas MR, Sayers LG, Parker PJ & Michell RH. 1997. Osmotic stress activates phosphatidylinositol-3,5-bisphosphate synthesis. *Nature,* **390,** 187-92.

Duex JE, Tang F & Weisman LS. 2006. The Vac14p-Fig4p complex acts independently of Vac7p and couples PI3,5P2 synthesis and turnover. *The Journal of cell biology,* **172,** 693-704.

Esteban JA. 2008. Intracellular machinery for the transport of AMPA receptors. *British Journal of Pharmacology,* **153,** S35-S43.

Evers DM, Matta JA, Hoe HS, Zarkowsky D, Lee SH, Isaac JT & Pak DTS. 2010. Plk2 attachment to NSF induces homeostatic removal of GluA2 during chronic overexcitation. *Nature neuroscience,* **13,** 1199-1207.

Fernandez-Monreal M, Brown TC, Royo M & Esteban JA. 2012. The Balance between Receptor Recycling and Trafficking toward Lysosomes Determines Synaptic Strength during Long-Term Depression. *Journal of Neuroscience,* **32,** 13200-13205.

Gainey MA, Hurvitz-Wolff JR, Lambo ME & Turrigiano GG. 2009. Synaptic Scaling Requires the GluR2 Subunit of the AMPA Receptor. *Journal of Neuroscience,* **29,** 6479-6489.

Gary JD, Wurmser AE, Bonangelino CJ, Weisman LS & Emr SD. 1998. Fab1p is essential for PtdIns(3)P 5-kinase activity and the maintenance of vacuolar size and membrane homeostasis. *The Journal of cell biology,* **143,** 65-79.

Gong LW & De Camilli P. 2008. Regulation of postsynaptic AMPA responses by synaptojanin 1. *Proceedings of the National Academy of Sciences of the United States of America,* **105,** 17561-17566.

Goold CP & Nicoll RA. 2010. Single-Cell Optogenetic Excitation Drives Homeostatic Synaptic Depression. *Neuron,* **68,** 512-528.

Haffner C, Di Paolo G, Rosenthal JA & De Camilli P. 2000. Direct interaction of the 170 kDa isoform of synaptojanin 1 with clathrin and with the clathrin adaptor AP-2. *Current Biology,* **10,** 471-474.

Hardingham N, Dachtler J & Fox K. 2013. The role of nitric oxide in pre-synaptic plasticity and homeostasis. *Frontiers in cellular neuroscience,* **7,** 190.

Harold D, Abraham R, Hollingworth P, Sims R, Gerrish A, Hamshere ML, Pahwa JS, Moskvina V, Dowzell K, Williams A, Jones N, Thomas C, Stretton A, Morgan AR, Lovestone S, Powell J, Proitsi P, Lupton MK, Brayne C, Rubinsztein DC, Gill M, Lawlor B, Lynch A, Morgan K, Brown KS, Passmore PA, Craig D, McGuinness B, Todd S, Holmes C, Mann D, Smith AD, Love S, Kehoe PG, Hardy J, Mead S, Fox N, Rossor M, Collinge J, Maier W, Jessen F, Schurmann B, van den Bussche H, Heuser I, Kornhuber J, Wiltfang J, Dichgans M, Frolich L, Hampel H, Hull M, Rujescu D, Goate AM, Kauwe JSK, Cruchaga C, Nowotny P, Morris JC, Mayo K, Sleegers K, Bettens K, Engelborghs S, De Deyn PP, Van Broeckhoven C, Livingston G, Bass NJ, Gurling H, McQuillin A, Gwilliam R, Deloukas P, Al-Chalabi A, Shaw CE, Tsolaki M, Singleton AB, Guerreiro R, Muhleisen TW, Nothen MM, Moebus S, Jockel KH, Klopp N, Wichmann HE, Carrasquillo MM, Pankratz VS, Younkin SG, Holmans PA, O'Donovan M, Owen MJ & Williams J. 2009. Genome-wide association study identifies variants at CLU and PICALM associated with Alzheimer's disease. *Nature genetics,* **41,** 1088-U61.

Henley JM & Wilkinson KA. 2013. AMPA receptor trafficking and the mechanisms underlying synaptic plasticity and cognitive aging. *Dialogues in clinical neuroscience,* **15,** 11-27.

Henry FE, McCartney AJ, Neely R, Perez AS, Carruthers CJL, Stuenkel EL, Inoki K & Sutton MA. 2012. Retrograde Changes in Presynaptic Function Driven by Dendritic mTORC1. *Journal of Neuroscience,* **32,** 17128-17142.

Horne EA & Dell'Acqua ML. 2007. Phospholipase C is required for changes in postsynaptic structure and function associated with NMDA receptor-dependent long-term depression. *Journal of Neuroscience,* **27,** 3523-3534.

Houlden H, King RHM, Wood NW, Thomas PK & Reilly MM. 2001. Mutations in the 5 ' region of the myotubularin-related protein 2 (MTMR2) gene in autosomal recessive hereditary neuropathy with focally folded myelin. *Brain,* **124,** 907-915.

Hu JH, Park JM, Park S, Xiao B, Dehoff MH, Kim S, Hayashi T, Schwarz MK, Huganir RL, Seeburg PH, Linden DJ & Worley PF. 2010. Homeostatic Scaling Requires Group I mGluR Activation Mediated by Homer1a. *Neuron,* **68,** 1128-1142.

Ikonomov OC, Sbrissa D, Delvecchio K, Xie YF, Jin JP, Rappolee D & Shisheva A. 2011. The phosphoinositide kinase PIKfyve is vital in early embryonic development: preimplantation lethality of PIKfyve(-/-) embryos but normality of PIKfyve(+/-) mice. *Journal of Biological Chemistry,* **286,** 13404-13413.

Ikonomov OC, Sbrissa D, Fenner H & Shisheva A. 2009. PIKfyve-ArPIKfyve-Sac3 core complex: contact sites and their consequence for Sac3 phosphatase activity and endocytic membrane homeostasis. *The Journal of biological chemistry,* **284,** 35794-806.

Ikonomov OC, Sbrissa D & Shisheva A. 2001. Mammalian cell morphology and endocytic membrane homeostasis require enzymatically active phosphoinositide 6-kinase PIKfyve. *Journal of Biological Chemistry,* **276,** 26141-26147.

Irie F, Okuno M, Pasquale EB & Yamaguchi Y. 2005. EphrinB-EphB signalling regulates clathrin-mediated endocytosis through tyrosine phosphorylation of synaptojanin 1. *Nature Cell Biology,* **7,** 501-U69.

Jakawich SK, Neely RM, Djakovic SN, Patrick GN & Sutton MA. 2010. An Essential Postsynaptic Role for the Ubiquitin Proteasome System in Slow Homeostatic Synaptic Plasticity in Cultured Hippocampal Neurons. *Neuroscience,* **171,** 1016-1031.

Jefferies HB, Cooke FT, Jat P, Boucheron C, Koizumi T, Hayakawa M, Kaizawa H, Ohishi T, Workman P, Waterfield MD & Parker PJ. 2008. A selective PIKfyve inhibitor blocks PtdIns(3,5)P(2) production and disrupts endomembrane transport and retroviral budding. *EMBO Rep,* **9,** 164-70.

Jin N, Chow CY, Liu L, Zolov SN, Bronson R, Davisson M, Petersen JL, Zhang Y, Park S, Duex JE, Goldowitz D, Meisler MH & Weisman LS. 2008. VAC14 nucleates a protein complex essential for the acute interconversion of PI3P and PI(3,5)P(2) in yeast and mouse. *The EMBO journal,* **27,** 3221-34.

Jones DR, Gonzalez-Garcia A, Diez E, Martinez AC, Carrera AC & Merida I. 1999. The identification of phosphatidylinositol 3,5-bisphosphate in T-lymphocytes and its regulation by interleukin-2. *J Biol Chem,* **274,** 18407-13.

Jungerius BJ, Hoogendoorn MLC, Bakker SC, van't Slot R, Bardoel AF, Ophoff RA, Wijmenga C, Kahn RS & Sinke RJ. 2008. An association screen of myelin-related genes implicates the chromosome 22q11 PIK4CA gene in schizophrenia. *Molecular psychiatry,* **13,** 1060-1068.

Jurado S, Benoist M, Lario A, Knafo S, Petrok CN & Esteban JA. 2010. PTEN is recruited to the postsynaptic terminal for NMDA receptor-dependent long-term depression. *The EMBO journal,* **29,** 2827-40.

Khuong TM, Habets RLP, Kuenen S, Witkowska A, Kasprowicz J, Swerts J, Jahn R, van den Bogaart G & Verstreken P. 2013. Synaptic PI(3,4,5)P-3 Is Required for Syntaxin1A Clustering and Neurotransmitter Release. *Neuron,* **77,** 1097-1108.

Kim JI, Lee HR, Sim SE, Baek J, Yu NK, Choi JH, Ko HG, Lee YS, Park SW, Kwak C, Ahn SJ, Choi SY, Kim H, Kim KH, Backx PH, Bradley CA, Kim E, Jang DJ, Lee K, Kim SJ, Zhuo M, Collingridge GL & Kaang BK. 2011. PI3K gamma is required for NMDA receptor-dependent long-term depression and behavioral flexibility. *Nature neuroscience,* **14,** 1447-U123.

Kim WT, Chang SH, Daniell L, Cremona O, Di Paolo G & De Camilli P. 2002. Delayed reentry of recycling vesicles into the fusion-competent synaptic vesicle pool in synaptojanin 1 knockout mice. *Proceedings of the National Academy of Sciences of the United States of America,* **99,** 17143-17148.

Knafo S & Esteban JA. 2012. Common pathways for growth and for plasticity. *Current Opinion in Neurobiology,* **22,** 405-411.

Krebs CE, Karkheiran S, Powell JC, Cao M, Makarov V, Darvish H, Di Paolo G, Walker RH, Shahidi GA, Buxbaum JD, De Camilli P, Yue ZY & Paisan-Ruiz C. 2013. The Sac1 Domain of SYNJ1 Identified Mutated in a Family with Early-Onset Progressive Parkinsonism with Generalized Seizures. *Human Mutation,* **34,** 1200-1207.

Lambo ME & Turrigiano GG. 2013. Synaptic and Intrinsic Homeostatic Mechanisms Cooperate to Increase L2/3 Pyramidal Neuron Excitability during a Late Phase of Critical Period Plasticity. *Journal of Neuroscience,* **33,** 8810-8819.

Lee HK, Kameyama K, Huganir RL & Bear MF. 1998. NMDA induces long-term synaptic depression and dephosphorylation of the GluR1 subunit of AMPA receptors in hippocampus. *Neuron,* **21,** 1151-1162.

Lee HW, Kim Y, Han K, Kim H & Kim E. 2010. The phosphoinositide 3-phosphatase MTMR2 interacts with PSD-95 and maintains excitatory synapses by modulating endosomal traffic. *J Neurosci,* **30,** 5508-18.

Lee KFH, Soares C & Beique JC. 2014. Tuning into diversity of homeostatic synaptic plasticity. *Neuropharmacology,* **78,** 31-37.

Lee KJ, Lee Y, Rozeboom A, Lee JY, Udagawa N, Hoe HS & Pak DT. 2011. Requirement for Plk2 in orchestrated ras and rap signaling, homeostatic structural plasticity, and memory. *Neuron,* **69,** 957-73.

Lee SH, Simonetta A & Sheng M. 2004. Subunit rules governing the sorting of internalized AMPA receptors in hippocampal neurons. *Neuron,* **43,** 221-236.

Lemaire JF & McPherson PS. 2006. Binding of Vac14 to neuronal nitric oxide synthase: Characterisation of a new internal PDZ-recognition motif. *FEBS Lett,* **580,** 6948-54.

Li X, Wang X, Zhang X, Zhao M, Tsang WL, Zhang Y, Yau RG, Weisman LS & Xu H. 2013. Genetically encoded fluorescent probe to visualize intracellular phosphatidylinositol 3,5-bisphosphate localization and dynamics. *Proceedings of*

the National Academy of Sciences of the United States of America, **110,** 21165-70.

Maffei A & Turrigiano GG. 2008. Multiple modes of network homeostasis in visual cortical layer 2/3. *Journal of Neuroscience,* **28,** 4377-4384.

Malinow R & Malenka RC. 2002. AMPA receptor trafficking and synaptic plasticity. *Annual review of neuroscience,* **25,** 103-26.

Man HY, Lin JW, Ju WH, Ahmadian G, Liu LD, Becker LE, Sheng M & Wang YT. 2000. Regulation of AMPA receptor-mediated synaptic transmission by clathrin-dependent receptor internalization. *Neuron,* **25,** 649-662.

Mani M, Lee SY, Lucast L, Cremona O, Di Paolo G, De Camlli P & Ryan TA. 2007. The dual phosphatase activity of synaptojanin1 is required for both efficient synaptic vesicle endocytosis and reavailability at nerve terminals. *Neuron,* **56,** 1004-1018.

McCartney AJ, Zhang Y & Weisman LS. 2014. Phosphatidylinositol 3,5-bis phosphate: Low abundance. High significance. . *Bioessays,* **36,** 52-64.

McPherson PS, Garcia EP, Slepnev VI, David C, Zhang X, Grabs D, Sossin WS, Bauerfeind R, Nemoto Y & De Camilli P. 1996. A presynaptic inositol-5-phosphatase. *Nature,* **379,** 353-7.

Naj AC, Jun G, Beecham GW, Wang LS, Vardarajan BN, Buros J, Gallins PJ, Buxbaum JD, Jarvik GP, Crane PK, Larson EB, Bird TD, Boeve BF, Graff-Radford NR, De Jager PL, Evans D, Schneider JA, Carrasquillo MM, Ertekin-Taner N, Younkin SG, Cruchaga C, Kauwe JSK, Nowotny P, Kramer P, Hardy J, Huentelman MJ, Myers AJ, Barmada MM, Demirci FY, Baldwin CT, Green RC, Rogaeva E, St George-Hyslop P, Arnold SE, Barber R, Beach T, Bigio EH, Bowen JD, Boxer A, Burke JR, Cairns NJ, Carlson CS, Carney RM, Carroll SL, Chui HC, Clark DG, Corneveaux J, Cotman CW, Cummings JL, DeCarli C, DeKosky ST, Diaz-Arrastia R, Dick M, Dickson DW, Ellis WG, Faber KM, Fallon KB, Farlow MR, Ferris S, Frosch MP, Galasko DR, Ganguli M, Gearing M, Geschwind DH, Ghetti B, Gilbert JR, Gilman S, Giordani B, Glass JD, Growdon JH, Hamilton RL, Harrell LE, Head E, Honig LS, Hulette CM, Hyman BT, Jicha GA, Jin LW, Johnson N, Karlawish J, Karydas A, Kaye JA, Kim R, Koo EH, Kowall NW, Lah JJ, Levey AI, Lieberman AP, Lopez OL, Mack WJ, Marson DC, Martiniuk F, Mash DC, Masliah E, McCormick WC, McCurry SM, McDavid AN, Mckee AC, Mesulam M, Miller BL, et al. 2011. Common variants at MS4A4/MS4A6E, CD2AP, CD33 and EPHA1 are associated with late-onset Alzheimer's disease. *Nature genetics,* **43,** 436-+.

Nicholson G, Lenk GM, Reddel SW, Grant AE, Towne CF, Ferguson CJ, Simpson E, Scheuerle A, Yasick M, Hoffman S, Blouin R, Brandt C, Coppola G, Biesecker LG, Batish SD & Meisler MH. 2011. Distinctive genetic and clinical features of CMT4J: a severe neuropathy caused by mutations in the PI(3,5)P-2 phosphatase FIG4. *Brain : a journal of neurology,* **134,** 1959-1971.

O'Brien RJ, Kamboj S, Ehlers MD, Rosen KR, Fischbach GD & Huganir RL. 1998. Activity-dependent modulation of synaptic AMPA receptor accumulation. *Neuron,* **21,** 1067-1078.

Opazo P, Sainlos M & Choquet D. 2012. Regulation of AMPA receptor surface diffusion by PSD-95 slots. *Current Opinion in Neurobiology,* **22,** 453-460.

Pak DTS & Sheng M. 2003. Targeted protein degradation and synapse remodeling by an inducible protein kinase. *Science,* **302,** 1368-1373.

Pozo K, Cingolani LA, Bassani S, Laurent F, Passafaro M & Goda Y. 2012. beta 3 integrin interacts directly with GluA2 AMPA receptor subunit and regulates AMPA receptor expression in hippocampal neurons. *Proceedings of the National Academy of Sciences of the United States of America,* **109,** 1323-1328.

Pozo K & Goda Y. 2010. Unraveling Mechanisms of Homeostatic Synaptic Plasticity. *Neuron,* **66,** 337-351.

Pribiag H & Stellwagen D. 2014. Neuroimmune regulation of homeostatic synaptic plasticity. *Neuropharmacology,* **78,** 13-22.

Qin Y, Zhu YH, Baumgart JP, Stornetta RL, Seidenman K, Mack V, van Aelst L & Zhu JJ. 2005. State-dependent Ras signaling and AMPA receptor trafficking. *Genes & development,* **19,** 2000-2015.

Rathje M, Fang HQ, Bachman JL, Anggono V, Gether U, Huganir RL & Madsen KL. 2013. AMPA receptor pHluorin-GluA2 reports NMDA receptor-induced intracellular acidification in hippocampal neurons. *Proceedings of the National Academy of Sciences of the United States of America,* **110,** 14426-14431.

Rudge SA, Anderson DM & Emr SD. 2004. Vacuole size control: Regulation of PtdIns(3,5)P-2 levels by the vacuole-associated Vac14-Fig4 complex, a PtdIns(3.5)P-2-specific phosphatase. *Molecular Biology of the Cell,* **15,** 24-36.

Saheki Y & De Camilli P. 2012. Synaptic Vesicle Endocytosis. *Cold Spring Harbor Perspectives in Biology,* **4**. DOI 10.1101/cshperspect.a005645.

Seebohm G, Neumann S, Theiss C, Novkovic T, Hill EV, Tavare JM, Lang F, Hollmann M, Manahan-Vaughan D & Strutz-Seebohm N. 2012. Identification of a Novel Signaling Pathway and Its Relevance for GluA1 Recycling. *Plos One,* **7,** e33889.

Seeburg DP, Feliu-Mojer M, Gaiottino J, Pak DT & Sheng M. 2008. Critical role of CDK5 and Polo-like kinase 2 in homeostatic synaptic plasticity during elevated activity. *Neuron,* **58,** 571-83.

Seeburg DP & Sheng M. 2008. Activity-induced Polo-like kinase 2 is required for homeostatic plasticity of hippocampal neurons during epileptiform activity. *The Journal of neuroscience : the official journal of the Society for Neuroscience,* **28,** 6583-91.

Senderek J, Bergmann C, Weber S, Ketelsen U-P, Schorle H, Rudnik-Schöneborn S, Büttner R, Buchheim E & Zerres K. 2003. Mutation of the SBF2 gene, encoding a novel member of the myotubularin family, in Charcot–Marie–Tooth neuropathy type 4B2/11p15. *Human Molecular Genetics,* **12,** 349-356.

Shepherd JD, Rumbaugh G, Wu J, Chowdhury S, Plath N, Kuhl D, Huganir RL & Worley PF. 2006. Arc/Arg3.1 mediates homeostatic synaptic scaling of AMPA receptors. *Neuron,* **52,** 475-484.

Shi SH, Hayashi Y, Esteban JA & Malinow R. 2001. Subunit-specific rules governing AMPA receptor trafficking to synapses in hippocampal pyramidal neurons. *Cell,* **105,** 331-343.

Siddoway B, Hou HL & Xia HH. 2014. Molecular mechanisms of homeostatic synaptic downscaling. *Neuropharmacology,* **78,** 38-44.

Siddoway BA, Altimimi HF, Hou H, Petralia RS, Xu B, Stellwagen D & Xia H. 2013. An essential role for inhibitor-2 regulation of protein phosphatase-1 in synaptic scaling. *The Journal of neuroscience : the official journal of the Society for Neuroscience,* **33,** 11206-11.

Stokes CE & Hawthorne JN. 1987. Reduced Phosphoinositide Concentrations in Anterior Temporal Cortex of Alzheimer-Diseased Brains. *Journal of neurochemistry,* **48,** 1018-1021.

Sun Q & Turrigiano GG. 2011. PSD-95 and PSD-93 Play Critical But Distinct Roles in Synaptic Scaling Up and Down. *Journal of Neuroscience,* **31,** 6800-6808.

Sutton MA, Ito HT, Cressy P, Kempf C, Woo JC & Schuman EM. 2006. Miniature neurotransmission stabilizes synaptic function via tonic suppression of local dendritic protein synthesis. *Cell,* **125,** 785-99.

Takasuga S, Horie Y, Sasaki J, Ge-Hong Sun-Wada G, Kawamura N, Iizuka R, Mizuno K, Eguchi S, Kofuji S, Kiyotaka K, Yamazaki M, Kontani K, Harada A, Katada T, Suzuki A, Wada O, Ohnishi H & Sasaki T. 2013. Critical roles of type III phosphatidylinositol phosphate kinase in murine embryonic visceral endoderm and adult intestine. *Proceedings of the National Academy of Sciences of the United States of America,* **110,** 1726-1731.

Takeuchi K, Gertner MJ, Zhou J, Parada LF, Bennett MV & Zukin RS. 2013. Dysregulation of synaptic plasticity precedes appearance of morphological defects in a Pten conditional knockout mouse model of autism. *Proceedings of the National Academy of Sciences of the United States of America,* **110,** 4738-43.

Tatavarty V, Sun Q & Turrigiano GG. 2013. How to scale down postsynaptic strength. *The Journal of neuroscience : the official journal of the Society for Neuroscience,* **33,** 13179-89.

Thalhammer A & Cingolani LA. 2014. Cell adhesion and homeostatic synaptic plasticity. *Neuropharmacology,* **78,** 23-30.

Thiagarajan TC, Lindskog M & Tsien RW. 2005. Adaptation to synaptic inactivity in hippocampal neurons. *Neuron,* **47,** 725-737.

Tsujita K, Itoh T, Ijuin T, Yamamoto A, Shisheva A, Laporte J & Takenawa T. 2004. Myotubularin regulates the function of the late endosome through the gram domain-phosphatidylinositol 3,5-bisphosphate interaction. *J Biol Chem,* **279,** 13817-24.

Tsuruta F, Green EM, Rousset M & Dolmetsch RE. 2009. PIKfyve regulates CaV1.2 degradation and prevents excitotoxic cell death. *J Cell Biol,* **187,** 279-94.

Turrigiano G. 2012. Homeostatic Synaptic Plasticity: Local and Global Mechanisms for Stabilizing Neuronal Function. *Cold Spring Harbor Perspectives in Biology,* **4**.

Turrigiano GG, Leslie KR, Desai NS, Rutherford LC & Nelson SB. 1998. Activity-dependent scaling of quantal amplitude in neocortical neurons. *Nature,* **391,** 892-6.

Unoki T, Matsuda S, Kakegawa W, Ngo TBV, Kohda K, Suzuki A, Funakoshi Y, Hasegawa H, Yuzaki M & Kanaho Y. 2012. NMDA Receptor-Mediated PIP5K Activation to Produce PI(4,5)P-2 Is Essential for AMPA Receptor Endocytosis during LTD. *Neuron,* **73,** 135-148.

Vitureira N, Letellier M & Goda Y. 2012. Homeostatic synaptic plasticity: from single synapses to neural circuits. *Current Opinion in Neurobiology,* **22,** 516-521.

Vorstman JAS, Chow EW, Ophoff RA, van Engeland H, Beemer FA, Kahn RS, Sinke RJ & Basset AS. 2009. Association of the PIK4CA Schizophrenia-Susceptibility Gene in Adults With the 22q11.2 Deletion Syndrome. *American Journal of Medical Genetics Part B-Neuropsychiatric Genetics,* **150B,** 430-433.

Wenk MR, Pellegrini L, Klenchin VA, Di Paolo G, Chang SH, Daniell L, Arioka M, Martin TF & De Camilli P. 2001. PIP kinase 1 gamma is the major PI(4,5)P-2 synthesizing enzyme at the synapse. *Neuron,* **32,** 79-88.

Whiteford CC, Brearley CA & Ulug ET. 1997. Phosphatidylinositol 3,5-bisphosphate defines a novel PI 3-kinase pathway in resting mouse fibroblasts. *Biochem J,* **323 (Pt 3),** 597-601.

Yamamoto A, Dewald DB, Boronenkov IV, Anderson RA, Emr SD & Koshland D. 1995. Novel Pi(4)P 5-Kinase Homolog, Fab1p, Essential for Normal Vacuole Function and Morphology in Yeast. *Molecular Biology of the Cell,* **6,** 525-539.

Yin HL & Janmey PA. 2003. Phosphoinositide regulation of the actin cytoskeleton. *Annual review of physiology,* **65,** 761-89.

Yu LMY & Goda Y. 2009. Presenilin 1 Modulates Glutamatergic Synaptic Transmission at Hippocampal Synapses. *Journal of Physiological Sciences,* **59,** 367-367.

Zhang Y, McCartney AJ, Zolov SN, Ferguson CJ, Meisler MH, Sutton MA & Weisman LS. 2012. Modulation of synaptic function by VAC14, a protein that regulates the phosphoinositides PI(3,5)P(2) and PI(5)P. *EMBO J,* **31,** 3442-56.

Zhang Y, Zolov SN, Chow CY, Slutsky SG, Richardson SC, Piper RC, Yang B, Nau JJ, Westrick RJ, Morrison SJ, Meisler MH & Weisman LS. 2007. Loss of Vac14, a regulator of the signaling lipid phosphatidylinositol 3,5-bisphosphate, results in neurodegeneration in mice. *Proceedings of the National Academy of Sciences of the United States of America,* **104,** 17518-23.

Zolov SN, Bridges D, Zhang Y, Lee W-W, Riehle E, Verma R, Lenk GM, Converso-Baran K, Weide T, Albin RL, Saltiel AR, Meisler MH, Russell MW & Weisman LS. 2012. In vivo, Pikfyve generates PI(3,5)P2, which serves as both a signaling lipid and the major precursor for PI5P. *Proceedings of the National Academy of Sciences,* **109,** 17472-17477.

Zubenko GS, Stiffler JS, Hughes HB & Martinez AJ. 1999. Reductions in brain phosphatidylinositol kinase activities in Alzheimer's disease. *Biological psychiatry,* **45,** 731-736.

CHAPTER 4

RAPID HOMEOSTATIC REGULATION OF SYNAPTIC FUNCTION AND INTRINSIC EXCITABILITY

4.1 SUMMARY

Chronic changes in neural activity are known to engage a diverse set of compensatory cellular mechanisms that promote stabilization of action potential firing rates, but how these distinct homeostatic adaptations are coordinately used by neurons is not well understood. Here we show that direct inhibition of AMPA receptors rapidly regulates the intrinsic excitability of neurons following activity blockade by increasing the level of voltage-gated sodium channels in the axon initial segment, in a protein synthesis-dependent manner. Earlier work has shown that AMPA receptor blockade acts locally to increase postsynaptic strength by increasing the synthesis of glutamate receptors and presynaptically through enhancement of presynaptic release probability, which also requires protein synthesis. In experiments where evoked release was blocked, it was possible to both measure spontaneous excitatory synaptic currents and the intrinsic excitability in the same neuron. This enabled us to examine all three points of homeostatic regulation; we found 1 hour of AMPA receptor blockade increases mEPSC amplitude, frequency and intrinsic excitability. Taken together, these results suggest that neurons engage multiple protein synthesis dependent cellular mechanisms

to compensate for a reduction in the excitatory drive at the local synaptic level and through modulation of the global excitability of the neuron.

4.2 INTRODUCTION

Neural networks maintain the ability to adapt to and compensate for changes in levels of synaptic activity by engaging a diverse set of homeostatic control mechanisms. Without such mechanisms, the high variability of network dynamics could promote network dysfunction and/or leave neurons insensitive to changes in synaptic drive (Turrigiano and Nelson, 2004; Davis, 2006; Marder and Goaillard, 2006; Pozo and Goda, 2010; Turrigiano, 2011; Vitureira et al., 2012). At the level of single neurons, multiple points of control have been shown to contribute to the overall homeostatic response, including postsynaptic strength (O'Brien et al., 1998; Turrigiano et al., 1998; Burrone et al., 2002; Desai et al., 2002; Thiagarajan et al., 2005; Wierenga et al., 2005; Gonzalez-Islas and Wenner, 2006; Stellwagen and Malenka, 2006; Echegoyen et al., 2007; Cingolani et al., 2008; Tokuoka and Goda, 2008; Jakawich et al., 2010; Henry et al., 2012), presynaptic probability of vesicle release (Bacci et al., 2001; Murthy et al., 2001; Burrone et al., 2002; Wang et al., 2004; De Gois et al., 2005; Thiagarajan et al., 2005; Frank et al., 2006; Wierenga et al., 2006; Cingolani et al., 2008; Tokuoka and Goda, 2008; Frank et al., 2009; Jakawich et al., 2010; Henry et al., 2012), inhibitory tone (Hendry and Jones, 1986, 1988; Hendry et al., 1994; Benevento et al., 1995; Marty et al., 1997; Rutherford et al., 1997; Kilman et al., 2002; Maffei et al., 2004; Gonzalez-Islas and Wenner, 2006; Hartman et al., 2006; Echegoyen et al., 2007; Bartley et al., 2008; Kim and Alger, 2010), and intrinsic excitability (Turrigiano et al., 1994; Desai et al., 1999b;

Burrone et al., 2002; Maffei and Turrigiano, 2008). Though each component of activity has been the focus of a number of studies, the detailed mechanisms of induction and expression for homeostatic control of network dynamics are still emerging. For example, some forms of homeostatic plasticity act globally, by either slowly altering neuronal firing rates (e.g., changes in intrinsic neuron excitability) or via cell-wide scaling of synaptic responsiveness over days (Turrigiano et al., 1998; Maffei and Turrigiano, 2008; Turrigiano, 2008; Yu and Goda, 2009). By contrast, more rapid forms of homeostatic plasticity occur over hours when synaptic activity is blocked directly and are implemented locally, at a restricted number of synapses (Ju et al., 2004; Sutton and Schuman, 2006; Branco et al., 2008; Hou et al., 2008; Jakawich et al., 2010; Henry et al., 2012). However, it is not known whether induction of homeostatic plasticity that acts locally may also induce global homeostatic mechanisms, such as changes in intrinsic excitability. Importantly, the coupling of the synaptic response with membrane excitability critically determines the output of the neuron.

Basal activation of AMPA receptors is important for homeostasis of presynaptic and postsynaptic strength. Chronic blockade, over 24h, of synaptic activation triggers compensatory increases in synaptic strength (Thiagarajan et al., 2002; Thiagarajan et al., 2005; Stellwagen and Malenka, 2006; Wang et al., 2011). Direct blockade of AMPA receptors for just hours increases AMPA receptor number and presynaptic release probability (Jakawich et al., 2010; Henry et al., 2012). Although the same stimulus was used to induce both forms of homeostatic control, each is controlled by distinct mechanisms. In response to antagonism of AMPA receptors by CNQX, cultured

hippocampal neurons synthesize and release BDNF locally in dendrites, which acts as a retrograde messenger signal to increase the probability of vesicle release in presynaptic terminals in hours(Jakawich et al., 2010; Henry et al., 2012). This rapid, retrograde signaling of BDNF-mediated modulation of presynaptic release is also dependent on postsynaptic mTOR activity (Henry et al., 2012). The rapid compensation concomitantly occurring in postsynaptic AMPA receptor number likely involves all-*trans* retinoic acid (Aoto et al., 2008; Wang et al., 2011) and TNFα (Stellwagen and Malenka, 2006; Steinmetz and Turrigiano, 2010). *In vivo*, it is likely that multiple homeostatic regulatory mechanisms work in concert to achieve homeostasis, and understanding the similarities and differences will be crucial for understanding normal brain function, as well as the etiology of pathological dysfunction underlying diseases such as epilepsy. Importantly, it is not known if in addition to regulating synaptic function, brief periods of AMPA receptor blockade engage homeostatic mechanisms to regulate the intrinsic excitability of pyramidal neurons.

In this study, we asked if cultured hippocampal neurons regulate membrane excitability in response to blockade of different facets of activity (action potentials, AMPA receptor or NMDA receptor activation) on timescales known to induce compensatory synaptic adaptations. To examine intrinsic excitability, we measured the number of action potentials in response to brief pulses of current of varying amplitudes. We found that blocking AMPA receptors (1h+), but not NMDA receptors or action potentials, for the same brief period leads to enhancement of intrinsic neuron excitability. The homeostatic plasticity in membrane excitability was observed

concomitantly, in the same neuron, with synaptic compensation. Similar to the synaptic adaptations induced by AMPA receptor blockade, these changes in intrinsic excitability depend on new protein synthesis. AMPA receptor blockade induced a protein synthesis-dependent increase in the voltage-gated Na^+ channel subunit $Na_V1.1$ in the axon initial segment, which suggests that voltage-gated Na^+ channels are one of the newly synthesized proteins. Our results suggest that a relatively brief period of decreased excitatory activity engages distinct cellular mechanisms to restore neurons to a "normal" level of activity. That a global form of homeostatic control is engaged in parallel with local regulation of synaptic function suggests that global and local homeostatic mechanisms cooperate to stabilize network function.

4.3 RESULTS

4.3.1 Brief blockade of synaptic activity increases network activity

Reduction in excitatory synaptic activation induces compensatory increases in multiple facets of neuronal excitability depending on the length of activity blockade and the method for decreasing activity. Homeostatic plasticity theory predicts that these compensatory enhancements are important for adjusting the firing rate of the neuronal network; however, this is rarely tested directly. We had previously demonstrated that relatively brief (3h) AMPA receptor blockade leads to rapid strengthening of postsynaptic sensitivity to glutamate and increases presynaptic probability of neurotransmitter release (Jakawich et al., 2010; Henry et al., 2012). In order to determine the consequence of these homeostatic changes to overall network activity, we tested the hypothesis that the compensation induced by AMPA receptor blockade is

sufficient to increase the level of neural activity when relieved of AMPA receptor blockade. To this end, cultured hippocampal neurons were treated for 3h with 40 μM CNQX in the media. Prior to recording action potentials and spontaneous excitatory postsynaptic currents (sEPSC), normal network function was re-established by replacing the media containing CNQX with extracellular recording solution without antagonists. We found that 3h AMPA receptor blockade is sufficient to impact network activity; the number of spontaneous action potentials significantly increased (Figure 4-1A-B). Action potentials were recorded extracellularly. Two-minute periods of high activity were isolated manually for analysis by identifying a period of high activity followed by no activity for at least 10 sec. The number of action potentials recorded from neurons incubated with CNQX for 3h was compared to action potentials recorded in sister-cultures on the same day.

Consistent with an increase in spontaneous action potentials following AMPA receptor blockade, whole-cell voltage-clamp recordings of sEPSCs revealed an increase in synaptic activity after AMPA receptor blockade (Figure 4-1C-D). We isolated sEPSCs by clamping the voltage at -70 mV, close to the reversal potential for chloride, and recorded spontaneous currents. The nature of sEPSCs was dramatically different following AMPA receptor blockade; sEPSCs were more frequent and higher in amplitude (Figure 4-1C). Similarly, analysis of the charge transfer in the first three minutes of recording shows that 3h AMPA receptor blockade increased the overall charge transfer by approximately 7-fold as compared to control neurons recorded on the same day (Figure 4-1D). Together, these data suggest that the changes in synaptic strength

following 3h of AMPA receptor blockade are indeed homeostatic in nature, promoting compensatory enhancements in excitatory drive in response to a period of reduction in synaptic activity. Additionally, these results raise the question of whether other compensatory changes in neuronal excitability are also induced homeostatically following AMPA receptor blockade.

4.3.2 Chronic blockade of action potentials or synaptic activity leads to compensatory increases in intrinsic excitability

In addition to engaging homeostatic mechanisms that change synaptic strength, neurons possess the ability to regulate the probability of firing through modifications of intrinsic excitability. Intrinsic excitability is a complicated phenotype that reflects the overall excitability of the cell. Modification in the expression levels or single channel properties of most voltage-gated ion channels would be predicted to increase or decrease the likelihood that a neuron will generate action potentials. To determine whether the increase in network activity following AMPA receptor blockade was mediated exclusively by compensatory responses in synaptic properties, we examined the intrinsic excitability of neurons following AMPA receptor blockade for brief or prolonged periods of time. These experiments also provide insight into the induction of these rapid forms of homeostatic regulation because intrinsic excitability is typically measured in the presence of a cocktail of inhibitors, including CNQX, used to pharmacologically isolate the neuron from ongoing synaptic activity. Thus, we were able test for compensatory changes in neuronal excitability without restoring AMPA receptor activity (required for recording sEPSCs and mEPSCs).

First, we examined the homeostatic regulation of intrinsic excitability induced by chronic blockade of action potentials (24h; 2µM TTX) in neurons compared to neurons treated chronically with AMPA receptor blockade (24h; 40µM CNQX). Intrinsic excitability was assessed by recording the change in membrane potential in response to a series of increasing 500ms depolarizing current steps in pharmacologically isolated neurons (10µM CNQX, 20µM APV, 10µM bicuculline) and counting the number of action potentials generated. Current was applied from resting membrane potential. The minimum current to generate at least one action potential is defined as the rheobase current. We found both chronic blockade of action potentials (24h; 2µM TTX) and AMPA receptors (24h; 40µM CNQX) caused an enhancement in intrinsic neuronal excitability (Figure 4-2A-B), no change in input resistance (Figure 4-2C) and a reduction in rheobase current (Figure 4-2D). These results agree with previous reports of homeostatic enhancement in intrinsic excitability in cultured cortical neurons following action potential blockade (Desai et al., 1999b) and show that intrinsic excitability is also homeostatically regulated following direct blockade of synaptic activation. Moreover, relief of AMPA receptor blockade was not necessary for the induction of CNQX-mediated homeostatic compensation in intrinsic excitability.

4.3.3 Brief blockade of synaptic activity (CNQX, 3h) but not blockade of action potentials (TTX, 3h) promotes rapid, compensatory enhancement of intrinsic excitability

Direct blockade of AMPA receptors induces a more rapid form of homeostatic synaptic plasticity (Jakawich et al., 2010; Henry et al., 2012), but it was not known if homeostatic regulation of intrinsic neuronal excitability was also induced faster in

response to AMPA receptor blockade. We compared the intrinsic excitability of neurons following brief (3h) AMPA receptor or action potential blockade by 40 µM CNQX or 2 µM TTX, respectively. For this relatively brief period of time, only neurons treated with AMPA receptor antagonists expressed a similar compensatory increase in intrinsic excitability as observed following chronic activity blockade (Figure 4-2A-B). Blocking action potentials with 2 µM TTX for just 3h produced no increase in firing rate in response to sustained current injection (Figure 4-2B and 4-2E) and no corresponding decrease in rheobase (Figure 4-2D).

4.3.4 Brief blockade of AMPA receptors, not NMDA receptors, enhances intrinsic excitability

In order to confirm the specific role of AMPA receptor activation in homeostatic regulation of intrinsic excitability, we used an alternative AMPA receptor antagonist, NBQX (20 µM), to block synaptic activity as well as examined the role of NMDA receptor activation. NMDA receptors are also activated by glutamate in the presence of co-agonists; however postsynaptic depolarization is required to remove the Mg^{2+} block of the pore of the channel and permit ion flux. Thus AMPA receptor blockade likely blocks NMDA receptor activity indirectly. To test the possibility that the homeostatic enhancement in intrinsic excitability is induced indirectly through loss NMDA receptor activity, we blocked NMDA receptor-mediated synaptic currents for 3h and measured intrinsic excitability. Previously published work demonstrated brief NMDA receptor blockade homeostatically increases miniature excitatory postsynaptic current (mEPSC) amplitude (Sutton et al., 2006) similarly to AMPA receptor blockade (Jakawich et al.,

2010; Henry et al., 2012). Thus, we predicted that both loss of NMDA receptor activity would produce a similar or greater homeostatic increase in intrinsic excitability. However, we found that brief AMPA receptor blockade (20 μM NBQX or 40 μM CNQX , 3h), but not NMDA receptor blockade (20 μM APV, 3h), increased intrinsic excitability (Figure 4-3A-B). Interestingly, loss of NMDA receptor activity decreased the number of action potentials fired (Figure 4-3B). These results suggest that the mechanisms underlying homeostatic compensation of synapse function and action potential properties are likely distinct.

4.3.5 Relatively brief AMPA receptor blockade induces multiple changes that contribute to enhancement of intrinsic excitability

In response to 3h AMPA receptor blockade, we found that neurons fired more action potentials in response to a given current injection (Figure 4-2 and Figure 4-3A-B). To determine whether AMPA receptor blockade increased the probability of firing by decreasing the threshold for action potential generation, we compared the average action potential generated during the rheobase current injection after AMPA receptor blockade to the average control action potential. We found that following 3h AMPA receptor blockade, action potentials are initiated at a slightly lower membrane potential (Figure 4-3C) and there was no change in the resting membrane potential (Figure 4-3D). We analyzed the threshold potential by measuring the membrane potential at which the change in potential is maximal and found a significantly lower threshold for firing after AMPA receptor blockade (Figure 4-3E). Normalization of the relationship between action potential number and current injection to the rheobase current does not fully

account for the increase in excitability (Figure 4-3D), suggesting other mechanisms also contribute to this homeostatic enhancement in excitability.

4.3.6 AMPA receptor blockade engages three distinct forms of compensation in the same neuron: mEPSC amplitude, mEPSC frequency, and intrinsic excitability

While neuronal network activity homeostasis is clearly important for network function, the exact mechanisms for achieving overall homeostasis are still emerging but will likely involve the coordinate control of multiple facets of activity. Synapse strength and intrinsic excitability are both important for setting the overall level of network activity, however it was not known if cells that express synaptic compensation will also express changes in intrinsic excitability. Typically mEPSCs are defined as TTX-resistant (TTX blocks voltage-gated sodium channels and prevents action potential initiation) EPSCs that result from spontaneous release of neurotransmitter. Analysis of intrinsic firing properties requires action potentials, thus typical strategies employed to study synaptic strength would not be useful. To overcome this limitation, after removing CNQX-containing media, neurons were placed in extracellular solution containing 100nM ω-Conotoxin-GVIA and 200 nM ω-Agatoxin-IVA to block P, Q, and N-type voltage-gated calcium channels and thereby suppress evoked release without affecting action potential generation. This enabled us to record mEPSCs and action potentials in the same neuron and extracellular solution.

In order to confirm that blockade of P, Q, and N-type calcium channels resulted in EPSCs that are similar to TTX-insensitive currents, we recorded synaptic currents after exposure to ω-Conotoxin-GVIA and ω-Agatoxin-IVA for 30min (necessary to achieve full

blockade of evoked release). Then, we applied TTX to the neurons and continued to record EPSCs (Figure 4-4A). We found that the subsequent addition of TTX had no impact on the kinetics (Figure 4-4B), the amplitude (Figure 4-4C), or the frequency (Figure 4-4D) of currents recorded in the presence of ω-Conotoxin-GVIA and ω-Agatoxin-IVA. Thus, these recorded currents are likely the same as TTX-insensitive currents typically called mEPSCs.

To determine whether the synaptic and intrinsic forms of homeostatic control are engaged at unique times or are expressed concomitantly, we blocked AMPA receptor activity for just 1h and recorded mEPSCs for 5min in voltage-clamp and then switched into current-clamp to record action potentials (Figure 4-4E). We found that even this brief (1h) blockade of AMPA receptors induced a compensatory increase in the amplitude (Figure 4-4F) and frequency (Figure 4-4G) of mEPSCs. Similarly, we found 1h AMPA receptor blockade increased the maximum number of action potentials fired (Figure 4-4H) and caused a leftward shift in the relationship between number of action potentials and the depolarizing current injection. These results indicate that both synaptic and intrinsic membrane properties are modulated following loss of synaptic activity on similar timescales.

4.3.7 Protein synthesis is required for enhancement of excitability

Although similar rapid compensatory regulation of both synaptic strength and intrinsic excitability may suggest overlapping mechanisms, distinct mechanisms were suggested by the lack of effect on intrinsic excitability following blockade of NMDA receptor activation (Figure 4-3A). To gain insight into the key intracellular signaling steps

involved in rapid homeostatic increases in intrinsic neuronal excitability, we examined three pathways known to be important for homeostatic regulation of synapse strength: protein synthesis (Jakawich et al., 2010; Henry et al., 2012), BDNF signaling (Jakawich et al., 2010, Desai, 1999 #169) and mTOR signaling (Henry et al., 2012).

Using two protein synthesis inhibitors, anisomycin and emetine, we tested whether homeostatic enhancement in excitability following AMPA receptor blockade requires protein synthesis. Anisomycin inhibits protein synthesis by blocking peptide elongation by inhibition of the animoacyl-transfer reaction in the 60S ribosome. Emetine is used as an alternative protein synthesis inhibitor that acts by blocking translocation by binding to the 40S ribosome. Indeed, we found that blocking protein synthesis with emetine applied 30 mins prior to blocking AMPA receptors for just 60 mins blocked the increase in excitability (Figure 4-5B). In a parallel set of experiments, we found pre-treating neurons anisomycin for 30min prior to 3h AMPA receptor blockade completely blocked the compensatory increase in excitability measured without inhibition of protein synthesis (Figure 4-5D). Protein synthesis inhibition for 1.5h-3.5h had no effect on the probability of firing action potentials in untreated neurons (Figure 4-5E). These data reveal that not only is protein synthesis critically important for homeostatic regulation of excitability, these changes are relatively rapid.

We previously found that loss of AMPA receptor activity, but not NMDA receptor activity, induced an increase in the presynaptic probability of vesicle release that requires mTORC1 activity (Henry et al., 2012) and BDNF (Jakawich et al., 2010; Henry et al., 2012). This differential effect raised the possibility that these pathways may be

required for homeostatic enhancement in probability of firing following AMPA receptor blockade as well. However, we found that the mTORC1 inhibitor rapamycin (100 nM) did not block the increase in excitability in response to AMPA receptor blockade (Figure 4-5F). Similarly, scavenging endogenous extracellular BDNF using 1 μg/mL TrkB-Fc during AMPA receptor blockade had no effect on intrinsic excitability (Figure 4-5G).

4.3.8 Voltage-Gated Sodium Channels in the axon initial segment are regulated by synaptic activity

That the loss of AMPA receptor activity reduces the threshold for firing an action potential (Figure 4-3E) without impacting resting membrane potential (Figure 4-3D) or input resistance (Figure 4-2C), suggests that voltage-gated sodium channels could be dynamically regulated during homeostatic enhancement of intrinsic excitability. Indeed, activity deprivation induces changes in the axon initial segment (Grubb and Burrone, 2010) where voltage-gated sodium channels are clustered. We examined the abundance of two voltage-gated sodium channels, $Na_V1.1$ and $Na_V1.2$, in the axon following AMPA receptor blockade for 3h by immunocytochemistry. After 3h, neurons were fixed, permeabilized and stained for either channel, MAP2 (dendritic marker) and ankyrin G (axon initial segment marker). We found that 3h AMPA receptor blockade increased the level of $Na_V1.1$ (Figure 4-6A-C) in the axon initial segment, but not the soma (Figure 4-6D). Similarly, $Na_V1.2$ levels were higher in the axon initial segment following AMPA receptor blockade (Figure 4-6E-G). $Na_V1.2$ was also observed in the soma and dendrites, neither of which was affected by AMPA receptor blockade (Figure 4-6H). Consistent with a requirement of protein synthesis in homeostatic enhancement

of intrinsic excitability, blockade of protein synthesis prior to AMPA receptor antagonism prevented the increase in both $Na_V1.1$ (Figure 4-6A-C) and $Na_V1.2$ (Figure 4-6E-G). Collectively, our results suggest that following loss of synaptic activity at excitatory synapses, neurons engage protein synthesis-dependent mechanisms that lead to increased excitability at the axon initial segment.

4.4 DISCUSSION

Together these data demonstrate that neurons possess the ability to rapidly engage multiple homeostatic mechanisms in the same cell to compensate for changes in excitatory synaptic activity. Blockade of AMPA receptors for as little as 1h causes three distinct changes in neural function through divergent, protein synthesis-dependent mechanisms: increased postsynaptic AMPA receptor expression, increased presynaptic probability of release and increased intrinsic excitability. The latter is mediated in part through increased expression of voltage-gated sodium channels in the axon initial segment. Unlike regulation of presynaptic function following loss of AMPA receptor activity, the enhancement in intrinsic excitability is independent of BDNF signaling. Thus, it is likely that the change in intrinsic excitability is regulated postsynaptically and not through retrograde signaling or axonal transport back to the soma. Moreover, the changes in intrinsic excitability were observed under conditions where presynaptic increases in probability of release are blocked (i.e. in the presence of TrkB-fc or rapamycin), thus demonstrating that homeostatic regulation of intrinsic excitability does not require homeostatic enhancement of presynaptic release.

The intrinsic excitability of a neuron is a polygenic, actively regulated and plastic property that describes the likelihood of firing an action potential. Although the electrical properties of neurons are complex, we identified that AMPA receptor blockade increases levels of two voltage-gated sodium channels, $Na_V1.1$ and $Na_V1.2$, in the axon initial segment, the site of action potential initiation (Stuart et al., 1997). Homeostatic regulation of Na^+ current was found previously following chronic changes in neural activity (Desai et al., 1999b). We found that both the increase in Na^+ channels and enhancement of intrinsic excitability require protein synthesis, which raises the possibility that these Na^+ channels or proteins that regulate them, such as the scaffolding protein ankyrin G (Garrido et al., 2003; Lemaillet et al., 2003), are candidates for the newly synthesized proteins. Moreover, local protein synthesis in the axon initial segment could be involved in activity-dependent control of the axon initial segment; indeed, ribosomes are found in the axon initial segment (Palay et al., 1968; Peters et al., 1968)}.

Together with the decrease in threshold detected following AMPA receptor blockade, the regulation of $Na_V1.1$ and $Na_V1.2$ in the axon initial segment strongly suggests that a critical component of the neuronal homeostatic response involves compensatory changes in this spike initiation zone. In addition to homeostatic regulation of Na^+ channel levels, Na^+ channel kinetics, changes in other ion channels in the axon initial segment (Bender and Trussell, 2012), or regulation of axon initial segment position (Grubb and Burrone, 2010; Kuba et al., 2010) may contribute to homeostatic regulation of neural excitability. Another possibility is that in addition to

homeostatic regulation at the axon initial segment, compensation could be expressed by modulation of dendritic excitability (Wong et al., 1979; Masukawa and Prince, 1984), such as observed in cortical layer 5 pyramidal neurons following sensory deprivation (Breton and Stuart, 2009). While we cannot exclude these possibilities, increases in Na^+ conductance alone may be sufficient to reduce threshold (Matzner and Devor, 1992) and thereby increase excitability.

Here, we have focused on more rapid regulation of intrinsic excitability in pyramidal-like hippocampal neurons. It is likely that other types of neurons have distinct mechanisms for expressing homeostatic changes on different timescales. Indeed, in cortical neurons, prolonged activity suppression leads to enhancement of intrinsic excitability that depends on BDNF (Desai et al., 1999a, b). In the rat prefrontal cortex, chronic *in vivo* exposure to ketamine, a non-competitive antagonist of the NMDA receptor, increases firing frequency by decreasing inhibition without changing the intrinsic excitability or excitatory synaptic drive (Zhang et al., 2008). This lack of effect on intrinsic excitability is reminiscent of our results showing there is no compensatory change in intrinsic excitability following NMDA receptor blockade with APV. Collectively, these findings suggest that activity manipulation triggers distinct compensatory strategies in different types of neurons to maintain 'normal' activity.

The compensatory changes in the synapse and in the axon initial segment occur in the same direction in the same neuron (i.e. loss of synaptic activity enhances both synaptic efficacy and intrinsic excitability), which likely increases the dynamic range of

the network. These results demonstrate that neurons can engage multiple, parallel modes of compensation to maintain a degree of activity in the neural network, which may have profound consequences on network function. Indeed, *in vivo* exposure of *Xenopus* tadpoles to a visual stimulation that drives decreases in excitatory synaptic strength also causes compensatory increases in the intrinsic excitability which increases the sensitivity of neurons to stimulus detection (Aizenman et al., 2003). The cooperation of homeostatic changes in synaptic strength and intrinsic excitability in response to manipulation of network activity is similar to the synergistic changes in synaptic strength and intrinsic excitability in response to tetanic stimulations known to cause Hebbian forms of plasticity in the hippocampus (Daoudal et al., 2002) and the cerebellum (Aizenman and Linden, 2000; Armano et al., 2000) .

In conclusion, our results support a role for activity-dependent changes in axon initial segment properties during control of neuronal excitability on fast timescales. We found that loss of AMPA receptor activity for just 1h drives rapid changes in the axon initial segment of hippocampal pyramidal-like neurons and increases intrinsic excitability. Moreover, increases in synapse strength and intrinsic excitability were observed in the same neurons, which is consistent with the hypothesis that neurons utilize redundant forms of compensation. These results suggest that in addition to activity-dependent changes in the axon initial segment driven by prolonged changes in membrane potential, the axon initial segment is also highly sensitive to brief changes in neuronal activity. These modes of control likely impact information processing and network stability broadly. Moreover, dysfunction in homeostatic control of intrinsic

excitability may contribute to the pathogenesis of neurological disorders, such as epilepsy (reviewed in (Meisler and Kearney, 2005; Wimmer et al., 2010)), Angelman Syndrome (Kaphzan et al., 2011; Kaphzan et al., 2013) and schizophrenia (Cruz et al., 2009). A more complete understanding of neuronal mechanisms that regulate the function of the axon initial segment, and a better understanding of the dynamic regulation of voltage-gate ion channels and their regulators, may reveal novel treatment strategies for these disorders.

4.5 CONCLUSIONS AND POSSIBLE CONNECTIONS TO PHOSPHOINOSITIDE LIPID SIGNALING

In these studies, AMPA-receptor blockade of cultured hippocampal neurons lead to protein-synthesis dependent changes in intrinsic excitability and voltage-gated sodium channel expression in the axon initial segment. While the intrinsic excitability of a neuron reflects the complex organization of a myriad of voltage-gated channels, the fact that a single stimulus – AMPA receptor blockade – causes both the enhancement of intrinsic excitability and increased sodium channel expression in the axon initial segment suggests these two changes are related. Indeed, increasing the number of voltage-gated sodium channels alone is expected to lower the threshold for firing an action potential, which was observed in the current-step elicited action potentials following AMPA receptor blockade. Note, however, that in addition to $Na_V1.1$ and $Na_V1.2$ other proteins involved in membrane excitability (discussed below) may be impacted by a sudden loss of excitatory synaptic drive. Additionally, the protein-synthesis dependent changes in sodium channel expression in the axon initial segment may not involve new

synthesis of these channels, but instead involve the synthesis of proteins that regulate voltage-gated sodium channel clustering or function.

In addition to the number of $Na_V1.1$ and $Na_V1.2$ in the axon initial segment, the functional properties of these channels are known to be modulated by accessory β-subunits, such as β1. In mice, loss of β1 (*Scn1b*$^{-/-}$) causes hypo-excitability in cerebellar granule neurons (Brackenbury et al. 2010). Consistent with a critical role in regulation of neuronal excitability, mutations in *SCN1B* have been identified in patients with generalized epilepsy with febrile seizure (GEFS+) and Dravet's syndrome (severe myoclonic epilepsy of infancy) (Wallace et al., 1998, Scheffer et al., 2007, Patino et al., 2009).

The cellular mechanisms that underlie these compensatory changes in excitability remain to be determined. Given that phosphoinositide lipid signaling has known roles in clustering integral membrane proteins in the plasma membrane and activating ion channels, there may be regulatory roles for these signaling lipids in the axon initial segment as well. For example, all inward rectifying potassium channels, which reduce excitability when activated, require the phosphoinositide lipid phosphatidylinostitol 4,5-bisphosphate for channel opening (Logothetis et al., 2007). Thus, control of membrane excitability could be achieved by changing the level of phosphatidylinostitol 4,5-bisphosphate on the plasma membrane. Functional studies are required to test this hypothesis. In conclusion, phosphoinositide lipid signaling is likely upstream of many cellular pathways that have been identified to be important for maintaining a normal level of neural activity. In the future, the identification of specific

protein effectors, a better understanding of the highly regulated lipid kinases and phosphatases, and the elucidation of the subcellular distribution of each phosphoinositide lipid will likely identify additional regulatory roles for phosphoinositide signaling lipids in homeostatic control of different facets of excitability, including at excitatory synaptic drive and intrinsic excitability.

4.6 MATERIALS & METHODS

4.6.1 Cell Culture

Dissociated postnatal (P1-2) rat hippocampal neuron cultures, plated at a density of 230-460 mm^2 in poly-D-lysine (Fisher, A-003-E) coated glass-bottom petri dishes (Mattek, P35G-0-14-C), were prepared as previously described (Sutton et al., 2006) and maintained for at least 21-24 DIV at 37ºC in growth medium [Neurobasal A (Invitrogen, 1088022) supplemented with B27 (Invitrogen, 17504-044) and Glutamax-1 (Invitrogen, 35050-061)] prior to use.

4.6.2 Drug Treatments

In indicated experiments, the following drugs were added to culture medium for indicated times at 37°C, 5% CO_2: 20 µM APV (Tocris, 0105), 40 µM anisomycin (Sigma, A9789), 40 µM CNQX (Sigma, C239), 25 µM emetine (Sigma, E2375), 20 µM NBQX (Sigma, N183), 100 nM rapamycin (LC Laboratories, R-5000), 1 µg/mL TrkB-fc (R&D Systems, 688-TK-100), and 2 µM TTX (EMD Bioscience, 554412).

4.6.3 Electrophysiology

Whole-cell patch-clamp recordings were made with an Axopatch 200B amplifier from cultured hippocampal neurons bathed in HEPES-buffered saline (HBS; 119 mM NaCl, 5 mM KCl, 2 mM $CaCl_2$, 2 mM $MgCl_2$, 30 mM Glucose, 10 mM HEPES, pH 7.4) plus 10 µM CNQX (Sigma, C239), 20 µM APV (Sigma, A8054) and 10 µM bicuculline (Tocris, O130) for intrinsic excitability recordings. For mEPSC recordings, neurons were bathed in HBS, plus 10 µM bicuculline (Tocris, O130) and 1 µM TTX (EMD Bioscience, 554412), or 10 µM bicuculline (Tocris, O130), 100 nM ω-Conotoxin GVIA (Sigma, C9915), and 200 nM ω-Agatoxin-IVA (Sigma, A6719). Whole-cell pipette internal solution (mEPSC recordings) contained: 115 mM $KMeSO_4$, 15 mM KCl, 5 mM NaCl, 0.02 mM EGTA, 1 mM $MgCl_2$, 10 mM Na2-Phosphocreatine, 4 mM ATP-Mg, 0.3 mM GTP-Na, pH 7.2, and had resistances ranging from 3-5 MΩ. Cultured neurons with a pyramidal-like morphology were voltage-clamped at –70 mV. Membrane potentials were recorded in current clamp and series resistance compensated for by >90%. Neurons found to have a resting membrane potential more depolarized that -55 mV were excluded from analysis. Input resistance was measured using a hyperpolarizing 25 pA current step. Intrinsic excitability was assessed in pharmacologically isolated neurons using a series of 500 ms current injections to depolarize the soma from resting membrane potential. For loose-patch recordings, pipette solution contained extracellular solution. Recordings in which seal resistance exceeded 50 MΩ were excluded from analysis. Miniature EPSCs were analyzed off-line using MiniAnalysis (Synaptosoft). Action potential properties and intrinsic excitability data were analyzed using Clampfit and custom MATLAB

(Mathworks) scripts. Statistical differences between experimental conditions were determined as indicated and all multiple comparisons were corrected for using the Tukey-Kramer post-hoc test.

4.6.4 Immunocytochemistry

Primary antibodies used were rabbit anti-MAP2 (1:1000, AB5622, Millipore Corporation, Billerica, MA, USA), mouse anti-$Na_v1.1$ (1:200, Clone K74/71, UC Davis/NIH NeuroMab Facility, Davis, CA, USA), mouse anti-$Na_v1.2$(1:500, Clone 69/3, UC Davis/NIH NeuroMab Facility, Davis, CA, USA) and mouse anti-Ankyrin-G (1:500, Clone 106/36, UC Davis/NIH NeuroMab Facility, Davis, CA, USA). Secondary antibodies were conjugated to Alexafluor 488, 555, and 647 (Invitrogen). Following treatment with 40µM CNQX (Sigma, C239) and/or 40 µM anisomycin (Sigma, A9789), cells were washed with phosphate-buffered saline supplemented with 1 mM $MgCl_2$ and 0.1 mM $CaCl_2$ (PBS-MC). Cells were fixed and permeabilized with methanol, washed and blocked with 2% bovine serum albumin (BSA) in PBS-MC. Neurons were incubated with antibody for 1h at room temperature. Images were acquired with an Olympus FV1000 confocal microscope (z-series, 0.41 µm intervals). Images were analyzed with ImageJ, Excel (Microsoft) and MATLAB (Mathworks).

4.7 ACKNOWLEDGMENTS

We are grateful to Cynthia Carruthers and Christian Althaus for preparing neuronal cultures. We thank Dr. Hisashi Umemori and his lab for helpful comments and suggestions. This work was supported by NIH grant RO1-MH085798-01 to MAS. AJM was supported in part by Neuroscience Training Grant T32EY017878, 5T32MH014279-

33, NRSA F31NS07470, and the Rackham Predoctoral Fellowship. NMC was supported in part by Undergraduate Research Opportunity Program at the University of Michigan.

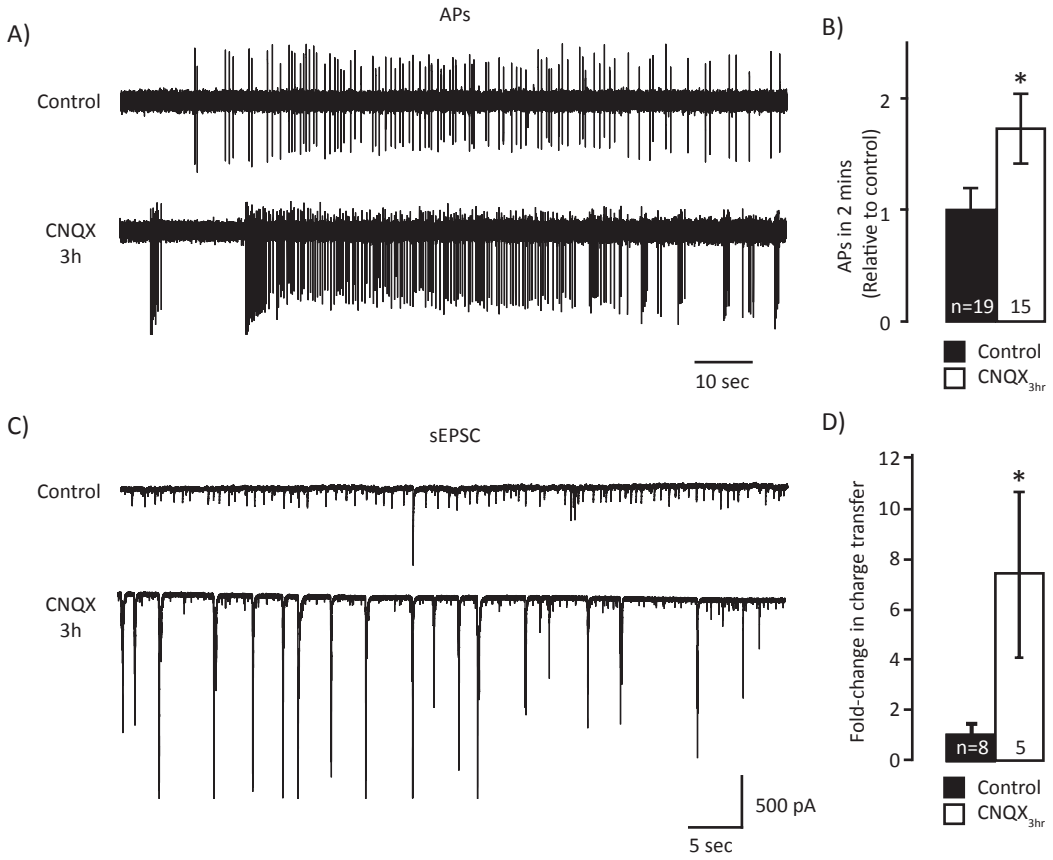

Figure 4-1. Loss of AMPAR activity rapidly enhances neural network activity
A) Representative extracellular recording of spontaneous action potentials in pyramidal-like neurons following AMPAR blockade for 3h with 40 µM CNQX or vehicle control. **B)** Mean (±SEM) fold change in the number of action potentials in a 2min period of high activity. High activity was defined as sustained firing for at least two min following at least 10 sec of silence. Following 3h AMPAR blockade, the number of APs increased (Control: 1.00±0.196, CNQX3h: 1.73±0.313; t-test, t(32)= -2.06, p=0.048). *p<0.05. n=number of cells. **C)** Representative intracellular record of spontaneous excitatory synaptic currents in pyramidal-like neurons following AMPAR blockade for 3h with 40 µM CNQX or vehicle control (Vcom= -70 mV). **D)** Mean (±SEM) fold change in normalized charge-transfer in the first 3min recorded. Following 3h AMPAR blockade, the level of spontaneous activity greatly increases (Control: 1.00±0.45, CNQX3h: 7.39±3.28; t-test, t(11)= -2.47, p=0.031). *p<0.05. n=number of cells.

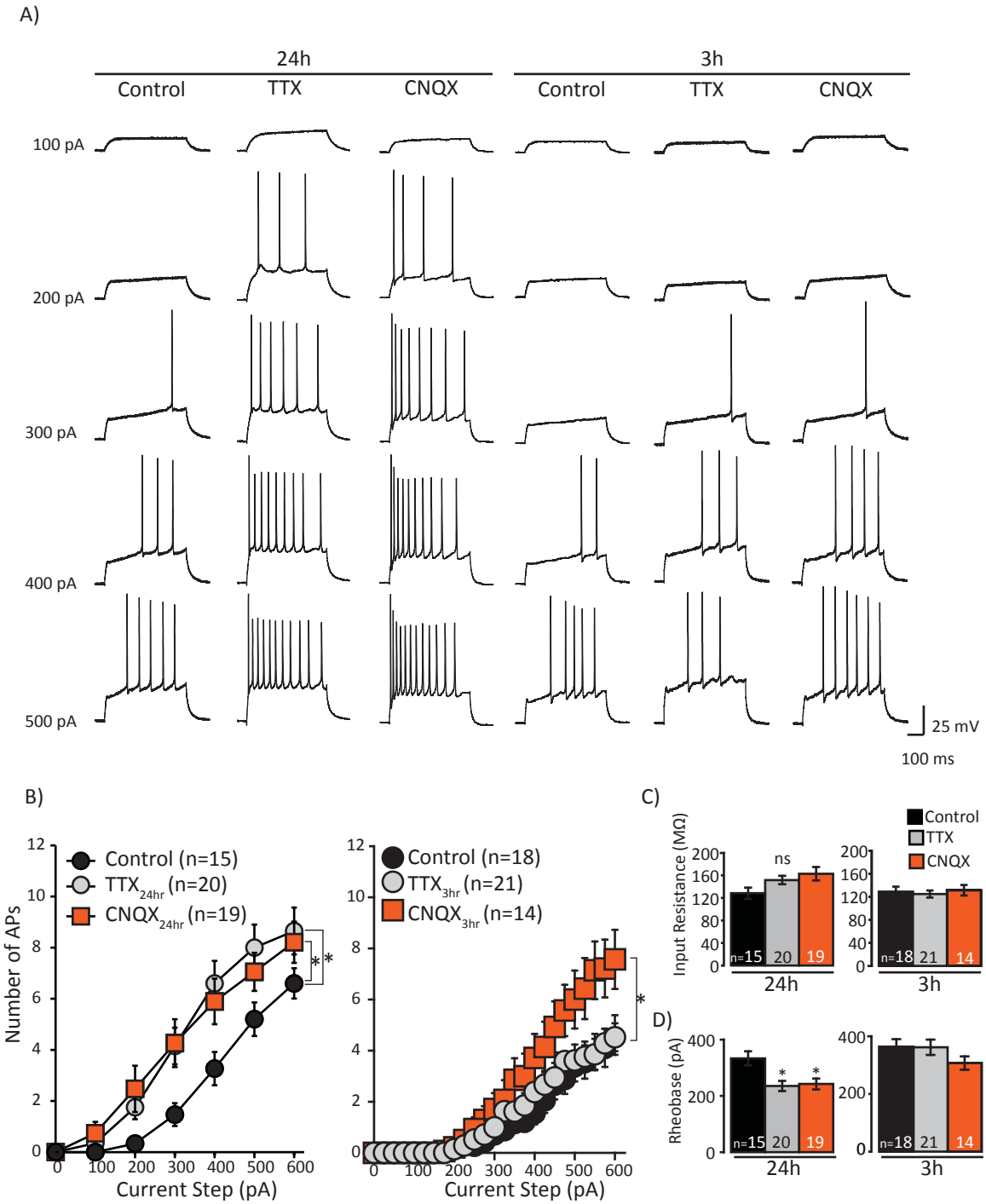

Figure 4-2. Increase in neural excitability following activity suppression

A) Representative action potential trains evoked by somatic current injections from resting membrane potential in pyramidal-like neurons in control neurons, following 24h and 3h of activity suppression with 2 µM TTX or 40 µM CNQX. **B)** Mean (±SEM) number of action potentials during 500 ms somatic current injection. Activity suppression for 24h decreases the current required to elicit action potentials (Kruskal-Wallis, $\chi2(2,429)=9.22$, $p=0.01$). *$p<0.05$ (Tukey-Kramer post hoc test). n=number of cells. **C)** Mean (±SEM)

input resistance of neurons recorded in A-B after 24h (left, in MΩ: Control-24h, 128.36±9.90; TTX-24h, 151.82±7.56, CNQX-24h, 162.99±11.84, ANOVA, F(2,51)=2.90, p=0.064) or 3h (right, in MΩ: Control-3h, 128.53±9.03; TTX-3h, 124.81±6.11, CNQX-3h, 131.36±6.11, ANOVA, F(2,50)=0.17, p=0.84) treatments. n=number of cells. **D)** Mean (±SEM) rheobase current after 24h (left) or 3h (right) treatments. Suppression of activity by either 24h TTX or 24h CNQX significantly lowered the current required to evoke at least one action potential (left, in pA: Control-24h, 333.33±25.20; TTX-24h, 235.0±18.17, CNQX-24h, 242.11±19.22, ANOVA, F(2,51)=6.49, p=0.0031). Brief activity blockade did not impact rheobase current (right, in pA: Control-3h, 363.89±26.14; TTX-3h, 361.90±26.37, CNQX-3h, 307.14±23.2, ANOVA, F(2,50)=1.33, p=0.27) treatments. *p<0.05 (Tukey-Kramer post hoc test). n=number of cells.

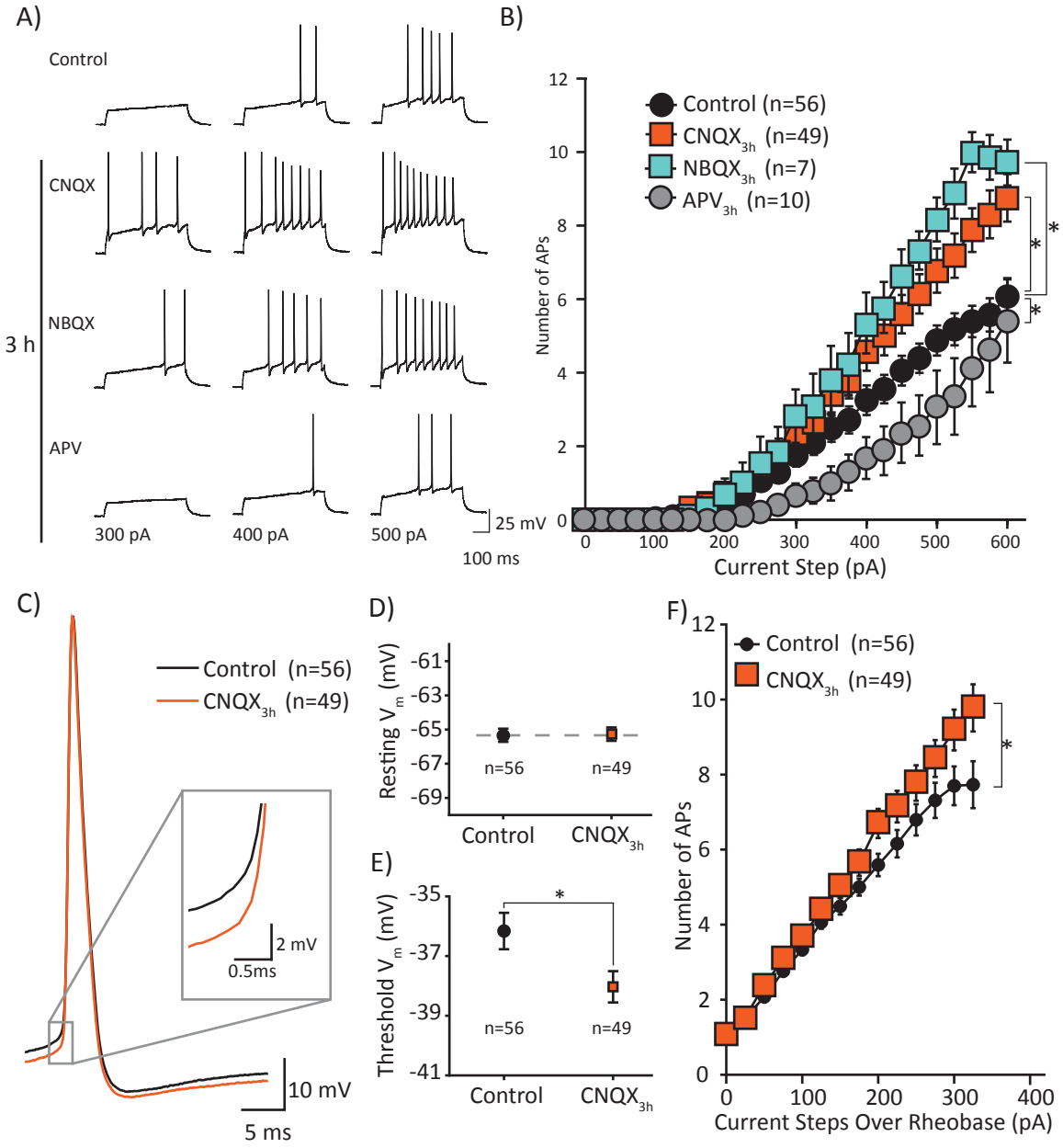

Figure 4-3. AMPAR blockade causes a compensatory decrease in the threshold for action potential generation

A) Representative action potential trains evoked by somatic current injections from resting membrane potential in pyramidal-like neurons treated with vehicle control, 40 µM CNQX, 20 µM NBQX, or 20 µM APV. **B)** Mean (±SEM) number of action potentials during 500 ms somatic current injection. AMPAR antagonism by NBQX recapitulates the enhancement of excitability induced by CNQX. Unlike AMPAR blockade, antagonism of NMDARs by 20 µM APV for just 3h decreases neural excitability (Kruskal-Wallis, $\chi2(3,3046)=60.26$, $p=5.18e-13$). *$p<0.05$ (Tukey-Kramer post hoc test). n=number of cells. **C)** Mean action potential. The first action potential generated in control and CNQX treated neurons was averaged and overlaid. The magnified region (gray box) shows the initial rising phase of the action potential is initiated at a lower membrane poten-

tial following AMPAR blockade. n=number of cells. **D)** Mean (±SEM) resting membrane potential is unaffected by AMPAR blockade (in mV: Control, -65.34±0.38; CNQX-3h, -65.27±0.39, t-test, t(103)= -0.12, p=0.90). n=number of cells. **E)** Mean (±SEM) threshold for firing an action potential. AMPAR blockade reduces the action potential threshold (in mV: Control, -35.98±0.63; CNQX-3h, -38.03±0.52, t-test, t(103)=2.47, p=0.015). *p<0.05. n=number of cells. **F)** Mean (±SEM) number of action potentials normalized to the rheobase current. Despite the normalization to rheobase, the mean number of action potentials evoked is higher following AMPAR blockade compared to control (two-sample Kolmogorov-Smirnov (K-S) test, D=0.13, p=1.7e-05). *p<0.05. n=number of neurons.

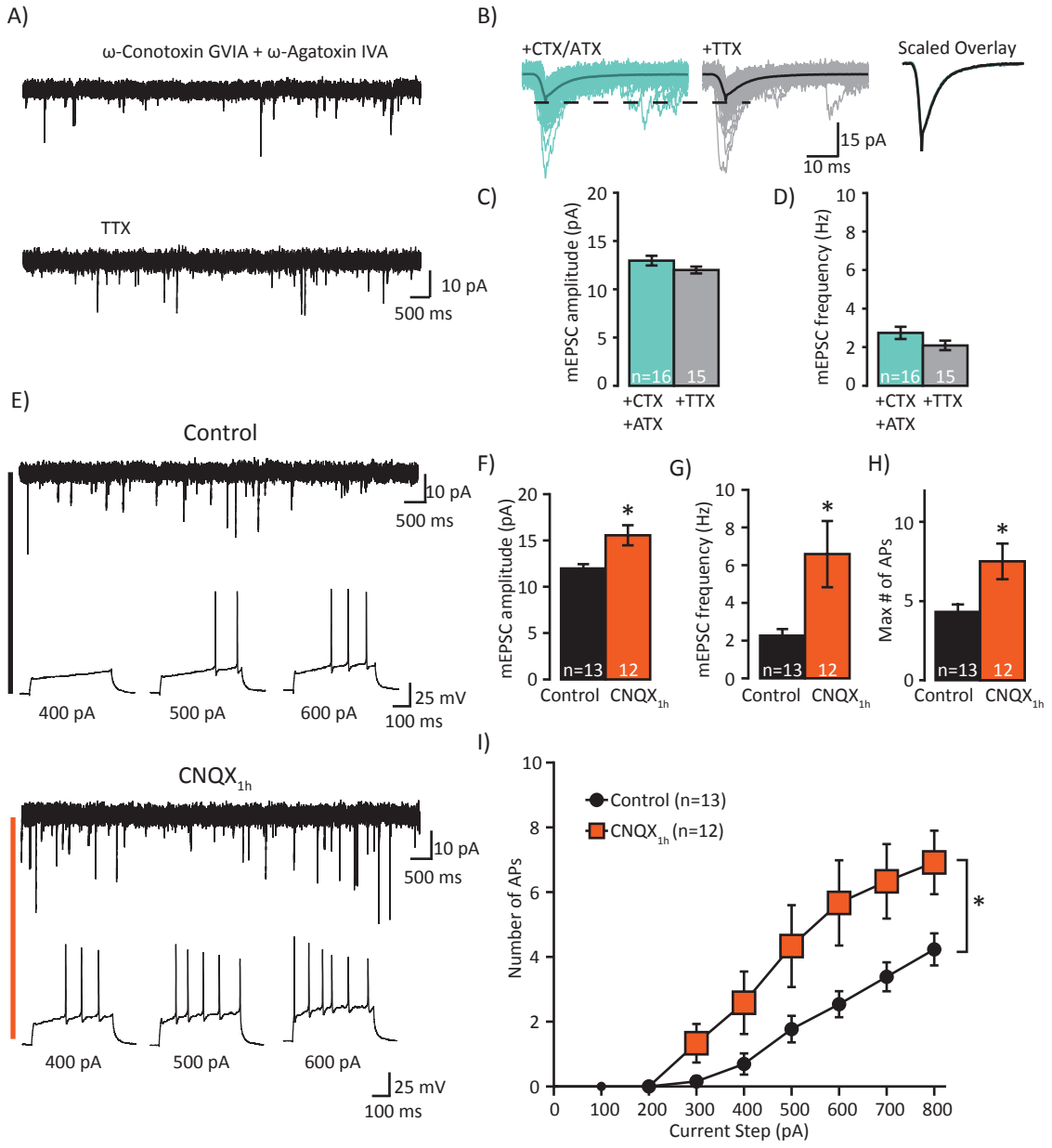

Figure 4-4. Coordinated onset of compensation at synapses and in intrinsic excitability **A)** Representative intracellular recording of synaptic currents in the presence of 100 nM ω-Conotoxin-GVIA (CTX) and 200 nM ω-Agatoxin-IVA (ATX) before (top) and after adding 1 µM TTX (bottom). **B)** Individual EPSCs aligned in time at the peak of the inward current (light color) and the average EPSC (dark line) in the presence of CTX and ATX before (blue) and after adding 1 µM TTX (gray/black). The scaled-to-peak overlays of each average EPSC are identical. Thus, suppression of evoked synaptic release CTX and ATX yields phenotypically similar EPSCs to miniature synaptic transmission recorded in the presence of TTX. **C)** Mean (±SEM) mEPSC amplitude. Blockade of action potentials by 1 µM TTX does not decrease the amplitude of mEPSCs after suppression with CTX and ATX (in pA: CTX/ATX, 12.96±0.50, +TTX, 11.99±0.35, t-test, t(29)= -1.58, p=0.124). **D)** Mean (±SEM) mEPSC frequency. Blockade of action potentials by 1 µM TTX does not decrease

the frequency of mEPSCs after suppression with CTX and ATX (in Hz: CTX/ATX, 2.74±0.32, +TTX, 2.07±0.35, t-test, t(29)= -1.60, p=0.121). **E)** Representative recording of mEPSCs (top) and action potential trains evoked by somatic current injections (bottom) in neurons treated with vehicle control or 40 µM CNQX for 1h. F) Mean (±SEM) mEPSC amplitude of neurons treated with vehicle control or 40 µM CNQX for 1h. AMPAR blockade rapidly increases mEPSC amplitude (in pA: control, 11.98±0.46, CNQX-1h, 15.56±1.09, t-test, t(23)= -3.11, p=0.0049). *p<0.05. n=number of cells. **F)** Mean (±SEM) mEPSC frequency of neurons treated with vehicle control or 40 µM CNQX for 1h. AMPAR blockade rapidly increases mEPSC frequency (in Hz: control, 2.26±0.36, CNQX-1h, 6.59±1.76, t-test, t(23)= -2.51, p=0.020). *p<0.05. n=number of cells. **G)** Mean (±SEM) maximum number of action potentials evoked by somatic current injections in neuron treated with vehicle control or 40 µM CNQX for 1h. AMPAR blockade rapidly increases the number of evoked action potentials (number of action potentials in 500 ms: control, 4.31±0.47, CNQX-1h, 7.5±1.12, t-test, t(23)= -2.69, p=0.013). *p<0.05. n=number of cells. **H)** Mean (±SEM) number of action potentials evoked with indicated current injections. AMPAR blockade rapidly increases the intrinsic excitability of neurons in 1h (two-sample K-S test, D=0.19, p=0.020). *p<0.05. n=number of neurons.

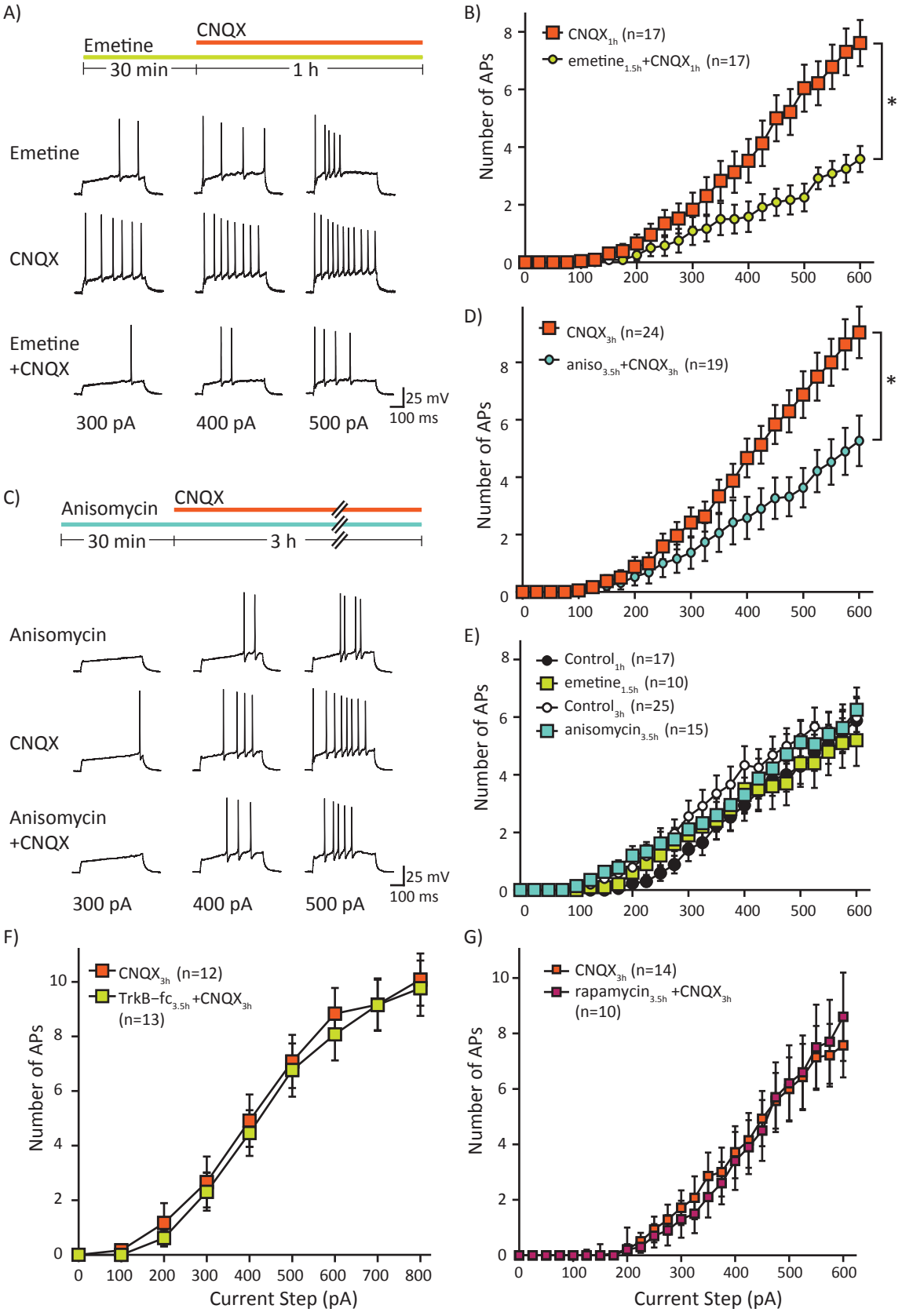
A)
Emetine
CNQX
30 min
1 h
Emetine
CNQX
Emetine
+CNQX
25 mV
100 ms
300 pA
400 pA
500 pA
B)
CNQX1h (n=17)
emetine1.5h+CNQX1h (n=17)
Number of APs
*
C)
Anisomycin
CNQX
30 min
3 h
Anisomycin
CNQX
Anisomycin
+CNQX
25 mV
100 ms
300 pA
400 pA
500 pA
D)
CNQX3h (n=24)
aniso3.5h+CNQX3h (n=19)
Number of APs
*
E)
Control1h (n=17)
emetine1.5h (n=10)
Control3h (n=25)
anisomycin3.5h (n=15)
Number of APs
F)
CNQX3h (n=12)
TrkB–fc3.5h +CNQX3h
(n=13)
Number of APs
Current Step (pA)
G)
CNQX3h (n=14)
rapamycin3.5h +CNQX3h
(n=10)
Number of APs
Current Step (pA)

Figure 4-5. Protein synthesis is required for rapid compensatory enhancement of intrinsic neural excitability

A) Representative intracellular recordings of action potential trains elicited by somatic current injections. Neurons treated with the protein synthesis inhibitor emetine (25 µM) for 30 min prior to and during AMPAR blockade with 40 uM CNQX for 1h were compared to either 25 µM emetine (90 min total) or 40 µM CNQX (1h) alone. **B)** Mean (±SEM) number of action potentials at indicated current steps. The increase in number of action potentials elicited after 1h AMPAR blockade is blocked when protein synthesis is inhibited (25 µM emetine) for 30 min prior to and during AMPAR blockade (two-sample K-S test, D=0.18, p=4.8e-06). *significantly different from CNQX ($p<0.05$). **C)** Representative intracellular recordings of action potential trains elicited by somatic current injections. The intrinsic excitability of neurons treated with the protein synthesis inhibitor anisomycin (40 µM) for 30 min prior to and during AMPAR blockade with 40 uM CNQX for 3h compared to both 40 µM anisomycin (3.5h total) or 40 µM CNQX (3h) alone. **D)** Mean (±SEM) number of action potentials at indicated current steps. The increase in number of action potentials elicited after 1h AMPAR blockade is blocked when protein synthesis is inhibited (40 µM anisomycin) for 30 min prior to and during AMPAR blockade (two-sample K-S test, D=0.16, p=2.7e-06). *significantly different from CNQX ($p<0.05$). n= number of neurons. **E)** Mean (±SEM) number of action potentials at indicated current steps. Inhibition of protein synthesis for 3.5h with 40 µM anisomycin significantly changed the distribution of action potentials evoked by current injections compared to control-3h, suggesting that protein synthesis alone can decrease excitability (Kruskal-Wallis test, $\chi2(3,1671)=41.45$, p=5.2e-09, Tukey-Kramer post hoc test). **F)** Mean (±SEM) number of action potentials at indicated current steps. Scavenging of endogenous BDNF (1 µg/mL TrkB-fc) for 30 min prior to and during 3h AMPAR blockade does not block homeostatic enhancement of intrinsic excitability (two-sample K-S test, D=0.033, p=0.997, not significant). **G)** Mean (±SEM) number of action potentials at indicated current steps. Inhibition of mTORC1 (100 nM rapamycin) for 30 min prior to and during 3h AMPAR blockade does not block homeostatic enhancement of intrinsic excitability (two-sample K-S test, D=0.055, p=0.991, not significant). B), D-G): n= number of cells.

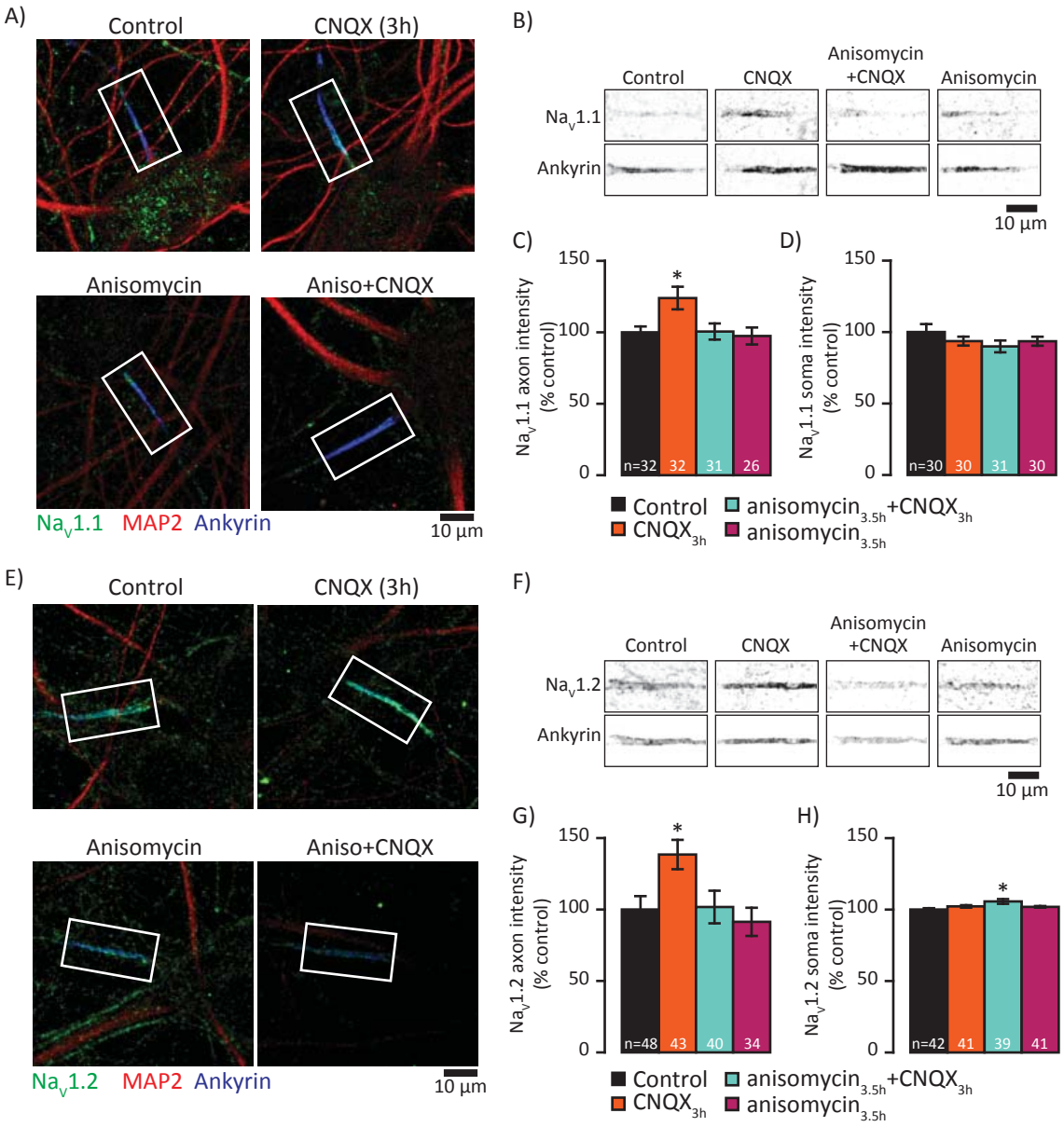

Figure 4-6. AMPAR blockade enhances the abundance of Na$_V$1.1 and Na$_V$1.2 in the axon initial segment

A) Representative images of neurons stained for Na$_V$1.1 (green), MAP2 (red) and ankyrin (blue) after vehicle control, 40 µM CNQX (3h), 40 µM anisomycin(3,5) plus 40 µM CNQX (3h), or 40 µM anisomycin (3.5h). **B)** The axon initial segments indicated by white boxes in (A) with the channels separated. **C)** Mean (±SEM) Na$_V$1.1 intensity in the axon initial segment normalized to control. AMPAR blockade significantly increases the abundance of Na$_V$1.1 in the axon initial segment (neurite colabeled with ankyrin) and this increase in blocked by pretreatment with protein synthesis inhibitors (in percent of control: control,100.00±4.081, 3h CNQX, 123.95±7.92, Anisomycin(3.5h)+CNQX(3h), 100.51±5.66, Anisomycin(3.5h), 97.40±5.92, ANOVA, F(3,117)=4.25, p=0.0068). *significantly different from control (p<0.05). n= number of axons. **D)** Mean (±SEM) Na$_V$1.1 intensity in the soma normalized to control. AMPAR blockade does not impact somatic

levels of $Na_V1.1$ (in percent of control: control, 100.00±5.58, 3h CNQX, 93.66±3.12, Anisomycin(3.5h)+CNQX(3h), 89.95±4.13, Anisomycin(3.5h), 93.57±3.14, ANOVA, F(3,117)=1.03, p=0.38). n= number of somas. **E)** Representative images of neurons stained for $Na_V1.2$, MAP2 and ankyrin after vehicle control, 40 µM CNQX (3h), 40 µM anisomycin(3,5) plus 40 µM CNQX (3h), or 40 µM anisomycin (3.5h). **F)** The axon initial segments indicated by white boxes in (E) with the channels separated. **G)** Mean (±SEM) $Na_V1.2$ intensity in the axon initial segment normalized to control. AMPAR blockade significantly increases the abundance of $Na_V1.2$ in the axon initial segment (neurite colabeled with ankyrin) and this increase in blocked by pretreatment with protein synthesis inhibitors (in percent of control: control, 100.00±9.31, 3h CNQX, 138.44±10.28, Anisomycin(3.5h)+CNQX(3h), 101.71±11.42, Anisomycin(3.5h), 91.34±9.87, ANOVA, F(3,161)=4.13, p=0.0074). *significantly different from control ($p<0.05$). n= number of axons. H) Mean (±SEM) $Na_V1.2$ intensity in the soma normalized to control. AMPAR blockade does not impact somatic levels of $Na_V1.2$ (in percent of control: control, 100.00±0.93, 3h CNQX, 102.21±0.85, Anisomycin(3.5h)+CNQX(3h), 105.66±1.65, Anisomycin(3.5h), 101.89±0.57, ANOVA, F(3,159)=4.89, p=0.0028). *significantly different from control ($p<0.05$). n= number of somas. (not shown) AMPAR blockade does not impact dendritic levels of $Na_V1.2$ (in percent of control: control, 100.00±3.02, 3h CNQX,102.26±4.33, t-test, t(120)= -0.4221, p=0.67). ◊Data were collected and analyzed with the help of Nick Carducci.

4.8 BIBLIOGRAPHY

Aizenman CD, Akerman CJ, Jensen KR & Cline HT. 2003. Visually driven regulation of intrinsic neuronal excitability improves stimulus detection in vivo. *Neuron,* **39,** 831-842.

Aizenman CD & Linden DJ. 2000. Rapid, synaptically driven increases in the intrinsic excitability of cerebellar deep nuclear neurons. *Nature Neuroscience,* **3,** 109-111.

Aoto J, Nam CI, Poon MM, Ting P & Chen L. 2008. Synaptic signaling by all-trans retinoic acid in homeostatic synaptic plasticity. *Neuron,* **60,** 308-20.

Armano S, Rossi P, Taglietti V & D'Angelo E. 2000. Long-term potentiation of intrinsic excitability at the Mossy fiber-granule cell synapse of rat cerebellum. *Journal of Neuroscience,* **20,** 5208-5216.

Bacci A, Coco S, Pravettoni E, Schenk U, Armano S, Frassoni C, Verderio C, De Camilli P & Matteoli M. 2001. Chronic blockade of glutamate receptors enhances presynaptic release and downregulates the interaction between synaptophysin-synaptobrevin-vesicle-associated membrane protein 2. *Journal of Neuroscience,* **21,** 6588-6596.

Bartley AF, Huang ZJ, Huber KM & Gibson JR. 2008. Differential activity-dependent, homeostatic plasticity of two neocortical inhibitory circuits. *Journal of Neurophysiology,* **100,** 1983-1994.

Bender KJ & Trussell LO. 2012. The physiology of the axon initial segment. *Annual review of neuroscience,* **35,** 249-65.

Benevento LA, Bakkum BW & Cohen RS. 1995. Gamma-Aminobutyric-Acid and Somatostatin Immunoreactivity in the Visual-Cortex of Normal and Dark-Reared Rats. *Brain Research,* **689,** 172-182.

Brackenbury WJ, Calhoun JD, Chen C, Miyazaki H, Nukina N, Oyama F, Ranscht B & Isom LL. 2010. Functional reciprocity between Na+ channel Nav1.6 and β1 subunits in the coordinated regulation of excitability and neurite outgrowth. *Proceedings of the National Academy of Sciences of the United States of America,* **107**, 2283–2288.

Branco T, Staras K, Darcy KJ & Goda Y. 2008. Local dendritic activity sets release probability at hippocampal synapses. *Neuron,* **59,** 475-485.

Breton JD & Stuart GJ. 2009. Loss of sensory input increases the intrinsic excitability of layer 5 pyramidal neurons in rat barrel cortex. *The Journal of physiology,* **587,** 5107-19.

Burrone J, O'Byrne M & Murthy VN. 2002. Multiple forms of synaptic plasticity triggered by selective suppression of activity in individual neurons. *Nature,* **420,** 414-418.

Cingolani LA, Thalhammer A, Yu LMY, Catalano M, Ramos T, Colicos MA & Goda Y. 2008. Activity-dependent regulation of synaptic AMPA receptor composition and abundance by beta 3 integrins. *Neuron,* **58,** 749-762.

Cruz DA, Weaver CL, Lovallo EM, Melchitzky DS & Lewis DA. 2009. Selective alterations in postsynaptic markers of chandelier cell inputs to cortical pyramidal neurons in subjects with schizophrenia. *Neuropsychopharmacology : official publication of the American College of Neuropsychopharmacology,* **34,** 2112-24.

Daoudal G, Hanada Y & Debanne D. 2002. Bidirectional plasticity of excitatory postsynaptic potential (EPSP)-spike coupling in CA1 hippocampal pyramidal neurons. *Proceedings of the National Academy of Sciences of the United States of America,* **99,** 14512-7.

Davis GW. 2006. Homeostatic control of neural activity: From phenomenology to molecular design. *Annual Review of Neuroscience,* **29,** 307-323.

De Gois S, Schafer MKH, Defamie N, Chen C, Ricci A, Weihe E, Varoqui H & Erickson JD. 2005. Homeostatic scaling of vesicular glutamate and GABA transporter expression in rat neocortical circuits. *Journal of Neuroscience,* **25,** 7121-7133.

Desai NS, Cudmore RH, Nelson SB & Turrigiano GG. 2002. Critical periods for experience-dependent synaptic scaling in visual cortex. *Nature neuroscience,* **5,** 783-9.

Desai NS, Rutherford LC & Turrigiano GG. 1999a. BDNF regulates the intrinsic excitability of cortical neurons. *Learning & Memory,* **6,** 284-291.

Desai NS, Rutherford LC & Turrigiano GG. 1999b. Plasticity in the intrinsic excitability of cortical pyramidal neurons. *Nature Neuroscience,* **2,** 515-520.

Echegoyen J, Neu A, Graber KD & Soltesz I. 2007. Homeostatic Plasticity Studied Using In Vivo Hippocampal Activity-Blockade: Synaptic Scaling, Intrinsic Plasticity and Age-Dependence. *Plos One,* **2**. ARTN e700

Frank CA, Kennedy MJ, Goold CP, Marek KW & Davis GW. 2006. Mechanisms underlying the rapid induction and sustained expression of synaptic homeostasis. *Neuron,* **52,** 663-677.

Frank CA, Pielage J & Davis GW. 2009. A Presynaptic Homeostatic Signaling System Composed of the Eph Receptor, Ephexin, Cdc42, and Ca(V)2.1 Calcium Channels. *Neuron,* **61,** 556-569.

Garrido JJ, Giraud P, Carlier E, Fernandes F, Moussif A, Fache MP, Debanne D & Dargent B. 2003. A targeting motif involved in sodium channel clustering at the axonal initial segment. *Science,* **300,** 2091-4.

Gonzalez-Islas C & Wenner P. 2006. Spontaneous network activity in the embryonic spinal cord regulates AMPAergic and GABAergic synaptic strength. *Neuron,* **49,** 563-575.

Grubb MS & Burrone J. 2010. Activity-dependent relocation of the axon initial segment fine-tunes neuronal excitability. *Nature,* **465,** 1070-4.

Hartman KN, Pal SK, Burrone J & Murthy VN. 2006. Activity-dependent regulation of inhibitory synaptic transmission in hippocampal neurons. *Nature Neuroscience,* **9,** 642-649.

Hendry SHC, Huntsman MM, Vinuela A, Mohler H, Deblas AL & Jones EG. 1994. Gaba(a) Receptor Subunit Immunoreactivity in Primate Visual-Cortex - Distribution in Macaques and Humans and Regulation by Visual Input in Adulthood. *Journal of Neuroscience,* **14,** 2383-2401.

Hendry SHC & Jones EG. 1986. Reduction in Number of Immunostained Gabaergic Neurons in Deprived-Eye Dominance Columns of Monkey Area-17. *Nature,* **320,** 750-753.

Hendry SHC & Jones EG. 1988. Activity-Dependent Regulation of Gaba Expression in the Visual-Cortex of Adult Monkeys. *Neuron,* **1,** 701-712.

Henry FE, McCartney AJ, Neely R, Perez AS, Carruthers CJL, Stuenkel EL, Inoki K & Sutton MA. 2012. Retrograde Changes in Presynaptic Function Driven by Dendritic mTORC1. *Journal of Neuroscience,* **32,** 17128-17142.

Hou Q, Zhang D, Jarzylo L, Huganir RL & Man HY. 2008. Homeostatic regulation of AMPA receptor expression at single hippocampal synapses. *Proceedings of the National Academy of Sciences of the United States of America,* **105,** 775-780.

Jakawich SK, Nasser HB, Strong MJ, McCartney AJ, Perez AS, Rakesh N, Carruthers CJL & Sutton MA. 2010. Local Presynaptic Activity Gates Homeostatic Changes in Presynaptic Function Driven by Dendritic BDNF Synthesis. *Neuron,* **68,** 1143-1158.

Ju W, Morishita W, Tsui J, Gaietta G, Deerinck TJ, Adams SR, Garner CC, Tsien RY, Ellisman MH & Malenka RC. 2004. Activity-dependent regulation of dendritic synthesis and trafficking of AMPA receptors. *Nature Neuroscience,* **7,** 244-253.

Kaphzan H, Buffington SA, Jung JI, Rasband MN & Klann E. 2011. Alterations in intrinsic membrane properties and the axon initial segment in a mouse model of Angelman syndrome. *The Journal of neuroscience : the official journal of the Society for Neuroscience,* **31,** 17637-48.

Kaphzan H, Buffington SA, Ramaraj AB, Lingrel JB, Rasband MN, Santini E & Klann E. 2013. Genetic reduction of the alpha1 subunit of Na/K-ATPase corrects multiple hippocampal phenotypes in Angelman syndrome. *Cell reports,* **4,** 405-12.

Kilman V, van Rossum MCW & Turrigiano GG. 2002. Activity deprivation reduces miniature IPSC amplitude by decreasing the number of postsynaptic GABA(A) receptors clustered at neocortical synapses. *Journal of Neuroscience,* **22,** 1328-1337.

Kim J & Alger BE. 2010. Reduction in endocannabinoid tone is a homeostatic mechanism for specific inhibitory synapses. *Nature Neuroscience,* **13,** 592-U104.

Kuba H, Oichi Y & Ohmori H. 2010. Presynaptic activity regulates Na+ channel distribution at the axon initial segment. *Nature,* **465,** 1075-U136.

Lemaillet G, Walker B & Lambert S. 2003. Identification of a conserved ankyrin-binding motif in the family of sodium channel alpha subunits. *The Journal of biological chemistry,* **278,** 27333-9.

Logothetis DE, Jin T, Lupyan D, & Rosenhouse-Dantsker A. 2007. Phosphoinositide-mediated gating of inward rectifying K(+) channels. *Pflugers Arch*, **455,** 83-95.

Maffei A, Nelson SB & Turrigiano GG. 2004. Selective reconfiguration of layer 4 visual cortical circuitry by visual deprivation. *Nature Neuroscience,* **7,** 1353-1359.

Maffei A & Turrigiano GG. 2008. Multiple modes of network homeostasis in visual cortical layer 2/3. *Journal of Neuroscience,* **28,** 4377-4384.

Marder E & Goaillard JM. 2006. Variability, compensation and homeostasis in neuron and network function. *Nature Reviews Neuroscience,* **7,** 563-574.

Marty S, Berzaghi MD & Berninger B. 1997. Neurotrophins and activity-dependent plasticity of cortical interneurons. *Trends in Neurosciences,* **20,** 198-202.

Masukawa LM & Prince DA. 1984. Synaptic control of excitability in isolated dendrites of hippocampal neurons. *The Journal of neuroscience : the official journal of the Society for Neuroscience,* **4,** 217-27.

Matzner O & Devor M. 1992. Na+ Conductance and the Threshold for Repetitive Neuronal Firing. *Brain Research,* **597,** 92-98.

Meisler MH & Kearney JA. 2005. Sodium channel mutations in epilepsy and other neurological disorders. *The Journal of clinical investigation,* **115,** 2010-7.

Murthy VN, Schikorski T, Stevens CF & Zhu YL. 2001. Inactivity produces increases in neurotransmitter release and synapse size. *Neuron,* **32,** 673-682.

O'Brien RJ, Kamboj S, Ehlers MD, Rosen KR, Fischbach GD & Huganir RL. 1998. Activity-dependent modulation of synaptic AMPA receptor accumulation. *Neuron,* **21,** 1067-1078.

Palay SL, Sotelo C, Peters A & Orkand PM. 1968. The axon hillock and the initial segment. *The Journal of cell biology,* **38,** 193-201.

Patino GA, Claes LR, Lopez-Santiago LF, Slat EA, Dondeti RS, Chen C, O'Malley HA, Gray CB, Miyazaki H, Nukina N, Oyama F, De Jonghe P & Isom LL. 2009. A functional null mutation of SCN1B in a patient with Dravet syndrome. *The Journal of neuroscience : the official journal of the Society for Neuroscience,* **29,** 10764–10778.

Peters A, Proskauer CC & Kaiserman-Abramof IR. 1968. The small pyramidal neuron of the rat cerebral cortex. The axon hillock and initial segment. *The Journal of cell biology,* **39,** 604-19.

Pozo K & Goda Y. 2010. Unraveling Mechanisms of Homeostatic Synaptic Plasticity. *Neuron,* **66,** 337-351.

Rutherford LC, DeWan A, Lauer HM & Turrigiano GG. 1997. Brain-derived neurotrophic factor mediates the activity-dependent regulation of inhibition in neocortical cultures. *Journal of Neuroscience,* **17,** 4527-4535.

Scheffer IE, Harkin LA, Grinton BE, Dibbens LM, Turner SJ, Zielinski MA, Xu R, Jackson G, Adams J, Connellan M, Petrou S, Wellard RM, Briellmann RS, Wallace RH, Mulley JC & Berkovic SF. 2007. Temporal lobe epilepsy and GEFS+phenotypes associated with SCN1B mutations. *Brain*, **130,** 100–109.

Steinmetz CC & Turrigiano GG. 2010. Tumor necrosis factor-alpha signaling maintains the ability of cortical synapses to express synaptic scaling. *The Journal of neuroscience : the official journal of the Society for Neuroscience,* **30,** 14685-90.

Stellwagen D & Malenka RC. 2006. Synaptic scaling mediated by glial TNF-alpha. *Nature,* **440,** 1054-9.

Stuart G, Schiller J & Sakmann B. 1997. Action potential initiation and propagation in rat neocortical pyramidal neurons. *The Journal of physiology,* **505 (Pt 3),** 617-32.

Sutton MA, Ito HT, Cressy P, Kempf C, Woo JC & Schuman EM. 2006. Miniature neurotransmission stabilizes synaptic function via tonic suppression of local dendritic protein synthesis. *Cell,* **125,** 785-799. DOI 10.1016/j.cell.2006.03.040.

Sutton MA & Schuman EM. 2006. Dendritic protein synthesis, synaptic plasticity, and memory. *Cell,* **127,** 49-58. DOI 10.1016/j.cell.2006.09.014.

Thiagarajan TC, Lindskog M & Tsien RW. 2005. Adaptation to synaptic inactivity in hippocampal neurons. *Neuron,* **47,** 725-37. 10.1016/j.neuron.2005.06.037.

Thiagarajan TC, Piedras-Renteria ES & Tsien RW. 2002. alpha- and beta CaMKII: Inverse regulation by neuronal activity and opposing effects on synaptic strength. *Neuron,* **36,** 1103-1114. Doi 10.1016/S0896-6273(02)01049-8.

Tokuoka H & Goda Y. 2008. Activity-dependent coordination of presynaptic release probability and postsynaptic GluR2 abundance at single synapses. *Proceedings of the National Academy of Sciences of the United States of America,* **105,** 14656-14661. DOI 10.1073/pnas.0805705105.

Turrigiano G. 2011. Too Many Cooks? Intrinsic and Synaptic Homeostatic Mechanisms in Cortical Circuit Refinement. *Annual Review of Neuroscience, Vol 34,* **34,** 89-103. DOI 10.1146/annurev-neuro-060909-153238.

Turrigiano G, Abbott LF & Marder E. 1994. Activity-dependent changes in the intrinsic properties of cultured neurons. *Science,* **264,** 974-7.

Turrigiano GG. 2008. The Self-Tuning Neuron: Synaptic Scaling of Excitatory Synapses. *Cell,* **135,** 422-435. DOI 10.1016/j.cell.2008.10.008.

Turrigiano GG, Leslie KR, Desai NS, Rutherford LC & Nelson SB. 1998. Activity-dependent scaling of quantal amplitude in neocortical neurons. *Nature,* **391,** 892-6. 10.1038/36103.

Turrigiano GG & Nelson SB. 2004. Homeostatic plasticity in the developing nervous system. *Nature Reviews Neuroscience,* **5,** 97-107. Doi 10.1038/Nrn1327.

Vitureira N, Letellier M & Goda Y. 2012. Homeostatic synaptic plasticity: from single synapses to neural circuits. *Current Opinion in Neurobiology,* **22,** 516-521. DOI 10.1016/j.conb.2011.09.006.

Wallace RH, Wang DW, Singh R, Scheffer IE, George AL Jr, Phillips HA, Saar K, Reis A, Johnson EW, Sutherland GR, Berkovic SF & Mulley JC (1998). Febrile seizures and generalized epilepsy associated with a mutation in the Na+-channel β1 subunit gene SCN1B. *Nature Genetics,* **19,** 366–370.

Wang HL, Zhang Z, Hintze M & Chen L. 2011. Decrease in calcium concentration triggers neuronal retinoic acid synthesis during homeostatic synaptic plasticity. *The Journal of neuroscience : the official journal of the Society for Neuroscience,* **31,** 17764-71. 10.1523/JNEUROSCI.3964-11.2011.

Wang XY, Engisch KL, Li YJ, Pinter MJ, Cope TC & Rich MM. 2004. Decreased synaptic activity shifts the calcium dependence of release at the mammalian neuromuscular junction in vivo. *Journal of Neuroscience,* **24,** 10687-10692. Doi 10.1523/Jneurosci.2755-04.2004.

Wierenga CJ, Ibata K & Turrigiano GG. 2005. Postsynaptic expression of homeostatic plasticity at neocortical synapses. *Journal of Neuroscience,* **25,** 2895-2905. Doi 10.1523/Jneurosci.5217-04.2005.

Wierenga CJ, Walsh MF & Turrigiano GG. 2006. Temporal regulation of the expression locus of homeostatic plasticity. *Journal of Neurophysiology,* **96,** 2127-2133. DOI 10.1152/jn.00107.2006.

Wimmer VC, Reid CA, So EY, Berkovic SF & Petrou S. 2010. Axon initial segment dysfunction in epilepsy. *The Journal of physiology,* **588,** 1829-40.

Wong RK, Prince DA & Basbaum AI. 1979. Intradendritic recordings from hippocampal neurons. *Proceedings of the National Academy of Sciences of the United States of America,* **76,** 986-90.

Yu LMY & Goda Y. 2009. Dendritic signalling and homeostatic adaptation. *Current Opinion in Neurobiology,* **19,** 327-335.

Zhang Y, Behrens MM & Lisman JE. 2008. Prolonged exposure to NMDAR antagonist suppresses inhibitory synaptic transmission in prefrontal cortex. *Journal of neurophysiology,* **100,** 959-65.

CHAPTER 5

CONCLUSIONS AND FUTURE DIRECTIONS

5.1 OUTSTANDING QUESTIONS

The critical role for the phosphoinositide lipid, PI(3,5)P_2, in bidirectional control of synapse function raises numerous questions in regards to the mechanism by which this minor component of the cytosolic-side of the membrane exerts control in neurons. What are the specific protein effectors of PI(3,5)P_2? Where is PI(3,5)P_2 synthesized? What activates the sole kinase responsible for the synthesis of PI(3,5)P_2, PIKfyve? Answering these questions will provide insights into cellular function and may suggest novel strategies for treatment of diseases linked to defects in phosphoinositide lipid synthesis. Below, I will outline possible future directions for addressing these questions.

5.2 IDENTIFICATION OF PIKFYVE ACTIVATORS

Identification of activators of PIKfyve is critical for understanding phosphoinositide lipid biology and the etiology of related disease. The [3H]-inositol labeling experiments are expensive and labor intensive, but are currently the best technique developed to examine PIKfyve activity. Alternatively, lysosome/vacuole size may be analyzed as PI(3,5)P_2 controls the size of this endosome. However, this phenotypic analysis is not sensitive enough because defects unrelated to PI(3,5)P_2 levels may also cause the enlargement of endosomes, including lysosomes. For example, in

TRPML1$^{-/-}$ cells the endolysosomal membranes are enlarged (reviewed in Cheng et al. 2010). These cells are phenotypically similar to PI(3,5)P_2 deficient cells. While the TRPML1 channels interact with PI(3,5)P_2 and (Dong et al. 2010), there is no evidence that loss of TRPML1 causes a change in PI(3,5)P_2 abundance. Instead, overexpression of TRPML1 in PI(3,5)P_2 deficient cells is sufficient to suppress the appearance of enlarged lysosomes (Dong et al. 2010). Thus, a change in vacuole or lysosome size could be driven by effects that are independent of PI(3,5)P_2 levels. The identification of upstream PIKfyve activators would be hastened greatly by the development of better tools to measure PIKfyve activity. For example, a highly dynamic fluorescent probe for PI(3,5)P_2 could be used to screen extracellular stimuli for an impact of PI(3,5)P_2 synthesis or conversion. Additionally, a better understanding of how the activity of PIKfyve is regulated – whether through phosphorylation or regulation by closely associated proteins – will be critical for a complete understanding endosomal function and may lead to the development of different PIKfyve activity assays. For example, if PIKfyve activity is regulated through phosphorylation, it may be possible to generate a phospho-specific antibody for the active kinase. This would be useful for measuring PIKfyve activity in neurons and other cells.

The results of my dissertation work, suggest that neural activity activates PIKfyve, as I found that PI(3,5)P_2 is elevated in neurons during NMDA stimulation and following chronic hyperactivation. An exciting possibility is that this activation of PIKfyve requires calcium influx as would be expected with strong activation of excitatory synapses. If PIKfyve activity is regulated in a calcium-dependent manner, then chelating

calcium or blocking calcium influx should decrease active PIKfyve and $PI(3,5)P_2$ levels. This could be investigated in neurons maintained in culture for 3 weeks and PIKfyve activity assessed by incubation various agents to test the hypothesis that calcium activates Fab1: (1) BAPTA/AM (cell-permeable) mediated chelation of calcium inside and outside the cells. (2) Calcium influx blockade by a cocktail of inhibitors which can be applied together or separately to isolate the source of calcium: APV (NMDA receptor antagonist), Nifedipine (L-type voltage-gated calcium channels), ω-conotoxin (blocks N-type calcium channels) and/or ω-agatoxin (blocks P/Q-type calcium channels). (3) Calcium influx could be increased by high-potassium stimulation (15 mM KCl) or NMDA stimulation.

5.3 WHAT IS THE ROLE OF THE PDZ-INTERACTING DOMAIN IN VAC14?

Vac14 is the scaffolding protein that regulates PIKfyve activity. Loss of Vac14 reduces the levels of $PI(3,5)P_2$ by 50% and leads to strengthening of synapses (Zhang et al., 2012). Additionally, we found that Vac14 is localized to excitatory synapses. Since loss of PIKfyve also results in a similar increase in synapse strength, we concluded that the changes in synapse strength require PIKfyve activity and do arise directly from the loss of Vac14. However, Vac14 contains a PDZ interacting domain which has the potential for interacting with numerous proteins in the postsynaptic density. These interactions may or may not be critical for Vac14-dependent regulation PIKfyve activity, but it is possible that the interaction of Vac14 with a synaptic protein is critical for synthesis of $PI(3,5)P_2$ at specific membrane subdomains. These observations, together with the finding that nNOS, which functions at the synapse in the regulation of

neurotransmission, binds Vac14 through a PDZ domain *in vitro* (Lemaire and McPherson, 2006), suggest that a functional interaction between Vac14 and nNOS exists. This has yet to be tested directly and in addition to direct tests of this interaction, exploration of other PDZ-containing proteins may be critical for understanding $PI(3,5)P_2$ in synaptic physiology.

There is an abundance of synaptic proteins with PDZ binding domains (Kim and Sheng, 2004) that may interaction with Vac14. One intriguing possibility is AMPA receptor subunits or adaptors that have known PDZ domains. For example, AMPA receptor subunits interact with PDZ domain containing proteins such as GRIP (Dong et al., 1997). Similarly, synapse strength is sensitive to PDZ-mediated interactions with the C-terminal domain of GluA1 subunit (Shi et al., 2001). Note, these results are in contrast to another study that examined synapse function and LTP, which were normal, in knockin mice lacking the C-terminal PDZ-interacting domain of GluA1 (Kim et al., 2005). In another example of the importance of PDZ domain interactions, the PDZ domain of PSD95 is necessary, but not sufficient, for scaling down after hyperactivation (Sun and Turrigiano, 2011).

5.4 SUBUNIT SPECIFIC TRAFFICKING TO THE LYSOSOME

A critical open question of my dissertation research is where, in the cell, does PIKfyve activity influence the plasma membrane, surface proteins. Does PIKfyve play a direct role on the plasma membrane? Do the roles of $PI(3,5)P_2$ that are known to occur in the late endosome/lysosome account for the change in the surface membrane

embedded proteins? Indeed the best understood endosomal compartments associated with $PI(3,5)P_2$, the late endosome and lysosome, are involved in activity-dependent modifications to synapse strength. After long-term depression, AMPA receptors are sent to lysosomes (Ehlers, 2000, Lee et al., 2004). How defects in the lysosomal degradation of AMPA receptors impacts the surface pools of AMPA receptors is unclear, but may involve subunit specific trafficking of AMPA receptors during synaptic plasticity, such as LTP (Hayashi et al., 2000, Passafaro et al., 2001, Shi et al., 2001) or NMDA stimulation which causes GluR2 and GluR3 containing AMPA receptors to accumulate with lysosomes (Lee et al., 2004). Note, however that no specific subunit is required for LTP (Kim et al., 2005, Panicker et al., 2008, Granger et al., 2013)} or chronic inactivity-induced homeostatic synaptic plasticity (Altimimi and Stellwagen, 2013). In my experiments that tested the hypothesis that PIKfyve activity is required for AMPA receptor trafficking, I found pHluorin-tagged GluA2, but not GluA1, were sensitive to PIKfyve inhibition. Notably, GluA2 trafficked more slowly to the surface following NMDA stimulation and PIKfyve inhibition eliminated the difference between GluA2 and GluA1 recycling rates. Thus, one possibility is that PIKfyve inhibition specifically blocked the trafficking of the pools of GluA2 destined to the lysosome and these results are consistent with a role for PIKfyve activity in trafficking GluA2 to the lysosome.

5.5 STUDYING PIKFYVE ACTIVITY IN INTACT NEURAL CIRCUITS

To further understand the role of $PI(3,5)P_2$ in regulation of synaptic function, it will be important to measure the impact on synapse function in intact networks due to loss of PIKfyve activity, pharmacologically or genetically. All mutant mice that have

impaired Fab1 activity (Vac14$^{-/-}$, Fig4$^{-/-}$, hypomorphic Fab1) die early, which has required the use of neuronal cultures. In the hippocampus, the Schaffer collateral pathway that connects hippocampal area CA3 to CA1 is well understood and has been the focus of a large number of studies of synapse function and plasticity (reviewed in (Bliss and Collingridge, 2013)). A conditional knockout of PIKfyve in pyramidal neurons would greatly aid the further investigation of these pathways. It may be possible for the examination of synapse function in the Fig4$^{-/-}$ mice, which can live up to 6 weeks. This is long enough for the brain to develop functional neural networks. LTP and LTD is reliably induced over a range of ages and commonly studied slices from two week old animals. The impact of reduced PI(3,5)P_2 synthesis on basal synaptic properties and forms of synaptic plasticity in intact networks is completely unknown.

Two inhibitors, YM201636 and apilimod, which are reversible, independent inhibitors of Fab1 may be useful *in vivo* or in *ex vivo* hippocampal slice experiments. Applied to slices while monitoring the response of CA1 pyramidal cells to Schaffer collateral stimulation, these inhibitors may reveal roles for PIKfyve in baseline conditions and during induction of plasticity. For example, LTP could be induced by high-frequency tetanic stimulation (4 trains of 100 Hz, separated by 1 min) and followed for 1 hour with pulses every minute. Expression of LTP is thought in part to involve the reduction of AMPA receptor internalization and stabilization on the cell surface. Thus, if the loss of PI(3,5)P_2 impairs AMPA receptor endocytosis as observed in cultured neurons, then LTP may be enhanced in Fig4$^{-/-}$ slices or in the presence of PIKfyve inhibitors as the defect in endocytosis prevents AMPA receptors from being normally

internalized. The inhibitors could also be used to investigate the temporal regulation of LTP by $PI(3,5)P_2$ by limiting their application to either during or after induction of LTP. Another, potential interesting experiment would be to re-examine LTD in slices, with electrical stimulation (as opposed to bath application of NMDA as I utilized in cultured hippocampal neurons). LTD could be induced by low-frequency stimulation (900 pulses at 1 Hz) and monitored for 1 hour with pulses every minute. Increased rate of AMPA receptor endocytosis is involved in LTD (reviewed in (Anggono and Huganir, 2012)). In rat hippocampal cultures, I found that Fab1 inhibition blocks the induction of chemical LTD. However, I also found that $Vac14^{-/-}$ neurons expressed cLTD. Together, these results suggest complete inhibition of PIKfyve activity, and not just decreased activity as in the $Vac14^{-/-}$ or $Fig4^{-/-}$ mice, may be necessary to block LTD.

5.6 BIBLIOGRAPHY

Altimimi HF & Stellwagen D. 2013. Persistent synaptic scaling independent of AMPA receptor subunit composition. *The Journal of neuroscience : the official journal of the Society for Neuroscience,* **33,** 11763-7. 10.1523/JNEUROSCI.1102-13.2013.

Anggono V & Huganir RL. 2012. Regulation of AMPA receptor trafficking and synaptic plasticity. *Current Opinion in Neurobiology,* **22,** 461-469.

Bliss TVP & Collingridge GL. 2013. Expression of NMDA receptor-dependent LTP in the hippocampus: bridging the divide. *Molecular Brain,* **6**. Artn 5

Cheng XP, Shen DB, Samie M & Xu HX. 2010. Mucolipins: Intracellular TRPML1-3 channels. *Febs Letters,* **584,** 2013-2021.

Dong H, O'Brien RJ, Fung ET, Lanahan AA, Worley PF & Huganir RL. 1997. GRIP: a synaptic PDZ domain-containing protein that interacts with AMPA receptors. *Nature,* **386,** 279-84.

Dong XP, Shen D, Wang X, Dawson T, Li X, Zhang Q, Cheng X, Zhang Y, Weisman LS, Delling M & Xu H. 2010. PI(3,5)P(2) controls membrane trafficking by direct activation of mucolipin Ca(2+) release channels in the endolysosome. *Nature communications,* **1,** 38.

Ehlers MD. 2000. Reinsertion or degradation of AMPA receptors determined by activity-dependent endocytic sorting. *Neuron,* **28,** 511-525.

Granger AJ, Shi Y, Lu W, Cerpas M & Nicoll RA. 2013. LTP requires a reserve pool of glutamate receptors independent of subunit type. *Nature,* **493,** 495-+.

Hayashi Y, Shi SH, Esteban JA, Piccini A, Poncer JC & Malinow R. 2000. Driving AMPA receptors into synapses by LTP and CaMKII: Requirement for GluR1 and PDZ domain interaction. *Science,* **287,** 2262-2267.

Kim CH, Takamiya K, Petralia RS, Sattler R, Yu S, Zhou W, Kalb R, Wenthold R & Huganir R. 2005. Persistent hippocampal CA1 LTP in mice lacking the C-terminal PDZ ligand of GluR1. *Nature neuroscience,* **8,** 985-7.

Kim E & Sheng M. 2004. PDZ domain proteins of synapses. *Nature reviews. Neuroscience,* **5,** 771-81.

Lee KJ, Lee Y, Rozeboom A, Lee JY, Udagawa N, Hoe HS & Pak DT. 2011. Requirement for Plk2 in orchestrated ras and rap signaling, homeostatic structural plasticity, and memory. *Neuron,* **69,** 957-73.

Lee SH, Simonetta A & Sheng M. 2004. Subunit rules governing the sorting of internalized AMPA receptors in hippocampal neurons. *Neuron,* **43,** 221-236

Lemaire JF & McPherson PS. 2006. Binding of Vac14 to neuronal nitric oxide synthase: Characterisation of a new internal PDZ-recognition motif. *FEBS letters,* **580,** 6948-54.

Panicker S, Brown K & Nicoll RA. 2008. Synaptic AMPA receptor subunit trafficking is independent of the C terminus in the GIuR2-lacking mouse. *Proceedings of the National Academy of Sciences of the United States of America,* **105,** 1032-1037.

Passafaro M, Piech V & Sheng M. 2001. Subunit-specific temporal and spatial patterns of AMPA receptor exocytosis in hippocampal neurons. *Nature Neuroscience,* **4,** 917-926.

Shi S, Hayashi Y, Esteban JA & Malinow R. 2001. Subunit-specific rules governing AMPA receptor trafficking to synapses in hippocampal pyramidal neurons. *Cell,* **105,** 331-43.

Sun Q & Turrigiano GG. 2011. PSD-95 and PSD-93 play critical but distinct roles in synaptic scaling up and down. *The Journal of neuroscience : the official journal of the Society for Neuroscience,* **31,** 6800-8.

Zhang YL, McCartney AJ, Zolov SN, Ferguson CJ, Meisler MH, Sutton MA & Weisman LS. 2012. Modulation of synaptic function by VAC14, a protein that regulates the phosphoinositides PI(3,5)P-2 and PI(5)P. *Embo Journal,* **31,** 3442-3456.

Appendix A

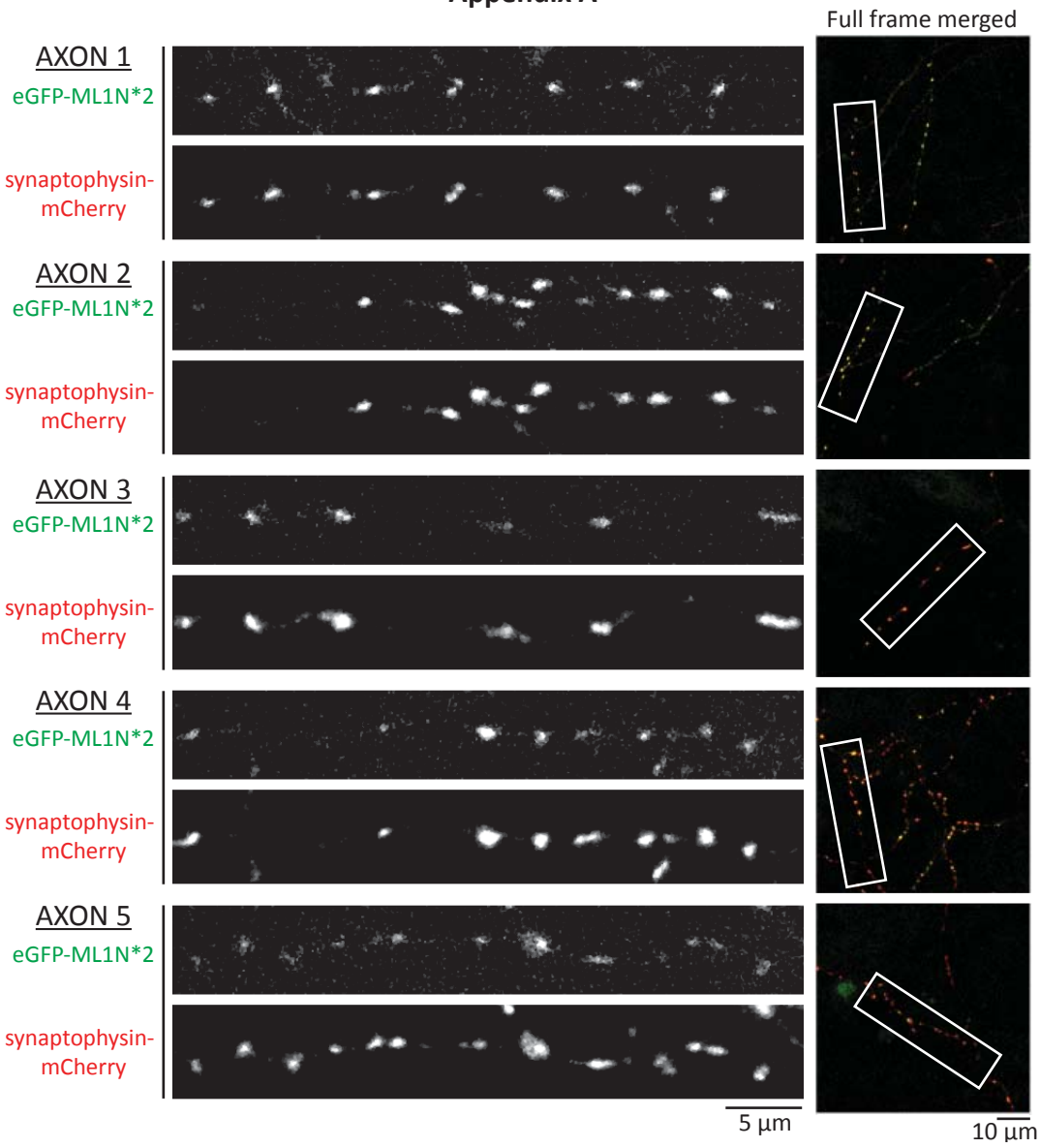

Figure A.1 - Neuronal expression of the PI(3,5)P_2 reporter (eGFP-ML1N*2) is found in axons

Cultured hippocampal neurons were transfected on DIV20 with 1 µg eGFP-ML1N*2 plasmid DNA and 0.5 µg synaptophysin-mCherry by the calcium phosphate transfection protocol and incubated for 24h in the 37C, 5%$C0_2$ incubator. Neurons expressing both plasmids were imaged live on the confocal microscope. The extracellular solution contained: 119 mM NaCl, 5 mM KCl, 2 mM CaCl2, 2 mM MgCl2, 30 mM glucose, 10 mM HEPES, pH 7.4. Z-projected, median filtered (0.5 pixel), background subtracted images are shown. 5 axons of 5 different neurons were analyzed. Most synaptophysin-mCherry positive puncta (likely presynaptic terminals) also have eGFP-ML1N*2; these results suggests that PI(3,5)P_2 may be localized to presynaptic terminals.

Appendix B

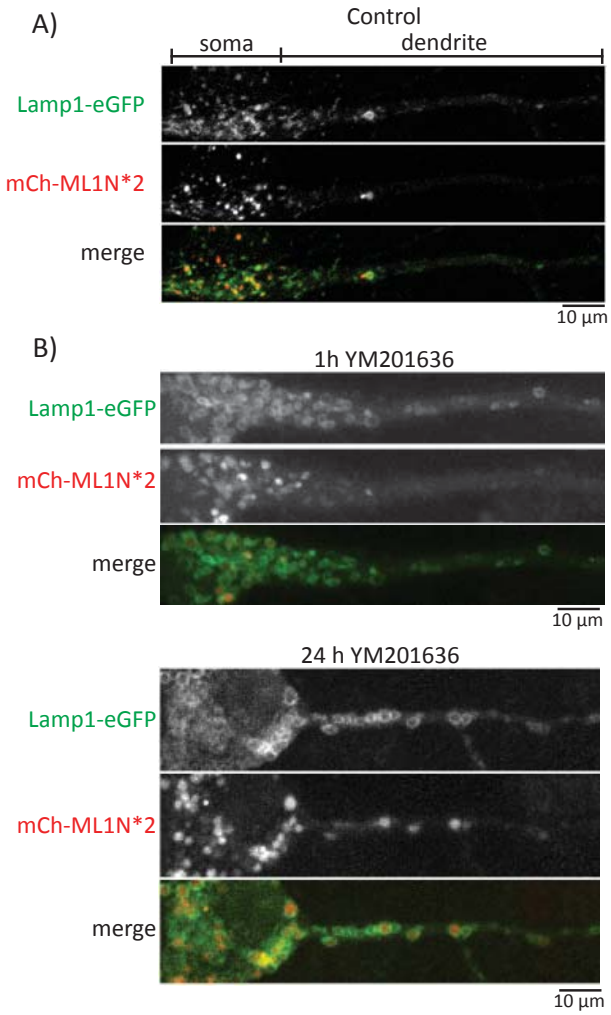

Figure A-2. Inhibition of PIKfyve increases Lamp1 compartment size and decreases the colocalization of the PI(3,5)P_2 reporter with lysosomes

Cultured hippocampal neurons were transfected on DIV19 with 1 µg mCherry-ML1N*2 plasmid DNA and 1.0 µg Lamp1-eGFP by the calcium phosphate transfection and incubated for 24h in the 37C, 5% C02. After 24h, a subset of dishes were treated with 2µM YM201636 for an addition 1 or 24h. Neurons expressing both plasmids were imaged live on the confocal microscope. The extracellular solution contained: 119 mM NaCl, 5 mM KCl, 2 mM CaCl2, 2 mM MgCl2, 30 mM glucose, 10 mM HEPES, pH 7.4. Z-projected images are shown. **A)** Representative image of a control neuron (one experiment, 10 cells). **B)** Representative image of a neuron treated with 2µM YM201636 for 1 or 24 hours prior to imaging (one experiment, 7-9 cells per timepoint). PIKfyve inhibition increases the size of the Lamp1 compartments within 1h and decreases the colocalization of Lamp1 and mCh-ML1N*2. After PIKfyve inhibition some punctate signal is still apparent in the mCh-ML1N*2 channel; these puncta appear to be inside Lamp1 compartments and thus are probably not binding PI(3,5)P_2 or reporting the localization of PI(3,5)P_2.

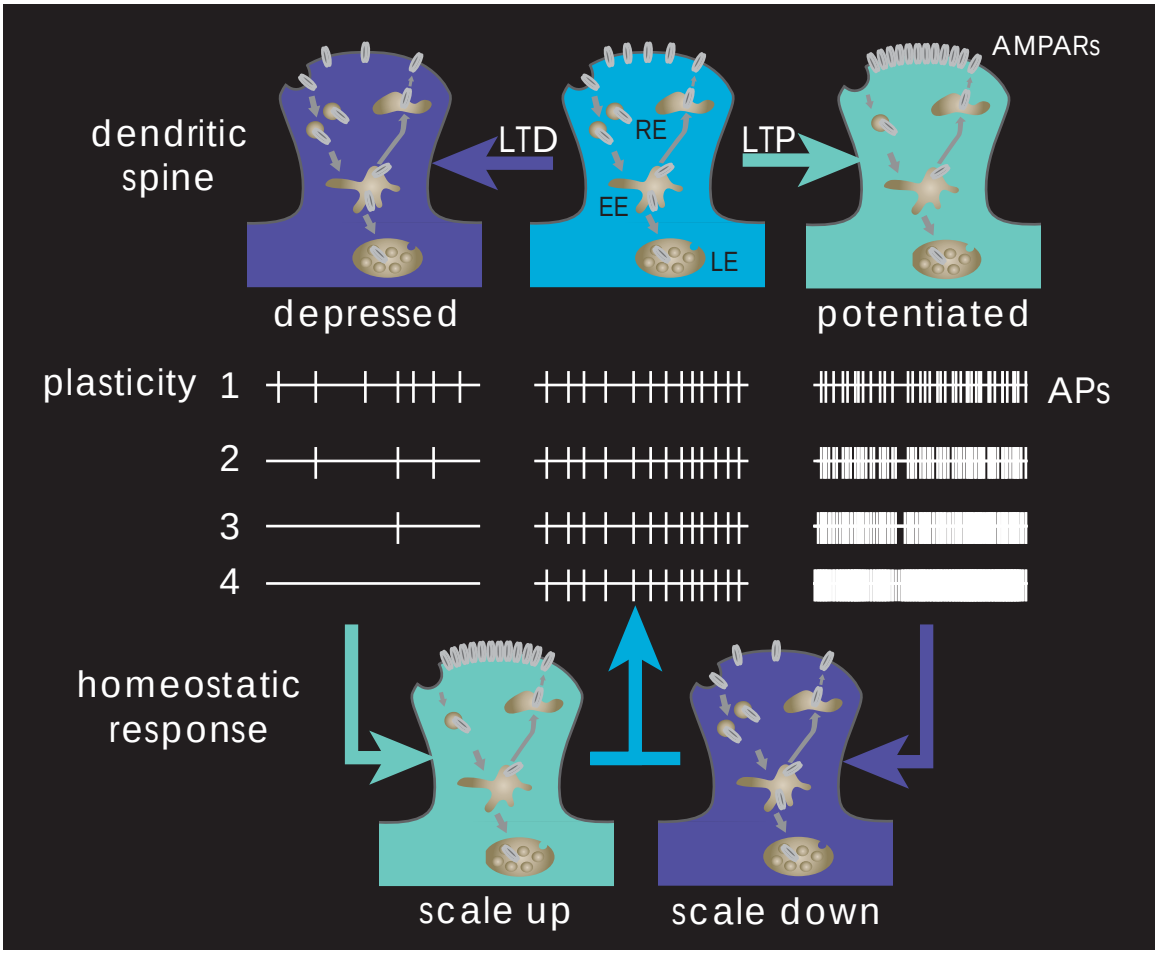

Figure A-3. Homeostatic responses to changes in activity maintain neural networks within a dynamic range

Changes in the strength postsynaptic dendritic spine – or sensitivity of the postsynaptic compartment to neurotransmitter – can drive changes in the level neural activity. Without compensatory regulation of the strength of the synapse, subsequent bouts of synaptic plasticity could eventually lead to saturation of the network, which would leave the network insensitive to further synaptic inputs.

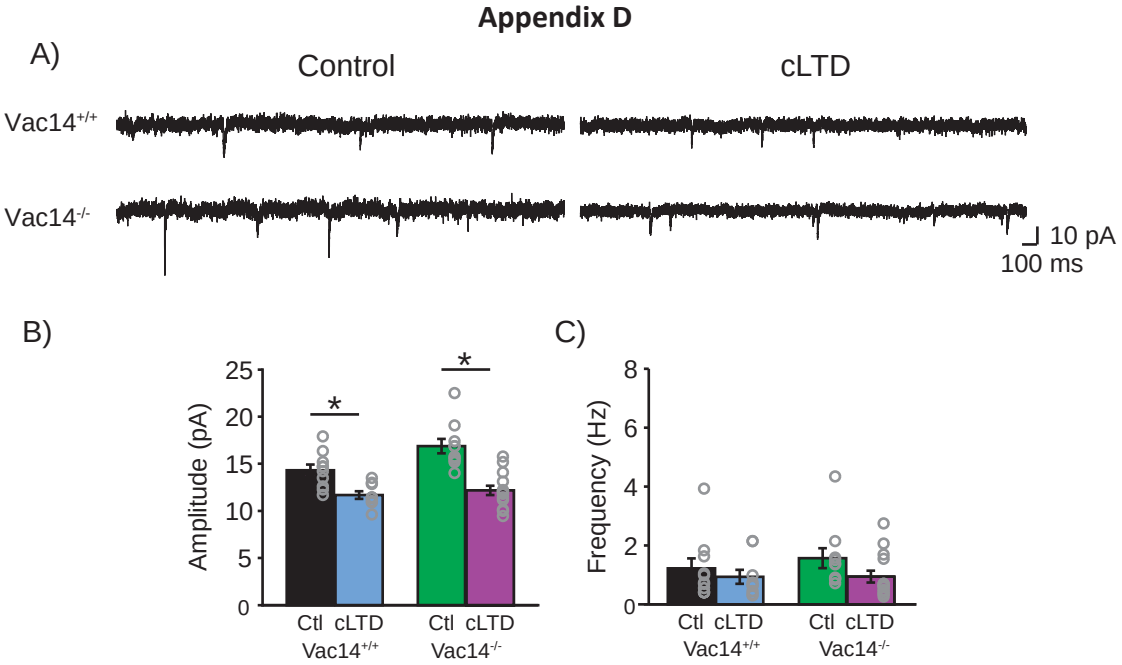

Figure A-4. Vac14 knockout neurons express normal long-term depression
A) Representative intracellular recordings of mEPSCs from DIV 14 wild-type and Vac14$^{-/-}$ neurons under basal conditions (top traces) and 30-90 min after induction of long-term depression (bottom traces). Long-term depression was induced by stimulating neurons for 5 min (followed by returning neurons to reserved media for 30 min) with the following solution: 20 µM NMDA, 1 µM glycine, 25 mM HEPES, 120 mM NaCl, 5 mM KCl, 1 mM $CaCl_2$, 0.2 mM $MgCl_2$, 30 mM D-glucose, pH 7.4. The extracellular recording solution contained HBS: 119 mM NaCl, 5 mM KCl, 2 mM $CaCl_2$, 2 mM $MgCl_2$, 30 mM Glucose, 10 mM HEPES, pH 7.4 plus 10 µM bicuculline (Tocris, O130) and 1 µM TTX (EMD Bioscience, 554412). The internal pipette solution contained: 100 mM cesium gluconate, 0.2 mM EGTA, 5 mM MgCl2, 40 mM HEPES, 2 mM Mg-ATP, 0.3 mM Li-GTP, 1 mM QX-314 (pH 7.2). Pipette resistance ranged from 3-5 MΩ. Neurons with a pyramidal-like morphology were targeted for analysis. For Vac14$^{-/-}$ neurons, neurons with minimal vacuolation were targeted for analysis. Neurons were voltage clamped at -70 mV, and series resistance was not compensated. mEPSC amplitude and frequency were analyzed offline using Minianalysis (Synaptosoft). Cultured neurons with a pyramidal-like morphology were voltage-clamped at –70 mV. **B)** Mean (±SEM) mEPSC amplitude. Induction of LTD reduces mEPSC amplitude similarly in both wild-type and Vac14$^{-/-}$ neurons (Wild-type: 14.32±0.60 pA, n=10. Wild-type+cLTD: 11.67±0.41 pA, n=9. Vac14$^{-/-}$: 16.87±0.77 pA, n=10. Vac14$^{-/-}$+cLTD: 12.17±0.49 pA, n=14. ANOVA, F(3,39)=15.93, p=6.47e-07, Tukey-Kramer post hoc).*significantly different (p<0.05). **C)** Mean (±SEM) mEPSC frequency. Induction of LTD does not significantly reduce the frequency of events (Wild-type: 1.22±0.34 Hz, n=10. Wild-type+cLTD: 0.93±0.24 Hz, n=9. Vac14$^{-/-}$: 1.56±0.34 Hz, n=10. Vac14$^{-/-}$+cLTD: 0.94±0.20Hz, n=14. ANOVA, F(3,39)=1.15, p=0.34).

Appendix E

Introduction to recording miniature excitatory postsynaptic currents (or 'minis')

In dissociated neuronal cultures, spontaneously active networks form with functional synapses. The strength of the synapse can be assessed by measuring the presynaptic probability of releasing a neurotransmitter-filled synaptic vesicle and the postsynaptic sensitivity to neurotransmitter. There are multiple ways to quantify synaptic properties, including visualizing synapse-specific proteins with immunocytochemistry and electrophysiological techniques. For my analysis of Vac14$^{-/-}$ synapses, I have focused on electrophysiology because I wanted to know if there are defects in functional synapses.

In all of my experiments, I have focused on glutamatergic synapses in "pyramidal-like" neurons, which were identified by morphology. Glutamate is released by the presynaptic terminal and acts as an agonist on glutamate receptors on the postsynaptic neuron. Ionotrophic glutamate receptors (AMPA-, NMDA-, and Kainate-type) open ion permeable pores when glutamate binds. The flux of ions through these channels can be measured using an electrophysiology approach called "voltage clamp."

In voltage clamp or more generally "patch clamping", a glass microelectrode is lowered onto the plasma membrane of a neuron and light suction is applied to for a tight seal between the membrane and the glass. Once the resistance of the seal is really

high (>1 GigaOhm) any current measured through the pipette must be due to opening and closing of ion channels inside the patched membrane. Typically, only one channel would be patched at a time ("single-channel recording") so this allows the analysis of the dynamics of opening and closing of that channel. In order to measure macroscopic whole-cell currents (such as synaptic currents), I break through the patched membrane by applying a pulse of suction through the pipette, thereby creating a hole in the membrane with low resistance (<25 MΩ). The tight seal between the glass pipette and the membrane is intact after making this hole, current doesn't leak through the seal and the extracellular solution does not get into the cell. Importantly, the solution filling the pipette does dialyze the cell, which provides the opportunity to deliver drugs or alter the ion composition inside the cell.

Electrical properties of cells can be investigated by applying an equivalent electrical circuit and then using the relationship between voltage (V), current(I) and resistance(R) defined by Ohm's Law (V = IR). In Figure A-5, V_R is the cell resting membrane potential or the difference in potential across the plasma membrane. The

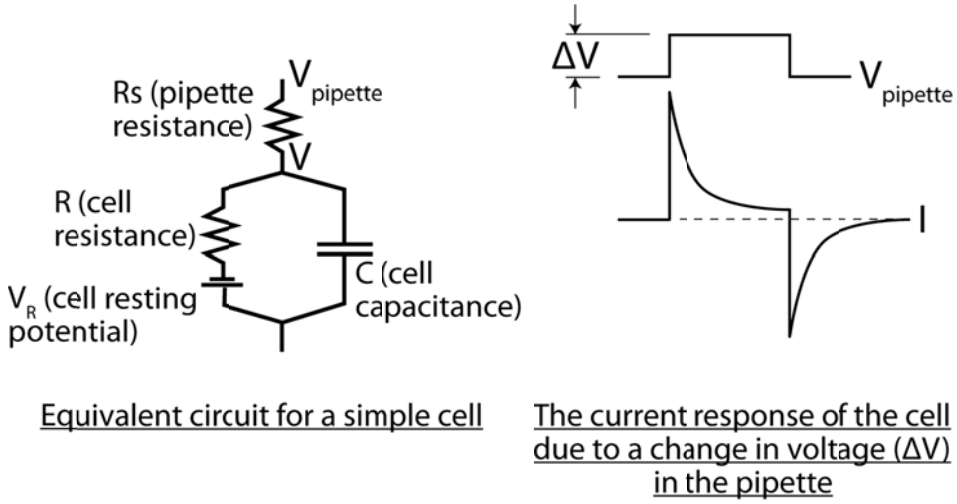

Figure A-5. Equivalent circuit schematic

plasma membrane can be thought of as a capacitor (C) since it is made of hydrophobic core, which means that there is a separation of charge across the membrane. The plasma membrane also has a resistance (R) to flow of current (I). The resistance is a function of the number of ion channels in the plasma membrane. If more ion channels open (e.g. in response to glutamate), then the membrane becomes less resistant to ion flux. If ion channels close, the membrane increases the resistance. A pipette in whole-cell configuration (described below), will be able to measure the voltage or current across the tip of the pipette as well as inject current into the cell to modulate the membrane potential. For example, the pipette can be used to depolarize the cell membrane by injecting current that makes the inside of the cell more positive and thereby decreases the separation of charge across the membrane. The amount of current required to depolarize the membrane a specific amount is calculated by Ohm's Law (I = V/R). Importantly, the pipette tip also acts as a resistor (R_s), so the voltage measured across the pipette tip is the result of the sum of R and R_s (resistance in series adds). If Rs is kept low and the injected current is also small, this error is negligible.

In order to measure synaptic currents, I use the same general approach: tight seal between pipette and membrane, then break through and record current flowing across the pipette tip. Then, I clamp the voltage of the membrane at -70 mV (the amplifier and pipette head stage calculate the amount of current to inject until the voltage equals -70mV). For healthy cells, the current required to reach -70mV is low (<100pA) and constant (doesn't change over the course of the experiment). The membrane potential of -70mV is chosen because it is near resting membrane potential

and the equilibrium potential for chloride-permeable ion channels (such as $GABA_A$ receptors), thereby allowing excitatory postsynaptic currents (EPSCs) to be isolated for analysis. The extracellular bath solution also helps to isolate EPSCs because it includes TTX (voltage-gated Na channel antagonist) to prevent neurons from firing action potentials and Bicuculline ($GABA_A$ receptor antagonist).

In the presence of TTX, neurons still spontaneously release single vesicles filled with neurotransmitter but evoked release is blocked. TTX-insensitive EPSCs are referred to as "minis" or mEPSCs since they are small compared to the amplitude of evoked release (also see Appendix 6 for a comparison of mEPSCs to spontaneous EPSCs). It is well accepted that minis are the result of a quantum of saturating levels of neurotransmitter (here glutamate), so the amplitude of mEPSCs can be used to measure the sensitivity of the postsynaptic cell to glutamate. If the number of AMPARs increases postsynaptically, then the amplitude of the current is expected to likewise increase. A few people have seen size of the quantal release change (presynaptic) in situations where the neurotransmitter transporter expression changes, however this is not common but is something to keep in mind. The most conservative conclusion to make about the increased amplitude of mEPSCs is that these results are consistent with postsynaptic changes in AMPAR expression. The frequency of mEPSCs is typically interpreted to reflect the number of synapses since the quantum of glutamate is released randomly, the more synapses the higher the frequency. Another interpretation could be that changes in frequency reflect a change in the probability of neurotransmitter release (or, in other words, vesicle fusion); however, this conclusion

requires further analysis (e.g. paired-pulse facilitation or imaging active terminals with fluorescent indicators).

In summary, I use whole-cell patch clamping to voltage clamp the postsynaptic neuron at -70 mV and record synaptic currents in the presence of TTX and bicuculline (mEPSCs). In voltage-clamp, the membrane potential is help constant by injecting current through the pipette. When a quantum of glutamate is released and opens ionotropic glutamate receptors (e.g. AMPA-type). The flux of ions through the ionotropic glutamate receptors acts to depolarize the membrane slightly. Since I'm using voltage-clamp mode the membrane potential is held constant, which means a small amount of current must be applied to oppose the depolarization. The pipette records this current and we call such events "mEPSCs." Data analysis is done manually using a specialized program called "MiniAnalysis" where each mEPSC is identified by eye (using kinetics). The program organizes the many parameters measured into a table, which can then be analyzed for average amplitude and frequency.

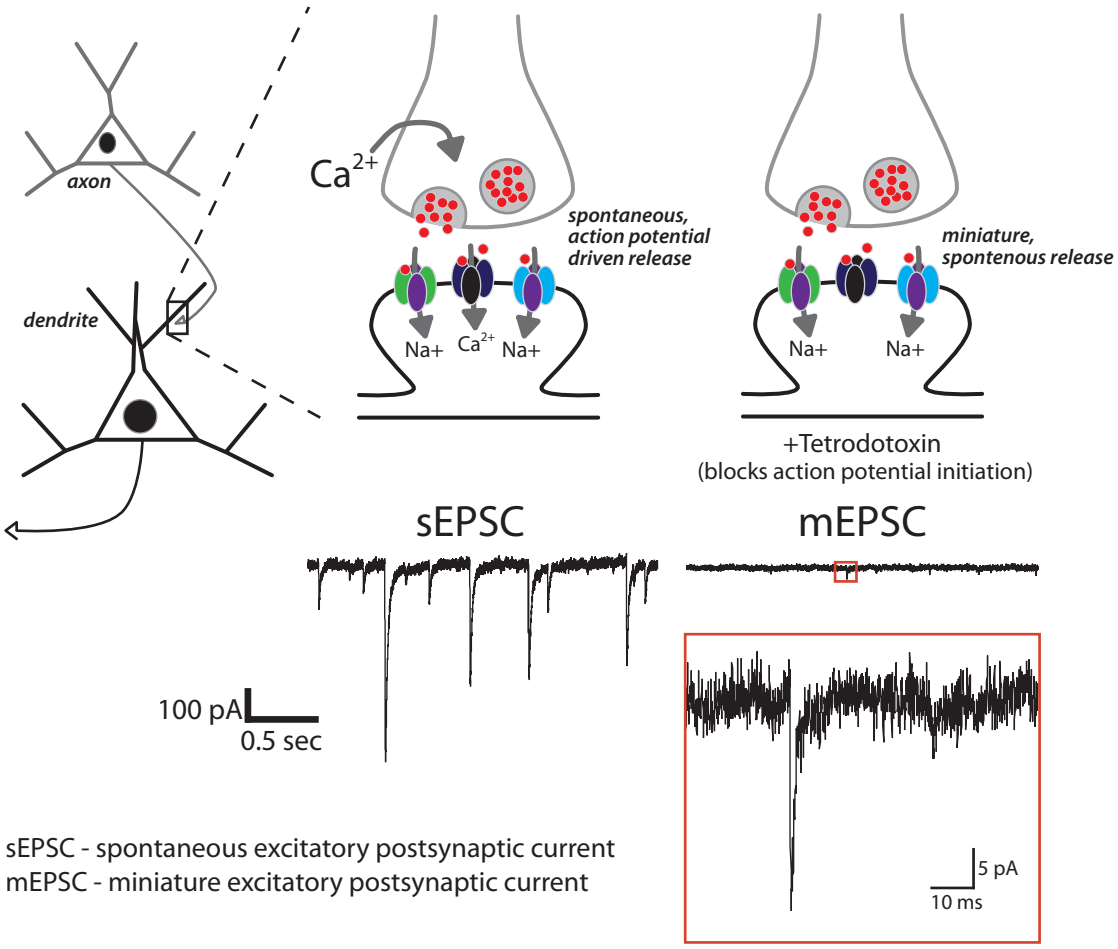

Figure A-6. Comparison of miniature and spontaneous postsynaptic currents
Cultured hippocampal neurons form spontaneously active networks that form function synaptic connections. In response to an action potential arrival in the presynaptic terminal, calcium influx increases and drives vesicle fusion with the plasma membrane. The fusion of the vesicle allows for neurotransmitter to release into the synapse and activate postsynaptic receptors. These events can be observed in the postsynaptic neurons by whole-cell voltage clamp and are called “spontaneous” excitatory postsynaptic currents (sEPSC). The spontaneous activity can be prevented by application of tetrodotoxin (TTX) which is an antagonist of voltage-gated sodium channels. Voltage-gated sodium channels are responsible for the initiation of action potentials, thus blocking these channels prevents action potential firing. In the absence of action potentials, seemingly random vesicle fusion events continue to occur. These synaptic events are called miniature EPSC s (mEPSC). As each event reflect the release of a quantum of neurotransmitter.

Appendix G

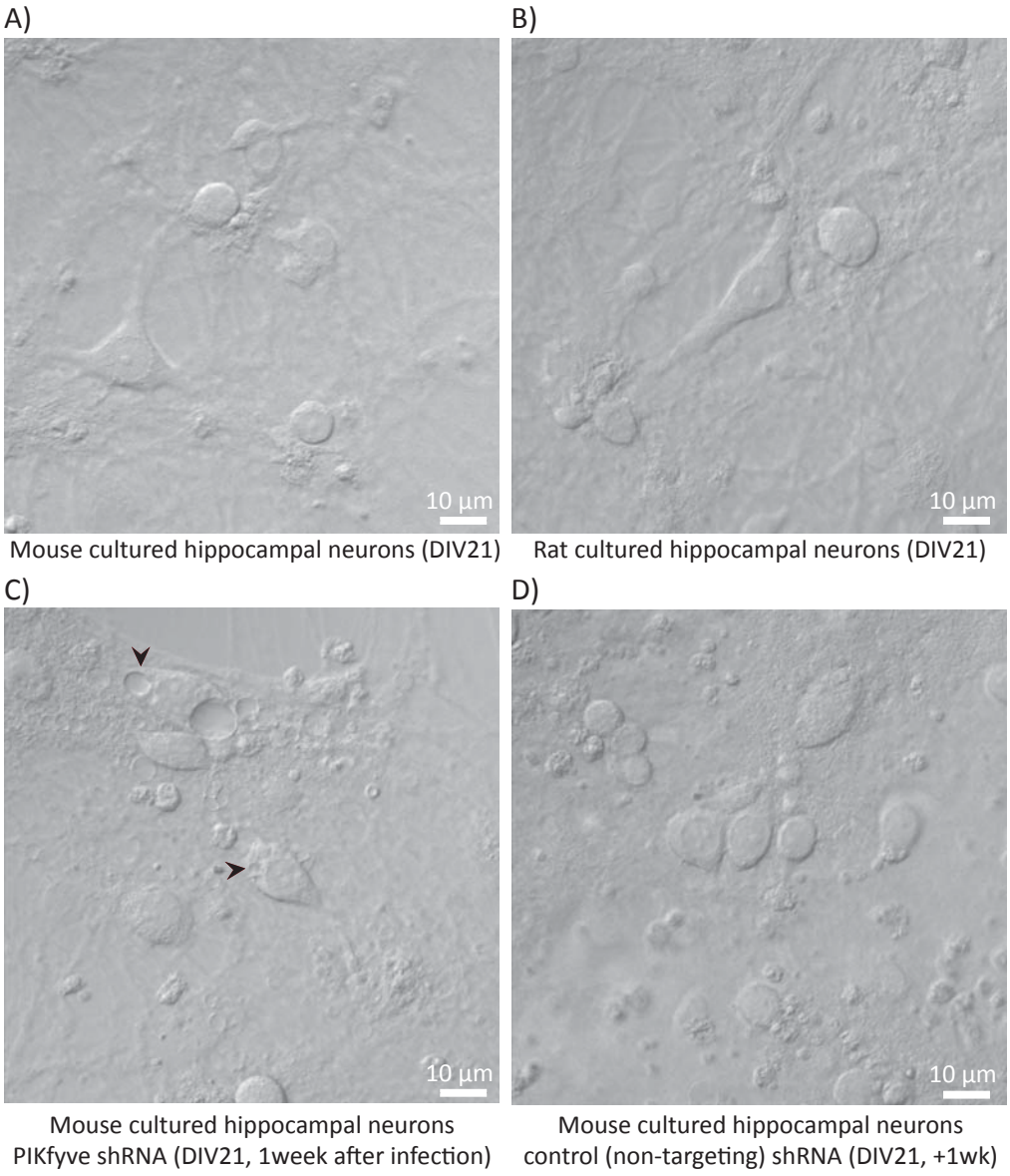

Figure A-7. Images of neurons after PIKfyve knockdown
A) Differential Interference Contrast (DIC) image of mature mouse cultured hippocampal neurons (DIV21). **B)** Rat hippocampal cultured neurons appear similar to (A) at DIV21. **C)** Vacuoles (arrowhead) are apparent in neurons infected with PIKfyve shRNA lentivirus after 7 days. Vacuoles began to appear 4 days after infection. **D)** Infection with non-targeting shRNA lentivirus did not cause vacuoles to form and was generally well tolerated. The experimental proceedures describing these experiments may be found in Chapter 3 (section 3.5.3).

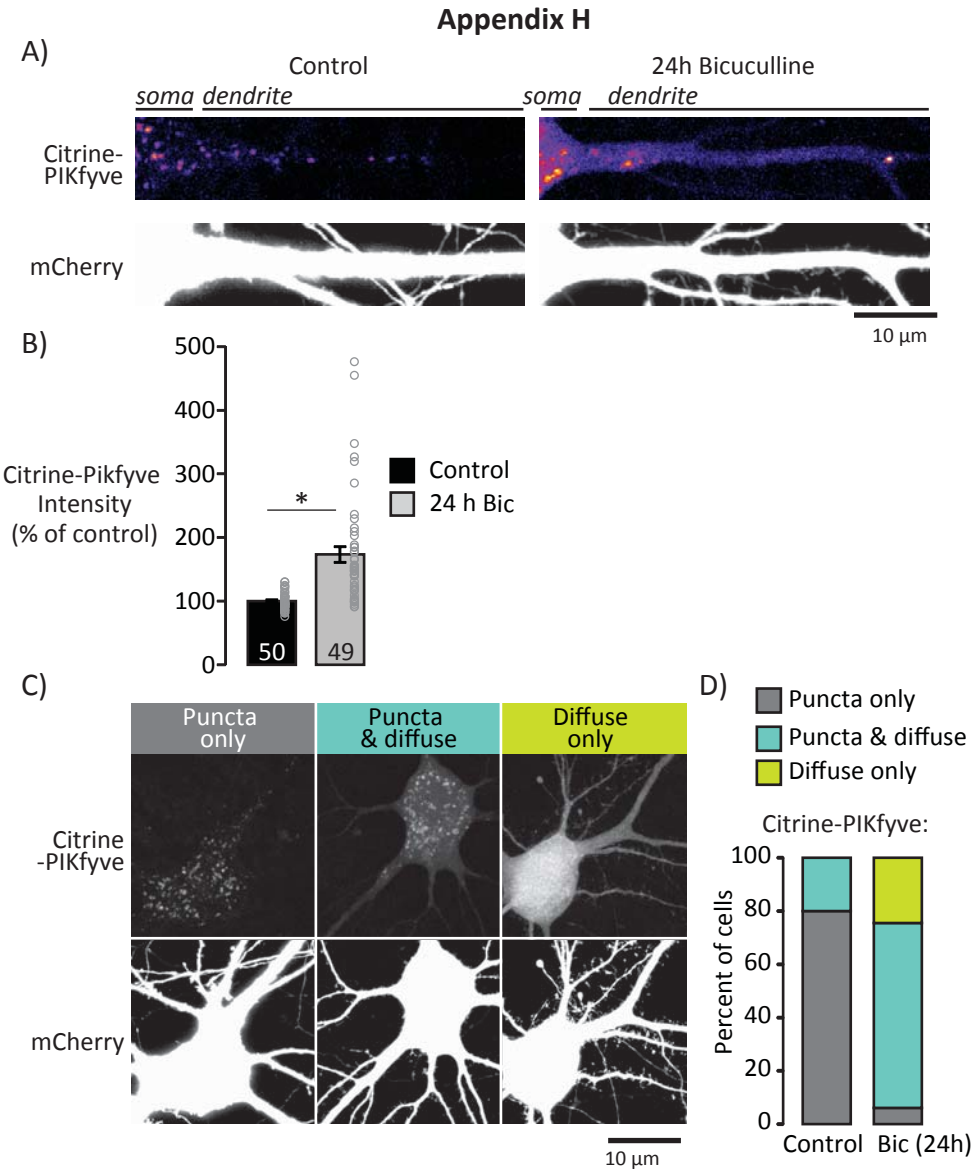

Figure A-8. Citrine-PIKfyve distribution changes after chronic hyperexcitation
A) To gain further insight into the subcellular sites of PI(3,5)P_2 synthesis following chronic hyperactivation, we examined the localization of fluorescently tagged PIKfyve (Citrine-PIKfyve) and found it was more abundant in dendrites and the soma after 24h Bic **(A-B)**. Notably, the increase iwas largely driven by increased diffuse fluorescence. Under basal conditions Citrine-PIKfyve is punctate and concentrated in the cell body **(A)**. Following Bic treatment, Citrine-PIKfyve becomes both more diffuse **(C-D)**. The increase in diffuse signal is unexpected since the PIKfyve substrate is embedded in membranes. One possibility is that with hyperactivity the compartments with which PIKfyve localizes became too small to resolve at the level of light microscope. The development of an antibody for activated PIKfyve would be required to determine the membrane subdomains where PIKfyve functions during synaptic weakening.

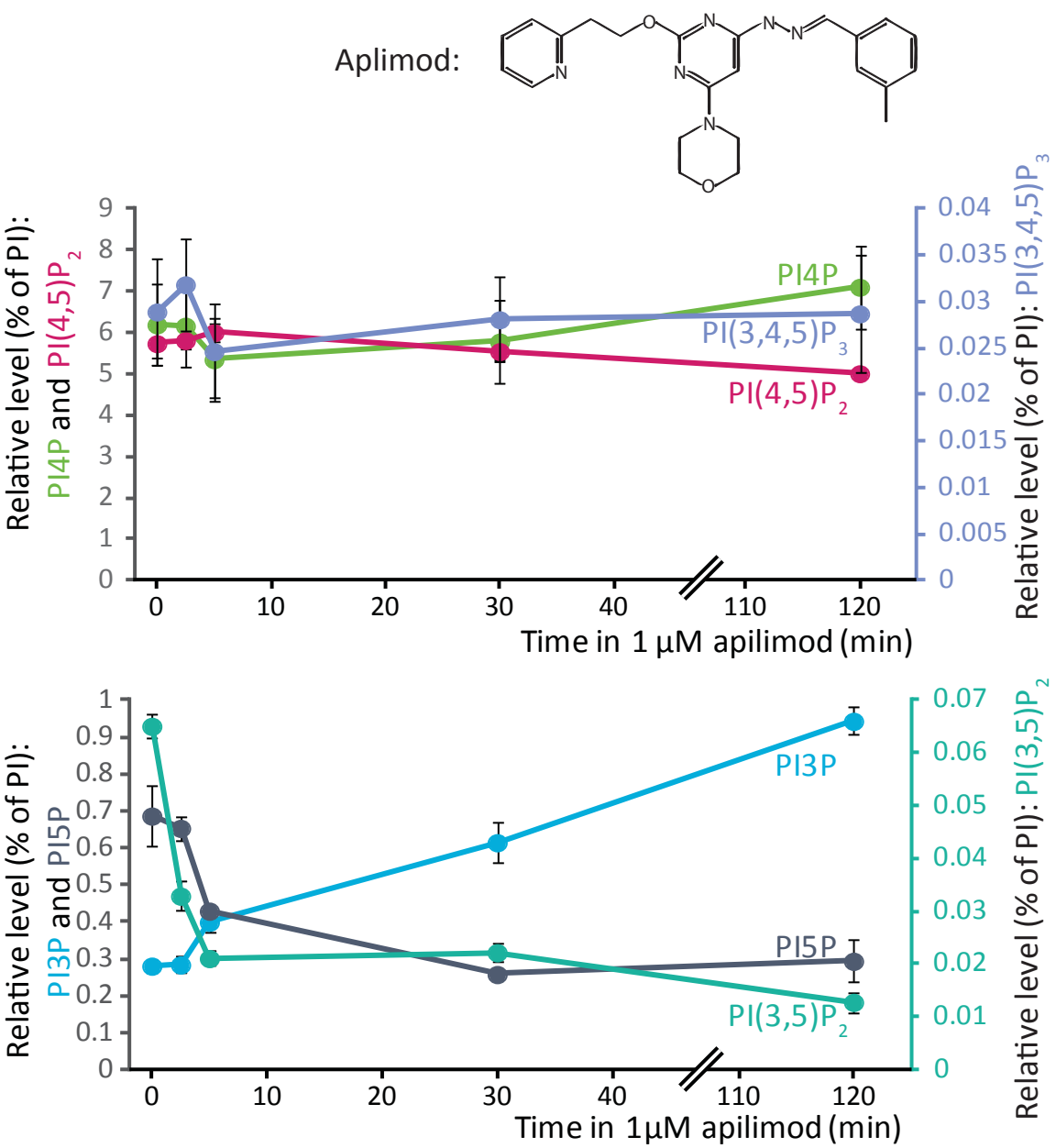

Figure A-9. Inhibition of PIKfyve in wild-type MEFs by 1 µM apilimod
Inhibition in mouse primary fibroblasts by 1 µM apilimod for the specified times (2.5, 5, 10, 30 and120 mins) results in a rapid depletion of PI(3,5)P_2 and PI5P (n=3). Note, the increase in PI3P during PIKfyve inhibition is likely due to accumulation of the pool of PI3P that is the precursor for PI(3,5)P_2 synthesis. These experiments were performed by Yanling Zhang and reanalyzed here for PI(3,4,5)P3 levels, which are stable with apilimod. Note, for each lipid, except PI(3,4,5)P_3, PIKfyve inhibition impacts the levels similarly (compare to Figure A-10).

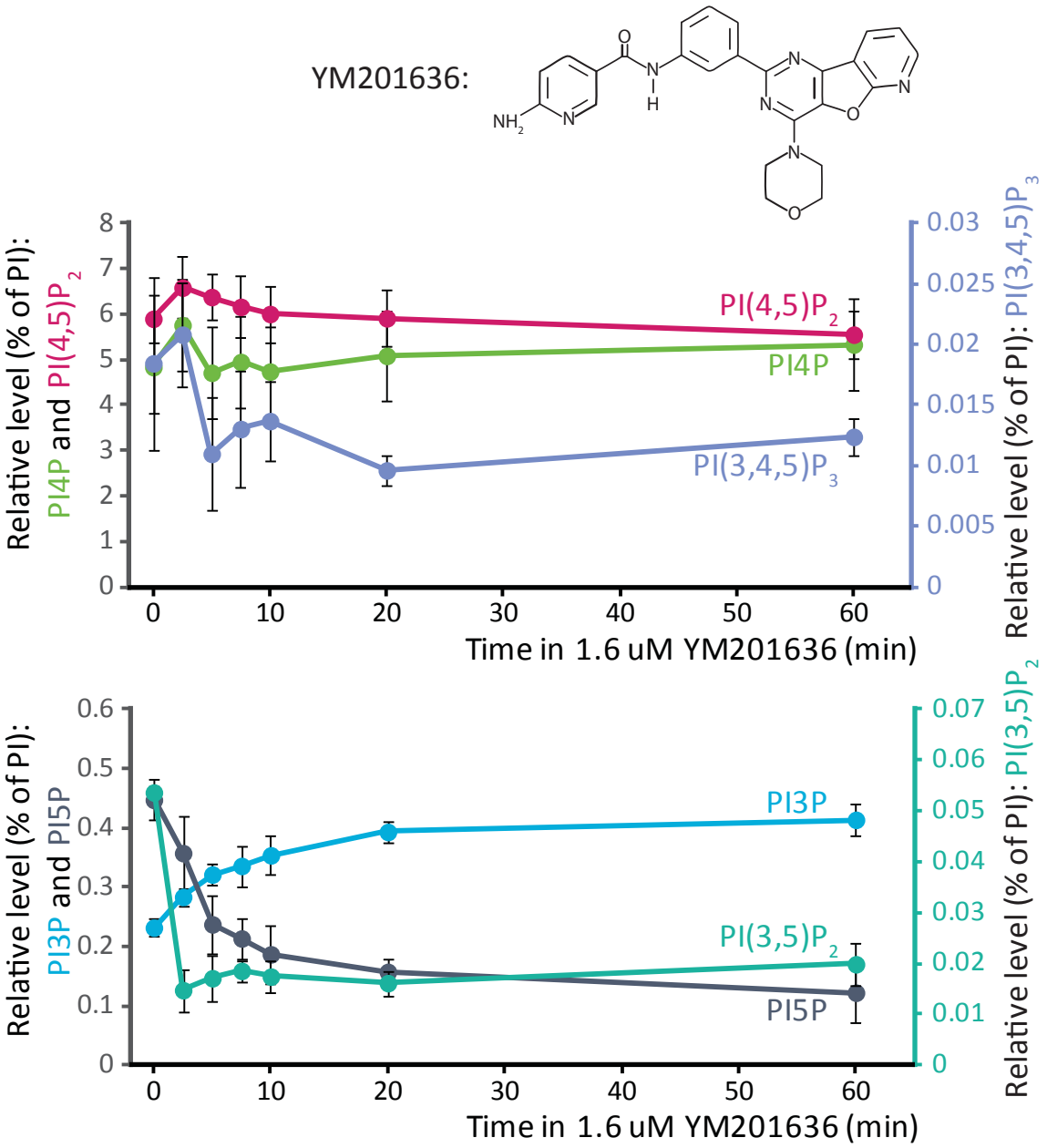

Figure A-10. Inhibition of PIKfyve in wild-type MEFs by 1.6 µM YM201636
Inhibition in mouse primary fibroblasts by 1.6 µM YM201636 for the specified times (2.5, 5, 7.5, 10, 20 and 60 mins) results in a rapid depletion of PI(3,5)P_2 and PI5P (n=4). Note, the increase in the level of PI3P during PIKfyve inhibition is likely due to accumulation of the pool of PI3P that is the precursor for PI(3,5)P_2 synthesis. The rapid decrease in the level of PI(3,4,5)P_3 observed following PIKfyve inhibition in as little as 5 min is likely due to off-target effects of the inhibitor. These experiments were performed by Sergey Zolov and portions published previously in Zolov et al. (2012).

Zolov SN, Bridges D, Zhang Y, Lee WW, et al., & Weisman LS. 2012. In vivo, Pikfyve generates PI(3,5)P2, which serves as both a signaling lipid and the major precursor for PI5P. *Proceedings of the National Academy of Sciences,* **109,** 17472-17477.

Appendix J

Table 4. Homeostatic changes in protein levels or activity following prolonged changes in neural activity (>12h; slow homeostatic synaptic plasticity)

KEY
Increased
Decreased
No Change

	INACTIVITY	HYPERACTIVITY	REFERENCE
A-actinin2	TTX	BIC	Ehlers, 2003
Arc	TTX	BIC	Shepherd et al., 2006
ARMS/Kidins220	TTX	BIC	Cortes et al., 2007
AKAP79/150	TTX	BIC	Ehlers, 2003
B3 Integrin	TTX	BIC	Cingolani et al., 2008
αCaMKII	TTX	BIC	Thiagarajan et al., 2002
	AP-5 or NBQX		Thiagarajan et al., 2002
	TTX	BIC	Ehlers, 2003
βCaMKII	TTX or NBQX	BIC	Thiagarajan et al., 2002
	AP-5		Thiagarajan et al., 2002
	TTX	BIC	Ehlers, 2003
CaMKII-T286P	TTX	BIC	Ehlers, 2003
p-EphA4		BIC	Fu et al., 2011
EphA4		BIC	Peng et al., 2013
GluA1	APV/CNQX	PTX/STRYCH	O'Brien et al., 1998
	TTX		Galvan et al., 2003
	NBQX		Thiagarajan et al., 2005
	AP-5		Thiagarajan et al., 2005
	TTX	BIC	Shepherd et al., 2006
	TTX	BIC	Hou et al., 2008
	Kir2.1 (PRE)		Hou et al., 2008
	TTX	BIC	Hu et al., 2010
	TTX	BIC	Jakawich et al., 2010
	TTX	BIC	Anggono et al., 2011
		BIC	Fu et al., 2011
		PTX	Lee et al., 2011
	TTX	BIC	Shin et al., 2012
		BIC	Peng et al., 2013
		BIC	Siddoway et al., 2013

GluA2	APV/CNQX	PTX/STRYCH	O'Brien et al., 1998
	NBQX		Thiagarajan et al., 2005
	TTX	BIC	Cingolani et al., 2008
	Kir2.1 (PRE)		Hou et al., 2008
	TTX	BIC	Hu et al., 2010
	TTX	BIC	Jakawich et al., 2010
	TTX	BIC	Anggono et al., 2011
		PTX	Lee et al., 2011
	TTX	BIC	Shin et al., 2012
	TTX		Altimimi and Stellwagen, 2013
		BIC	Peng et al., 2013
		BIC	Siddoway et al., 2013
GKAP	TTX	BIC	Ehlers, 2003
	TTX	BIC	Shin et al., 2012
GRIP	Kir2.1 (PRE)		Hou et al., 2008
HCN1	TTX		Arimitsu et al., 2009
Homer	TTX	BIC	Ehlers, 2003
Homer1a	TTX	BIC	Hu et al., 2010
I-2 p-S43	TTX	BIC	Siddoway et al., 2013
mGluR1α	TTX	BIC	Ehlers, 2003
Myosin Va	TTX	BIC	Ehlers, 2003
nNOS	TTX	BIC	Ehlers, 2003
NR1, NR2B	TTX	BIC	Ehlers, 2003
	TTX		Galvan et al., 2003
		BIC	Casanova et al., 2013
NR2A	TTX	BIC	Ehlers, 2003
		BIC	Casanova et al., 2013
NSF	TTX	BIC	Ehlers, 2003
PICK1	TTX	BIC	Anggono et al., 2011
		BIC	Peng et al., 2013
PKA-cat	TTX	BIC	Ehlers, 2003
PKA-RIIβ	TTX	BIC	Ehlers, 2003
PKCβ	TTX	BIC	Ehlers, 2003
PKCε	TTX	BIC	Ehlers, 2003
PKCγ	TTX	BIC	Ehlers, 2003
Plk2 (SNK)		PTX	Pak and Sheng, 2003
		PTX	Seeburg and Sheng, 2008
PP1	TTX	BIC	Ehlers, 2003
PSD95 (hippocampus)	Kir2.1 (pre)		Hou et al., 2008
	TTX	BIC	Jakawich et al., 2010
		BIC	Peng et al., 2013
		PTX	Lee et al., 2011
		PTX	Pak and Sheng, 2003
	TTX	BIC	Shin et al., 2012

PSD95 (cortical)	TTX	BIC	Fu et al., 2011
		BIC	Fu et al., 2011
	TTX or DNQX	PTX OR BIC	Sun and Turrigiano, 2011
PSD93	TTX	BIC	Ehlers, 2003
	TTX or DNQX	PTX OR BIC	Sun and Turrigiano, 2011
	TTX	BIC	Shin et al., 2012
Active Rap2		PTX	Lee et al., 2011
Active Ras		PTX	Lee et al., 2011
PSD93	TTX	BIC	Ehlers, 2003
Sap102	TTX	BIC	Ehlers, 2003
	TTX or DNQX	PTX OR BIC	Sun and Turrigiano, 2011
Shank	TTX	BIC	Ehlers, 2003
Spinophilin	TTX	BIC	Ehlers, 2003
SynGAP	TTX	BIC	Ehlers, 2003
Tubulin	TTX	BIC	Ehlers, 2003
Rap GAP (SPAR)		PTX	Pak and Sheng, 2003
		PTX	Lee et al., 2011

Bibliography

Altimimi HF & Stellwagen D. 2013. Persistent synaptic scaling independent of AMPA receptor subunit composition. *The Journal of neuroscience : the official journal of the Society for Neuroscience,* **33,** 11763-7.

Anggono V, Clem RL & Huganir RL. 2011. PICK1 loss of function occludes homeostatic synaptic scaling. *The Journal of neuroscience : the official journal of the Society for Neuroscience,* **31,** 2188-96.

Arimitsu T, Nuriya M, Ikeda K, Takahashi T & Yasui M. 2009. Activity-dependent regulation of HCN1 protein in cortical neurons. *Biochemical and Biophysical Research Communications,* **387,** 87-91.

Casanova JR, Nishimura M, Le J, Lam TT & Swann JW. 2013. Rapid hippocampal network adaptation to recurring synchronous activity - a role for calcineurin. *European Journal of Neuroscience,* **38,** 3115-3127.

Cingolani LA, Thalhammer A, Yu LM, Catalano M, Ramos T, Colicos MA & Goda Y. 2008. Activity-dependent regulation of synaptic AMPA receptor composition and abundance by beta3 integrins. *Neuron,* **58,** 749-62.

Cortes RY, Arevalo JC, Magby JP, Chao MV & Plummer MR. 2007. Developmental and activity-dependent regulation of ARMS/Kidins220 in cultured rat hippocampal neurons. *Developmental Neurobiology,* **67,** 1687-1698.

Ehlers MD. 2003. Activity level controls postsynaptic composition and signaling via the ubiquitin-proteasome system. *Nature neuroscience,* **6,** 231-42.

Fu AK, Hung KW, Fu WY, Shen C, Chen Y, Xia J, Lai KO & Ip NY. 2011. APC(Cdh1) mediates EphA4-dependent downregulation of AMPA receptors in homeostatic plasticity. *Nature neuroscience,* **14,** 181-9.

Galvan CD, Wenzel JH, Dineley KT, Lam TT, Schwartzkroin PA, Sweatt JD & Swann JW.

2003. Postsynaptic contributions to hippocampal network hyperexcitability induced by chronic activity blockade in vivo. *European Journal of Neuroscience,* **18,** 1861-1872.

Hou Q, Zhang D, Jarzylo L, Huganir RL & Man HY. 2008. Homeostatic regulation of AMPA receptor expression at single hippocampal synapses. *Proceedings of the National Academy of Sciences of the United States of America,* **105,** 775-80.

Hu JH, Park JM, Park S, Xiao B, Dehoff MH, Kim S, Hayashi T, Schwarz MK, Huganir RL, Seeburg PH, Linden DJ & Worley PF. 2010. Homeostatic scaling requires group I mGluR activation mediated by Homer1a. *Neuron,* **68,** 1128-42.

Jakawich SK, Neely RM, Djakovic SN, Patrick GN & Sutton MA. 2010. An essential postsynaptic role for the ubiquitin proteasome system in slow homeostatic synaptic plasticity in cultured hippocampal neurons. *Neuroscience,* **171,** 1016-31.

Lee KJ, Lee Y, Rozeboom A, Lee JY, Udagawa N, Hoe HS & Pak DT. 2011. Requirement for Plk2 in orchestrated ras and rap signaling, homeostatic structural plasticity, and memory. *Neuron,* **69,** 957-73.

O'Brien RJ, Kamboj S, Ehlers MD, Rosen KR, Fischbach GD & Huganir RL. 1998. Activity-dependent modulation of synaptic AMPA receptor accumulation. *Neuron,* **21,** 1067-78.

Pak DT & Sheng M. 2003. Targeted protein degradation and synapse remodeling by an inducible protein kinase. *Science,* **302,** 1368-73.

Peng YR, Hou ZH & Yu X. 2013. The kinase activity of EphA4 mediates homeostatic scaling-down of synaptic strength via activation of Cdk5. *Neuropharmacology,* **65,** 232-43.

Seeburg DP & Sheng M. 2008. Activity-induced Polo-like kinase 2 is required for homeostatic plasticity of hippocampal neurons during epileptiform activity. *The Journal of neuroscience : the official journal of the Society for Neuroscience,* **28,** 6583-91.

Shepherd JD, Rumbaugh G, Wu J, Chowdhury S, Plath N, Kuhl D, Huganir RL & Worley PF. 2006. Arc/Arg3.1 mediates homeostatic synaptic scaling of AMPA receptors. *Neuron,* **52,** 475-84.

Shin SM, Zhang N, Hansen J, Gerges NZ, Pak DT, Sheng M & Lee SH. 2012. GKAP orchestrates activity-dependent postsynaptic protein remodeling and homeostatic scaling. *Nature neuroscience,* **15,** 1655-66.

Siddoway BA, Altimimi HF, Hou H, Petralia RS, Xu B, Stellwagen D & Xia H. 2013. An essential role for inhibitor-2 regulation of protein phosphatase-1 in synaptic scaling. *The Journal of neuroscience : the official journal of the Society for Neuroscience,* **33,** 11206-11.

Sun Q & Turrigiano GG. 2011. PSD-95 and PSD-93 play critical but distinct roles in synaptic scaling up and down. *The Journal of neuroscience : the official journal of the Society for Neuroscience,* **31,** 6800-8.

Thiagarajan TC, Lindskog M & Tsien RW. 2005. Adaptation to synaptic inactivity in hippocampal neurons. *Neuron,* **47,** 725-37.

Thiagarajan TC, Piedras-Renteria ES & Tsien RW. 2002. alpha- and betaCaMKII. Inverse regulation by neuronal activity and opposing effects on synaptic strength. *Neuron,* **36,** 1103-14.